

**STUDIES ON PREPARATION, CHARACTERIZATION
AND EVALUATION OF MICRON TO NANOSIZED
DISPERSIONS IN LATEX TECHNOLOGY**

Thesis submitted to

Cochin University of Science and Technology

in partial fulfilment of the requirements

for the award of the degree of

Doctor of Philosophy

Under the Faculty of Technology

by

Anand K.



**Department of Polymer Science and Rubber Technology
Cochin University of Science and Technology
Kochi- 682 022, Kerala, India**

January 2017

Studies on preparation, characterization and evaluation of micron to nanosized dispersions in latex technology

Ph.D. Thesis

Author

Anand K.

Advanced Centre for Rubber Technology
Rubber Research Institute of India
Kottayam- 686 009, Kerala, India.
E-mail: anand.rrii@gmail.com

Supervising Teachers

Dr. Siby Varghese

Joint Director
Advanced Centre for Rubber Technology
Rubber Research Institute of India
Kottayam- 686 009, Kerala, India.
E-mail: sibyvarghese100@yahoo.com

Dr. Thomas Kurian

Professor
Department of Polymer Science and
Rubber Technology
Cochin University of Science and
Technology (CUSAT)
Kochi- 682 022, Kerala, India.
E-mail: drtkurian@gmail.com

Department of Polymer Science and Rubber Technology
Cochin University of Science and Technology
Kochi- 682 022, Kerala, India

January 2017



Dr. Siby Varghese

Joint Director

Advanced Centre for Rubber Technology
Rubber Research Institute of India
Kottayam- 686 009, Kerala, India.
E-mail: sibyvarghese100@yahoo.com



Dr. Thomas Kurian

Professor

Department of Polymer Science
and Rubber Technology
Cochin University of Science and
Technology (CUSAT)
Kochi- 682 022, Kerala, India.

Date:

Certificate

This is to certify that the thesis entitled “**Studies on preparation, characterization and evaluation of micron to nanosized dispersions in latex technology**” which is being submitted by Mr. Anand K., in partial fulfilment of the requirements of the degree of Doctor of Philosophy, to Cochin University of Science and Technology (CUSAT), Kochi, Kerala, India is a record of the bonafide research work carried out by him under our joint guidance and supervision.

Mr. Anand has worked on the research problem for about five years at the Rubber Research Institute of India, Kottayam. All the relevant corrections and modifications suggested by the audience during the pre-synopsis seminar and recommended by the Doctoral Committee of the candidate have been incorporated in the thesis. In our opinion, the thesis fulfills all the requirements according to the regulations. The results embodied in this thesis have not been submitted for the award of any other degree or diploma.

Siby Varghese
(Supervising Guide)

Thomas Kurian
(Co-Guide)

Declaration

I hereby declare that the thesis entitled, “**Studies on preparation, characterization and evaluation of micron to nanosized dispersions in latex technology**”, is the original research work carried out by me under the joint guidance and supervision of Dr. Siby Varghese, Joint Director, Advanced Centre for Rubber Technology Division, Rubber Research Institute of India, Kottayam-686 009 and Dr. Thomas Kurian, Professor, Department of Polymer Science and Rubber Technology, Kochi-682 022. No part of this thesis has been presented for any other degree from any other institution.

Kottayam
30-01-2017

Anand K.

Acknowledgement

I bow my head before God Almighty for showering His blessings throughout the course of my research programme. I express my sincere gratitude to my research supervisors Dr. Siby Varghese, Joint Director Technical Consultancy Division, Rubber Research Institute of India, Kottayam and Dr. Thomas Kurian, Professor, Department of Polymer Science and Rubber Technology, Cochin University of Science and Technology (CUSAT), Kochi for their generous and inspiring guidance throughout the tenure of my research work.

I am thankful to Dr. James Jacob, Director Research, Rubber Research Institute of India, Kottayam for providing me with the laboratory facilities and for his providence. I am thankful to Prof. Sunil K. Narayanankutty (HOD) and all the Faculty Members of the Department of Polymer Science and Rubber Technology, CUSAT for their interest in the progress of my work. I would like to extend my sincere thanks to Dr. K.T. Thomas, Dr. Rosamma Alex, Dr. Jacob Varkey, Dr. Benny George, Dr. Manoj Kurian Jacob, Mr. Joy Joseph, Dr. Shera Mathew, Smt. Tessy George, Dr. Reethamma Joseph, Dr. Jinu Jacob George, Smt. Fancy, Mr. Jinesh, Dr. Sasidharan, Smt. Rejitha Rajan, Smt. Anu Mary Joseph, Sri. Eldho Abraham, and Smt. Shybi. The staff members of Instrumentation Division of Rubber Research Institute of India are acknowledged. I thank Mr. Baby, Mr. Jose and Mr. Vijayan for the preparation of test samples. I express my thanks to the library staffs for literature search and documentation. The support rendered by the scientific, technical and administrative staff during my stay at Rubber Research Institute of India is gratefully acknowledged.

Dr. Balagopal N. Nair, Dr. Anandhan Srinivasan Prof. Suresh Pillai and Dr. Suryasarathy Bose are thankfully remembered for suggestions and discussions. Sincerely acknowledges Prof. Kuruvilla Joseph, Prof. Sabu Thomas and Prof. M.K. Jayaraj for providing necessary lab and instrument facilities. Thanks to Manjunatha Ganiga for AFM analysis. I am indebted to Prof. Jacob Philip for offering course work as a part of Ph.D. programme. Thanks to Sofian Ibrahim, Chai Chee Keong and Albert V. Tamashauski for chemicals and latex samples for study.

The prayers, care and sacrifices of my parents and sister is greatly acknowledged. Their consolation and moral support helped me to tackle every difficult situation during the research tenure.

Last but not least, I extend my thanks to my relatives and well-wishers for their unstinting support without which it would be difficult to complete the research work satisfactorily.

Anand K,

||| Preface |||

For latex compounding and latex product manufacturing, chemicals are added to the latex in the form of dispersions. Properly stabilized fine particle dispersions are essential for satisfactory processing and end use properties. Ball milling is a widely used technique by latex industry for the preparation of chemical dispersions. Since most of the latex chemicals are water insoluble, it requires careful formulations and may take many hours to prepare these dispersions. Moreover, ball milling is a complicated process and the parameters such as milling time, milling speed, milling atmosphere, ball to powder weight ratio, concentration of the surfactant, *etc.* determines the milling efficiency.

With the advancement of nano/fine particle technology, latex product manufacturers are looking for processes/chemicals which can improve the technological properties and can impart novel functionalities to the finished product. Moreover, for intimate mixing, the particle size of dispersions should be comparable with that of latex particle size and is around 580 nm. In addition, the incorporation of fine/nanoparticles minimizes the sedimentation rate and improves the transparency of thin latex products such as condoms. The present study aims at the optimization of process parameters for the preparation of chemical dispersions of various latex compounding ingredients by simple ball milling, synthesis, stabilization and evaluation of nano zinc oxide (ZnO) dispersion and their effect on pre-vulcanized natural rubber latex properties, degradation studies of nano filler dispersions incorporated natural rubber latex nanocomposites, influence of starch nanocrystals on latex vulcanizate properties and fabrication of radiation vulcanized natural rubber latex (RVNRL)-graphene nanocomposites.

The thesis consists of nine chapters. A concise introduction to the subject and literature review is presented in the first chapter. The objective of the work is also mentioned in this chapter.

The second chapter describes the details of materials used in the present work, experimental techniques and the instruments used for the preparation and characterization of the ultra-fine/nanomaterials and the rubber vulcanizates prepared using these materials.

Chapter 3 is divided into part A, part B and part C. Part A describes the ball milling process which was used to prepare dispersions of ZnO with lowest possible size by varying process parameters. The effect of milling time and ultrasonication on the particle size of the dispersions were assessed. The particles in the dispersions were characterized by dynamic light scattering (DLS) and zeta potential measurements. The effect of varying the concentration of surfactant (SA) on dispersion stability was explained. The effect of ball size on the milling efficiency of ZnO dispersions is presented in Part B. Part C presents the preparation of dispersions of various latex compounding ingredients (LCI) such as china clay, zinc diethyl dithiocarbamate (ZDEC), zinc 2- mercapto benzothiazole (ZMBT) and butylated reaction product of p-cresol and dicyclopentadiene (wingstay L) by wet ball milling. Effect of varying the ball size 6.35 mm (small), 12.7 mm (medium), 19.05 mm (large) and composite balls and milling time on particle size and stability of aqueous of dispersions of latex compounding ingredients were studied.

Chapter 4 is divided into part A and part B. Part A explores the synthesis of nano-ZnO by a solvent-free mechano-chemical method and was characterized by X-ray diffraction (XRD), FT-IR spectroscopy,

thermogravimetric analysis (TGA), dynamic light scattering measurements (DLS) and transmission electron microscopy (TEM). The effect of various surfactants [Triton X 100, polyethylene glycol- 6000 (both non-ionic), cetyltrimethylammonium bromide (cationic) and sodium dodecyl sulphate (anionic)] on the stability of nano-ZnO dispersions are explained in Part B. In order to examine the stability of the dispersion, particle size analysis, zeta potential measurements and sedimentation tests were conducted.

Effect of synthesized nano-ZnO on swelling, antimicrobial, mechanical and ageing properties of pre-vulcanized natural rubber latex films are described in Chapter 5.

The degradation behavior of nano silica (SiO_2) and nano titania (TiO_2) filled natural rubber latex (NR) nanocomposites against various degrading environments (thermal, gamma radiation, UV radiation and chlorination) is presented in Chapter 6. The mechanical properties such as tensile strength, elongation at break and modulus at 100% elongation were recorded after exposing the latex film vulcanizates to various degrading environments.

Chapter 7 describes the addition of starch nanocrystals (SNC) on the properties of natural rubber latex vulcanizates. Starch nanocrystals were isolated from modified corn starch and the size of the SNC suspension was analyzed from dynamic light scattering (DLS) studies and X-ray diffraction (XRD) measurements.

Chapter 8 reports the fabrication of radiation vulcanized natural rubber latex (RVNRL) - graphene based nanocomposites. The synthesis of graphene derivatives such as exfoliated graphene oxide (XGO) and reduced graphene oxide (RGO) has been made through a hydrazine free

route and were characterized by various analytical and spectroscopic tools. The effect of filler content on mechanical, morphological and electrical properties of the nanocomposites were studied and the distribution of filler in polymer matrix is explained by theoretical predictions.

The summary and conclusions of the studies presented in the thesis is given in chapter 9.

Abstract

In latex industry, the chemical dispersions required for latex product manufacturing are usually prepared by ball-milling. The ultimate properties of finished latex products are highly dependent on particle size as well as the stability of added dispersions. The central aim of the present research work was the optimization of process parameters for the preparation of aqueous dispersions of latex compounding ingredients such as zinc oxide, china clay, zinc diethyl dithiocarbamate (ZDEC), zinc 2-mercapto benzothiazole (ZMBT) and butylated reaction product of p-cresol and dicyclopentadiene (wingstay L) with lowest possible size by ball-milling. The process parameters such as ball size, milling time and concentration of the surfactant were optimized. The size and stability of as-prepared dispersions were evaluated by dynamic light scattering (DLS), zeta potential measurements and sedimentation test. The use of smaller and composite balls (mixture of balls with different diameters) for milling resulted maximum size reduction.

Zinc oxide (ZnO) nanoparticles were synthesized through mechano-chemical route and the effect of various surfactants on the size and stability of the dispersions were studied. ZnO stabilized with anionic surfactant, sodium dodecyl sulphate (SDS) showed good stability. The addition of synthesized nano-ZnO on swelling, antimicrobial, mechanical and ageing properties of pre-vulcanized latex vulcanizates were examined and compared with conventional ZnO filled vulcanizates. The degradation behaviour of silica (SiO₂) nanoparticles and titania (TiO₂) nanoparticles incorporated natural rubber latex (NR) nanocomposites

against various degrading agents *viz.* thermal, γ - radiation, UV radiation and chlorination were studied. The addition of nano silica and nano titania in latex formulations improved the degradation resistance of latex films. Starch nanocrystals (SNC) were isolated from modified corn starch and its efficacy as a potential bio-filler for natural rubber latex were explored. The barrier properties of latex films were improved with the addition of SNC suspension. Finally, graphene derivatives such as exfoliated graphene oxide (XGO) and reduced graphene oxide (RGO) were prepared and characterized by various analytical and spectroscopic tools and fabricated radiation vulcanized natural rubber latex (RVNRL) - graphene nanocomposite. The addition of RGO in RVNRL matrix yielded significant improvement in electrical conductivity and theoretical predictions showed random distribution of filler in the polymer matrix.

Keywords: Natural rubber latex, RVNRL, Ball-milling, Latex-compounding ingredients, Ultra-fine dispersions, Nano-ZnO, Surfactants, Stabilization, Pre-vulcanization, Starch nanocrystals, Graphene, Ageing, Degradation, Mechanical-properties.

Contents

<i>Preface</i>	i
<i>Abstract</i>	v

Chapter 1

General Introduction01 - 74

1.1 Natural rubber latex	02
1.1.1 Structure and composition	02
1.1.2 Preservation	03
1.1.3 Changes in physico-chemical properties of latex upon storage.....	05
1.2 Latex compounding	06
1.3 Principles of latex compounding.....	08
1.4 Vulcanization	09
1.5 Importance of ZnO in rubber	12
1.6 Reinforcement of elastomers	18
1.6.1 Filler characteristics and vulcanizate properties	20
1.7 Nanotechnology in rubber	27
1.8 Preparation of nanomaterials	28
1.8.1 Top-down approach.....	30
1.8.2 Bottom-up approach	33
1.8.2.1 Vapour phase synthesis	33
1.8.2.2 Liquid phase synthesis.....	34
1.8.3 Synthesis of nano ZnO	36
1.9 Polymer nanocomposites	42
1.9.1 Melt intercalation	43
1.9.2 Intercalation of polymer or pre-polymer from solution.....	43
1.9.3 <i>In-situ</i> intercalative polymerization.....	44
1.9.4 Exfoliation/adsorption	44
1.10 Rubber nanocomposites.....	48
1.11 Scope and objectives of the study	59
References	62

Chapter 2

Experimental75 - 96

2.1 Centrifuged natural rubber latex	75
2.2 Radiation vulcanized natural rubber latex (RVNRL).....	76

2.3	Materials used	76
2.4	Compounding ingredients.....	81
2.5	Characterization	81
2.5.1	Dynamic light scattering (DLS).....	81
2.5.2	Zeta potential	83
2.5.2.1	<i>Determination of stability of dispersion</i>	83
2.5.3	XRD	84
2.5.4	FT-IR.....	84
2.5.5	SEM.....	84
2.5.6	TEM	85
2.5.7	Raman analysis	86
2.5.8	AFM analysis	87
2.5.9	UV-visible spectra.....	87
2.5.10	TG-DTA studies	87
2.6	Degradation studies	88
2.6.1	Thermal ageing	88
2.6.2	UV ageing.....	88
2.6.3	Chlorination	88
2.6.4	Gamma ageing	88
2.7	Properties of latex vulcanizate	89
2.7.1	Viscosity	89
2.7.2	pH meter	89
2.7.3	Chloroform number	89
2.7.4	Equilibrium swelling and crosslink density	90
2.7.5	Sorption studies.....	92
2.7.6	Mechanical properties.....	93
2.7.7	Electrical properties.....	93
2.7.8	Morphology	94
2.8	Theoretical modeling.....	94
	References.....	96

Chapter 3

Preparation of dispersions by ball-milling:

State- of- the- art..... 97 - 143

Part-A

Preparation of ultra-fine dispersions of zinc oxide by ball-milling: Optimization of process parameters

3A.1 Introduction.....98

3A.2	Experimental	100
3A.2.1	Materials	100
3A.2.2	Methods	100
3A.3	Results and discussion	102
3A.3.1	Effect of milling time on volume weighed mean at various concentrations of surfactant	102
3A.3.2	Effect of surfactant on the specific surface area of zinc oxide.....	103
3A.3.3	Effect of the concentration of the surfactant on the size (%) of zinc oxide particles	104
3A.3.4	Effect of ultrasonication.....	109
3A.3.5	Effect of ultrasonication on the specific surface area of zinc oxide particles	109
3A.3.6	Effect of ultrasonication on the size (%) of zinc oxide Particles	110
3A.3.7	Effect of milling and ultrasonication on polydispersity	111
3A.3.8	Variation of zeta potential with SA concentration	112
3A.4	Conclusions	113
	References	114

Part-B

Effect of ball size on milling efficiency of zinc oxide dispersions

3B.1	Introduction	115
3B.2	Experimental	116
3B.2.1	Methods	116
3B.2.2	Characterization	117
3B.3	Results and discussion	117
3B.3.1	Effect of ball size on cumulative size distribution	117
3B.3.2	Effect of ball size on specific surface area.....	119
3B.3.3	Effect of ball size on D50	119
3B.3.4	Effect of ball size on size (%) of ZnO	121
3B.3.5	Effect of ball size on stability of ZnO dispersions	122
3B.4	Conclusions	123
	References	123

Part-C

Aqueous dispersions of latex compounding ingredients by wet ball-milling: Effect of ball size and milling time on dispersion quality

3C.1	Introduction	126
3C.2	Experimental	128

3C.2.1	Materials	128
3C.2.2	Methods	128
3C.2.3	Free volume determination	129
3C.2.4	Determination of stability of dispersion	129
3C.3	Results and discussion	130
3C.3.1	Effect of ball size and milling time on D [4, 3]	130
3C.3.2	Effect of ball size on size (%)	133
3C.3.3	Effect of milling time on specific surface area (SSA) of latex compounding ingredients	134
3C.3.4	Effect of milling time on cumulative size distribution of latex compounding ingredients.....	136
3C.3.5	Stability of dispersions	140
3C.4	Conclusions	142
	References	142

Chapter 4

Preparation characterization and stabilization of zinc oxide nanodispersions 145 - 169

Part-A

Synthesis of zinc oxide nanorods through mechano-chemical route: A solvent free approach.

4A.1	Introduction	146
4A.2	Experimental	148
4A.2.1	Methods	148
	4A.2.1.1 <i>Preparation of nano-ZnO</i>	148
	4A.2.1.2 <i>Characterization</i>	148
4A.3	Results and discussion	149
4A.3.1	TG-DTA analysis	149
4A.3.2	XRD analysis	150
4A.3.3	FT-IR analysis.....	151
4A.3.4	DLS analysis	152
4A.3.5	HR-TEM analysis.....	153
4A.3.6	Mechanism of ZnO nanoparticle formation.....	153
4A.3.7	Role of CTAB in morphology of ZnO nanoparticles	155
4A.4	Conclusions	155
	References	156

Part-B

Role of surfactants on the stability of nano zinc oxide dispersions

4B.1 Introduction	159
4B.2 Experimental	161
4B.2.1 Materials	161
4B.2.2 Methods	161
4B.2.2.1 <i>Preparation of ZnO dispersion</i>	161
4B.2.2.2 <i>Characterization</i>	162
4B.3 Results and discussion	162
4B.3.1 Impact of various surfactants on ZnO dispersion	162
4B.3.1.1 <i>Particle size of ZnO in various surfactants</i>	162
4B.3.1.2 <i>Size after storage</i>	163
4B.3.1.3 <i>Effect of sonication</i>	164
4B.3.1.4 <i>Stability of ZnO dispersion</i>	165
4B.4 Conclusions	168
References	168

Chapter 5

Effect of micro and nano zinc oxide on the properties of pre-vulcanized natural rubber

(NR) latex films 171 - 186

5.1 Introduction	172
5.2 Experimental	174
5.2.1 Methods	174
5.3 Results and discussion	176
5.3.1 Sorption behavior	176
5.3.2 Antimicrobial activity	177
5.3.3 Mechanical properties	179
5.3.4 Effect of ageing	182
5.4 Conclusions	184
References	185

Chapter 6

Degradation behaviour of nano silica and nano titania filled natural rubber (NR) latex

nanocomposites 187 - 204

6.1 Introduction	188
6.2 Experimental	190

6.2.1	Methods	190
6.2.1.1	<i>Preparation of latex films</i>	191
6.3	Results and discussion	191
6.3.1	Swelling studies	192
6.3.2	TGA studies	193
6.3.3	Effect of thermal ageing	194
6.3.4	Effect of chlorination.....	197
6.3.5	Effect of UV light.....	199
6.3.6	Effect of gamma radiation	201
6.4	Conclusions.....	202
	References.....	202

Chapter 7

Effect of starch nanocrystals on natural rubber latex vulcanizate properties 205 - 220

7.1	Introduction.....	206
7.2	Experimental	208
7.2.1	Materials	208
7.2.2	Methods	208
7.2.2.1	<i>Preparation of starch nanocrystals</i>	208
7.2.2.2	<i>Characterization</i>	209
7.2.2.3	<i>Composite preparation</i>	209
7.2.2.4	<i>Mechanical property measurements</i>	210
7.3	Results and discussion	210
7.3.1	DLS analysis	210
7.3.2	XRD analysis	212
7.3.3	SEM analysis	213
7.3.4	Swelling studies	214
7.3.5	Mechanical properties.....	215
7.3.6	Effect of leaching	216
7.3.7	Theoretical predictions	218
7.4	Conclusions.....	219
	References.....	219

Chapter 8

Properties of radiation vulcanized natural rubber latex (RVNRL) - graphene nanocomposites 221 - 240

8.1	Introduction.....	222
8.2	Experimental	224

8.2.1	Materials	224
8.2.2	Methods	225
8.2.2.1	<i>Preparation of exfoliated graphene oxide (XGO) dispersion</i>	225
8.2.2.2	<i>Preparation of reduced graphene oxide (RGO) dispersion</i>	225
8.2.2.3	<i>Preparation of nanocomposites</i>	226
8.2.2.4	<i>Characterization</i>	227
8.3	Results and discussion	228
8.3.1	Particle size analysis.....	228
8.3.2	FT-IR analysis.....	229
8.3.3	UV-Visible analysis	230
8.3.4	Raman analysis	231
8.3.5	AFM analysis of RGO	232
8.3.6	TEM analysis of RGO	233
8.3.7	Visual features of the composite	233
8.3.8	Electrical conductivity studies	234
8.3.9	Mechanical properties.....	236
8.3.10	Theoretical modeling	237
8.4	Conclusions	238
	References	239

Chapter 9

Summary and conclusions241 – 247

List of abbreviations and symbols249 - 253

List of publications and presentations.....255 - 256

Curriculum vitae.....257 - 258

.....✻.....

Chapter 1

GENERAL INTRODUCTION

<i>Contents</i>	1.1 <i>Natural rubber latex</i>
	1.2 <i>Latex compounding</i>
	1.3 <i>Principles of latex compounding</i>
	1.4 <i>Vulcanization</i>
	1.5 <i>Importance of ZnO in Rubber</i>
	1.6 <i>Reinforcement of elastomers</i>
	1.7 <i>Nanotechnology in rubber</i>
	1.8 <i>Preparation of nanomaterials</i>
	1.9 <i>Polymer nanocomposites</i>
	1.10 <i>Rubber nanocomposites</i>
	1.11 <i>Scope and objectives of the study</i>

This chapter describes the structure and composition of natural rubber latex, latex compounding, vulcanization methods etc. Role of zinc oxide (ZnO) in rubber industry was highlighted. The concept of rubber reinforcement and its effect on vulcanizate properties were explained with adequate literature support. The evolution of nanotechnology and preparation of nanomaterials are explained well. Synthesis of nano ZnO by different methods was explained. Finally, the preparation of polymer/rubber nanocomposites was explained and the effect of addition of various nanomaterials on rubber composites was discussed.

1.1 Natural rubber latex

1.1.1 Structure and composition

Hevea Brasiliensis, popularly known as rubber trees account for 99 per cent of world's natural rubber (NR) production. Rubber latex is a stable dispersion of rubber particles in aqueous medium and is essentially a two phase system comprising a dispersed phase (discontinuous phase of rubber molecules) and dispersion medium (aqueous continuous phase of serum). It is chemically *cis*-1, 4- polyisoprene having the following structure

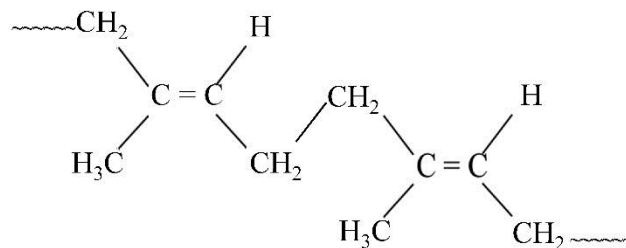


Figure 1.1: Structure of natural rubber (NR)

The field latex is a negatively charged colloidal dispersion of rubber particles suspended in an aqueous serum. The rubber particles are surrounded by a layer of proteins and phospholipids (Figure 1.2). The rubber particles in NR latex are polydispersed and have a wide range of diameters varying from 0.01 to 5 μm . Besides rubber particles, non-rubber constituents are also present in latex which include protein (1 - 1.5%), resin (1 - 2.5%), sugar (1%), ash (< 1%) and water (55 - 65%). The non-rubber constituents like proteins, carbohydrates, sugars *etc.* in latex make it a susceptible environment for bacterial

growth and cause latex putrefaction. Hence the latex collected from tree should be properly preserved.

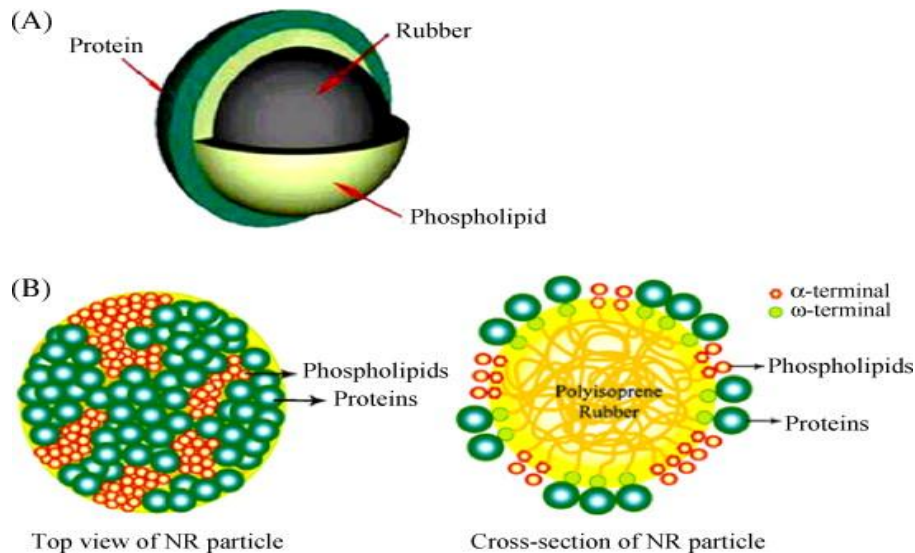


Figure 1.2: Two possible models: (A) current model and (B) rubber particle consisting of a mixed layer of proteins and lipids [1]

1.1.2 Preservation

Preservatives protect the latex against spontaneous coagulation by suppressing the activity and growth of micro-organisms, deactivating trace metals and increase the colloidal stability. Ammonia is the most widely used preservative for NR latex. The preservative effect of ammonia upon NR latex was first recorded in 1953 [2]. Ammonia at a concentration of 1 per cent by weight on latex is added for field latex and 0.7 per cent by weight on latex for concentrated latex. It is an effective bactericide and ensures latex stability by improving the pH. The main disadvantages of high ammonia latex are strong odour, processing

difficulties, zinc oxide (ZnO) thickening *etc.* Considering these drawbacks, a preservation system with lesser amount of ammonia was introduced during the seventies [3]. Various types of commercially available latex preservative systems are given in Table 1.1.

Table 1.1: Type of latex preservative systems

Type of system	Requirements
High ammonia (HA) system	0.6% ammonia (min.)
LA-SPP system	0.2% ammonia + 0.2% sodium pentachlorophenate
LA-BA system	0.2% ammonia + 0.24% boric acid + 0.05% lauric acid
LA-ZDEC system	0.2% ammonia + 0.1% zinc diethyl dithiocarbamate + 0.05% lauric acid.

However the last three systems failed to have any serious impact on the latex preservation. The major drawbacks of these systems are:

- 1) High toxicity and poor film colour in the case of LA-SPP system.
- 2) Poor chemical stability and slow rate of cure in the case of LA-BA system.
- 3) Lower mechanical and storage stability in the case of LA-ZDEC system.

To overcome these problems, a composite preservative system comprising 0.2 - 0.3 per cent ammonia along with 0.013 per cent each of TMTD and ZnO, known as LATZ system has been introduced in 1975 [4]. LATZ system of preservation can be applied to both field latex and concentrated latex. Mathew *et al.*, [5] reported the use of monomethyl amine as an effective alternative for ammonia in preserving concentrated

latex. A non-toxic latex preservative system consisting of 0.4 per cent ammonia and 0.05 per cent Dowicil [1-(3-chloroallyl)-3,5,7-triaza-1-azonia adamantane chloride] was found to be as good as the LATZ preservative system for both field latex and latex concentrate [6]. The identification of ammonia loving bacteria by Shum and Wren [7] intensified the search for alternative preservative systems for latex.

1.1.3 Changes in physico-chemical properties of latex upon storage

The chemical constitution of ammonia preserved latex after ammoniation and storage differs considerably from that of fresh, unammoniated NR latex. The amount of proteins and resinous substances decrease on storage as they are converted to polypeptides, amino acids, soaps, and glycerol. The overall concentration of ions present in the aqueous phase tends to increase, particularly the concentrations of carboxylate anions of high and low molecular masses, phosphate anions and amino-acid anions. These chemical changes significantly affect the colloidal properties, processing characteristics and technological properties of vulcanized latex films.

The latex properties having major significance are dry rubber content (DRC), non-rubber solids (NRS) content, alkalinity, volatile fatty acid number (VFA), mechanical stability time (MST) and potassium hydroxide number (KOH). Among them principal changes occurs for the last three parameters.

The anions of volatile fatty acids such as formic, acetic and propionic may be generated in the latex system by the action of bacteria.

Lowe [8] reported that the concentration of these anions increases rapidly over a period of few days, until a stage is reached after which very little further increase occurs and rate of formation initially increases with increasing temperature. As temperature is further increased, the rate of formation decreases sharply. These indications suggest an enzyme-catalyzed process. As the VFA number increases, latex coagulation occurs. There exist several theories for the coagulation of natural rubber latex [9].

KOH number is a measure of the ionic strength of the serum in the presence of ammonia. It was reported that the electrical conductivity of ammonia-preserved latex increases significantly during storage [10]. This indicates a progressive increase in ionic strength of aqueous phase as the formation of additional anions.

Mechanical stability time of latex increases steadily upon storage. Addition of external soaps such as ammonium laurate will cause instant increase in MST. The increase in MST during storage is attributed to the hydrolysis of lipids which produce fatty acid soaps and get adsorbed on the particle surface.

1.2 Latex compounding

The art of mixing various compounding ingredients with latex is known as latex compounding. All ingredients added to latex should be brought to a physical state comparable to latex, before they are mixed. Water soluble ingredients are added to latex as solutions and water insoluble ingredients as dispersions/emulsions.

All chemicals that are used as stabilizers, dispersing agents, emulsifiers, wetting agents, foam promoters, foam stabilizers, viscosity modifiers *etc.*, come under surface active agent's category. To prevent coagulation of latex compound while adding chemicals, stabilizers are first added to latex before compounding. Surfactant usually acts to reduce the interfacial free energy of two phases and allows easy mixing.

Normal vulcanizing agent for natural rubber latex is sulphur. Sulphur is added at different levels ranging from 0.3 - 2.5 phr on dry basis and 50 per cent dispersion in water is desirable. In sulphurless cure, TMTD is used as vulcanizing agent.

Accelerators are chemicals added to latex to reduce vulcanization time and also to improve the technological properties of vulcanized product. The common accelerators used with rubber bands, elastic thread, gloves and foam rubber is ZDEC and its dosage ranges from 0.5 - 1.5 phr. ZMBT is used in addition to ZDEC in latex compounds where increased modulus for the product is required. TMTD is used in low sulphur formulations and its dosage varies from 2 - 3 phr, where high heat resistance of the product is needed.

Zinc oxide (ZnO) is the activator used in latex compounds to boost up the cure time and also to impart additional heat resistance to the product. Its dosage is very low (0.1 phr) for rubber bands and high (2 - 3 parts) with elastic thread. When transparency of the finished product is required, concentration of the ZnO should be 0.5 phr (max.).

Antioxidants protect rubber from deterioration by other agencies such as oxygen, heat, light, ozone, trace metals *etc.* The level of antioxidant to be added varies from 0.5 - 2 phr. Amine derivatives and phenolic types of antioxidants are generally used in latex industry.

Inorganic fillers and pigments are added in latex compounds to cheapen and stiffen the product or to colour it. Clays, mica powder, whiting *etc.* are used as fillers. About 5 - 10 phr clay or whiting as dispersions are added in the production of latex products.

Plasticizers are used in latex compounds to reduce the modulus of the products such as gloves balloons *etc.* Mineral oils and non-volatile esters come under this category. Mineral oils of the paraffinic and naphthenic types are commonly used.

1.3 Principles of latex compounding [11]

- Particle size of the chemical dispersions used in a latex compound must be comparable to the particles size of the latex.
- Intimate mixing of the chemical dispersions and latex particles are essential.
- The particle size of the compounding ingredients should be lower (< 1micron)
- For thin film high strength latex product like condoms, sub-micron (500 - 1000 nm) and nano (50 - 100 nm) sized particle dispersions should be used.

- Stabilization of the chemical dispersions should be ensured to minimize the sedimentation during storage and in the process lines.
- The colloidal stability of the chemical dispersions should match well with that of latex. *i.e.* the electrical double layer at the latex particle surface should be maintained.
- To prevent colloidal destabilization, pH of the compounding ingredients (chemical dispersions) should be the same with that of latex.
- For latex dipping compounds the ‘surface free energy’ of the compound must be lower than the ‘surface free energy’ of the former.

1.4 Vulcanization

Vulcanization, also known as cross-linking or curing, is the process where the rubber chains are joined together, increasing strength and elasticity, and reducing the tendency of the rubber to creep when extended.

Latex can be vulcanized in three principal ways. They are:

- 1) Allowing latex particles to react with sulphur and one or more vulcanization accelerator, and possibly also with an inorganic activator.
- 2) By heating the latex with organic peroxides and hydroperoxides, and possibly also with activators for those compounds.
- 3) By exposing latex to high energy radiation.

Latices vulcanized using these techniques are commonly known as pre-vulcanized latex (PVL). Pre-vulcanized latex refers to chemically modified latex that on drying gives a vulcanized film. Most of the dipped goods were manufactured using pre-vulcanized latex.

Schematic representation of sulphur pre-vulcanization of latex is shown in Figure 1.3.

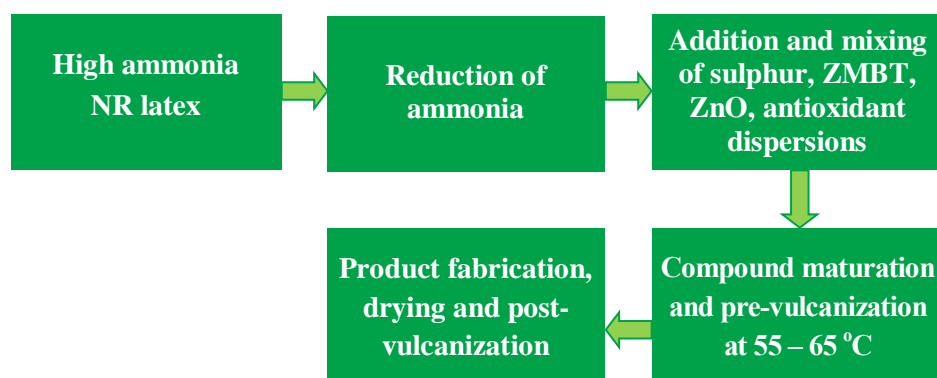


Figure 1.3: Schematic representation of sulphur pre-vulcanization of latex [12]

Philpott [13, 14] discovered that sulphur pre-vulcanized latex can be prepared from compounds containing a sulphur donor such as tetramethylthiuram disulphide accelerated with a nucleophile such as thiourea and formulation for the system have been described. The advantages of pre-vulcanized NR latex are: simple to use, long shelf life, no need for maturation and vulcanization and better efficiency in leaching.

The crosslinking of latex by free radicals generated from peroxide and hydroperoxide systems has been known [15]. The general mechanism of peroxide vulcanization consists of three step process *viz.*

initiation, propagation and termination [16]. The process involves initial thermal homolytic cleavage of a peroxide molecule forming two free radicals. This follows first order kinetics and the rate of reaction depends only on the concentration of the peroxide. During propagation step, the free radicals generated react with the polymer chain removing the more labile allylic hydrogen atoms from the polymer (H-abstraction) or radical addition across the unsaturation of the polymer chain resulting the formation of a polymer radical. Finally, in the termination step, two polymer radicals couple to form a carbon-carbon crosslink. Owing to low toxicity, they are more suitable for medical applications.

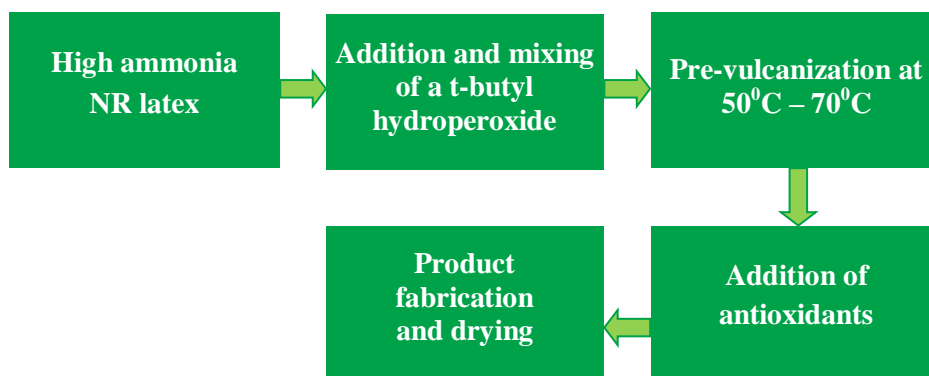


Figure 1.4: Schematic representation of peroxide vulcanization of latex [12]

Natural rubber latex can be cross-linked using high energy γ -radiation [17, 18].

The degree of crosslinking relates to dosage of radiation and the process may be accelerated by the use of sensitizers such as chloroform, carbon tetrachloride or monofunctional monomers [19, 20]. The crosslinks in irradiated latex are carbon-carbon ones similar to those in peroxide cures.

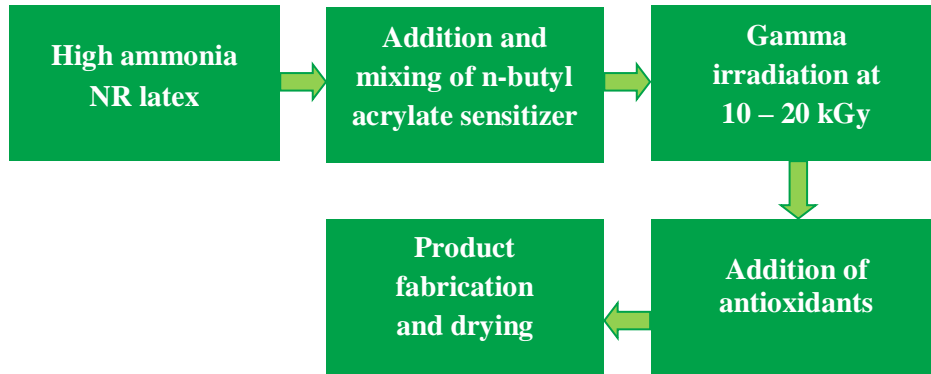


Figure 1.5: Schematic representation of radiation vulcanization of NR latex [12]

1.5 Importance of ZnO in Rubber

Zinc oxide primarily acts as an activator in sulphur vulcanization. In addition, it is normally added to peroxide cure systems and is also used as a crosslinking agent for rubbers containing halogens or carboxyl groups (CR, CSM, CIIR, XNBR, XSBR *etc.*). World-wide use of zinc oxide is in excess of 1.2 million tonnes annually. Rubber industry holds the major share of usage of ZnO.

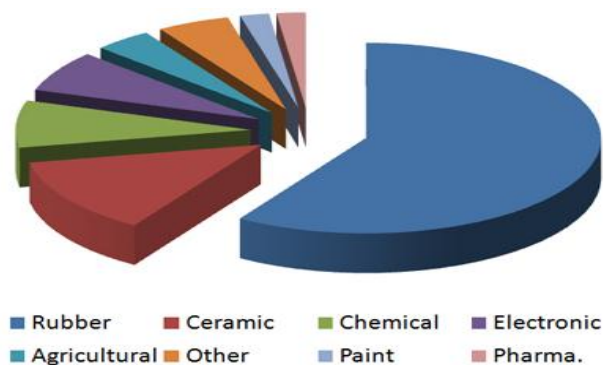


Figure 1.6: World wide applications of ZnO [21]

French process zinc oxide, made from metallic zinc, is preferred for rubber formulations. The major reason for this is that they have nearly spherical particle shape and have narrow particle size distribution. With a finer particle size, it is more reactive and gives faster cure rate. Further the purity of assay is >99.5%. Latex rubber products are often formulated with very fine zinc oxide known as active grades which have low levels of opacity [21]. The important role played by zinc oxide in rubber industry is given below [22]:

Activation

In the curing process of natural rubber and most types of synthetic rubbers, the chemical reactivity of zinc oxide is utilized to speed up the rate of cure with the organic accelerator. The unreacted share of the zinc oxide remains available as a basic reserve to neutralize the sulphur bearing acidic decomposition products formed during vulcanization. Adequate levels of zinc oxide distinctly contribute to chemical reinforcement, scorch control and resistance to heat ageing and compression fatigue.

Acceleration

Zinc oxide serves as an accelerator with some types of elastomer. The cross-linking that it induces takes several forms. With some systems, zinc oxide serves as an effective co-accelerator in the vulcanization process.

Heat stabilization

Zinc oxide retards the de-vulcanization of numerous types of rubber compounds operating at elevated temperatures. French process zinc oxides impart heat-ageing resistance superior to that of American-

process zinc oxides. The former type, being sulphur-free, has a higher pH and can neutralize more effectively the acidic decomposition products formed during ageing. Moreover, the finer French-process zinc oxides proved as superior grades in heat-ageing resistance.

Latex gelation

Zinc oxide is particularly effective in the gelation of the foam, with sufficient stability, as part of the production process of latex foam rubber products.

Light stabilization

Zinc oxide's absorption of ultraviolet rays is exceptional among white pigments and extenders. It therefore serves as an effective stabilizer of white and tinted rubber compounds under prolonged exposure to the sun's destructive rays.

Pigmentation

Zinc oxide provides a high degree of whiteness and tinting strength for rubber products such as tyre sidewalls, sheeting and surgical gloves, owing to its high brightness, refractive index and optimum particle size.

Reinforcement

Zinc oxide provides reinforcement in natural rubber, as well as in some synthetic elastomers, such as polysulphides and chloroprenes. The degree of reinforcement depend upon a combination of the oxide's particle size, with the finest size being the most effective; and the oxide's reactivity with the rubber. Additionally, it imparts heat stabilization by reacting with acidic decomposition products.

Rubber-metal bonding

In the bonding of rubber to brass, zinc oxide reacts with copper oxide on the brass surface, forming a tightly adhering zinc-copper salt.

Tack retention

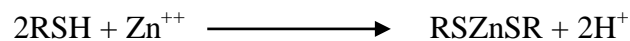
One of the unique properties of zinc oxide is its ability to retain the tack of uncured rubber compounds for adhesive tapes on storage.

A simple mechanism on the action of zinc oxide in conventional sulphur vulcanization is explained below [23]:

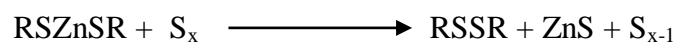
Step 1: Rubber hydrocarbon reacts with sulphur to form a rubber hydrosulphide.



Step 2: When ZnO and fatty acids are present, the thiol groups form zinc mercaptides.



Step 3: The zinc mercaptides thus formed is oxidised by sulphur to give disulphide crosslinks and zinc sulphides.



Role of metal oxides in tetramethylthiuram disulphide vulcanization is explained by Dogadkin and Shershnev [24]. They found that vulcanization in the presence of MBT (mercaptobenzothiazole) or DPG (diphenylguanidine) as accelerators; activators have almost no effect on

the rate of addition of sulphur to rubber, but have a significant influence on the rate and degree of crosslinking of the rubber molecules. Special interest attaches to studies of the action of metal oxides in vulcanization with tetramethylthiuram disulphide (TMTD). In the absence of zinc oxide this accelerator does not bring about vulcanization.

Manik and Banerjee [25] studied about the salient features of both non-elemental sulphur vulcanization by TMTD and elemental sulphur vulcanization promoted by TMTD both in presence and absence of ZnO and stearic acid. They found that the entire course of the reaction can be altered by ZnO or ZnO-stearic acid. Both the crosslink formation and TMTD decomposition are much higher in presence of ZnO or ZnO-stearic acid, but stearic acid seems to have no effect.

Mechanism of the gelling of *hevea* latex by zinc compounds were studied [26]. The effect of zinc distribution on the mechanical stability of NR latex concentrates were studied by Davies and Pendle [27]. They found that the mechanical stability of latex concentrates, particularly for LATZ latices can be increased by using dithiothreitol (DTT). Zinc ions tend to destabilize latex by neutralizing some of the fatty acid anions on the rubber particle surface and DTT increases the stability of latex by removing a large proportion of these zinc ions.

Johnson and Scott [28] made experiments on the preparation of transparent vulcanized rubbers. Tests with other activators zinc carbonate, zinc oleate, and zinc stearate with magnesium carbonate showed that these are less effective than zinc oxide and the vulcanizates obtained had

inferior mechanical properties. Results indicated that in most cases vulcanizates containing 1 per cent of ZnO were transparent, but were not so when cured with Zn salts of organic acids [29]. Though it is necessary to use ZnO as an adjuvant in curing with organic accelerators but when transparent products are required, it is practicable to use only 1 per cent ZnO or lower.

To study the accelerating power of zinc salts of organic accelerators as well as to find the relation between these Zn salts and ZnO, zinc salts of mercaptobenzothiazole and tetramethylthiuram disulphide were synthesized and vulcanization tests were carried out [30]. It has been found that in the absence of ZnO, Zn salts had no accelerating power. Saijo and Kaneko [31] reported that rubber to brass bonding can be improved by increasing the ZnO content up to 40 phr. It is suggested that bonding is promoted by the formation of zinc-copper sulphide from acidic copper sulphide and basic ZnO. Finely divided ZnO is treated with normal zinc propionate which provides easy dispersion in rubber and improved physical properties [32].

Carboxylic elastomers can be cured by standard compounding recipes utilizing sulphur and zinc oxide. The zinc oxide, besides aiding the sulphur cure, also gives a secondary cure through an ionic bond with the carboxyl groups. However, because of the affinity of the zinc oxide for the carboxyl group, the stocks tend to have an excessive scorch and a short shelf-life. To prevent this excessive scorch, the zinc oxide must be isolated from the carboxyl group until the desired cure temperature is reached. Heat and light stability of ethylene propylene terpolymers

containing zinc oxide and titanium dioxide were studied [34]. Oven ageing properties at 350° F and 300° F of EPT polymers were substantially improved with additions of zinc oxide up to 10 and 20 phr.

In situ surface-modified nano-zinc oxide has been prepared by the sol-gel method and its effect on conventional NR vulcanization has been studied recently [35]. Results demonstrated that the dispersal of *in situ* surface-modified nano-ZnO in NR vulcanizate was better than that of ordinary ZnO.

1.6 Reinforcement of elastomers

The concept of reinforcement is important to obtain vulcanizates with desired properties [36]. It is generally accepted that the reinforcement of elastomers is dependent, to a large extent, on polymer properties, filler properties and processing [37]. Generally speaking, the factors influencing elastomer reinforcement are:

- The primary particle size or specific surface area, which together with loading determines the effective contact area between the filler and polymer matrix.
- The surface activity, which is the prominent factor with regard to filler-filler and filler- polymer interaction.

The excellent wear resistance of rubber with carbon black was first noticed in England in about 1912. Until then, the normal filler used in tyre treads was ZnO. Substitution of carbon black for ZnO increased the mileage many-fold. Since the early 1950's, carbon black have been complemented by the group of highly active silica's.

Three possible types of filler-polymer interactions can be visualized as follows [38]:

Type 1

The filler is only physically present in a non-polar polymer with no interaction at all. The filler then merely acts as a diluent and is expected to weaken the material by its presence.

Type 2

The filler is physically present in the polymer and its surface is wetted by the polymer either because of the inherent polymer affinity for the filler or because the filler is appropriately surface treated to provide this affinity. A physical bond is developed causing an increase in the frictional resistance to the movement of the filler and thereby resulting in an increase in the tensile strength and a decrease in the elongation at break.

Type 3

The filler establishes a true chemical bond with the polymer. This results in an exceptional strengthening effect. The type of interaction present in carbon black filled rubber might be of this kind. The nature of interaction present in carbon black filled rubber has been studied and generally agreed that *van der Waals* forces are sufficient to give reinforcing effects [39]. However, evidence of chemical grafting between carbon black and rubber also exists [40].

1.6.1 Filler characteristics and vulcanizate properties

Filler morphology such as particle size, structure and surface characteristics have a large influence on the physical performance of the elastomeric material. Most important are the surface characteristics and the chemically active sites, which determine the interaction between the filler and the polymer chains. This polymer-filler interaction is responsible for rubber reinforcement and better understanding of this interfacial interaction is essential for understanding the mechanism of rubber reinforcement [41].

The important characteristics of filled vulcanizate in comparison with the gum vulcanizate are the increased modulus at 300 per cent elongations and reduced swelling in solvents. Bound rubber is regarded to be the result of rubber-filler interaction and is often taken as a measure of the surface activity of the filler. It is the rubber portion that can no longer be separated from filler when the rubber batch is extracted in rubber solvent over a specific period of time, usually at room temperature [42].

Particle size is directly related to the reciprocal of surface area/gram of the filler. Smaller particles actually reflect their greater extent of interface between polymer and solid material. Thus, fillers with smaller particle size improve the tensile strength and modulus. For carbon black filled elastomers, it has been shown that for significant reinforcement, the mean particle diameter between 0.02 μm and 0.05 μm is most effective [43]. The reduction in properties at higher filler loading is due to dilution effect. This is merely due to a diminishing volume fraction of polymer in the composite. If the volume percentage of filler increases,

there will not be enough rubber matrix to hold the filler particles together. In this situation, strength approaches to zero. Before this stage of loading is reached, the compound attains a level of stiffness where it becomes brittle and would show poor strength.

The specific features (mechanical response) exhibited by reinforced elastomers related to energy dissipation phenomena are Payne effect and Mullins effect. The first one is observed at small deformations and is characterized by a strong decrease in storage modulus G' with corresponding increase in loss modulus G'' . The second one is observed at high extensions and is characterized by a pronounced lowering in the stress when the filled vulcanizate is extended second time. It is also known as “stress softening.” Unfilled rubbers exhibit less stress softening. Mullins and Tobin considered that filled rubber consists of hard and soft regions. When the sample is pre-stretched, a fraction of hard regions become soft. This might be attributed due to the breakage of filler particle aggregates or the breaking of loose rubber-filler bonds [44].

In the general background of the reinforcement of rubbers, the non-linear effect at small strains, generally referred as Payne effect, has been investigated in the case of silica filled styrene butadiene rubber (SBR) [45]. The experimental results demonstrate that the Payne effect occurs even at low silica content, below the percolation threshold.

The role of active fillers like carbon black and silica has been studied in the rubber matrix for a better understanding of the rubber performance and the mechanism of reinforcement [46]. The influence of basic properties of carbon blacks, such as specific surface area, structure

and surface activity on the Payne-effect, were investigated with a rubber process analyzer (RPA). The effect of carbon black loading and type on the properties of ferrite filled natural rubber (NR) composites was investigated [47]. The tensile strength and elongation at break of ferrite filled natural rubber composites were found to decrease with the increase of both types carbon black loading. The microstructure showed that filler dispersion of ferrite filled natural rubber composites become poorer with increasing carbon black loading. Effect of grafted carbon black (GCB) on properties of vulcanized natural rubber was investigated by Xu *et al.* [48]. To modify carbon black (CB) surface, *in situ* grafting of natural rubber (NR) onto the CB surface by solid-state method was used to get grafted carbon black (GCB). As a result, it was found that GCB could improve both cure rate and crosslinking density. Moreover, the mechanical properties of vulcanized NR filled with GCB were enhanced to a large extent compared with vulcanized NR filled with CB.

Azura *et al.* [49] investigated the effects of the filler loading and ageing time on the mechanical and electrical conductivity of natural rubber. The mechanical properties increased with a filler loading up to a certain loading, and a decrease in the mechanical properties was observed with higher filler loadings.

Experiments on mixing silica, carbon black, and CaCO_3 into various elastomers (EPDM, NBR, and SBR) were carried out by White *et al.* [50]. Characterization of carbon black distribution and mechanical properties in NR/SBR blends were studied by Kunizawa and NI [51]. A bias dispersion state of carbon black (CB) in styrene butadiene rubber (SBR)

and natural rubber (NR) was observed by scanning probe microscope (SPM). The results indicated that the SBR/CB interaction in rubber composite was stronger than that of the NR/CB interaction by measuring tensile strength in NR/SBR blended rubber composites. It was found that island patterns of SBR phase were formed in the polymer and more carbon blacks were segregated in SBR phase than in NR phase and the concentration of CB in SBR phase was estimated to be about twice as large as that in NR phase. The SPM photographs of NR/SBR blend composite is shown in Figure 1.7.

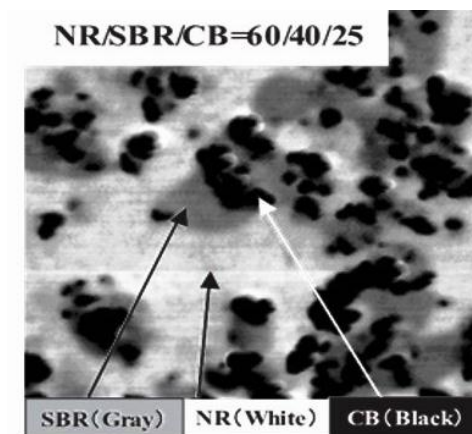


Figure 1.7: SPM photograph of NR/SBR blend composites [51]

Thermal diffusivity (α), thermal conductivity (λ) and specific heat capacity (C) of tyre tread rubber filled with different carbon black were studied [52]. The results showed that α and λ increased with the increase in amount of carbon black, and C of tread rubber decreased. With the increase of amount of carbon black, the difference of λ of three types of tread rubber filled with different carbon black augmented firstly, and diminished afterwards.

The crosslink density and thermal stability of the silica/rubber composites treated by silane coupling agents, *i.e.*, γ -aminopropyl triethoxysilane (APS), γ -chloropropyltrimethoxysilane (CPS), and γ -methacryloxypropyltrimethoxysilane (MPS), were investigated [53]. The composites treated by MPS showed the superior crosslink density and thermal stability. Yan *et al.* [54] investigated the effect of nitrile rubber (NBR) on the properties of silica-filled natural rubber (NR) compounds in the presence of a new silane coupling agent, 3-octanoylthio-1-propyltriethoxysilane (NXT). The properties of silica-filled NR compounds were improved by adding NBR. The dispersion of silica was improved by adding NBR. The scorch time and optimum cure time became shorter with increasing NBR content. The crosslink density of silica-filled NR vulcanizates also increased with increasing NBR content.

The effect of magnesium carbonate (MgCO_3) loading on the compound properties of polychloroprene (CR), natural rubber (NR), and their blends was investigated [55]. The results revealed that, regardless of the rubber type and blend ratio, increasing MgCO_3 loading resulted in not only an increase in the compound viscosity, but also in the enhancements of the cure rate and state of cure.

A novel rubber composite of acrylonitrile–butadiene rubber (NBR) filled with anhydrous copper sulphate (CuSO_4) particles were investigated by Yuan *et al.* [56]. Results indicated that the composite had wonderful mechanical properties, which profited from the *in situ* coordination crosslinking interactions between the nitrile group (-CN) of NBR and solid CuSO_4 particles.

Bound rubber (BdR) is considered as a measure of the filler–polymer interaction in rubber compounds. Sridhar *et al.* [57] studied the variation of the bound rubber (BdR) content with storage time in chlorobutyl compounds filled with fillers like carbon black, carbon-silica dual phase filler (CSDPf), silica, and nanoclays. The effect of $\text{Ni}_{0.25}\text{Co}_{0.25}\text{Zn}_{0.5}\text{Fe}_2\text{O}_4$ ferrite on magnetic and thermal properties of thermoplastic natural rubber composites were studied [58]. The results showed that magnetization (M), saturation magnetization (M_s), remanent magnetization (M_R), initial susceptibility (χ_i) and initial permeability (μ_i) increase with increasing filler content at all compositions. The thermal conductivity of the composites was found to be in the range of 0.26 to $0.52 \text{ W m}^{-1} \text{ K}^{-1}$.

Poompradub [59] used cuttle bone as reinforcing filler for natural rubber. Presence of chitin on the surface of the cuttlebone particles was speculated to result in a good interaction between cuttlebone particles and NR, which may be ascribed to the mechanical properties of cuttlebone filled NR samples. Role of lignin filler in stabilization of natural rubber based composite was studied by Košíková *et al.* [60]. It was shown that incorporation of lignin improved the physico-mechanical properties of the rubber vulcanizates and increased the resistance of NR vulcanizates to thermo-oxidative degradation in air. Sukumar and Menon [61] used organically modified kaolin as reinforcing filler for natural rubber. Effect of chemically modified waste rubber powder as filler in natural rubber vulcanizates were studied by Yehia *et al.* [62]. The chemically modified RP was incorporated in natural rubber mixes either alone or in combination

with carbon black (HAF). It was found that the chemically modified RP improves tensile strength and ageing resistance of NR vulcanizates compared with untreated RP.

The effects of concentration and modification of fibre surface in sisal/oil palm hybrid fibre reinforced rubber composites have been studied by Jacob *et al.* [63]. They claim that increasing the concentration of fibres resulted in reduction of tensile strength and tear strength, but increased modulus of the composites. Formation of a controlled morphology of fillers in polymeric composites may be difficult to achieve by conventional methods such as mechanical shear or chemical methods. A tunable structure of filler and anisotropic properties in composites can be obtained by exploiting dielectrophoretic assembly of fillers in a polymer composite by using electric fields [64]. In their work, different concentrations of titanium dioxide (TiO₂) particles in silicone rubber matrix were assembled in a chain-like structure by using an alternating electric field. It was shown that dielectric permittivity of the oriented composite is higher whereas its dielectric loss is lower in the orientation (thickness) direction than those for composites with random distribution of filler.

Table 1.2: Percentage change in dielectric permittivity as a result of titania addition in oriented samples at 1000 Hz frequency [64]

Titania Vol.%	2	5	8	11
Percentage increase in dielectric permittivity (%)	9.7	10.7	10.9	15.1
Percentage decrease in dielectric loss (%)	-12.3	-15.5	-20.4	-33.3

Silicone rubber filled with thermally conductive, but electrically insulating Al₂O₃ or ZnO fillers were investigated to be used as elastomeric thermal pads, a class of thermal interface materials by Sim *et al.* [65].

The effect of Al₂O₃ or ZnO fillers on the thermal conductivity and coefficient of thermal expansion (CTE) of the silicone rubber were investigated, and it was found that with increasing Al₂O₃ or ZnO fillers, the thermal conductivity of the thermal pads increases, while the coefficient of thermal expansion (CTE) decreases. The effects of alumina (Al₂O₃) and zinc oxide (ZnO) fillers on the curing characteristics, thermal and mechanical properties of silicone rubber were studied [66]. Comparison of mechanical strength between the two silicone rubber hybrids indicates that ZnO is a better reinforcing filler, as evidenced in the tensile strength, elongation at break, and modulus at 300 per cent elongation. The thermal conductivities of silicone rubber filled with ZnO in a wide volume range were studied [67].

1.7 Nanotechnology in rubber [68]

Nano particles and rubber nanocomposites are getting more attention now-a-days due to their novel functionalities. They show enhanced material properties which cannot be seen in conventional composites. However, commercial applications of rubber nanocomposites are yet to gain real momentum. The homogeneous dispersion of nanoparticles such as carbon nanotubes, layered silicates *etc.* in the rubber matrix is a real challenge because the degree of dispersion decides the ultimate performance of the material. This issue has to be seriously looked into. Generally spoken, reduction of particle sizes to nano dimensions will make the added materials more reactive.

Advantages of rubber nanocomposites over conventional rubber composites are –

- 1) Lighter weight due to low loading of nanoparticles.
- 2) Improved material properties (*i.e.* mechanical, thermal, electrical) and new functionalities (antimicrobial, barrier, flame retardant *etc.*).
- 3) Easy processing in comparison to conventional composites.

1.8 Preparation of nanomaterials

Depending on the number of dimensions which are reduced to nanometre size range, nanomaterials can be defined as zero-dimensional (quantum dots), one-dimensional (nanowires, nanorods, and nanotubules) and two-dimensional (quantum well, nanosheet, graphene). In zero-dimensional nanomaterials, all the three dimensions are reduced to nanometre range. In one-dimensional nanomaterials, two dimensions are in the nanometre range and one can remain large. In two-dimensional nanomaterials, one dimension is reduced to nanometre range and the other two dimensions remain large [69].

Size, shape and composition controlled synthesis of different class of nanomaterials is an interesting subject among researchers and continuous efforts are still pursued to scale up the preparation of various kinds of nanomaterials for various applications. A large number of methods such as physical, chemical, biological and hybrid techniques are available to synthesize different types of nanomaterials in the form of colloids, powders, rods, wires, tubes, thin films *etc.*. Generally, nanomaterials can be synthesized *via* two approaches; top-down and bottom-up. Using appropriate methods, a wide range of nanomaterials with different morphology and combination can be synthesized.

Various techniques employed for the synthesis of nanomaterials are shown in Figure 1.8.

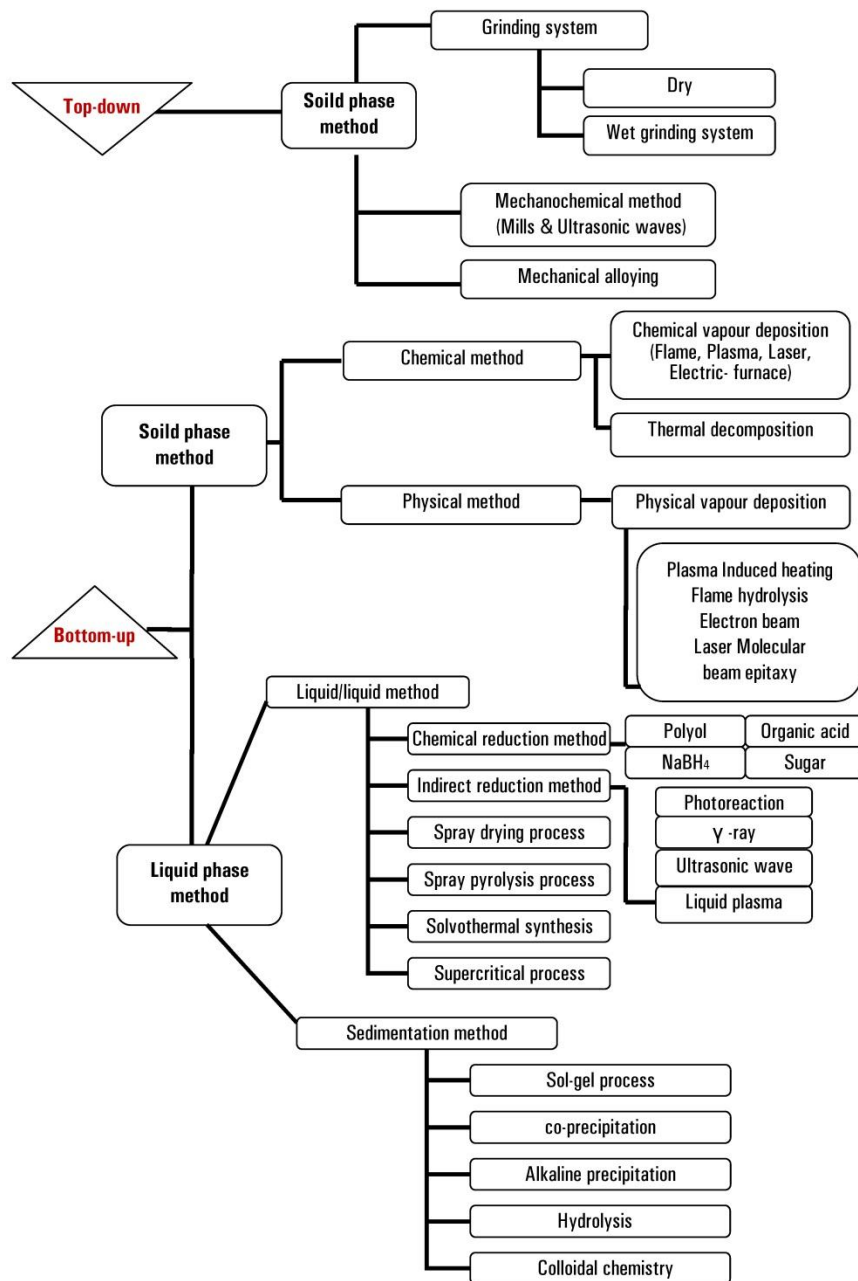


Figure 1.8: Nanomaterials - synthesis techniques

1.8.1 Top-down approach

Top-down approach refers to crushing or grinding of a bulk material to get nano sized particle. Attrition or milling is an important technical operation used for the size reduction of materials. It is commonly used in microelectronics industry and also well accepted in processing of materials for the manufacture of cements, pigments and paints, ceramics, pharmaceuticals and dispersions.

Among all top down approaches, high energy ball milling, has been widely exploited for the synthesis of various nanomaterials, nanograins, nanoalloys, nanocomposites and nano-quasi- crystalline materials. Some inherent advantages of high energy ball milling in processing nanomaterials are: excellent versatility, scalability, and cost-effectiveness. In high-energy ball milling, plastic deformation, cold-welding and fracture are predominant factors that lead to the deformation and change in shape of the particles. Cold-welding leads to an increase in particle size and fracture leads to a decrease in particle size [70]. The physico-chemical and mechanical aspects involved in the process of grinding are reviewed by various authors [71, 72].

The main objectives of the milling process are to reduce the particle size, mixing, blending and particle shaping. In order for a material to be ground in a mill, the particles of that material have to be trapped and crushed between two balls or between a ball and the mill wall. If the particles to be digested are brittle, they will be ground into a very fine powder when trapped between two colliding surfaces. On the

other hand, non-brittle particles change their shape when trapped between two colliding surfaces [73].

The grinding (dry/wet) action comprises a combination of friction, attrition and impact. The main stress types involved in high energy ball milling process are compression, shear (attrition), impact (stroke), impact (collision) and are represented in Figure 1.9.

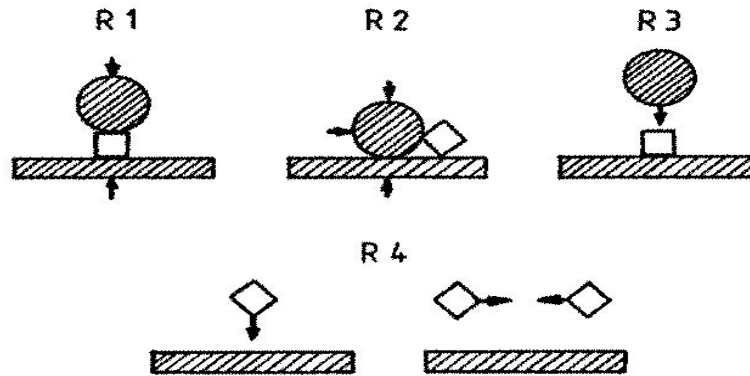


Figure 1.9: Main stress types in mills, R1- compression, R2- shear (attrition), R3- impact (stroke), R4- impact (collision), *circle-* mass of milling media, *square-* mass of material charge, *rectangle-* mass of mill wall [74]

For satisfactory grinding, the presence of air space inside the grinding vessel is essential (~ 40-50% of the total volume). During ball milling, motion of the balls along with the charge undergoes cascading effect resulting in particle size reduction. The motion of the balls against each other, and also against the walls of the container brings about the reduction of the particle size of the solid material. Depending upon the speed of the mill and the character of the material, the balls which rise to the top may undergo cascading, cataracting and sliding. At the end of the cascading process, the balls strike the bottom of the container with

impact, and are again folded into the revolving mass. A temperature rise in the range of 100-1100°C is expected to take place during collisions. Lower temperature favours amorphous particle formation. Cryo-grinding technique is often used for the preparation of certain nanostructured materials.

Factors affecting the efficiency of ball milling are:

- Speed of rotation of the jar
- Size and size distribution of the balls
- Material of the balls
- Viscosity of the slurry (in the case of dispersions)
- Ball to powder ratio (BPR) or charge ratio.
- Period of ball milling
- Milling atmosphere

The effect of increasing speed of rotation of the container first increases the rate of grinding until a certain speed is reached. Further increase of speed will cease the grinding efficiency. The critical rotational frequency is $29.92/\sqrt{R}$ minute⁻¹, where R is the radius of the container in meters [75].

Mechanochemical processing and thermo-mechanical processing are included in top-down approach for nanoparticle synthesis. The technology uses high energy dry milling to mechanically induce chemical reactions to occur at low temperature [76]. The main problem involved in top-down approach includes imperfection of surface structure. In addition to surface defects, it can also induce internal stress and material contamination.

1.8.2 Bottom-up approach

Bottom-up approach refers to materials synthesis: atom-by-atom, molecule-by-molecule or cluster-by-cluster and has been in industrial use for over a century. It utilizes the concept of molecular self-assembly. This technique enables the production of nanostructures with less defects and better chemical composition. According to the phases involved, bottom-up approach is roughly classified into vapour phase synthesis and liquid phase synthesis.

1.8.2.1 Vapour phase synthesis

Nanostructured materials in the form of thin films can be prepared by evaporating the materials on some substrates. The material of interest is brought in gaseous state which can form clusters and are then deposited on appropriate substrates. Most of gas phase synthetic routes are based on homogeneous nucleation in the gas phase and subsequent condensation.

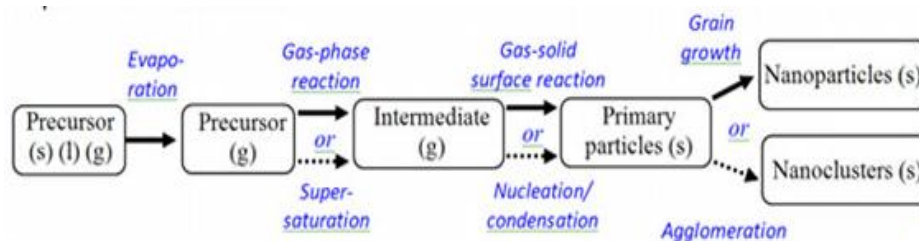


Figure 1.10: Flow chart showing vapour phase synthesis of nanomaterials [77]

In laser ablation technique, vapourization of the material is effected using pulses of laser beam of high power. Single Walled Carbon Nanotubes (SWNT's) are mostly synthesized by this method. Sputtering is a method of vaporizing materials from a solid surface by bombardment with high-velocity ions of an inert gas like Ar, causing an ejection of

atoms and clusters. It is a very good technique to deposit multi-layer thin films and non-porous compact films.

Flame synthesis is the most commercially successful approach to nanoparticle synthesis-producing millions of metric tons per year of carbon black and metal oxides. In chemical vapour deposition (CVD) method substrate is exposed to one or more volatile precursors. Molecular beam epitaxy (MBE) is considered as a special case of evaporation for single crystal film growth in ultra-high vacuum. In MBE, evaporated atoms or molecules from one or more sources do not interact with each other in the vapour phase under low pressure. This ensures the absence of contamination, and thus gives highly pure film with precise control of chemical composition of deposit. This allows deposition of quantum dots and quantum wires in a very controlled fashion. Low rate of deposition and high substrate temperature allows sufficient mobility of the elements on the substrate and allows layer by layer growth to obtain nanostructures.

1.8.2.2 Liquid phase synthesis

The liquid phase fabrication entails a wet chemistry route.

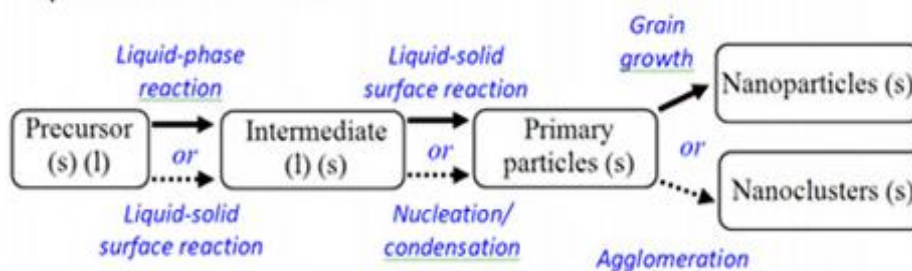


Figure 1.11: Flow chart showing liquid phase synthesis of nanomaterials [77]

The sol-gel technique is a long-established process used for the preparation of colloidal nanoparticles from liquid phase. Sol-gel-processes are well adapted for the synthesis of oxide nanoparticles and ceramic nanoparticles. Typical precursors are metal alkoxides and metal chlorides, which undergo hydrolysis and poly-condensation reactions to form a colloid, a system composed of nanoparticles dispersed in a solvent. This process involves transition of a system from a liquid “sol” into a solid “gel” phase.

A variety of materials with different morphologies *such as* wire (1D), rod (2D), sphere (3D) can be prepared by solvothermal process. The process is carried out in a sealed vessel and involves the use of a solvent under moderate to high pressure (typically between 1 atm. and 10,000 atm.) and temperature (typically between 100°C and 1000°C) that facilitates the interaction of precursors during synthesis. If water is used as solvent, it is termed hydrothermal processing.

Microwave heating is often used for the preparation of different nanostructured materials. The general advantages of microwave mediated synthesis over conventional ones are (1) simple and fast optimization of experimental parameters, (2) reaction rate acceleration, (3) wide range of reaction conditions, (4) high reaction yields and (5) excellent control over reaction conditions [78].

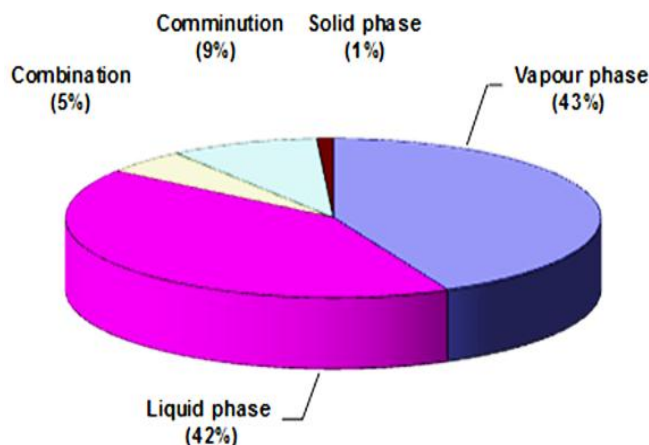


Figure 1.12: Statistics showing nanomaterials preparation methods [76]

Nanomaterials preparation methods can be divided into five categories, namely, comminution (mechanical milling), solid, liquid and vapour phase techniques and a combination of those (Figure 1.12). All the methods are potentially important. However, several factors such as consistency in product quality and cost related with raw materials, operation, yield, capital equipment, safety, waste disposal and other environmental issues should also be considered for the commercialization of nano products.

1.8.3 Synthesis of nano ZnO

Preparation of ZnO nanoparticles has been of significant research attention over the past few years. ZnO has probably the richest variety of nanostructures. Its range includes nano wires, nanorods, nanobelts, nanosprings, nanocombs nanorings, tower like structures *etc.* attracts much interest [79]. ZnO nanostructures are now widely used in solar cell [80], gas sensors [81, 82] chemical absorbent [83], drug delivery [84], varistors [85, 86], displays [87], electrical and optical devices [88],

electrostatic dissipative coating [89], catalysts for photo-degradation [90, 91] *etc.*

Chemical solution method was found to be one of the favourite method to prepare 1D nanostructured materials in terms of its low cost, versatility and potential large scale production [92]. Qian *et al.* [92] synthesized single crystalline ZnO nanorods with diameter of 5 nm by a simple chemical solution route method using zinc acetate dihydrate and NaOH as precursors. By adjusting the NaOH concentration or reaction time, ZnO nanorods with various aspect ratios can be prepared. Room temperature precipitation method for the synthesis of ZnO nanoparticles with average particle size of 60.1 nm using ZnCl₂ and NH₄OH in presence of surfactant cetyltrimethylammonium bromide were reported [93]. Flower like 3D ZnO nanomaterials have been synthesized by hydrothermal method using KNO₃ as inorganic mineralizer [94]. Mammori *et al.* [95] used a combination of sol-gel and combustion method (gel combustion method) to prepare ZnO nano powder using citric acid as the fuel for the first time. Muhammed *et al.* [96] used chemical precipitation method for the synthesis of ZnO nanoparticles using ammonium carbamate as precipitating agent. They also suggested that moderate ammonia concentration was beneficial for limiting the particle growth. In aqueous or solution based synthesis, the tendency for the formation of bonds of Zn-O-Zn among nanoparticles is high due to the existence of water molecules resulting agglomeration which impede the potential application of nanoparticles.

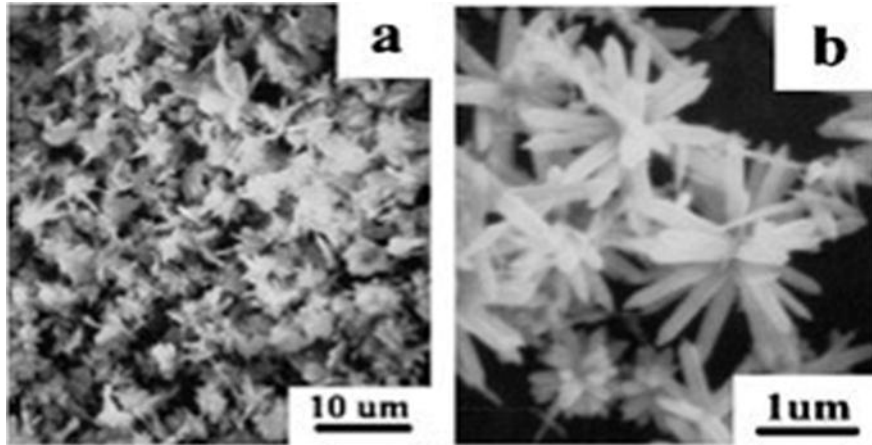


Figure 1.13: SEM images (a and b) of synthesized ZnO 3D nanostructures [94]

Studies on surface coating of nanoparticles are also well documented. Hong *et al.* [97] prepared ZnO nanoparticles by direct precipitation from zinc acetate and ammonium carbonate followed by calcinating the precursor at 450°C for 3h. Silica coating on the surface of ZnO nanoparticles improves the dispersibility and hence reduces the agglomeration of nanoparticles. Ashtaputre *et al.* [98] used a chemical route for the synthesis of ZnO nanoparticles using thioglycerol as capping agent. Li *et al.* [99] synthesized flower like ZnO microstructures with different sizes and shapes *via* a simple aqueous solution route using ZnCl_2 and NaOH as reagents and triethanolamine as modifying agent. Aqueous solution of monodispersed ZnO nanorods with a diameter of 10 nm and a length of 50 nm were synthesized in presence of PVP [100]. The size of ZnO could be controlled by altering Zn^{2+} /PVP weight ratio. Spherical ZnO nanoparticles synthesized by non-aqueous routes (using organic solvents) are also reported [101, 102].

Surface modification of nanoparticle by grafting polymers onto it is an effective way to improve its dispersibility in polymer matrix and enhances the properties of resulting composites. ZnO/polystyrene composite particles were synthesized by pickering emulsion polymerization and their pH adjusting ability were well studied [103]. The grafting of polymers on to surface of ZnO nanoparticles and radical copolymerization of methylmethacrylate (MMA) and methacrylic acid (MAA) were investigated [104].

Wan *et al.* [105] prepared tetrapod-like ZnO nanostructures by rapid heating metal zinc pellet at 900°C under air ambient. Another evaporating synthesis method to synthesize ZnO particles is metal-organic chemical vapor deposition (MOCVD) [106]. Zhang *et al.* [107] have reported that ZnO tubes were epitaxially grown on sapphire (0001) substrate by MOCVD. The growth pressure and temperature were 0.3-3 torr and 475°C respectively. Oxygen and diethyl zinc were used as precursors and nitrogen gas was used as the carrier gas. A simple efficient thermal evaporation technique, oxidizing zinc foils in a tube furnace at 700°C in air without the presence of catalyst and carrier gas was developed [108]. By controlling the heating rate, different morphologies have been achieved: porous membranes, nanowires (or nanorods), nanobelts, nanoneedles, and nanotetrapods have been achieved. In pulsed laser deposition method laser power has been utilized as growth parameter to control the diameter of nanorods by controlling the dimension of 3D nucleation [109]. Well aligned ZnO nanowires have been grown on certain substrates by thermal reduction

method [110, 111]. Ordered semiconductor ZnO nanowire arrays embedded in anodic alumina membranes (AAM) were fabricated by generating alumina templates with nanochannels, electrodepositing Zn in them, and then oxidizing the Zn nanowire arrays [112]. The polycrystalline ZnO nanowires with the diameters ranging from 15 to 90 nm were uniformly assembled into the hexagonally ordered nanochannels of the AAM.

Microwave assisted synthesis of ZnO micro and nano particles are reported [113]. Microwave irradiation of solutions of $\text{Zn}(\text{NO}_3)_2$ and urea provides a straightforward route to a-axis oriented needle shaped crystals of ZnO [114]. Unalan *et al.* [115] demonstrated a rapid method to synthesize large area, vertically aligned ZnO nanowires on various substrates using microwave heating. ZnO nanostructures have been successfully prepared by a microwave irradiation method. The role of albumen as a template in addressing the size and morphology of ZnO has been investigated. Pure ZnO nanostructures, consisting of rod- and whisker-like nanoparticles embedded in a sheet matrix, were obtained in the presence of albumen whereas a heterogeneous mixture of $\text{Zn}(\text{OH})_2$ and ZnO was obtained in absence of albumen [116]. Compared to conventional methods, microwave synthesis has the advantage of producing ultra-fine metal oxides with high purity owing to short reaction time [117].

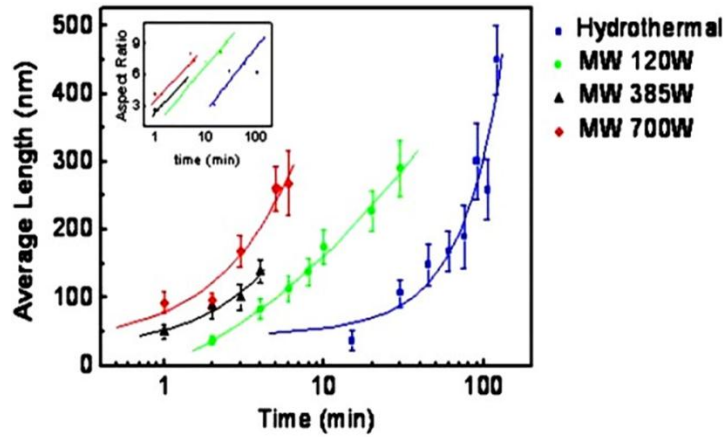


Figure 1.14: Axial growth rates of samples at different microwave powers as compared to hydrothermal growth with standard deviation [115]

Solid state mechanochemical processing which is not only a physical size reduction process in conventional milling; but also a chemical reaction that is mechanically activated at the nanoscale [118-120]. In contrast to most other synthesis methods involving high temperatures and complex reaction conditions, this method is a simple and efficient method for preparing ZnO nanoparticles with high yield at low cost. Since such reaction does not involve organic solvents, they are attractive from an environmental point of view.

The major parameters determining the characteristics of final oxidic products are reaction time, temperature, concentration of reagents and concentration of surfactants. By judicious adjustment of these conditions, formation of metal oxide nanoparticles with outstanding monodispersity and astonishing particle morphologies is possible [121].

1.9 Polymer nanocomposites

The technology of polymer nanocomposites is a versatile branch of materials science with several new prospects. It seems probable that this family of composites is becoming a structural material of high importance in the 21st century. The small size, high surface area, and possibly a high aspect ratio of nanoscale reinforcements potentially allow polymeric composites to exceed classical limitations and display synergistic properties. Reduction of the reinforcing phase size to nanoscale dimensions conceptually produces a hybrid macromolecule of the organic and inorganic components [122].

Polymer nanocomposites can be broadly classified as-

- Nanoclay- reinforced composites
- Carbon nanotube- reinforced composites
- Nanofibre- reinforced composites and
- Inorganic particle- reinforced composites

The preferred attributes of clays for polymer reinforcement include high purity and uniformity, large aspect ratio, good dispersibility and thermal stability [122]. Hectorite, saponite, and montmorillonite are the most commonly used smectite type layered silicates for the preparation of nanocomposites. In polymer-layered silicate (PLS) nanocomposites, stacking of the layers leads to a regular *van der Waals* gap between the layers called the interlayer or gallery. Isomeric substitution (for example tetrahedral Si^{4+} by Al^{3+} or octahedral Al^{3+} by Mg^{2+} or Fe^{2+}) within the layers generates negative charges that are counterbalanced by alkali and

alkaline earth cations (typically Na^+ or Ca^{2+}) situated inside the galleries [123]. This type of layered silicate is characterized by a moderate surface charge known as the cation exchange capacity (CEC). The traditional routes to prepare nanocomposites using layered compounds as reinforcement, especially clays, can be as follows [124, 125].

1.9.1 Melt intercalation

This is the most popular procedure to prepare nanocomposites for industrial applications. In this approach, the polymer is first melted at high temperature and the filler is then blended with the polymer melt at high temperature under shear. This technique has an advantage that no solvent is required for the nanocomposite synthesis. The polymer can intercalate between the interlayers.

1.9.2 Intercalation of polymer or pre-polymer from solution

In this mode of nanocomposite synthesis, the organically modified silicate is dispersed in a solvent in which the polymer is also soluble. It is well known that such layered silicates, owing to the weak forces that stack the layers together can be easily dispersed in an adequate solvent. The polymer then adsorbs on to the delaminated sheets and when the solvent is evaporated (or the mixture precipitated), the sheets re-assemble, sandwiching the polymer to form, in the best case, an ordered multi-layer structure. The polymer chains lose entropy owing to diffusion inside the silicate interlayers, however, such a process is still thermodynamically viable, owing to the gain in the entropy by the solvent molecules due to desorption from the silicate interlayers [126].

1.9.3 *In-situ* intercalative polymerization

The *in-situ* intercalation mode of polymerization was the method reported by Toyota researchers. In this mode of polymerization, the layered silicate mineral is swollen in monomer. The monomer being of low molecular weight can also diffuse easily into the interlayers thereby swelling the interlayers. On initiation of the reaction, the monomer present in and out of the interlayers polymerizes to generate nanocomposites in which the layered silicate platelets are delaminated to the nanometre level. However, a control of the polymerization in and out of the layers is required in order to achieve high extents of filler exfoliation.

1.9.4 Exfoliation/adsorption

First the layered host is exfoliated in a solvent, in which the polymer is soluble (water, toluene, *etc.*). The polymer is adsorbed onto the single-layer surfaces and after evaporation of the solvent or a precipitation procedure, the single layers are re-stacked, trapping the polymer as hydrated/ solvated. There is a general agreement in the literature that exfoliated systems lead to better mechanical properties, particularly higher modulus, than intercalated nanocomposites [127].

It should be noted that, intercalation is based on ionic interactions and exothermic heats of mixing, whereas exfoliation is prompted by a mutual interaction of the hydrophobic groups of the surfactant with the hydrophobic polymer chains. This is essentially parallel to the compatibilization process in a polymer blend [128].

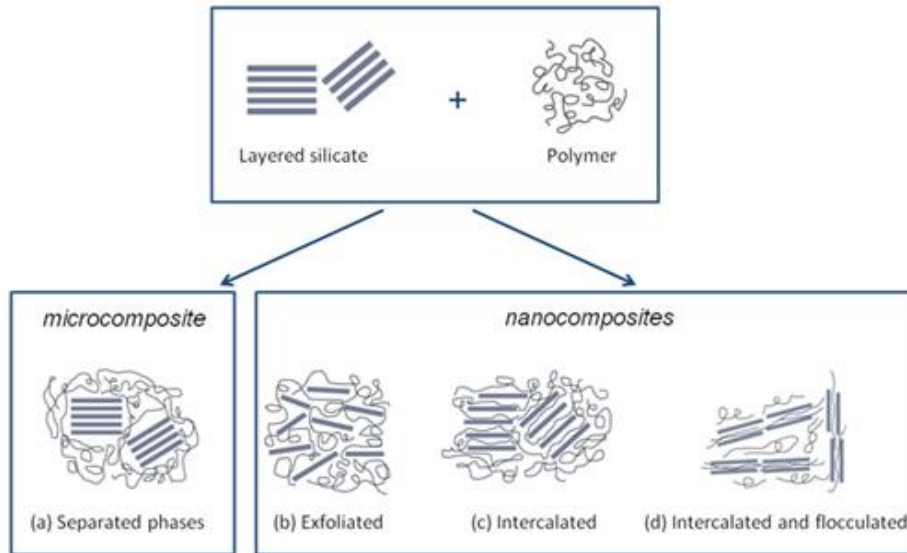


Figure 1.15: Structure of polymer-clay nanocomposites [129]

Carbon nano tubes (CNT's) were first noticed and fully characterized in 1991 by Sumio Iijima [130]. Carbon nanotubes are produced by two possible ways: a catalytic chemical vapour decomposition process at medium temperatures (600-1000°C) and an electric discharge (arc) process under helium at high temperature (3000 to 4000°C). Both processes produce a mix between SWCNT, DWCNT and MWCNT, with surface defects (*e.g.* some pentagonal cycles in place of aromatic rings). The first nanotubes observed were multi-walled nanotubes (MWNT). MWNTs consist of two or more concentric cylindrical shells of graphene sheets coaxially arranged around a central hollow core with interlayer separation, as in graphite (0.34 nm) [131]. Yu *et al.* [132] showed that if only the nanotubes on the outer edge of a SWNT in a bundle are used to calculate the modulus, it is close to the predicted 1 TPa. However, if the whole area of the bundle is used, the calculated

modulus is considerably lower. This suggests that, unless the SWNTs are isolated from the bundles, the modulus of the composites made from these materials will be limited. Other major benefits of incorporating CNT's in polymer are it can impart exceptional mechanical strength and increase the electrical and thermal properties of the composites. Thermal conductivities of SWCNT are as high as $6000 \text{ W m}^{-1}\text{K}^{-1}$ and that of individual MWCNT are $3000 \text{ W m}^{-1}\text{K}^{-1}$ at room temperature. Surface modification of CNT's is well documented [133]. Metal oxide coated CNT's and inorganic nanowires were prepared by Gomathi *et al.* [134]. The ceramic oxide coating provides improved compatibility with polar matrices as well as improved thermal stability of the nanotubes and nanowires. Various methods used for the preparation of polymer-CNT composites are shown in Figure 1.16.

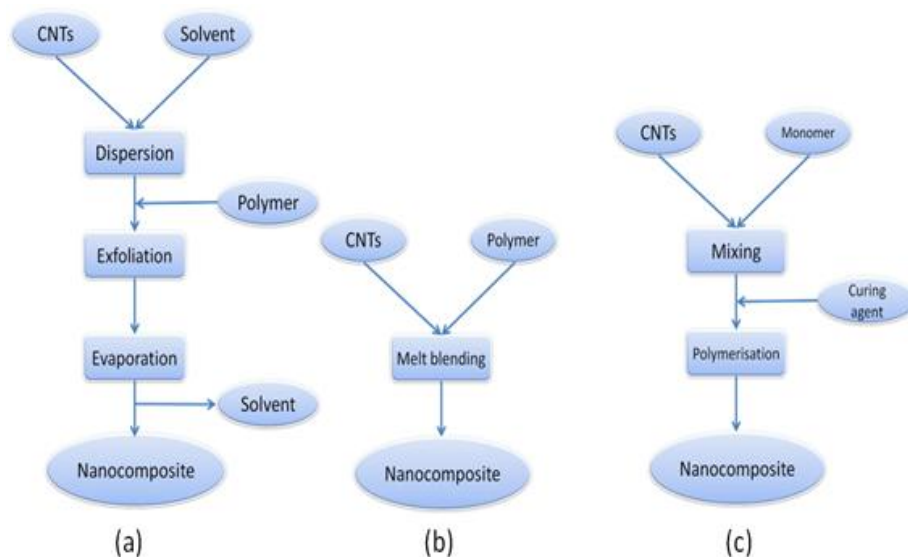


Figure 1.16: Schematic representation of various steps of polymer CNT composite processing (a) Solution mixing (b) Melt mixing and (c) In-situ polymerization [135]

Carbon nanofibres (CNF's) are expected to be promising nano-filler in polymers for the preparation of composites because of their mechanical and physical properties (Young's Modulus ~ 500 GPa, tensile strength ~ 3 GPa, electrical conductivity $\sim 10^3$ S/cm, thermal conductivity ~ 1900 $\text{Wm}^{-1}\text{K}^{-1}$) [136]. They are unique form of vapour grown carbon fibres that fill the gap in physical properties between conventional carbon fibres (5-10 μm) and carbon nanotubes (1-10 nm). The reduced diameter of nanofibre provides a larger surface area with surface functionalities in the fibre [137]. Typically CNF are not concentric cylinders; the length of the fibre can be varied from about 100 μm to several cm, and the diameter is of the order of 100-200 nm with an average aspect ratio greater than 100.

Nanometer-sized particles have been made from different organic-inorganic precursors and these impart improved properties to composite materials [138]. Polymer/inorganic particle-based nanocomposites (PINC's) have shown significant improvement in mechanical, thermal and electrical properties. Optical and magnetic applications of polymer-inorganic nanocomposites were reviewed [139].

Different particles have been used to prepare polymer/inorganic particle nanocomposites, including:

Metals (Al, Fe, Au, Ag, *etc.*)

Metal oxides (ZnO, Al_2O_3 , CaCO_3 , TiO_2 , *etc.*)

Non-metal oxide (SiO_2) [140]

Other (SiC)

The selection of nanoparticles depends on the desired thermal, mechanical, and electrical properties of the nanocomposites. For example, Al nanoparticles are often selected due to their high conductivity; calcium carbonate particles are chosen because of the relative low cost of the material, and silicon carbide (SiC) nanoparticles are used because of their high hardness, corrosion resistance, and strength [141].

1.10 Rubber nanocomposites

The concept of filler reinforcement at the nano level is highly relevant in rubber compounds with better performance applications [142, 143]. Rubber nanocomposites have great importance now-a-days because of high reinforcement property associated with small filler concentration [144]. The thrust importance of this route is to improve the material properties at lower filler content (0.5 to 5 wt. %) which are superior and cannot be achieved with conventional micro fillers. The advantages of incorporating nanoparticles include efficient reinforcement with minimal loss of ductility and impact strength, heat stability, flame retardance, improved abrasion resistance, better gas permeability, reduced shrinkage and residual stress and altered electronic and optical properties [145].

The reinforcement of rubber requires rigid entities, such as carbon black, clays, silicates, calcium carbonate, zinc oxide, magnesium hydroxide and metal oxides, and this important phenomena has been discussed at length by various authors [146, 147]. The small size of fillers provides exceptionally large interfacial area in the composites. The interface controls the degree of interaction between filler and the polymer and thus controls the properties [148].

The ultimate property of nanocomposite strongly depends on uniform dispersion/ distribution of nanoparticles in the polymer matrix. NR vulcanizates containing various fillers were prepared and their mechanical properties were compared and related to degree of filler dispersion [149].

Rubber layered-silicate nanocomposites are the foremost members of high performance nanocomposites. Improvements in mechanical, thermal and barrier properties and flame retardancy *etc.* are claimed for this class of polymer nanocomposites which could not be achieved by conventional fillers at low loading (below 10 phr) [150, 151]. Layered silicates can be easily dispersed in water. Hence the production of silicate NR latex nanocomposites is easy. Conditions for dispersing clay nano-layers into both IR (synthetic *cis* 1, 4 polyisoprene) and ENR (epoxidized natural rubber) have been reported [152].

Elastomer nanocomposites are currently prepared in the following ways:

- Solution blending
- Latex compounding
- Melt intercalation
- *In-situ* polymerization

Elastomer nanocomposites with different nanofillers, their preparation, explaining the properties with existing theories and models have been reviewed [153].

The inclusion of highly anisotropic clay nanoparticles (nanoclays) on natural rubber (NR) micro structure is studied by González *et al.* [154]. It was found that the presence of nanoclay introduces a dual crystallization

mechanism due to the alignment of nanoparticles during stretching. The improved properties in NR-nanoclay nanocomposites can be attributed to both microstructural morphological changes induced by nanoclay as well as to the nanoclay mobility in the NR matrix during crystallization.

Varghese *et al.* [155] tried conventional latex compounding technique for the preparation of NR latex nanocomposites. Teh *et al.* [156] (2003) reported that mechanical properties were improved upto 2 phr loading of organoclay (grade 1.28E) in natural rubber and thereafter it decreased. Natural rubber/sodium montmorillonite nanocomposites were prepared by using natural rubber latex without acid coagulation [157]. Cure characterization indicated that Na-MMT retarded the vulcanization reaction of NR. The mechanical properties of the NR/Na-MMT nanocomposites were improved with addition of Na-MMT which is attributed to the reinforcing effect of Na-MMT with rubber. The viscoelastic and dielectric properties of nano structured layered silicates reinforced natural rubber (NR), carboxylated styrene butadiene rubber (XSBR) and their blends have been analyzed by Stephen *et al.* [158]. Upon the addition of filler, the storage modulus of nanocomposites was found to increase due to the enhancement in stiffness of the material. Due to the restricted mobility of polymer chain segments, the damping values decreased as a function of filler loading.

Gatos [159] investigated the role of the aspect ratio of the layered silicate platelets on the mechanical and oxygen permeation properties of hydrogenated nitrile rubber (HNBR)/organophilic layered silicate nanocomposites. Montmorillonite (MMT) and fluorohectorite (FHT)

bearing the same type of intercalant (*i.e.*, octadecylamine; ODA), however, showing different aspect ratio was explored in their study. Authors claims that, increasing aspect ratio (MMT < FHT) resulted in higher stiffness under uniaxial tensile loading. Recently, Swapna *et al.* [160] prepared nanocomposites based on natural rubber latex as the matrix and naturally occurring tubular shaped nanoclay, halloysite nanotubes (HNTs) as the reinforcing phase through co-coagulation method. Solvent transport properties of nanocomposites were found to decrease at lower concentration of HNT because of the tortuosity of the path.

Table 1.3: Percentage of reduction of $\tan \delta_{\max}$ of nanocomposites [158]

Sample	% reduction of $\tan \delta_{\max}$		Sample	% reduction of $\tan \delta_{\max}$	
	NR phase	XSBR phase		NR phase	XSBR phase
N _{100sP} E _{2.5}	44.8	-	N _{0sP} F _{2.5}	-	40.3
N _{100sP} E ₅	55.9	-	N _{0sP} F ₅	-	55.6
N _{100sP} E _{7.5}	69.4	-	N _{0sP} F _{7.5}	-	59.0
N _{100sP} F _{2.5}	28.0	-	N _{70sP} E _{2.5}	43.6	18.7
N _{100sP} F ₅	30.6	-	N _{70sP} E ₅	51.4	34.5
N _{100sP} F _{7.5}	46.5	-	N _{70sP} E _{7.5}	53.5	37.1
N _{0sP} E _{2.5}	-	35.5	N _{70sP} F _{2.5}	43.7	12.7
N _{0sP} E ₅	-	38.7	N _{70sP} F ₅	55.7	25.9
N _{0sP} E _{7.5}	-	55.8	N _{70sP} F _{7.5}	47.3	24.5

[In the sample code N stands for NR, the subscript numbers 100, 70 and 0 denotes the weight percentage of NR, sP represents sulphur prevulcanization, E and F represent sodium bentonite and sodium fluorohectorite and the subscript numbers 2.5, 5 and 7.5 indicate filler concentration in phr.]

The influence of inorganic nanoparticles on crosslinking mechanism of elastomers has been evaluated [161]. The results have shown that a highly ordered structure with a huge amount of entanglements, wherein the polymer is nanoscopically confined, is formed by the addition of nanoparticles. Peng *et al.* [162] studied NR/nano SiO₂ composite by latex compounding technique. Meera *et al.* [163] showed more pronounced Payne effect at higher silica loading in NR silica nanocomposites. A novel natural rubber/silica (NR/SiO₂) nanocomposite with a SiO₂ loading of 4 wt. per cent was developed by latex compounding with self-assembly techniques [164]. The SiO₂ nanoparticles were homogeneously distributed throughout the NR matrix as spherical nano-clusters with an average size of 75 nm. A small amount of synthetic precipitated amorphous white silica nanofiller, pre-treated with *bis* (3-triethoxysilylpropyl) tetrasulphide (TESPT), was used to crosslink and reinforce natural rubber (NR) by Ansarifar *et al.* [165]. The silica particles were fully dispersed in the rubber, which was cured primarily by using sulphur in TESPT. The effect of precipitated silica nanofiller on the curing and mechanical properties of natural rubber and synthetic polyisoprene was investigated [166]. Kohjia *et al.* [167, 168] recently reported an interesting investigation on the applicability of 3D-TEM, a technique that combines transmission electron microscopy with computerized tomography; to visualize and analyze the three dimensional state of NR containing silica or carbon black dispersion in nanocomposites.

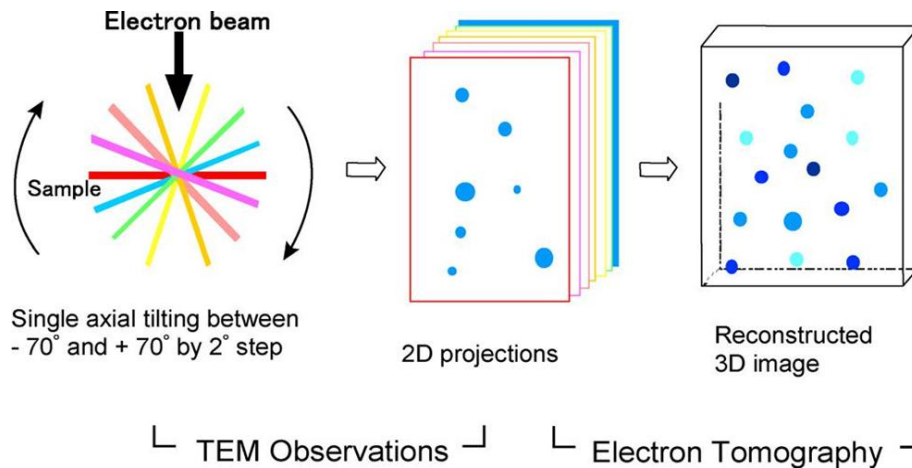


Figure 1.17: Procedure for 3D-TEM measurements [167]

The erosion resistance of silicone rubber (SIR) filled with 12 nm size fumed silica (nanofiller) to those filled with 5 μ m size silica filler (micro filler) were studied [169]. The erosion resistance of the SIR materials increased with increasing percentage of the fillers, and it was observed that 10 per cent by weight of nano filled SIR gives a performance that is similar to that obtained with 50 per cent by weight of micro filled SIR. Kemalolu and Aytac [170] studied the effects of loading level of micro or nano sized BN particles on the thermal, mechanical, and morphological properties of silicone rubber. The addition of BN particles in silicone matrix decreases the tensile strength, strain at break and coefficient of thermal expansion (CTE) values, on the other hand increases modulus, hardness and thermal conductivity.

Latex compounding has been successfully applied for dispersing nano calcium carbonate in NR latex [171]. Nano-calcium carbonate composites have been incorporated in NR *via* melt intercalation

technique [172]. Natural rubber (NR) based ternary nanocomposites containing both calcium carbonate and organoclay have been characterized on the basis of morphology, cure characteristics, and physico-mechanical behavior [173]. The cure and mechanical properties of natural rubber vulcanizates with nano CaCO_3 as filler and linseed oil as an extender were studied [174]. CaCO_3 /NR latex nanocomposite and its properties were studied by Deng *et al.* [175]. The results showed that the structure and properties of composites could be clearly improved by NRL mixed with surface-treated nanometre CaCO_3 .

Reports on melt mixing mode incorporation of oxides like nano titanium dioxide [176], nano zinc oxide [177] are available. Natural rubber/rutile- TiO_2 nanocomposites (NR/n- TiO_2 (R) composites) with different n- TiO_2 (R) contents were prepared by Seentrakoon *et al.* [178]. They reported that NR incorporated with n- TiO_2 (R) shows the good performance in mechanical properties as well as UV-protection and antibacterial properties. The mechanical performance of NR/n- TiO_2 (R) composites was enhanced with an increase of n- TiO_2 (R) content up to the optimum level of 5 phr and then declined. Huang *et al.* [179] prepared TiO_2 /NR nanocomposites and evaluated their antibacterial and antifungal activity. Mechanical properties of TiO_2 dispersed NR latex films were reported [180].

Cellulose nanofibres (CNF) with diameter 10-60 nm were isolated from raw banana fibres by steam explosion process. These CNF were used as reinforcing elements in natural rubber (NR) latex along with crosslinking agents to prepare nanocomposite films and physico-mechanical properties

were studied [181]. Kueseng *et al.* [182] prepared NR nanocomposites with SiC nanoparticles and carbon nanotubes. The report claims that the modulus and strength of NR with 1.5 per cent SiC nanoparticles appear to be superior to those of SWCNT's. Effect of 1-octadecanol functionalization of carbon nano tubes (CNT) on electrical properties of NR nanocomposites was studied by Thomas *et al.* [183]. TEM studies revealed that functionalization causes improvement in dispersion of CNT in NR matrix, which was corroborated by increase in electrical resistivity in the case of functionalized CNT/NR composites. Natural rubber, carbon nanotubes and cotton yarns were mixed to give a uniformly mixed composite containing 15 volume per cent carbon nanotubes and 3 volume per cent cotton and exhibiting heat resistance temperature $\leq 300^{\circ}\text{C}$ [184]. Natural rubber/carboxylated styrene butadiene rubber (NR/XSBR) (80/20) nanocomposites containing different loadings of carbon black (CB) (3-9 phr) and carbon nanotube (CNT) (0.1-0.4 phr) have been prepared by a latex stage compounding method [185]. The CNT-filled nanocomposites (0.2 phr) provided a comparable tensile strength with that of the CB-filled nanocomposites (5 phr) (*i.e.* 25-fold lower filler loading).

Atieh *et al.* [186] studied the properties of natural rubber NR/MWCNT nanocomposites. Natural rubber (NR)/ multi-walled carbon nanotube (MWCNT) composites were prepared by combining self-assembly and latex compounding techniques [187]. Results show that MWCNTs are homogeneously distributed throughout the NR matrix as single tube and present a great interfacial adhesion with NR phase when MWCNT

contents are less than 3 wt. per cent. Reinforcement of natural rubber using carboxylated multi-walled carbon nanotubes (c-MWCNT) dispersed with sodium dodecyl sulphate is reported [188]. The structure of the reinforced latex films was investigated by TEM and AFM.

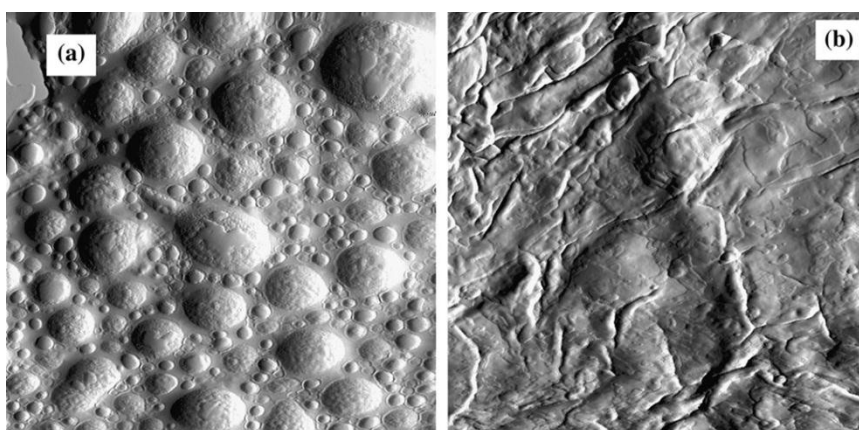


Figure 1.18: AFM image of the surface of a composite with 2.8 wt. % MWCNT before (a) and after (b) coagulation of the latex at 60⁰C [188]

Cataldo *et al.* [189, 190] used multi-walled carbon nanotubes (MWCNTs) as reinforcing filler in natural rubber and styrene-butadiene copolymer (E-SBR) based formulation as partial replacement of carbon black.

Preparation, properties and applications of graphene-elastomer nanocomposites are reviewed by several authors [191-193].

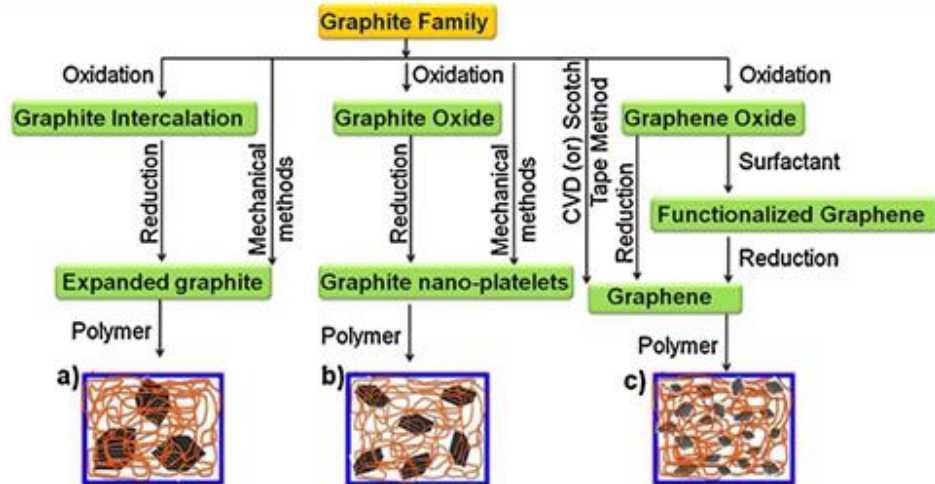


Figure 1.19: Schematic representation of graphitic based filler systems and elastomer nanocomposite containing (a) expanded graphite (b) graphite nanoplatelets and (c) graphene [192]

Ozbas *et al.* [194] studied the effects of functionalized graphene sheets (FGS) on the mechanical properties and strain-induced crystallization of NR and compared it with that of conventional carbon black (CB) filled one. They claim that the onset of crystallization occurs at much lower strains for FGS filled NR than for CB filled NR. Recently, Yang *et al.* [195] fabricated high-nanofiller-content graphene/natural rubber nanocomposites with high electrical conductivity (up to 104 S m^{-1}) and excellent mechanical properties (tensile strength, 48 MPa; modulus, 1.2 GPa) *via* vacuum-assisted self-assembly for the first time. She *et al.* reported 87 per cent improvement in tensile strength and 8.7 fold increase in modulus at 200 per cent elongation with the addition of 0.7 wt. per cent GO addition compared with those of ENR [196]. Aqueous solutions with different concentrations of GO and RGO were mixed with NR latex under magnetic stirring followed by sonication. The thermal,

mechanical and electrical properties of the resulting composites were estimated with filler content. The biodegradability of the composite was also studied [197]. Zhan *et al.* prepared NR/GE composites by ultrasonically assisted latex mixing and *in situ* reduction process. Compared to pure rubber, tensile and tear strength for NR/GE composites (2 wt. per cent) were increased by ~47 and 50 per cent. Also, the maximum torque, cross link density, elastic modulus and thermal conductivity of NR/GE composites were found to increase [198].

Natural rubber latex / potato starch nanocrystal nanocomposites were reported by Emilie *et al.* [199]. They synthesized potato starch nanocrystals by acid hydrolysis of potato starch powder and incorporated to natural rubber latex at different levels (0-20 wt. per cent). The morphology, structure and the electrical properties of the resulting composites were studied. Structural and mechanical properties of NR based nanocomposites reinforced with starch nanocrystals extracted from different botanical sources (normal maize, amylo maize, potato and wheat starch) were reported [200]. Mechanical, morphological, curing and thermal properties of SBR-starch composites were reported. To improve the reinforcement, a variety of starch modifications were tried by Tang *et al.* [201]. Mele *et al.* proposed a modelling approach to study the reinforcing mechanisms of starch nanocrystals in non-vulcanized natural rubber latex. The non-linear dynamic mechanical experiments confirmed the significant reinforcing effect of waxy maize starch nanocrystals [202]. Greater reduction in oxygen permeability was reported to NR with the addition of starch nanocrystals [203].

From the above discussion, it is possible to extract the behaviour of elastomer nanocomposites based on the nature of the polymer and the interaction between the filler and matrix. The elastic modulus tends to increase with the volume fraction of inclusions in every case. Interaction between matrix and filler may play an important role on composite properties. The addition of nanoparticles with poor interaction with the matrix causes the yield stress to decrease, compared to the neat matrix, regardless of the filler concentration or size. A poor filler–matrix interaction leads to a decrease in the ultimate and yield stress as compared to the pure matrix system [125].

Although nanocomposites are realizing many key applications in numerous industrial fields, a number of technical and economic barriers exist for their widespread commercialization. These include impact performance, the complex formulation relationships and routes to achieve nano-filler dispersion and exfoliation in the polymer matrix. Investment in state-of-the-art equipment and the enlargement of core research team's is another bottleneck to bring out innovative technologies on nanocomposites [204].

1.11 Scope and objectives of the study

For latex compounding, the solid ingredients are to be added as fine dispersions. The size of the ingredients added to the latex must be comparable to the size of the rubber particles in latex for intimate mixing. The practical importance of this technique is to minimize the sedimentation during storage of the mixes and to achieve a satisfactory processing rate. To obtain finely ground, stable dispersions it is usual to use milling devices

such as ball-mills, vibration mills, attrition mills *etc.* The main disadvantage of using these techniques is that it is a very slow process and may take several hours to produce a fine dispersion. Moreover by using conventional micro-dispersions, sedimentation rate of chemicals during storage and amount of unreacted chemicals in the product will be high causing more release of more chemicals to the environment as effluents. The release of zinc ions in effluents from rubber industries is also of great concern as it is creating environmental problems. Moreover, higher the particle size of dispersions, poorer the clarity to the thin walled latex articles and are more prone to defects. This causes high rejection rate to the products. Latex users therefore spend a great deal of time and money for achieving stable dispersions of compounding ingredients having very small particle sizes.

With the advancement of nanotechnology and rapid advances in new chemicals and milling process, “fine particle” technology has come within the reach of every industry. Natural rubber latex being a nano-sized dispersion of rubber in aqueous medium (average size 580 nm), the new concept has got great importance in latex dipping industry. By matching the particle size of dispersions with that of latex, sedimentation in chemical dispersions during storage can be minimized. The main problems associated with nano dispersions is the agglomeration followed by settling. To avoid this, nano-dispersions are to be stabilized by using suitable stabilizing agents.

The nano-ZnO dispersion has got wide acceptance in latex technology as it offers good latex stability and better product clarity. The nano-ZnO dispersions are required in small quantities compared to

micro-dispersions and are completely consumed in the system so that the release to effluents will be minimum.

The central aim of this research work was to study the effect of ultrafine/nanoparticle dispersions in latex technology. The specific objectives of the present work are:

- Preparation of chemical dispersions of latex compounding ingredients [zinc oxide, china clay, zinc diethyl dithiocarbamate (ZDEC), zinc 2-mercapto benzothiazole (ZMBT) and butylated reaction product of p-cresol and dicyclopentadiene (wingstay L)] by ball-milling.
- Optimization of ball-milling parameters such as milling time, concentration of surfactant (SA) and ball size on dispersion quality.
- Evaluation of dispersion quality of the compounding ingredients by dynamic light scattering (DLS), zeta potential measurements and sedimentation test.
- Synthesis of nano-ZnO through a simple mechano-chemical route and its characterization using various analytical and spectroscopic techniques.
- Stabilization of synthesized ZnO nanoparticles using various surfactants and their size and stability evaluation by dynamic light scattering (DLS), zeta potential measurements and sedimentation test.

- Evaluation of nano-ZnO dispersions for physical and antimicrobial properties in natural rubber latex vulcanizates.
- The effect of nano silica and nano titania dispersions on natural rubber latex vulcanizate properties after ageing under various degrading environments viz. thermal, γ -radiation, UV radiation and chlorination.
- Preparation and characterization of starch nanocrystals isolated from modified corn starch and their evaluation in natural rubber latex.
- Preparation of graphene dispersions and the evaluation of their effect on the properties of radiation vulcanized natural rubber latex (RVNRL).

References

- [1] K. Nawamawat, J. T. Sakdapipanich, C. C. Ho, Y. Ma, J. Song, and J. G. Vancso, *Colloids and Surfaces A: Physico-chemical and Engg. Aspects*, **390**, 157 (2011).
- [2] W. Johnson, *British Patent No.467*, Aug 18(1953).
- [3] S. F. Cheong, and C. O. Ong, *J. Rubber Res. Inst. Malaysia* **24(2)**, 118 (1974).
- [4] C. K. John, M. Nadarajah, P. S. Rama Rao, C. M. Lau, and C. S. Ng, *Proceedings of the Intl. Rubber Conf., 1975*, Kuala Lumpur, Malaysia Vol. IV p.339.
- [5] N. M. Mathew, L. Varghese, R. Kothandaraman, and E. V. Thomas, *Rubber Board Bull.* **13(3)**, 58 (1976).
- [6] C. K. John, N. P. Wong, H. C. Chin, P. S. Rama Rao, and A. Latiff (1985) *Proceedings of the Intl. Rubber Conf., 1985*, Kuala Lumpur, Malaysia Vol. II p. 451.

- [7] K. C. Shum, and W. G. Wren, *J. Rubber Res. Inst. Malaysia*, **25(2)** 69 (1977).
- [8] J. S. Lowe, *Trans. Inst. Rubber Indus.* **35(1)** 10 (1959).
- [9] M. R. Sethuraj, and N. M. Mathew (eds.) “Natural Rubber: Biology, Cultivation, and Technology. Developments in Crop Science 23”: Chapter 17 Elsevier Publishers, (1992).
- [10] H. C Chin, M. M. Singh, and S. E. Loke, *Plastics and Rubber: Mater. And Appli.* **(4)**, 164 (1979).
- [11] J. John and R. K. Matthan 21st Rubber Conference on “Emerging Trends in Developing Eco-Friendly and Energy Efficient Elastomeric Material and Processing Technology”(2012), p. 77.
- [12] www3.lgm.gov.my/irpec.
- [13] M. W. Philpott, *Proc. 4th Rubber Technol. Conf., 1962, MRPRA, London*, p.470.
- [14] M. W. Philpott, *J. Rubber Res. Inst. Malaysia* **(22)**, 441 (1969).
- [15] G. F. Bloomfield, *Rubber Develop.* **(5)**, 34 (1952).
- [16] R. Rajan, S. Varghese, and K. E. George, *Rubber Science.* **27(1)**, 98 (2014).
- [17] Y. Minoura, and M. Asao, *J. Appl. Polym. Sci.* **(5)**, 233 (1961).
- [18] F. I. Sundardi, and S. Kartawardoyo, *J. Appl. Polym. Sci.* **(21)**, 3077 (1977).
- [19] K. Makuuchi, and H. Nakayama, *Prog. Org. Coat.* **11(3)**, 241 (1983).
- [20] H. Ambroz, *J. Polym. Sci: Polym. Symp.* **42(3)**, 1339 (1973).
- [21] www.zinc.org.
- [22] www.numenor.com
- [23] B. C. Barton, *Rubber Chem. Technol.* **23(4)**, 888 (1950).
- [24] B. A. Dogadkin, and V. A. Shershnev, *Rubber Chem. Technol.* **33(2)**, 412 (1960).
- [25] S. P. Manik, and S. Banerjee, *Rubber Chem. Technol.* **43(6)**, 1294 (1970).

- [26] G. M. Kraay and M. van den Tempel, *Rubber Chem. Technol.* **25(4)**, 995 (1952).
- [27] R. T. Davies, and T. D. Pendle, *Rubber Chem. Technol.* **66(4)**, 578 (1993).
- [28] E. B. Johnson, and J. R. Scott, *Rubber Chem. Technol.* **16(2)**, 445 (1943).
- [29] R. Thiollet, and G. Martin, *Rubber Chem. Technol.* **(4)**, 1 (1931).
- [30] G. Shobayashi, *J. Soc. Rubber Ind. Japan* **20**, 1 (1947).
- [31] T. Saijo, and H. Kaneko, *Nippon Gomu Kyokaishi* **32**, 100 (1959).
- [32] M. K. Coulter US Patent 2785990 A, March 19, 1957.
- [33] V. L. Hallenbeck, *Rubber Chem. Technol.* **46(1)**, 78 (1973).
- [34] H. Baldyga, and H. C. Jones, *Rubber Chem. Technol.* **39(4)**, 1347 (1966).
- [35] Z. Man, Li Deng, M. Yang, Y. Chen, and Z. Jin, *Rubber Chem. Technol.* **87(1)**, 21 (2014).
- [36] M. Morton (Ed.), "Rubber Technology" 3rd edition, Van Nostrand Reinhold, New York (1987).
- [37] S. O. Movahed, and M. Alimardani, *Reinforcement of Rubber Compounds by Different Fillers: Recent Achievements* in "Rubber Types, Properties and Uses" Ed. Gabriel A Popa, Chapter 1, Nova Science Publishers, NY, 2013.
- [38] Chih-Cheng Peng *Dissertation Doktors der Naturwissenschaften*, Universität Bayreuth (2005)
- [39] J. H. Bachmann, J. W. Sellers, M. P. Wagner, and R. F. Wolf, *Rubber Chem. Technol.*, **32**, 1286 (1959).
- [40] W. F. Watson, *Rubber Chem. Technol.* **28(4)**, 1032 (1955).
- [41] L. Bokobza, and O. Rapoport, *J. Appl. Polym. Sci.* **85** 2301 (2002).
- [42] S. Wolff, *Rubber Chem. Technol.* **69(3)**, 325 (1996).
- [43] G. Kraus, *Rubber Chem. Technol.* **38(5)**, 1070 (1965).
- [44] L. Mullins, and N. R Tobin, *J Appl. Polym. Sci.* **9**, 2993 (1965).

- [45] C. Gauthier, E. Reynaud, R. Vassoille, and L. Ladouce-Stelandre, *Polymer* **45(8)**, 761 (2004).
- [46] J. Fröhlich, W. Niedermeier, and H. D. Luginsland, *Composites Part A: Appl. Sci. and Manufacturing* **36(4)**, 449 (2005).
- [47] S. T. Sam, H. Ismail, M. N. Ahmad Fauzi, and A. Abu Bakar, *J. of Reinforced Plastics and Composites* **27**, 1893 (2008).
- [48] H. Xu, J. Han, L. Fang, F. Shen, and C. Wu *Polymer Bull.* **58(5-6)**, 951 (2007).
- [49] A. R. Azura, S. Ghazali, and M. Mariatti, *J Appl. Polym. Sci.* **110(2)**, 747 (2008).
- [50] J. L. White, D. Liu, and S. H. Bumm, *J Appl. Polym. Sci.* **102(4)**, 3940 (2006).
- [51] T. Kunizawa, and Qing-Qing NI *J. Japan Soc. Comp. Mater.* **35(4)**, 157 (2009).
- [52] He Yan, Ma Lianxiang, and Cui Qi, *China Synthetic Rubber Industry* 2007-03.
- [53] Soo-Jin Park, and Ki-Sook Cho *J. Colloid and Interface Sci.* **267(1)**, 86 (2003).
- [54] H. Yan, K. Sun, Y. Zhang, and Y. Zhang, *Polym. Test.* **24(1)**, 32 (2005).
- [55] P. Sae-Oui, C. Sirisinha, K. Hatthapanit, and N. Phewthongin, *J Appl. Polym. Sci.* **110(5)**, 2763 (2008).
- [56] X. Yuan, F. Shen, G. Wu, and C. Wu, *J. Polym. Sci. B Polym. Phys.* **45(5)**, 571 (2007).
- [57] V. Sridhar, B. R. Gupta, and D. K. Tripathy, *J. Appl. Polym. Sci.*, **102(1)**, 715 (2006).
- [58] D. Puryanti, Sahrim Hj. Ahmad, Mustaffa Hj. Abdullah, and Ahmad Nazlim Hj. Yusoff, *Intl. J. of Polym. Mater.*, **56(3)**, 327 (2007).
- [59] S. Poompradub, Y. Ikeda, Y. Kokubo, and T. Shiono, *Euro. Polym. J.* **44(12)**, 4157 (2008).

- [60] B. Košíková, A. Gregorová, A. Osvald, and J. Krajčovičová, *J. Appl. Polym. Sci.* **103(2)**, 1226 (2007).
- [61] R. Sukumar, and A. R. R. Menon, *J. Appl. Polym. Sci.* **107(6)**, 3476 (2008).
- [62] A. A. Yehia, M. A. Mull, M. N. Ismail, Y. A. Hefny, and E. M. Abdel-Bary, *J. Appl. Polym. Sci.* **93(1)**, 30 (2004).
- [63] M. Jacob, S. Thomas, and K. T. Varughese, *Comp. Sci. and Technol.* **64(7–8)** 955 (2004).
- [64] M. R. Kashani, S. Javadi, and N. Gharavi, *Smart Mater. Struct.* **19(3)**, 035019 (2010).
- [65] L. C. Sim, S. R. Ramanan, H. Ismail, K. N. Seetharamu, and T. J. Goh, *Thermochim. Acta.* **430(1-2)**, 155 (2005).
- [66] L. C. Sim, C. K. Lee, S. R. Ramanan, H. Ismail, and K. N. Seetharamu, *Polymer- Plastics Technol. Engg.* **45(3)**, 301 (2006).
- [67] Q. Mu, S. Feng, and G. Diao, *Polymer Comp.* **28(2)**, 125 (2007).
- [68] www.dailymirror.lk, March, 31(2011).
- [69] M. K. Sharma, *Ph.D. Thesis*. Homi Bhabha National Institute, (2012).
- [70] T. P. Yadav, R. M. Yadav, and D. P. Singh, *Nanosci. and Nanotechnol.* **2(3)**, 22 (2012).
- [71] H. El-Shall, and P. Somasundaran, *Powder Technol.* **38**, 275 (1984).
- [72] C. Suryanarayana, *Prog. Mater. Sci.* **46**, 1 (2001).
- [73] A. O. Gezerman, and B. D. Corbacioglu *Intl. J. Modern Chem.* **1(3)**, 116 (2012).
- [74] P. Balaz, “Mechanochemistry in Nanoscience and Minerals Engineering”, Springer- Verlag, Berlin Heidelberg p.103 (2008).
- [75] E. K. Fischer, *Ind. Engg. Chem.* **33**, 1465 (1941).
- [76] T. Tsuzuki, *Intl. J. Nanotechnol.* **6(5/6)**, 567 (2009).
- [77] www.news-medical.net/health/Synthesis-of-Nanoparticles.aspx.
- [78] G. P. Barreto, G. Morales, and Ma. Luisa López Quintanilla, *J. Mater.* **2013**, Article ID 478681 (2013).

- [79] L. S. Mende, and J. L. M. Driscoll, *Mater. Today* **10**(5), 40 (2007).
- [80] Z. S. Wang, C. H. Huang, Y. Y. Huang, Y. J. Hou, P. H. Xie, B. W. Zhang, and H. M. Cheng, *Chem. Mater.* **13**, 678 (2001).
- [81] J. Q. Xu, Q. Y. Pan, Y. A. Shun, and Z. Z. Tian, *Sens. Actuators B-Chem.* **66**, 277 (2000).
- [82] D. H. Yoon, and G. M. Choi, *Sensors Actuators B-Chem.* **45**(3), 251 (1997).
- [83] I. Rosso, C. Galletti, M. Bizzi, G. Saracco, and V. Specchia, *Ind. Engg. Chem. Res.* **42**, 1688 (2003).
- [84] L. Palanikumar, S. Ramasamy, G. Hariharan, and C. Balachandran, *Appl. Nanosci.* **3**(5), 441 (2013).
- [85] J. Wu, C. S. Xie, Z. K. Bai, B. L. Zhu, K. J. Huang, and R. Wu, *Mater. Sci. Engg. B* **95**, 157 (2002).
- [86] S. C. Pillai, J. M. Kelly, D. E. McCormack, P. O' Brien, and R. Ramesh, *J. Mater. Chem.* **13**, 2586 (2003).
- [87] Y. Nakanishi, A. Miyake, H. Kominami, T. Aoki, Y. Hatanaka, and G. Shimaoka, *Appl. Surf. Sci.* **142**, 233 (1999).
- [88] C. Feldman, *Adv. Fundam. Mater.* **13**, 101 (2003).
- [89] M. Kitano, and M. Shiojiri, *Powder Technol.* **93**, 267 (1997).
- [90] V. P. Kamat, R. Huehn, and R. Nicolaescu, *J Phys. Chem. B* **106**, 788 (2002).
- [91] A. C. Dodd, A. J. McKinley, M. Saunders, and T. Tsuzuki, *J. Nanoparticle Res.* **8**, 43 (2006).
- [92] H. L. Cao, X. F. Qian, Q. Gong, W. M. Du, X. D. Ma, and Z. K. Zhu, *Nanotechnology*, **17**, 3632 (2006).
- [93] Y. D. Wang, C. L. Ma, X. D. Sun, and H. D. Li, *Inorg. Chem. Commun.* **5**, 751 (2002).
- [94] F. Zhou, X. Zhao, H. S. Zheng, and T. C. Tang, *Chem. Lett.* **34**, 1114 (2005).
- [95] N. R. Noori, R. S. Mamoory, P. Alizadeh and A. Mehdikhani, *J. Ceram. Process. Res.* **9**(3), 246 (2008).

- [96] L. Wang, and M. Muhammed, *J. Mater. Chem.* **9**, 2871 (1999).
- [97] R. Hong, T. Pan, J. Qian, and H. Li, *Chem. Engg. J.* **119**, 71 (2006).
- [98] S. S. Ashtaputre, A. Deshpande, S. Marathe, M. E. Wankhede, J. Chimanpure, R. Pasricha, J. Urban, S. K. Haram, S. W. Gosavi, and S. K. Kulkarni, *PRAMANA- J of Phys.* **65(4)**, 615 (2005).
- [99] P. Li, H. Liu, Y. F. Zhang, Y. Wei, and X. K. Wang, *Mater. Chem. Phys.* **106**, 63 (2007).
- [100] F. Bai, P. He, Z. Jia, X. Huang, Y. He, *Mater. Lett.* **59**, 1687 (2005).
- [101] M. Shim, and P. Guyot-Sionnest, *J. Am. Chem. Soc.* **123**, 11651 (2001).
- [102] P. D. Cozzoli, M. L. Curri, A. Agostiano, G. Leo, and M. Lomascolo, *J Phys. Chem. B* **107**, 4756 (2003).
- [103] J. H. Chen, C. Y. Cheng, W. Y. Chiu, C. F. Lee, and N. Y. Liang, *Euro. Poly. J.* **44**, 3271 (2008).
- [104] E. Tang, G. Cheng, and X. Ma, *Powder Technol.* **161**, 209 (2006).
- [105] Q. Wan, K. Yu, T. H. Wang, and C. L. Lin, *Appl. Phys. Lett.* **83**, 2253 (2003).
- [106] X. L. Yuana, B. P. Zhang, J. Niitsumaa, and T. Sekiguchia, *Mat. Sci. Semicon. Proc.* **9**, 146 (2006).
- [107] B. P. Zhang, N. T. Binh, K. Wakatsuki, Y. Segawa, Y. Yamada, N. Usami, M. Kawasaki, and H. Koinuma, *Appl. Phys. Lett.* **84**, 4098 (2004).
- [108] J. Zhang Y. Yang, B. Xu, F. Jiang, and J. Li, *J. Cryst. Growth* **280(3-4)**, 509 (2005).
- [109] S. Choopun, H. Tabata, and T. Kawai, *J. Cryst. Growth*, **274**, 167 (2005).
- [110] W. I. Park, and G. C. Yi, *Adv. Mater.* **16**, 87 (2004).
- [111] W. Lee, M. C. Jeong, and J. M. Myoung, *Acta Mater.* **52**, 3949 (2004).
- [112] Y. Li, G. W. Meng, L. D. Zhang, and F. Phillipp, *Appl. Phys. Lett.* **76**, 2011 (2000).
- [113] H. Wang, J. Z. Xu, J. J. Zhu, and H. Y. Chen, *J. Cryst. Growth*, **244**, 88 (2002).

- [114] D. Ledwith, S. C. Pillai, G. W. Watson, and J. M. Kelly, *Chem. Commun.* **20**, 2294 (2004).
- [115] H. E. Unalan, P. Hiralal, N. Rupesinghe, S. Dalal, W. I. Milne, and G. A. J. Amaratunga, *Nanotechnology* **19**, 255608 (2008).
- [116] T. Prakash, R. Jayaprakash, G. Neri, and S. Kumar, *J. Nanoparticles* **2013**, Article ID 274894, (2013).
- [117] N. F. Hamedani, and F. Farzaneh, *J. Sci. Islamic Rep. Iran* **17(3)**, 231 (2006).
- [118] L. Shen, N. Bao, K. Yanagisawa, K. Domen, A. Gupta, and C. A. Grimes, *Nanotechnology* **17**, 5117 (2006).
- [119] A. Azam, F. Ahmed, N. Arshi, M. Chaman, and A. H. Naqvi, *Intl. J. Theo. and Appl. Sci.* **1(2)**,12 (2009).
- [120] Zhi-Peng Sun, L. Liu, Li Zhang, and Dian- Zeng Jia, *Nanotechnology* **17**, 2266 (2006).
- [121] N. Niederberger, and M. Antonietti “Nanomaterials Chemistry”, (eds. C. N. R. Rao, A. Muller and A. K. Cheetham) WILEY- VCH, Chapter **3**, 119 (2007).
- [122] L. A. Goettler, K. Y. Lee, and H. Thakkar, *Polymer Rev.* **47(2)**, 291 (2007).
- [123] S. S. Ray, and M. Okamoto, *Prog. Polym. Sci.* **28**, 1539 (2003).
- [124] V. Mittal, *Materials* **2**, 992 (2009).
- [125] W. E. Gacitua, A. A. Ballerini, and J. Zhang, *Maderas. Ciencia y tecnología* **7(3)**, 159 (2005).
- [126] H. R. Fischer, L. H. Gielgens, and T. P. M. Koster, *Acta Polym.* **50**, 122 (1999).
- [127] J. Jordan, K. Jacob, R. Tannenbaum, M. Sharaf, and I. Jasiuk, *Mater. Sci. and Engg.- A*, **393**, 1 (2005).
- [128] R. D. Kroshefsky, J. L. Price, and D. Mangaraj, *Rubber Chem. Technol.* **82(3)**, 340 (2009).
- [129] M. Galimberty, “Advanced Elastomers- Technology, Properties and Applications”(ed. Anna Boczkowska) *chapter 4*, InTech Open (2012).

- [130] S. Iijima, *Nature*, **354**, 56 (1991).
- [131] P. M. Ajayan, and T. W. Ebbesen, *Rep. Prog. Phys.* **60(10)**, 1025 (1997).
- [132] M. F. Yu, B. S. Files, A. Sivaram, and R. S. Ruoff, *Phys. Rev. Lett.* **84(24)**, 5552 (2000).
- [133] S. R. C. Vivekchand, A. Govindaraj, and C. N. R. Rao, "Nanotubes and Nanowires: Recent Developments" in '*Nanomaterials Chemistry*', Eds. C. N. R. Rao, A. Müller, and A. K. Cheetham, WILEY-VCH Verlag, Weinheim, (2007).
- [134] A. Gomathi, S. R. C. Vivekchand, A. Govindaraj, and C. N. R. Rao, *Adv. Mater.* **17**, 2757 (2005).
- [135] E. Beyou, S. Akbar, P. Chaumont, and P. Cassagnau, "*Syntheses and Applications of carbon nanotubes and their composites*"(ed. Satoru Suzuki), *chapter 5*, In Tech Open (2013).
- [136] S. Bal, *Materials and Design* **31(5)**, 2406 (2010).
- [137] K. Jayaraman, M. Katakai, Y. Zhang, X. Mo, and S. Ramakrishna, *J. Nanosci. Nanotechnol.* **4(1-2)**, 52 (2004).
- [138] J. Tang, Y. Wang, H. Liu, Y. Xia and B. Schneider, *J. Appl. Polym. Sci.* **90(4)**, 1053 (2003).
- [139] S. Li, M. M. Lin, M. S. Toprak, D. K. Kim and M. Muhammed, *Nano Rev.* **1**, 5214 (2010).
- [140] Y. P. Zheng, Y. Zheng, and R. C. Ning, *Mater. Lett.* **57(19)**, 2940 (2003).
- [141] F. Hussain, M. Hojjati, M. Okamoto, and R. E. Gorga, *J. Comp. Mater.* **40 (17)**, 1511 (2006).
- [142] A. Usuki, A. Tukigase, and M. Kato, *Polymer* **43**, 2185 (2002).
- [143] A. I. Nakatani, W. Cen, R. C. Schmidt, G. V. Gordon, and C. C. Han, *Polymer* **42**, 3713 (2001).
- [144] R. A. Vaia, and E. P. Giannelis, *Macromolecules*, **30(25)**, 7990 (1997).
- [145] M. S. Sreekala, and C. Eger, "*Polymer Composites from Macro- to Nano-scale*", *chapter 6* (eds. K. Friedrich, S. Fakirov, and Z. Zhang) *Science+ NY*, (2005) p.91.

- [146] G. Kraus, *Reinforcement of Elastomers*, Interscience, NY.
- [147] A. K. Bhowmick, M. M. Hall, and H. Benary, “*Rubber Products Manufacturing Technology*”, Marcel Dekker Inc., USA (1994).
- [148] R. V. Kurahatti, A. O. Surendranathan, S. A. Kori, N. Singh, A. V. Ramesh Kumar, and S. Srivastava, *Defence Sci. J.*, **60(5)**, 551 (2010).
- [149] N. Rattanasom, S. Prasertsri, and T. Ruangritnumchai, *Polym. Test.* **28(1)**, 8 (2009).
- [150] Uthirakumar *Ph.D. thesis*, School of Chonbuk National Univ. Chonju, Korea (2005).
- [151] L. Theodore, and R. G. Kunz, “*Nanotechnology: Environmental implications and Solutions*”, John Wiley & Sons, NJ p.61 (2005).
- [152] Y. T. Vu, J. E. Mark, L. H. Pham, and M. Engelhardt, *J. Appl. Polym. Sci.* **82**, 1391 (2001).
- [153] M. Maiti, M. Bhattacharya, and A. K. Bhowmick, *Rubber Chem. Technol.*, **81(3)**, 384 (2008).
- [154] J. C. González, H. Retsos, R. Verdejo, S. Toki, B. S. Hsiao, E. P. Giannelis, and M. A. López-Manchado, *Macromolecules* **41(18)**, 6763 (2008).
- [155] S. Varghese, and J. Karger- Kocsis, *Polymer* **44**, 4921 (2003).
- [156] P. L. Teh, Z. A. Mohd. Ishak, U. S. Ishiaku, and J. Karger- Kocsis, *jurnal teknologi* **39(A)**, 1 (2003).
- [157] U. Sookyung, C. Nakason and W. Thaijaroen, *Adv. Mater. Res.* **626**, 62 (2013).
- [158] R. Stephen, S. Thomas, K. V. S. N. Raju, S. Varghese, K. Joseph, and Z. Oommen *Rubber Chem. Technol.* **80(4)**, 672 (2007).
- [159] K. G. Gatos, and J. Karger-Kocsis, *Euro. Polym. J.* **43(4)**, 1097 (2007).
- [160] V. P. Swapna, R. Stephen, T. Greeshma, C. Sharan Dev, and M. S. Sreekala, *Polymer Comp.* **37(2)**, 602 (2016).
- [161] M. A. L. Manchado, J. L. Valentín, J. Carretero, F. Barroso, and M. Arroyo, *Euro. Polym. J.* **43(10)**, 4143 (2007).

- [162] Z. Peng, L. X. Kong, S. D. Li, Y. Chen, and M. F. Huang, *Comp. Sci. Technol.* **67**, 3130 (2007).
- [163] A. P. Meera, S. Said, Y. Grohens, and S. Thomas, *J. Phys. Chem. C* **113(42)**, 17997 (2009).
- [164] S. D. Li, Z. Peng, L. X. Kong, and J. P. Zhong, *J. Nanosci. Nanotechnol.* **6(2)**, 541 (2006).
- [165] A. Ansarifar, S. F. Shiah, N. Ibrahim, and A. Azhar, "Rubber chem 2004," *4th International Rubber Chemicals, Compounding and Mixing Conference*, Birmingham, United Kingdom (2004).
- [166] S. O. Movahed, K. A. Yasin, A. Ansarifar, M. Song, and S. Hameed, *J. Appl. Polym. Sci.* **109(2)**, 869 (2008).
- [167] S. Kohjiya, A. Kato, and Y. Ikeda, *Prog. Polym. Sci.* **33**, 979 (2008).
- [168] S. Kohjiya, A. Kato, J. Shimanuki, T. Hasegawa, and Y. Ikeda, *Polymer* **46**, 4440 (2005).
- [169] A. H. El-Hag, L. C. Simon, S. H. Jayaram, and E. A. Cherney, *IEEE Transactions on Dielectrics and Electrical Insulation* **13(1)**, 122 (2006).
- [170] S. Kemaloglu, G. Ozkoc, and A. Aytac *Thermochim. Acta* **499(1-2)**, 40(2010).
- [171] S. Manroshan, and A. Baharin, *J. Appl. Polym. Sci.* **96**, 1550 (2005).
- [172] J. Gu, D. Jia, Y. Luo, and R. Cheng, *Hecheng Xiangjiao Gongye* **28**, 374 (2005).
- [173] H. S. Ghari, A. J. Arani, and Z. Shakouri, *Rubber Chem. Technol.* **86(2)**, 330 (2013).
- [174] S. Fernandez, and S. Kunchandy, *Orient. J. Chem.* **29(1)**, 219 (2013).
- [175] C. M. Deng, M. Chen, N. J. Ao, D. Yan, and Z. Q. Zheng, *J. Appl. Polym. Sci.* **101**, 3442 (2006).
- [176] G. Lin, M. Tian, Y. L. Lu, X. J. Zhang, and L. Q. Zhang, *Polymer J.* **38**, 498 (2006).
- [177] Y. Chen, (for Shanghai University of Engineering Technology), *Chinese Patent*, CN1386788A, Dec. 25, (2002).

- [178] B. Seentrakoon, J. Banja, and W. Chawasiri, *Polym. Degrad. Stab.* **98(2)**, 566 (2013).
- [179] M. Huang, A. Ding, T.Gao, M.Lv, and P. Li, *3rd Intl. Conf. on Biomed. Engg. and Informatics (BMEI-2010)* (2010).
- [180] S. S. Ochigbo, and A. S. Luyt, *Intl. J. Comp. Mater.* **1(1)**, 7 (2011).
- [181] E. Abraham, B. Deepa, L. A. Pothan, M. John, S. Narine, S. Thomas, and R. Anandjiwala, *Cellulose* **20(1)**, 417 (2013).
- [182] K. Kueseng, K. I. Jacob, *Euro. Polym. J.* **42(1)**, 220 (2006).
- [183] P. S. Thomas, A. A. Abdullateef, M. A. Al- Harthi, M. A. Atieh, S. K. De, M. Rahaman, T. K. Chaki, D. Khastgir, and Bandyopadhyai, *J. Mater. Sci.* **47(7)**, 3344 (2012).
- [184] T. Noguchi, and A. Magario, (for Nissin Kogyo Co., Ltd,) *US Patent No. US 7619029B1*, November 17, (2009).
- [185] A. Boonmahitthisud, and S. Chuayjuljit, *J. Metals, Mater. and Minerals*, **22(1)**, 77 (2012).
- [186] M. A. Atieh, N. Girun, F. R. Ahmadun, C. T. Guan, El-Sadig Mahdi, and D. R. Baik, *Online J. Nanotechnol.* **1**, 1 (2005).
- [187] Z. Peng, C. Feng, Y. Luo, Z. Yi, Y. Li and L. X. Kong *J. Wuhan Univ. Technol. - Mater. Sci. Ed.* **26(6)**, 807 (2011).
- [188] S. Bhattacharyya, C. Sinturel, O. Bahloul, M. L. Saboungi, S. Thomas, and J. P. Salvetat, *Carbon* **46(7)**, 1037 (2008).
- [189] F. Cataldo, O. Ursini, and G. Angelini, *Fullerenes, Nanotubes and Carbon Nanostructures* **17(1)**, 38 (2009).
- [190] F. Cataldo, O. Ursini, and G. Angelini, *Fullerenes, Nanotubes and Carbon Nanostructures* **17(1)**, 55 (2009).
- [191] D. G. Papageorgiou, I. A. Kinloch and R. J. Young *Carbon* **95**, 460 (2015).
- [192] K. K. Sadasivuni, D. Ponnamma, S. Thomas and Y. Grohens *Prog. Polym. Sci.* **39 (4)**, 749 (2014).

- [193] A. Das and G. Heinrich Graphene-rubber nanocomposites in Encyclopedia of polymeric nanomaterials, S. Kobayashi and K. Mullen (eds.), Springer-Verlag Berlin Heidelberg, 1-5 (2014).
- [194] B. Ozbas, S. Toki, B. S. Hsiao, B. Chu, R. A. Register, I. A Aksay, R. K. Prud'homme and D. H. Adamson, *J. Polym. Phys. PART B: Polym. Phys.* **50**, 718 (2012).
- [195] H. S. Yang, P. Liu T. P. Zhang, Y. X. Duan, and J. M. Zhang, *RSC Adv.* **4**, 27687 (2014).
- [196] X. She, C. He, Z. Peng and L. Kong, *Polymer* **55**, 6803 (2014).
- [197] C. F. Matos, F. Galembeck and A. J. G. Zarbin *Carbon* **78**, 469 (2014).
- [198] Y. Zhan, J. Wu, H. Xia, N. Yan, G. Fei, and G. Yuan *Macromol. Mater. Engg.* **296**, 590 (2011).
- [199] B. Emilie, K. R. Rajisha, K. Nandhakumar, J. M. Saiter and S. Thomas, *Mater. Lett.* **65**, 3615 (2011).
- [200] D. S. LeCorre, J. Bras, and A. Dufresne, *Macromol. Mater. Engg.* **297**, 969 (2012).
- [201] H. Tang, Q. Qi, Y. Wu, G. Liang, L. Zhang and J. Ma, *Macromol. Mater. Engg.* **291**, 629 (2006).
- [202] P. Mele, H. Angellier, S. M. Boisseau and A. Dufresne, *Biomacromolecules* **12**, 1487 (2011).
- [203] H. Angellier, S. M. Boisseau, L. Lebrun and A. Dufresne, *Macromolecules* **38(9)**, 3783 (2005).
- [204] S. Baksi, S. Biswas, Nanocomposites – An overview, *The Sci. Technol. J.I* **1(5)**, 22 (2014).

.....✂.....

Chapter 2

EXPERIMENTAL

Contents	2.1 <i>Centrifuged natural rubber latex</i>
	2.2 <i>Radiation vulcanized natural rubber latex (RVNRL)</i>
	2.3 <i>Materials used</i>
	2.4 <i>Compounding ingredients</i>
	2.5 <i>Characterization</i>
	2.6 <i>Degradation studies</i>
	2.7 <i>Properties of latex vulcanizate</i>
	2.8 <i>Theoretical modelling</i>

This chapter describes the details of materials, specifications, experimental techniques and instruments used for the preparation and characterization of the ultra-fine/nanomaterials and their vulcanizates. Different characterization techniques such as dynamic light scattering (DLS), zeta potential measurements, X-ray diffraction (XRD), Fourier Transform infrared spectroscopy (FT-IR), Raman analysis, Atomic force microscopy (AFM), UV-visible spectroscopy and thermogravimetric analysis (TGA) are explained. Properties of latex vulcanizates are also discussed.

2.1 Centrifuged natural rubber latex

The characteristic specification, requirement and properties of centrifuged natural rubber latex (high ammonia type) used for pre-vulcanization and latex compounding are given in Table 2.1. The tests were carried out as per IS specifications shown in Table 2.1.

Table 2.1: Specification, requirement and properties of centrifuged latex used for pre-vulcanization and latex compounding

Property	Value	Requirement (BIS 5430-1981)	Test method
Dry rubber content (%)	60.5	60 min.	IS 3708 (part 1) 1985
Non rubber solids (%)	1.6	2 max.	IS 9316 (part 4) 1988
Ammonia content (%)	0.9	0.6 min.	IS 3708 (part 4) 1985
Volatile fatty acid number	0.035	0.15 max.	IS 3708 (part7) 1986
Mechanical stability time (sec.)	980	475 min.	IS 3708 (part 6) 1985

2.2 Radiation vulcanized natural rubber latex (RVNRL)

Radiation vulcanized natural rubber latex (RVNRL) having a total solid content of 53.49% was supplied by Raymintex, Malaysian Nuclear Agency, Selangor, Malaysia. The formulation for the preparation of RVNRL is shown in Table 2.2. The radiation dose selected was 12 kGy at a dose rate of 2 kGy/hour. The sensitizer used was n - butylacrylate. The stabilizer used was potassium laurate and Irganox 1520 was used as antioxidant. These materials were used as received.

Table 2.2: Formulation used for the preparation of RVNRL

Materials	phr
Latex	100
Stabilizer	0.02
Antioxigant (Irganox)	1.0
n-BA	5.0
Water	Required

2.3 Materials used

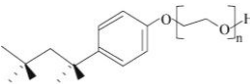
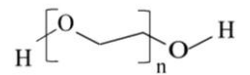


Zinc acetate dehydrate ($\text{Zn}(\text{OAc})_2 \cdot 2\text{H}_2\text{O}$) and sodium hydroxide (NaOH) used were of analytical grade supplied by MERCK, Mumbai, India. The sources of all the chemicals used were given in Table 2.3.

Table 2.3: Manufacturers/suppliers of chemicals

Materials/chemicals	Chemicals suppliers
Zinc oxide (white seal grade)	Sumit chemicals Pvt. Ltd., Kanpur, India & Hari Narain Industries Pvt. Ltd., Chandigarh, India.
Dispersol F	ICI limited, Calcutta, India
Sulphur	Jocil Ltd., Andhra Pradesh, India
ZDEC	Lanxess, India
ZMBT	Lanxess, India
Wingstay L	RT Vanderbuilt Inc., USA
Chinaclay	Bharathy Minerals Pvt. Ltd., Trivandrum, India
Zinc acetate dehydrate (AR grade)	MERCK, Mumbai, India
Sodium hydroxide	MERCK, Mumbai, India
Cetyl trimethylammonium bromide	CDH, New Delhi, India
Distilled water (HPLC grade)	Spectrochem, Mumbai, India
Sulphuric acid (98%,GR grade)	Merck, Mumbai, India
Hydrogen peroxide solution (purified)	Merck, Mumbai, India
Potassium permanganate	Qualigens fine chemicals, Mumbai, India
Potassium hydroxide	Qualigens fine chemicals, Mumbai, India
Triton X 100	Sigma Aldrich, Germany
Polyethylene glycol-6000	Merck, Mumbai, India
Sodium dodecyl sulphate	Sigma Aldrich, Germany
Nano zinc oxide dispersion	Sigma Aldrich, Germany
Nano titanium dioxide dispersion	Sigma Aldrich, Germany
Nano silica dispersion	Sigma Aldrich, Germany
Modified corn starch	Jemsons starch and derivatives, Aroor, Kerala, India
Antioxidant Irganox	Ciba Specialty Chemicals, Switzerland
Coarse low-density flake graphite	Asbury carbons, USA
Centrifuged natural rubber latex	Central Experimental Station, Rubber Research Institute India, India
Radiation vulcanized natural rubber latex (RVNRL)	Raymintex, Malaysian Nuclear Agency, Selangor, Malaysia
Ceramic balls	Platinum Ceramics, Namakkal, Tamil Nadu, India

The surfactants used are Triton X 100, PEG 6000 (both non-ionic), CTAB (cationic) and SDS (anionic). Triton-X 100 and SDS were purchased from Sigma - Aldrich. PEG 6000 was procured from MERCK and LR grade CTAB from CDH, New Delhi. Millipore distilled water having a conductivity of 0.240 $\mu\text{S}/\text{cm}$ was used for the preparation of surfactant solutions. Details of the surfactants are given in Table 2.4.

Table 2.4: Details of the surfactants used

Surfactant used	IUPAC name	Formula	Molar mass (g mol^{-1})	Structure
Triton X 100 (Non-ionic)	Polyoxyethylene octyl phenyl ether	$(\text{C}_{14}\text{H}_{22}\text{O}(\text{C}_2\text{H}_4\text{O})_n)$	647	
PEG 6000 (Non-ionic)	Poly(oxyethylene)	$\text{H}-(\text{O}-\text{CH}_2-\text{CH}_2)_n-\text{OH}$	5000-7000	
CTAB (Cationic)	Hexadecyltrimethylammonium bromide	$(\text{C}_{16}\text{H}_{33})\text{N}(\text{CH}_3)_3\text{Br}$	364.45	
SDS (Anionic)	Sodium dodecyl sulphate	$\text{NaC}_{12}\text{H}_{25}\text{SO}_4$	288.37	

Nano-ZnO dispersion (50 wt. % in water) with an average particle size of 35 nm was procured from Sigma Aldrich (Buhler Inc.). Table 2.5 shows the details of the filler dispersions used.

Table 2.5: Details of the filler dispersions used

Filler used	Details
Nano silicon dioxide dispersion (silica dispersion)	Silicon dioxide, alumina doped nanoparticles dispersion (20 wt.% in water) 99.99% trace metal basis.
Nano titanium dioxide dispersion (titania dispersion)	Titanium (IV) oxide, mixture of rutile and anatase (33-37 wt.% in water) 99.9% trace metal basis.

Modified corn starch was supplied by Jemsons Starch and Derivatives, Aroor, Kerala, India. The characteristics of modified corn starch used is given in Table 2.6.

Table 2.6: Characteristics of modified corn starch

Appearance	Pale white powder
Moisture content	6%
pH	12.4
Solubility	Fully soluble

Coarse low-density flake graphite (Grade 3780) obtained from Asbury Carbons, United States was used for the preparation of graphene derivatives (exfoliated graphene oxide and reduced graphene oxide). The specification of the graphite used is shown in Table 2.7.

Table 2.7: Specifications of graphite used

Carbon	98.6%
Sulphur	0.058%
Size	1/8" x 0 mesh
Bulk density	21.56 (g/100 ml)
Resistivity	0.0334 Ω cm

Zinc oxide used in this study was white seal grade supplied by Sumit chemicals Pvt. Ltd., Kanpur, India. Details of the zinc oxide used are given in Table 2.8. Disodium methylene *bis*-naphthalene sulphonate (Dispersol F) used was from ICI limited, Calcutta, India.

Table 2.8: Details of zinc oxide

Product name	Physical form	Solubility in water (%)	Bulk density (g/cc)
Zinc oxide active	Fine powder	Up to 1	0.5-0.6

High performance inert Al₂O₃ ceramic balls with different sizes *viz.* 6.35 mm (small), 12.7 mm (medium) and 19.05 mm (large) in diameter were used for ball milling. The specifications of the balls are shown in Table 2.9.

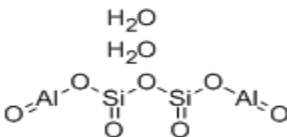
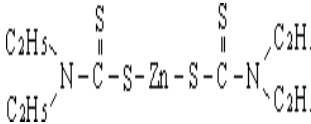
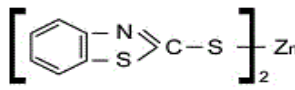
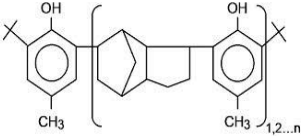
Table 2.9: Specifications of the balls used

Balls used	High performance inert Al ₂ O ₃ ceramic balls
Composition	SiO ₂ + Al ₂ O ₃ (9%) + others
Water absorption	0.03%
Density	2.8
Hardness	7.5 mohs
Properties	High mechanical strength, resistance to abrasion, chemically non-reactive, low coefficient of thermal expansion.

2.4 Compounding ingredients

Details of latex compounding ingredients are shown in Table 2.10.

Table 2.10: Details of latex compounding ingredients

Ingredients	Molecular weight	Water solubility	Structure
China clay	258.2	0.1% max.	
Zinc diethyl dithiocarbamate (ZDEC)	361.91	Insoluble	
Zinc 2-mercapto benzothiazole (ZMBT)	397.9	Insoluble	
Butylated reaction product of p-cresol and dicyclopenta diene (Wingstay L)	650 (Avg.)	Insoluble	

2.5 Characterization

2.5.1 Dynamic light scattering (DLS)

Particle size of materials in the nano-size range was performed in a particle size analyzer (Zetasizer Nano S, Malvern, UK) using dynamic light scattering (DLS) technique. Micron sized particle analysis, specific surface area and cumulative size distributions of dispersions were

measured using a particle size analyzer (Mastersizer 3000, Malvern, UK) by dynamic light scattering (DLS) technique.

Dynamic light scattering (DLS) is a non-invasive, well-established technique for measuring the size of particles and macromolecules typically in the submicron region. It can be used to measure size of samples which consist of particles suspended in a liquid *e.g.* proteins, polymers, micelles, carbohydrates, nanoparticles, colloidal dispersions, and emulsions. The particle size has a direct influence on material properties such as stability of suspension, appearance, flowability and handling, packing density and porosity, viscosity, reactivity *etc.* [1].

The basic principle of DLS is that, particles in suspension undergo Brownian motion caused by thermally induced collisions between the suspended particles and solvent molecules. If the particles are illuminated with a laser, the intensity of the scattered light fluctuates over very short intervals at a rate that is dependent upon the size of the particles; smaller particles are displaced further by the solvent molecules and move more rapidly. Analysis of these intensity fluctuations yields the velocity of the Brownian motion and hence the particle size using the Stokes-Einstein relationship.

The diameter measured in dynamic light scattering is called the hydrodynamic diameter and refers to the way a particle diffuses within a fluid. The diameter obtained by this technique is that of a sphere that has the same translational diffusion coefficient as the particle being measured.

2.5.2 Zeta potential

Zeta potential was measured by a Zetasizer (Nano Z, Malvern, UK) at 25⁰C. The magnitude of the zeta potential gives an indication of the stability of the suspension. A good suspension will not sediment quickly and will have long shelf-life. If all the particles in the suspension have a large negative or positive zeta potential then they will tend to repel each other and there will be no tendency for the particle for aggregation/agglomeration. If the particles have low zeta potential values then there will be no force to prevent particles coming together and flocculating.

A powder dispersion in water is considered stable when the zeta potential is greater than +30 mV or less than -30 mV. Problems with dispersion stability would arise at pH values between 4 and 7.5 as the zeta potential values are between +30 and -30mV [2].

2.5.2.1 Determination of stability of dispersion

Sedimentation test was used to examine the stability of wet ball-milled dispersions after different milling intervals. Around 1-2 g of dispersions wet milled at various intervals were added to about 20 ml distilled water taken in a measuring vessel. The depth of sedimentation column was recorded after 24 h. Higher the length of the column; the better will be the stability of the dispersions. The sedimentation percentage of aqueous dispersions was determined by the following equation:

The sedimentation percentage of aqueous dispersions

$$= \frac{H}{H_0} \times 100(\%) \quad \dots\dots\dots (2.1)$$

where H (cm) is the length of the sedimentation column and H₀ (cm) is the total length of suspension [3]. Higher the magnitude better will be the dispersion stability.

2.5.3 XRD

The X-ray diffraction (XRD) of ZnO nano particles were recorded on PANalytical X'pert machine with Cu-K α radiation ($\lambda=1.54056\text{\AA}$). The mean grain size (D) of the particles was determined from Scherrer equation [4].

Wide angle and small angle 2D-X-ray scattering were measured using Xeuss simultaneous WAXS/SAXS instruments. Cu-K α is the X-ray source with collimated area of 0.64 mm². Silver behenate is used for distance calibration. 2D-X-ray scattering data were azimuthally integrated using Fit-2D software. The hydrolyzed starch samples were placed in a sample holder of the machine for X-ray measurements.

2.5.4 FT-IR

FT-IR spectra were recorded on a FT-IR spectrometer (Varian 660-IR model - USA) in the wavelength range 400 - 4000 cm⁻¹.

2.5.5 SEM

Scanning Electron Microscopy (SEM) analysis of hydrolyzed starch sample was performed using a SEM machine (Zeiss Evo 18 Cryo) with variable pressure working at 15-30 kV.

2.5.6 TEM

TEM images were taken on HRTEM machine (Model tecnai G² F30, Netherlands) operating at an accelerating voltage of 300 kV. HRTEM of graphene dispersions was carried out in Jeol/JEM 2100 operated with a voltage of 200 kV having a magnification capacity of 2000 – 1500000 x. Graphene dispersions were drop casted on carbon coated copper grid 300 mesh (manufacture company - Electron microscopy sciences). Excess sample on the copper grid were washed out and allowed to dry for 15 minutes under infrared lamp and taken for TEM imaging.

Transmission electron microscope (TEM) is a microscopic technique in which the beam of electrons is transmitted through an ultra-thin specimen. An image is formed when the beam of electrons are transmitted through the specimen.

The main components of a basic TEM are vacuum system, electron gun, electron lens, apertures, specimen stage and an imaging system which can be either a fluorescent screen or a CCD camera.

Sample preparation in TEM is a complex procedure. The sample should be the size of below 3mm and a few hundreds to nanometers thin. The sample can be prepared by the dispersion in a solvent (powder samples), or sectioning (of plastic embedded biological specimens and polymers) with ultramicrotome (with or without cryo attachment).

Metallic, ceramic and semiconductor samples were prepared by mechanical milling, simple grinding, ion milling *etc.*

The main parts of TEM are shown in Figure 2.1.

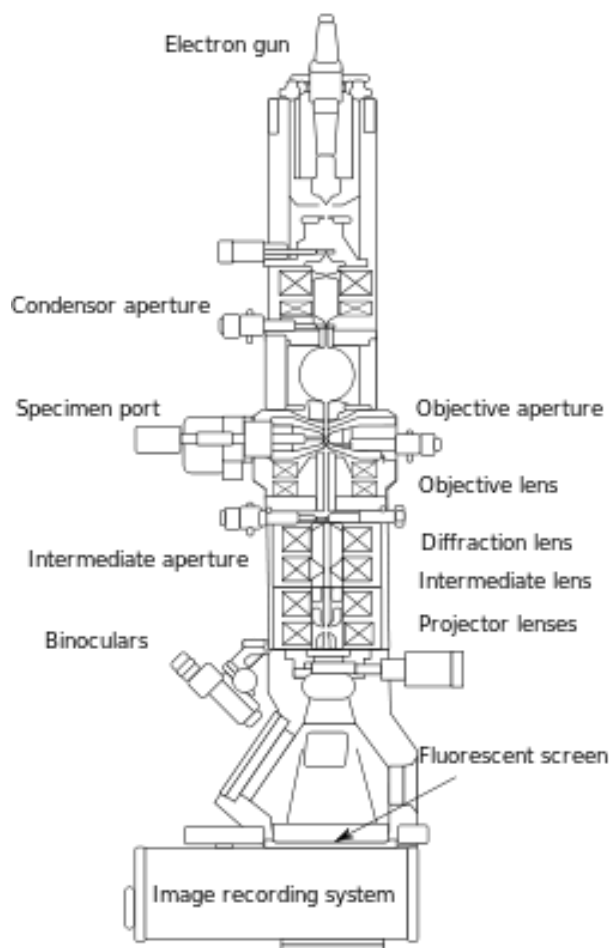


Figure 2.1: The main parts of TEM

2.5.7 Raman analysis

Raman spectroscopy is one of the most powerful analytical techniques in materials science research. It can be used to rapidly characterize the chemical composition and structure of a sample, whether solid, liquid, gas, gel, slurry or powder.

High resolution Raman spectrometer (Horiba JY) band analysis with a resolution in the order of $0.3 - 1 \text{ cm}^{-1}$ was used to record the Raman spectra of XGO and RGO. Ar ion laser operating at 514 nm was used for this purpose.

2.5.8 AFM analysis

AFM analysis of RGO was measured with a WITec Alpha 300RA, GmbH using tapping mode by drop casting on a glass substrate. The scan area was $5 \mu\text{m} \times 5 \mu\text{m}$.

2.5.9 UV-visible spectra

The UV-visible spectra of XGO and RGO were recorded on Spectro UV-VIS double beam spectrometer (model UVD-3500) of Labomed Inc., Los Angeles, CA.

2.5.10 TG-DTA studies

Thermogravimetric analysis is a branch of thermal analysis in which the change in mass (weight) of a substance is measured with respect to temperature. This can be carried out in air or inert atmosphere and the weight is recorded as a function of increasing temperature.

Thermogravimetric analysis of nano ZnO was carried out on a Perkin Elmer TGA 4000 model machine under N_2 atmosphere at a heating rate of $10 \text{ }^\circ\text{C}/\text{min}$. in the temperature range $30 - 900 \text{ }^\circ\text{C}$.

2.6 Degradation studies

2.6.1 Thermal ageing

The thermal stability of latex vulcanizates were studied by heating the specimens in a hot air circulated oven at 70 °C for 7 days. Dumb-bell shaped specimens were punched and mechanical properties were measured thereafter.

2.6.2 UV ageing

For UV degradation studies, radiation from a UV chamber (PHILIPS TLD 30W Holland) was used. The UV source used consists of two fluorescent tubes each having a capacity of 15W. The dumb-bell shaped specimens were kept on a glass plate which is fixed at the middle of the chamber horizontally with the radiation source. Both the sides of the samples were simultaneously exposed to the UV radiation for about 48 h. The mechanical properties of UV aged latex films were measured thereafter.

2.6.3 Chlorination

Chlorination was carried out in a closed vessel by immersing the latex films in 0.1 per cent chlorine solution for 3 min. After chlorination the product was washed in dilute ammonia solution (1%) and thereafter in water and then dried. The mechanical properties of the films were measured thereafter.

2.6.4 Gamma ageing

Dumb-bell shaped test specimens were irradiated with γ -rays from a ^{60}Co radiation source. The samples were irradiated to different levels

i.e. 30, 50 and 100 kGy. The dose rate was 1.06 kGy/h in air at room temperature. The mechanical properties of the gum and the composite films were measured after irradiation.

2.7 Properties of latex vulcanizate

2.7.1 Viscosity

Viscosity measurements were performed at 25°C (ASTM D 2526-229) using a Brookfield viscometer (LVT Model, Brookfield Laboratories, Stoughton-USA).

Around 200 ml of latex compound was taken in a beaker. The spindle (spindle no. 2) is attached to the viscometer and immersed into the latex compound. Dip the spindle to the compound up to the mark. The spindle is then allowed to rotate at a speed of 60 rpm to obtain reading. This value multiplied by 5 (multiplication factor) is expressed as viscosity in cPs.

2.7.2 pH meter

Mettler Toledo AG digital pH Meter (Switzerland) was used to record the pH of latex samples.

2.7.3 Chloroform number

The extent of vulcanization was assessed from the chloroform number. A portion of latex sample was mixed with equal volume of chloroform and after 2 minutes the coagulum was examined and graded. The grading is shown in Table 2.11.

Table 2.11: Grading of vulcanized latex as per chloroform number

Chloroform number	Nature of coagulum
1	Tacky mass and break in a stringy manner when stretched
2	Weak lump which breaks upon stretching
3	Non-tacky agglomerates
4	Small dry crumbs

2.7.4 Equilibrium swelling and crosslink density

For swelling studies, circular samples having a diameter of 2cm were cut from the vulcanized film using a circular die. Initial weights of the samples were noted. The films were immersed in toluene and were taken at various intervals of time and weighed again after removing the solvent from the surface of the samples using blotting paper. This procedure was continued until no more solvent uptake by the polymer was noted. The amount of solvent absorbed at various time intervals was measured and graphs were plotted.

The volume fraction of rubber (V_r) was determined by equilibrium swelling in toluene at 30°C by Ellis and Welding [5] method.

$$V_r = \frac{(D - FT)\rho_r^{-1}}{(D - FT)\rho_r^{-1} + A_0 \rho_s^{-1}} \dots\dots\dots(2.2)$$

Where D is the de-swollen weight, F is the weight fraction of the filler, A_0 is the solvent absorbed, T is the sample weight, ρ_r is the density of rubber (0.92) and ρ_s is the density of the solvent (0.866).

The swelling index was determined by immersing a small portion of the composite film in toluene for 48 h and measuring the increase in the weight.

The swelling index can be calculated using the equation:

$$\text{Swelling index } (Q) = \frac{W_2 - W_1}{W_1} \dots\dots\dots(2.3)$$

where W_1 and W_2 are the initial and swollen weights of the latex films respectively.

The variation of swelling index for vulcanized natural rubber specimens can be broadly classified as follows: unvulcanized (>15), lightly vulcanized (7-15), moderately vulcanized (5-7) and fully vulcanized (< 5) [6].

The crosslink density was determined using Florey-Rehner equation [7].

$$\nu = \frac{1}{2M_c} \dots\dots\dots(2.4)$$

$$M_c = \frac{-\rho_r V_s \phi^{1/3}}{\ln[1 - \phi] + \phi + \chi\phi^2} \dots\dots\dots(2.5)$$

where M_c is the molecular weight between the cross-links.

ρ_r is the density of the polymer, V_s is the molar volume of solvent (106.2868) and χ is rubber-solvent interaction parameter (0.391).

Volume fraction of rubber ϕ can be calculated as follows:

$$\phi = \frac{D_w/\rho_r}{(D_w/\rho_r) + (S_w - D_w)/\rho_s} \dots\dots\dots (2.6)$$

Where S_w is swollen weight, D_w is deswollen weight and ρ_s is density of solvent.

2.7.5 Sorption studies

Circular specimens having 2 cm in diameter were cut from the film and immersed in toluene up to 48h. The solvent absorption was periodically monitored and the swelling index at various intervals was calculated using the equation:

$$Q (\%) = \frac{W_t - W_0}{W_0} \times 100 \dots\dots\dots (2.7)$$

where W_0 and W_t are the weight of the films before and after an immersion time of 't'.

The toluene uptake (TU %) and sorption coefficient (S) of composite samples were calculated using the equations. [8].

$$TU (\%) = \frac{m_t - m_0}{M_w \times m_0} \times 100 \dots\dots\dots(2.8)$$

$$S (\%) = \frac{M_\infty}{M_0} \times 100 \dots\dots\dots (2.9)$$

where m_0 and m_t are the weights of the samples before and after immersion at time t and M_w is the molecular weight of toluene (92.14 gmol^{-1}). M_0 and M_∞ are the initial mass of the polymer film and mass of the solvent adsorbed at equilibrium.

2.7.6 Mechanical properties

The mechanical properties of the composite films are measured using a Zwick universal testing machine (Model 1474) according to ASTM D 412.

The percentage retention in tensile strength was calculated as follows [9]

$$\text{Tensile strength retention (\%)} = \frac{\text{Tensile strength after ageing}}{\text{Tensile strength before ageing}} \times 100 \dots (2.10)$$

Tear strength of samples was measured according to ASTM D-624.

Tension set was measured as per IS 4148. Tensile specimens having 40 mm length and 6 mm width were punched out and extended up to five times to its length (200 mm) on Instron 4411 machine and kept for 10 minutes. The samples were released and kept on a flat surface at room temperature for 10 minutes to attain equilibrium and measured the change in length.

All mechanical tests were carried out at 27 °C.

2.7.7 Electrical properties

The electrical conductivity of the composite films was measured by a two-probe technique. The cut specimens having dimensions (1.3cm x 1.3cm) were kept between two copper plates and a constant voltage of 6V from a DC source (Systronics Model 615 D) is applied and the current flowing through them was monitored using a digital multimeter (Fluke 187). The conductivity of the sample was measured using the following equation

$$\sigma = \frac{t}{RA} \dots\dots\dots(2.11)$$

where t is the thickness of the specimen, A is the area of cross-section of the sheet and R is the resistance of the film. R can be calculated using the equation

$$R = \frac{E}{I} \dots\dots\dots(2.12)$$

where E is the applied voltage and I is the current passing through the specimen.

2.7.8 Morphology

The optical images of the nanocomposites were taken on Wild Heerbrugg (M8) zoom stereomicroscope (Switzerland) connected with Leica digital camera (model DFC 320), Germany.

2.8 Theoretical modelling

The relative moduli of the films were predicted using the following theoretical models and compared with the experimental results [10-13].

Einstein equation

$$E' = E_0 (1 + 2.5c) \dots\dots\dots(2.13)$$

Guth equation

$$E' = E_0 (1 + 2.5c + 14.1c^2) \dots\dots\dots (2.14)$$

Brinkman equation

$$E' = E_0 (1-c)^{-5/2} \dots\dots\dots(2.15)$$

Ponte Castaneda equation

$$E' = E_0 / (1-3c) \dots\dots\dots(2.16)$$

where E_0 and E' represents modulus of gum and filled samples respectively and ‘ c ’ indicates filler fraction.

Halpin Tsai model is an effective tool to predict the mechanical properties of filled composites. The orientation of filler particles in the polymer matrix can be effectively predicted using this model. The modulus of randomly oriented RGO (E_r) and unidirectionally oriented RGO (E_u) in RVNRL matrix can be calculated [14].

$$E_r = E_m \left[\frac{3}{8} \left(\frac{1 + \eta_L \xi V_g}{1 - \eta_L V_g} \right) + \frac{5}{8} \left(\frac{1 + \eta_T V_g}{1 - \eta_T V_g} \right) \right] \dots\dots(2.17)$$

$$E_u = E_m \left[\frac{(1 + \eta_L \xi V_g)}{(1 - \eta_L V_g)} \right] \dots\dots\dots(2.18)$$

$$\eta_L = \frac{\left[\left(\frac{E_g}{E_m} \right) - 1 \right]}{\left[\left(\frac{E_g}{E_m} \right) + \xi \right]} \dots\dots\dots(2.19)$$

$$\eta_T = \frac{\left[\left(\frac{E_g}{E_m} \right) - 1 \right]}{\left[\left(\frac{E_g}{E_m} \right) + 2 \right]} \dots\dots\dots (2.20)$$

$$\xi = \left(\frac{2l_g}{3t_g} \right) \dots\dots\dots(2.21)$$

where l_g and t_g are the average length and thickness of RGO. V_g is the volume fraction of RGO. E_g is the Young’s modulus of RGO and E_m is

the M_{100} of the unfilled RVNRL. ξ is the shape fitting parameter and depends on filler geometry and orientation.

References

- [1] www.malvern.com, A basic guide to particle characterization.
- [2] Zetasizer nano series Technical Note.
- [3] E. Tang, G. Cheng, X. Ma, *Powder Technol.* **161**, 209 (2006).
- [4] L. Shen, N. Bao, K. Yanagisawa, K. Domen, A. Gupta, and C. A. Grimes, *Nanotechnology* **17**, 5117 (2006).
- [5] B. Ellis, and G. N. Welding, *Rubber Chem. Technol.* **37**, 571 (1964).
- [6] K. K. Sasidharan, R. Joseph, S. Palaty, K. S. Gopalakrishnan, G. Rajammal, and V. Pillai, *J. Appl. Polym. Sci.*, **97**, 1804 (2005).
- [7] Flory and Rehner, *J. Chem. Phys.* **11**, 521 (1943).
- [8] D. LeCorre, J. Bras, and A. Dufresne, *Macromol. Mater. Engg.* **297**, 969 (2012).
- [9] S. Mathew, S. Varghese, and R. Joseph, *Prog. Rubber Plastics and Recycl. Technol.* **29**(1), 1 (2013).
- [10] A. R. Payne, Dynamic properties of filler-loaded rubbers in reinforcement of elastomers G. Kraus (Ed.) Inter Science Publishers **1965** chapter 3.
- [11] J. S. Bergstrom, and M. C. Boyce, *Rubber Chem. Technol.* **72**, 633 (1999).
- [12] D. D. Nguyen, and K. M. Dinh, *Vietnam J. Mechanics*, *VAST* **34**(1), 19 (2012).
- [13] H. C. Brinkman, *J. Chem. Phys.* **20**, 571 (1952).
- [14] X. She, C. He, Z. Peng, and L. Kong, *Polymer* **55**, 6803 (2014).

.....✂.....

Chapter 3

PREPARATION OF DISPERSIONS BY BALL-MILLING: STATE- OF- THE- ART

Part A

Preparation of Ultra-Fine Dispersions of Zinc Oxide by Ball-milling: Optimization of Process Parameters

Part B

Effect of Ball Size on Milling Efficiency of Zinc Oxide Dispersions

Part C

Aqueous Dispersions of Latex Compounding Ingredients by Wet Ball-Milling: Effect of Ball Size and Milling Time on Dispersion Quality

Contents

PREPARATION OF ULTRA-FINE DISPERSIONS OF ZINC OXIDE BY SIMPLE BALL-MILLING: OPTIMIZATION OF PROCESS PARAMETERS

Contents	<i>3A.1 Introduction</i>
	<i>3A.2 Experimental</i>
	<i>3A.3 Results and Discussion</i>
	<i>3A.4 Conclusions</i>

Ultra-fine aqueous dispersions of zinc oxide (ZnO) were prepared by a combination of wet ball-milling and ultrasonication in presence of a surfactant (SA). The particles in the dispersions were characterized by dynamic light scattering (DLS) and zeta potential measurements. Six hours of ball-milling of the zinc oxide dispersion containing 3 wt. % SA followed by ultrasonication resulted in the formation of particles having size below 500 nm.

3A.1 Introduction

Stable colloidal dispersions of zinc oxide are in great demand for a broad range of products such as paints, dyes, cosmetics, pharmaceuticals, ceramics and micro-electronics. The annual worldwide demand of zinc oxide is about 1,200,000 metric tons [1]. Incorporation of fine particles of zinc oxide in rubber latex based formulations improves the strength of the product as a result of the improved homogeneity, solubility, and reactivity of the additive [2]. Addition of a suitable dispersant

*Part of work presented in this chapter has been published in **Powder Technology**, 271, 187-192, (2015).*

(surfactant) is one of the methods to improve the dispersability and stability of aqueous dispersions [3].

Wet ball-milling is one of the most economic and efficient techniques for the preparation of ultra-fine dispersions of particulate materials. This technique is also used for the blending of materials [4, 5]. Finely divided materials undergo spontaneous aggregation, adsorption and recrystallization in an activated system during grinding or after the grinding has been completed [6]. Homogenization, dispersion and stability are very difficult goals at submicron and nano-scales where the particles have a strong tendency to agglomerate and form larger structures [7]. Ultrasonication is commonly used for the disintegration of particle assemblies. A combination of ball-milling followed by ultrasonication may lead to stable dispersions with lower particle size [8].

Stabilization of colloidal dispersions of many metal oxide nano powders by electrostatic and steric methods has been reported [9, 10]. In electrostatic stabilization, charges generated at the surface of particles prevent the re-agglomeration of fine particles. Steric stabilization occurs when large molecules adsorb on to the surface of particles thereby providing a physical barrier between them. A combination of these two may stabilize the fine dispersions.

One of the objectives of the work reported in this chapter was to assess the stability of zinc oxide dispersions by zeta potential measurements. Zeta potential (ζ) is a function of the surface charge of the particles. A highly negative or positive ζ potential value (more than 30 mV or less than -30 mV) shows dispersions with reasonable stability [11].

Dry milling processes are the popular methods for the production of micro particles of materials. These dry particles agglomerate during the preparation of aqueous dispersions. To the best of the knowledge of the author, no research reports were reported regarding the production of ultra-fine dispersions of zinc oxide by simple wet ball-milling. The pioneering efforts to prepare and characterize the stable ultra-fine dispersions of zinc oxide by a combination of wet ball-milling and ultrasonication in presence of a surfactant is discussed in this chapter.

3A.2 Experimental

3A.2.1 Materials

The details of the ZnO used and its specifications are given in experimental section.

3A.2.2 Methods

Ball-milling (wet grinding) was performed in a stainless steel vessel having a capacity of 2.5 L (20.5 cm diameter x 15.5 cm height). Porcelain balls of 18-20 mm diameter were used as grinding media and the powder to ball weight ratio was maintained as 1:5. The mixture (formulations shown in Table 3A.1) was ball milled at 35 rpm so as to ensure the cascading action of the slurry inside the jar. The batch size of the dispersion was 500 g. Around 1-2 g samples were withdrawn at regular intervals of time (say 6, 12, 18, 24 and 30 h) for particle size analysis. Disodium methylene *bis*-naphthalene sulphonate (Dispersol F) was used as the surfactant. The SA was added along with the powder before starting the milling process. Particle size, size distributions and specific

surface area of the zinc oxide dispersion was measured using a particle size analyzer (Mastersizer 3000, Malvern, UK) by dynamic light scattering technique. Size distribution was determined as the average of three replicates. Aggregation of particles has been avoided by subjecting the samples to ultrasonication performed in a Vibra Cell ultrasonics (model VCX-750) at a frequency of 20 kHz having a power rate of 750W. The amplitude of vibration, time of ultrasonication and pulsation rate were recorded and are 45%, 15 minute and 10 sec. respectively. Ultrasonication of the particle dispersions were carried out in a water bath maintained at a constant temperature (28 °C). The stability of wet ball-milled zinc oxide dispersion was measured using a Zetasizer (Nano Z, Malvern UK) at 25 °C.

Table 3A.1: Formulations used for preparing zinc oxide dispersions

Ingredients	Parts by weight (%)		
	A	B	C
Zinc oxide	100	100	100
Dispersol F (SA*)	2	3	4
Water (Distilled)	198	197	196

*SA = Surfactant

The poly dispersity index or width of particle size distribution of the dispersion was expressed by span.

$$Span = \frac{[D(v,90)-D(v,10)]}{D(v,50)} \dots\dots\dots (3.1)$$

Where D (v, 90), D (v, 10) and D (v, 50) are the equivalent volume diameters at 90, 10 and 50 per cent cumulative volume respectively. A small span indicates a narrow size distribution [12].

3A.3 Results and Discussion

3A.3.1 Effect of milling time on volume weighed mean at various concentrations of surfactant

Volume weighed mean, $D [4, 3]$ is also known as the De Broucker Mean. $D [4, 3]$ is very relevant for many samples as it reflects the size of those particles which constitute the bulk of the sample volume. It is most sensitive to the presence of large particulates in the size distribution. The effect of concentration of SA on $D [4, 3]$ of ball-milled zinc oxide at various intervals of wet ball-milling is shown in Figure 3A.1.

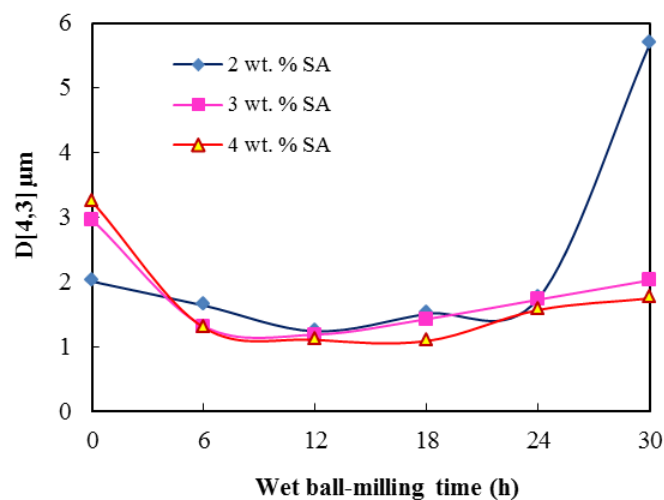


Figure 3A.1: Effect of wet ball-milling time on the volume weighed mean ($D [4, 3]$) of zinc oxide dispersions containing various concentrations of SA

As evident from the figure, irrespective of the concentration of the SA, the size of the zinc oxide particles is larger in all the cases. The particle size of zinc oxide decreases considerably in all the formulations after

6 hours of wet ball-milling. The particle size remained almost unchanged as the ball-milling was continued up to 18 h. The zinc oxide dispersions containing 3 and 4 wt. % of SA showed a gradual increase in D [4, 3] after 18 h of wet ball-milling. On the other hand, a sharp rise in D [4, 3] was observed in the case of the zinc oxide dispersion stabilized with 2 wt. % SA after 24 h of wet ball-milling. The sharp increase in particle size after 24 h of wet ball-milling is apparently due to the agglomeration of the zinc oxide particles as the low SA concentration (2 wt. %), is inadequate to prevent the interaction among the particles.

3A.3.2 Effect of surfactant on the specific surface area of zinc oxide

The specific surface area (SSA) of wet ball-milled zinc oxide dispersion with various concentrations of SA as a function of milling time is shown in Figure 3A.2.

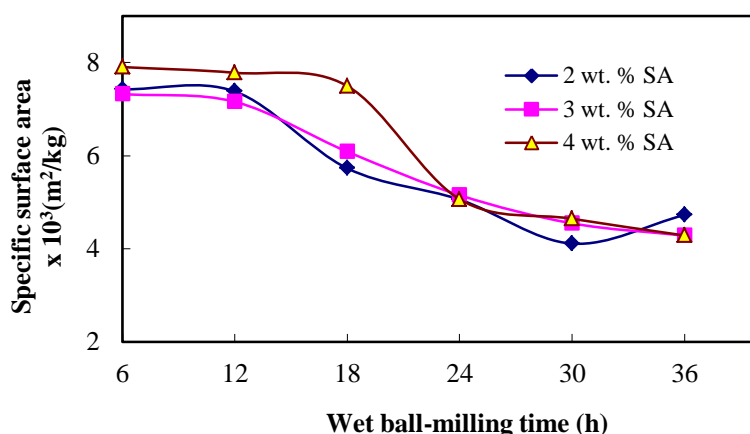


Figure 3A.2: Variation of specific surface area of zinc oxide dispersions with wet ball-milling time

For the first 12 h of ball-milling, SSA of zinc oxide stabilized with 2 and 3 wt. % of SA remains almost steady at 7377 and 7156 m²/kg respectively. After 12 h of ball-milling, there has been a marginal decline in SSA of zinc oxide irrespective of the concentration of SA. An interesting observation is that the SSA of zinc oxide stabilized with 2, 3 and 4 wt. % SA coincides after 24 h of ball-milling. The decrease in SSA after prolonged ball-milling indicates that the ultra-fine particles produced during extended period of milling leads to the aggregation of the particles. The size of the ultra-fine particles with high surface energies quickly increases to micro-scale range in water due to rapid particle collision, *Van der Waals* attraction, water bridging and high surface energy [13].

3A.3.3 Effect of the concentration of the surfactant on the size (%) of zinc oxide particles

The effects of wet ball-milling time (6, 12, 18, 24 and 30h) on the particle size of zinc oxide in the dispersions containing various concentrations (2, 3 and 4 wt. %) of the SA are shown in Figures 3A.3, 3A.4 and 3A.5.

The particle size distributions in each case are grouped into three discrete categories and designated as sizes below 500 nm (ultra-fine), sizes in between 500-1000 nm (fine), and sizes above 1000 nm (coarse). For convenience they can be designated as ultra-fine, fine and coarse particles.

In the case of the zinc oxide dispersion containing 2 wt. % SA (Figure 3A.3), 20 per cent of the particles were in the ultra-fine range

and 44 per cent of the particles were in the coarser range after 6 h of wet ball-milling. After 30 h of ball-milling the quantity of ultra-fine particles decreased to 3.5 per cent whereas the quantity of coarser particles increased to 74 per cent.

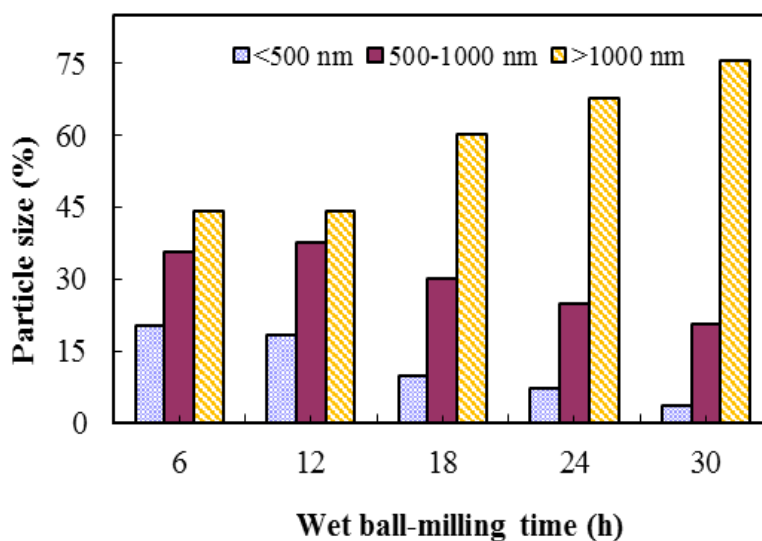


Figure 3A.3: Effect of wet ball-milling time on the size (%) of zinc oxide particles in aqueous dispersions containing 2 wt. % SA

After 6 h of wet ball-milling, 19 per cent of the particles were in the ultra-fine range and 45 per cent of the particles were in the coarser range in the case of the zinc oxide dispersion containing 3 wt. % SA (Figure 3A.4). After 30 h of ball-milling the quantity of ultra-fine particles decreased to 6 per cent whereas the quantity of coarser particles increased to 74 per cent.

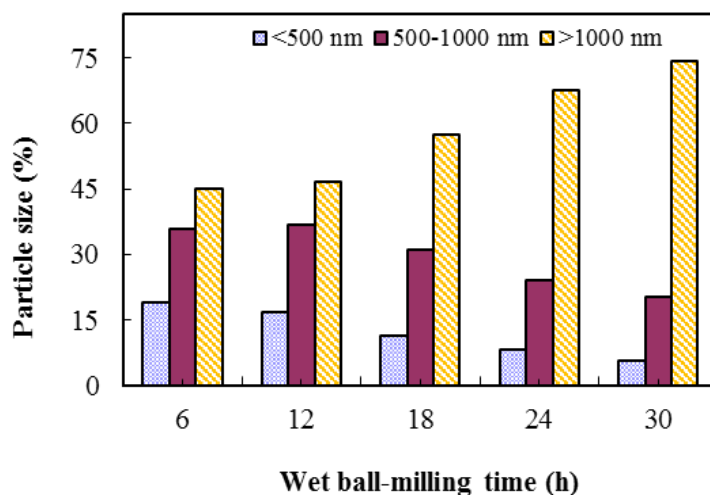


Figure 3A.4: Effect of wet ball-milling time on the size (%) of zinc oxide particles in aqueous dispersions containing 3 wt. % SA

In the case of the zinc oxide dispersion containing 4 wt. % SA (Figure 3A.5), the share of ultra-fine particles after 6, 12 and 18 h of wet ball-milling was 22, 20 and 18 per cent. As the milling time was increased to 24 and 30 h, the share of the ultra-fine particles decreased to 5 and 4 per cent. The share of coarser particles after 6 h and 12 h of milling was 41 per cent only and it increased to 44, 67, and 72 per cent respectively after 18, 24 and 30 h of milling.

The results cited above show that the portion of lower sized particles decreases as the milling time increases, irrespective of the concentration of the surfactant. Though prolonged milling is expected to decrease the average size of the particles, the reason for the reverse trend might be due to the agglomeration of particles. As the milling time increases apparently the cold welding mechanism (*i.e.*, the bond

formation between smaller particles) predominates over the expected fracturing mechanism. However up to a milling time of 6 h, the share of the lower particle size is maximum at all concentrations of the SA and thereafter it decreases gradually.

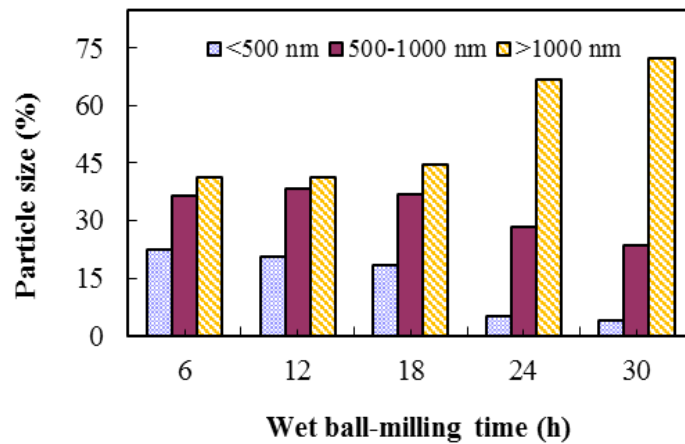


Figure 3A.5: Effect of wet ball-milling time on the size (%) of zinc oxide particles in aqueous dispersions containing 4 wt. % SA

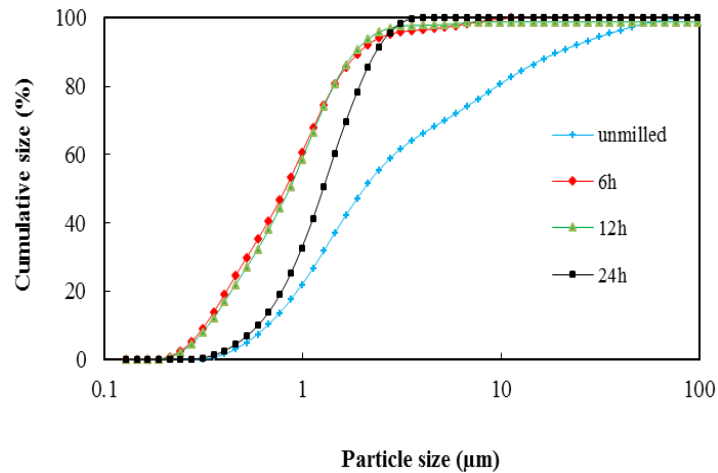


Figure 3A.6: Cumulative particle size distributions of unmilled zinc oxide and after 6, 12 and 24 hours of wet ball-milling with 4 wt. % SA

The cumulative particle size curves of unmilled zinc oxide and after 6, 12, 24 h of ball-milling with 4 wt. % of SA are shown in Figure 3A.6.

A shift in the curve towards left is observed after 6 h of milling indicating samples size reduction. A slight increase in size distribution was observed after 12 h of ball-milling. However, the shift of the curves towards right (increase in particle size) is more pronounced at higher milling time. Thus with the same concentration of the SA, prolonged ball-milling increases the size of the zinc oxide particles in the dispersion due to agglomeration.

A schematic representation of the changes in the particle size of zinc oxide during wet ball-milling is shown in Figure 3A.7.

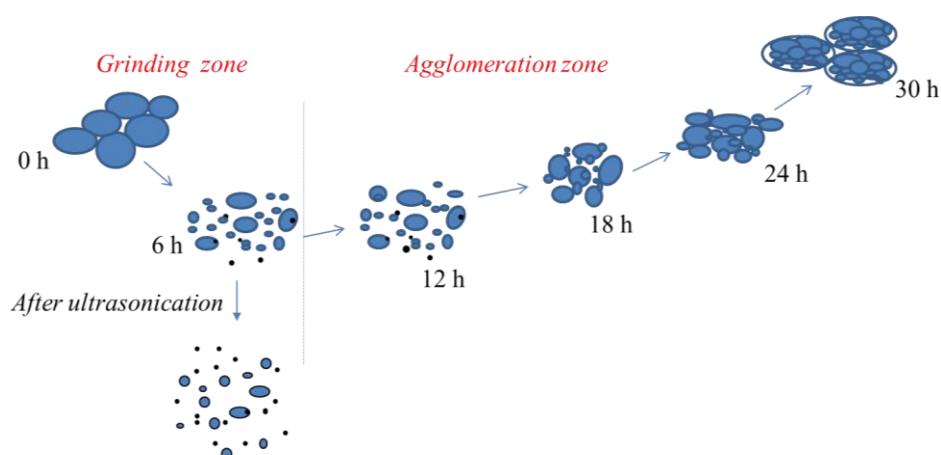


Figure 3A.7: Schematic diagram showing the formation of agglomerated (coarse) zinc oxide particles in aqueous dispersion upon prolonged wet ball-milling

The reduction in particle size is due to the formation of fresh surfaces during the course of grinding [14]. However, a slight increase in particle size was observed after 12 h of milling. The increase in particle size of zinc oxide after 12 h of ball-milling is expected to be due to the heat generation inside the milling vessel. As milling time increases the heat generated in the milling jar leads to the agglomeration causing an increase in the size of the particles [15] as evident from the decrease in specific surface area.

3A.3.4 Effect of ultrasonication

Ultrasonication is an effective tool for preparing aqueous dispersion of ultra-fine particles. Ultrasonic cavitation is very effective in breaking agglomerates and aggregates. When ultrasound is used for dispersing highly concentrated batches, the liquid jet streams resulting from ultrasonic cavitation make the particles collide with each other at velocities of up to 1000 km/h. This breaks the primary particles and the *Van der Waals* forces in agglomerates. Large particles are subjected to surface erosion (*via* cavitation collapse in the surrounding liquid) or particle size reduction (due to fission through inter-particle collision or the collapse of cavitation bubbles formed on the surface) [16].

3A.3.5 Effect of ultrasonication on the specific surface area of zinc oxide particles

The effect of ultrasonication on the specific surface area of wet milled zinc oxide dispersions with various concentrations of SA (2, 3 and 4 wt. %) is shown in Figure 3A.8.

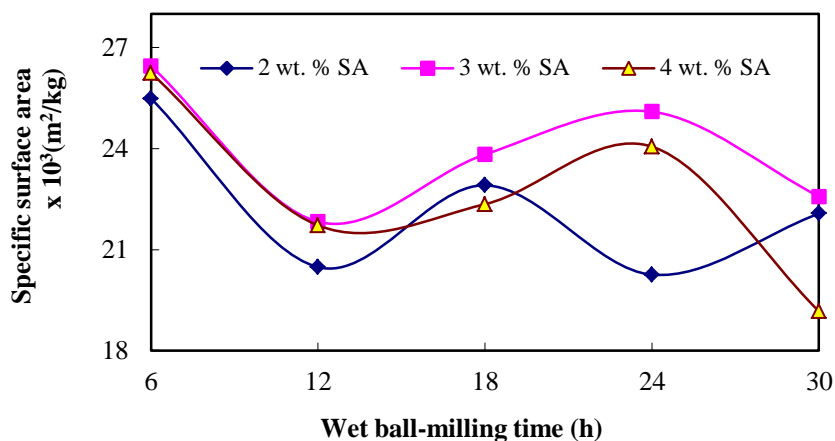


Figure 3A.8: Specific surface area of zinc oxide particles in aqueous dispersion after wet ball-milling followed by ultrasonication

The specific surface area of the particles in the ultrasonicated zinc oxide dispersions after 6 h of ball-milling with 3 and 4 wt. % SA are almost same whereas a reduction in SSA is observed with 2 wt. % SA. The decrease in SSA of the samples sonicated after 12 h of milling indicates re-agglomeration of the particles. The extent of agglomerate breakage depends on the nature of inter-particle bonds. Once agglomerates or aggregates are formed in a synthesis process it would be difficult to convert them back to their primary particles [9].

3A.3.6 Effect of ultrasonication on the size (%) of zinc oxide particles

A higher reduction in the size of the zinc oxide particles has been achieved by wet ball-milling followed by ultrasonication. Effect of ultrasonication on wet ball-milled zinc oxide dispersion containing 3 wt. % SA is shown in Figure 3A.9. Ultrasonication after 6 h ball-milling gave

88 per cent of the particles in the ultra-fine size range. However on ultrasonication after 30 h of wet ball-milling, the share of ultra-fine size zinc oxide particles in the dispersion decreased to 76 per cent.

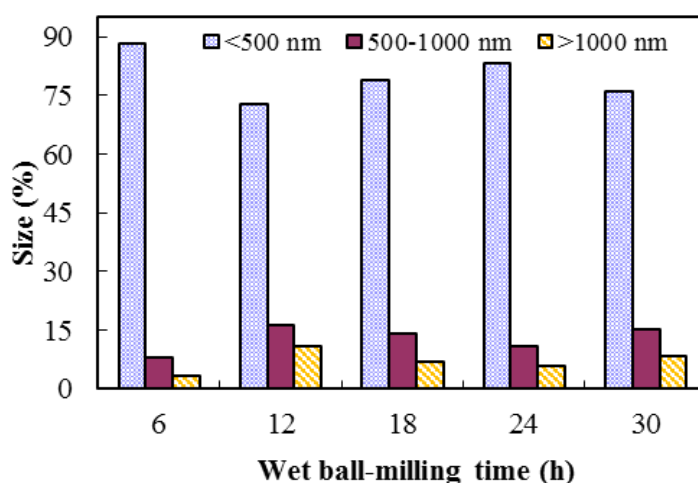


Figure 3A.9: Size (%) of zinc oxide particles in aqueous dispersions containing 3 wt. % SA after wet ball-milling for various durations followed by ultrasonication

3A.3.7 Effect of milling and ultrasonication on polydispersity

The polydispersity indices (span) of ball-milled zinc oxide stabilized with 2, 3 and 4 wt. % SA before and after ultrasonication are shown in Table 3A.2. A lower span value of 1.57 was observed for zinc oxide dispersion containing 3 wt. % SA after 6 h of ball-milling followed by sonication. This indicates that 6 h of ball-milling followed by sonication at a SA concentration of 3 wt. % is the ideal condition for the preparation of monodispersed zinc oxide suspensions. A broad span indicates highly polydispersed particles. Polydispersity index values greater than 2 are not desirable.

Table 3A.2: Polydispersity (span) of aqueous dispersions of zinc oxide containing 2, 3 and 4 wt. % SA

Milling time (h)	Span 2 wt. % SA		Span 3 wt. % SA		Span 4 wt. % SA	
	BS [†]	AS	BS	AS	BS	AS
6	2.30	1.72	1.89	1.57	1.90	1.65
12	1.78	3.70	1.59	3.11	1.66	2.99
18	1.69	2.41	1.60	2.35	1.59	2.95
24	1.70	2.43	1.68	1.89	1.40	2.14
30	2.09	2.85	1.61	2.6	1.39	2.91

[†]BS- Before ultrasonication

AS- After ultrasonication

3A.3.8 Variation of zeta potential with SA concentration

The colloidal stability and the evaluation of optimal dispersing conditions of zinc oxide dispersion after various wet ball-milling intervals were measured using zeta potential analysis. The criterion for surface stability is identified to be $|\zeta| > 30$. Figure 3A.10 shows the change in zeta potential with SA concentration at various milling intervals.

In all the cases, higher negative zeta potential values were observed for samples stabilized with 4 wt. % of SA. As the concentration of SA decreases, the value also decreases. Lowest zeta potential value of -28.4 mV was obtained after 24 h wet ball-milling with 2 wt. % of SA. The schematic representation shown along with Figure 3A.10 indicates the effect of concentration of SA on the particle-particle interaction. As the concentration of SA increases; particle-particle interaction decreases resulting in a stable dispersion. Thus, irrespective of the milling time, greater negative surface charges on zinc oxide particles in the aqueous dispersion can be achieved with 3-4 wt. % SA, which imparts better stability to the dispersion.

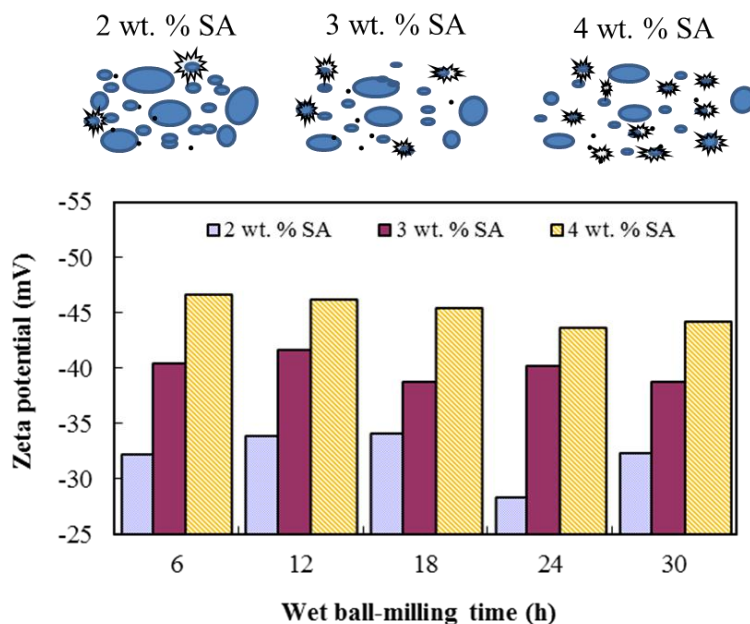


Figure 3A.10: Variation of the magnitude of zeta potential with SA concentration after various ball-milling intervals

3A.4 Conclusions

The particle size of zinc oxide in aqueous dispersions containing various concentrations of surfactant decreases considerably after 6 h of wet ball-milling. The decrease in specific surface area after prolonged ball-milling indicates that the ultra-fine particles produced during extended period of ball-milling leads to the aggregation of the particles. As the milling time increases apparently the cold welding mechanism predominates over the expected fracturing mechanism. A higher reduction in the size of the zinc oxide particles has been achieved by wet ball-milling followed by ultrasonication. The zeta potential value decreases as the concentration of the surfactant in the aqueous dispersion decreases.

References

- [1] J. Walter, *Tire Technology International*, p18 March (2009).
- [2] M. Asif Inam, S. Ouattara, and C. Frances, *Powder Technol.*, **208**, 329 (2011).
- [3] K. Gharanjig, F. Sadr Dadras, M. Sadeghi-Kiakhani, and S. Tafaghodi, *J. Disp. Sci. Technol.*, **34**, 381 (2013).
- [4] H. B. Fadhel, C. Frances, and A. Mamourian, *Powder Technol.*, **105**, 362 (1999).
- [5] V. Monov, B. Sokolov, and S. Stoenchev, *Cybernetics and Information Technologies*, **12**(2), 51 (2012).
- [6] M. K. Beyer, and H. Clausen-Schaumann, *Chem. Rev.* **105**(8), 2921 (2005).
- [7] C. Saliel, Q. Chen, S. Manickavasagam, L. S. Schadler, R. W. Siegel, and M. P. Menguc, *J. Nanoparticle Res.*, **6**, 35 (2004).
- [8] G. Mani, Q. Fan, S. C. Ugbolue, and I. F. Eiff, *Mater. Res. Soc. Symp. Proc.*, **740**, 113 (2003).
- [9] N. Mandzy, E. Grulke, and T. Druffel, *Powder Technol.*, **160**, 121 (2005).
- [10] S. G. J. Heijman, and H. N. Stein, *Langmuir*, **11**(2), 422 (1995).
- [11] www.malvern.co.uk (Technical Notes on Dispersion Stability and Zeta Potential).
- [12] O. Y. Toraman, *Particulate Sci. and Technol.*, **29**, 475 (2011).
- [13] C.P. Tso, C.M. Zhung, Y. H. Shih, Y. M. Tseng, S. C. Wu, and R. Doong, *Water Sci. Technol.- WST*, **61**(1), 127 (2010).
- [14] G. Du, Q. Xue, H. Ding, and Z. Li, *Ind. J. Engg. Mater. Sci.* **20**, 7 (2013).
- [15] M. Ramezani, and T. Neitzert, *J. Achievements Mater. Manu. Eng.* **55**(2), 790 (2012).
- [16] T. Hielscher, ENS'05, Paris, France, December (2005).

**EFFECT OF BALL SIZE ON MILLING EFFICIENCY OF
ZINC OXIDE DISPERSIONS**

Contents	<i>3B.1 Introduction</i>
	<i>3B.2 Experimental</i>
	<i>3B.3 Results and Discussion</i>
	<i>3B.4 Conclusions</i>

Zinc oxide (ZnO) was wet milled using inert Al₂O₃-ceramic balls having different diameter at various milling intervals and the milling efficiency of the resultant dispersion was followed through particle size analysis and zeta potential measurements. The results indicated that smaller sized balls improved the milling efficiency.

3B.1 Introduction

Ball-milling is a widely used technique for the size reduction of particles which may have different nature and have a wide diversity in physical and chemical characteristics [1-4]. In this technique, powder particles are trapped between colliding balls in a vial, which causes repeated deformation, re-welding, and fragmentation of powders resulting in the formation of fine, dispersed particles [5]. Ball-milling is a complicated process and are governed by several factors such as

*Part of work presented in this chapter has been published in **Particulate Science and Technology**, DOI: 10.1080/02726351.2016.1248258 (2016).*

ball size, ball to powder weight ratio, milling time, amount of dispersing agent and also of the jar rotation speed. The influence of grinding conditions in the preparation of fine particles produced by ball-milling was reported [6, 7].

Nano-ZnO is one of the multifunctional inorganic materials with broad range of applications. Preparation of stable dispersions of ultra-fine ZnO particles is a subject of interest among researchers. Preparation of ZnO dispersion using ball-milling has been studied extensively [5, 8-10]. The optimum milling conditions for the preparation of ultra-fine ZnO dispersions have been reported [11]. The aim of the present research work is to study the effect of balls having different diameters on wet milling of ZnO dispersion. The average particle size and stability of ZnO wet milled using different ball sizes as a function of milling time is also explored.

3B.2 Experimental

3B.2.1 Methods

A recipe consisting of 500 g ZnO, 10 g Dispersol F and 490 g water each were taken in three separate stainless-steel cylindrical vessels (ball mills) and milled for various durations (0.5, 6, 12, 18, 24 and 30 h). The ball sizes used in the three separate vessels were 6.35 mm, 12.7 mm and 19.05 mm. In all the cases, the ball to powder weight ratio has been 5:1 and the jar rotation speed was 35 rpm.

3B.2.2 Characterization

The average particle size of wet milled ZnO dispersion was measured at frequent intervals using a Mastersizer 3000 (Malvern Instruments - UK) particle size analyzer. Zetasizer (Nano Z, Malvern UK) was used to measure the zeta potential of the dispersions.

3B.3 Results and Discussion

3B.3.1 Effect of ball size on cumulative size distribution

Figures 3B.1(a, b and c) represents the cumulative distribution curves of particles of ZnO dispersions milled with balls having diameter 6.35, 12.7 and 19.05 mm respectively. From the Figure 3B.1a it is obvious that, smaller sized balls shift the curve towards the left side (*i.e.* particle size decreases). As the ball size increases, with increase in milling time, curve shift towards right side (particle size increases). Larger balls provide greater free volume in between the balls. This results in agglomeration of particles. Further, larger balls deliver low collision rate, as a result the bonding mechanism dominates over fracture mechanism [12]. However, irrespective of the ball size, 30 h of wet ball-milling generated larger particles. The results are in accordance with our earlier findings [11].

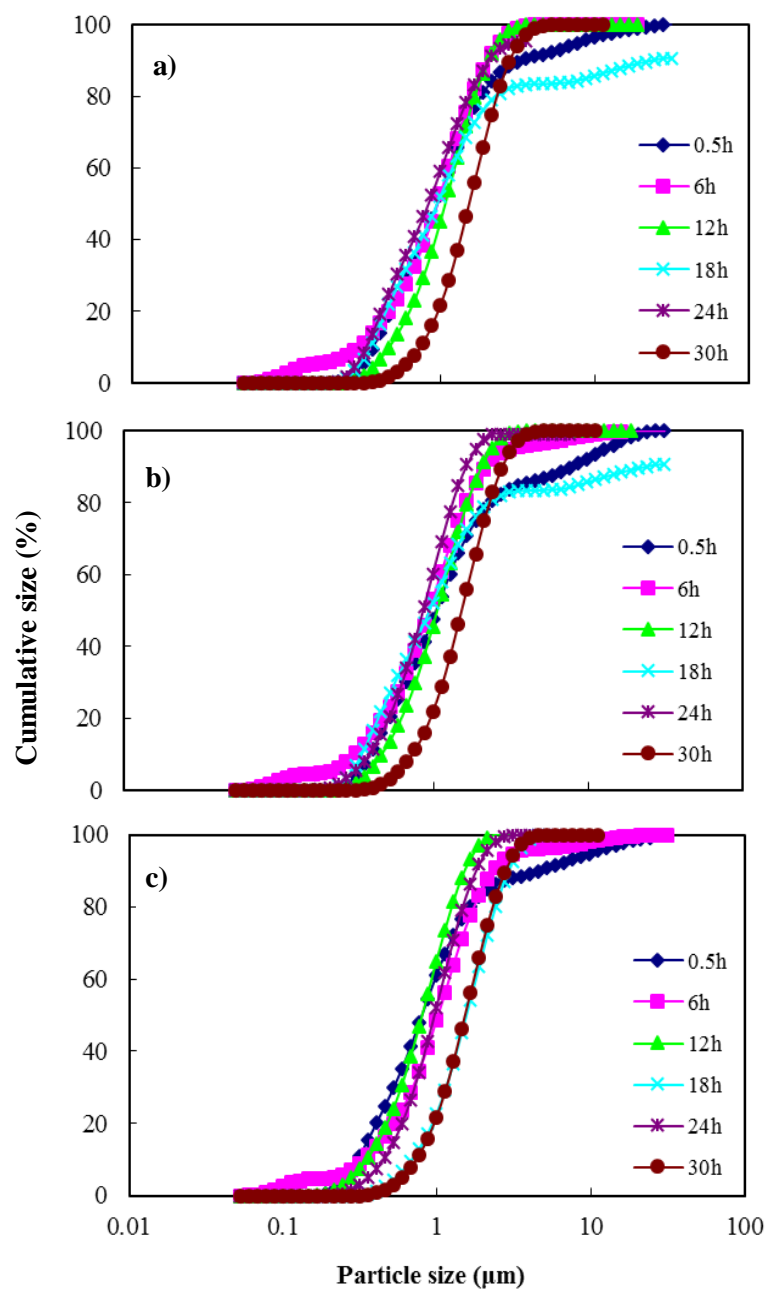


Figure 3B.1: Cumulative distribution curves of ZnO wet ball milled with a) 6.35 mm balls b) 12.7 mm balls and c) 19.05 mm balls

3B.3.2 Effect of ball size on specific surface area

The specific surface area of wet ball milled zinc oxide dispersion with different ball size as a function of milling time is shown in Figure 3B.2.

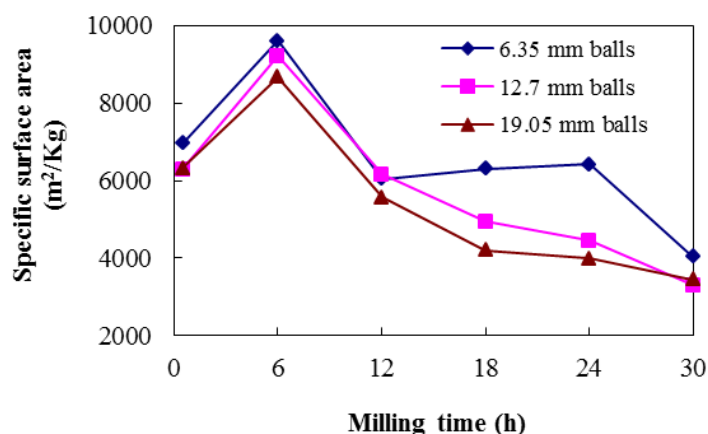


Figure 3B.2: The specific surface area of ZnO for varying ball size as a function of milling time

In the beginning of ball-milling (up to 6 h), irrespective of the ball size, sharp increase in SSA of ZnO was observed followed by a sharp decline. An increase in specific surface area of zinc oxide is observed after 18 and 24 h of wet milling with balls having 6.35 mm in diameter. However, irrespective of the ball size, reduction in SSA was observed after 30 h of milling. The decrease in SSA after prolonged ball-milling indicates that the ultra-fine particles undergo aggregation [11].

3B.3.3 Effect of ball size on D50

The average particle size (D50) of the wet milled ZnO dispersion is shown in Figure 3B.3 as a function of milling time for different ball

sizes. For the first 12 h of ball-milling no significant variation in mean particle size was noticed with ball size. The optimum size of 0.98 μm has been achieved after 24 h of ball-milling using 6.35 mm balls. Reduction of particle size would result an increase in the formation of fresh surfaces [15]. Reduction in particle size after 18 h of grinding with smaller sized balls indicates that the rate of formation of fresh surfaces is high compared to other cases. Further increase in milling time resulted an increase in particle size. This might be due to cold welding of particles caused by the repetitive shear forces [12]. In the case of 12.7 mm and 19.05 mm balls also, increase in D50 is observed after 18 h of milling.

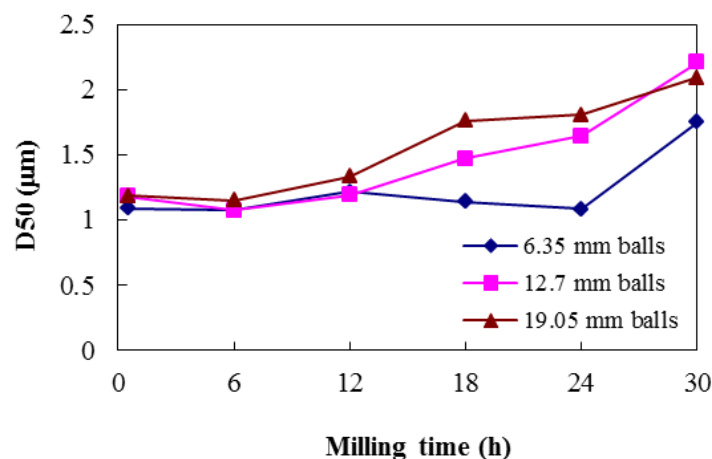


Figure 3B.3: Variation in the mean particle size (D50) of ZnO with the milling time for different ball sizes

When the particle becomes smaller, the milling efficiency decreases with increase in milling time [13]. As the milling process advances, the temperature goes up very fast and the impact of energy will not be enough to break down the particle. Results on mechanical

alloying of Al powder shows that it started to agglomerate when the milling time was increased up to 40 h [14]. From this result it can be said that the optimum milling time (24 h) for ZnO results in efficient milling, when the ball size is 6.35 mm in diameter.

3B.3.4 Effect of ball size on size (%) of ZnO

The size (%) of ZnO (particles having size $< 0.5 \mu\text{m}$) after milling with balls having different diameters is shown in Figure 3B.4. It can be seen that the size (%) of ZnO ball milled with 6.35 mm balls was high in comparison with balls having larger diameter (12.7 mm and 19.05 mm). The highest share of 23.4 per cent was achieved after 24 h of milling. Further increase in milling time resulted in a drastic reduction in the share of lower sized particles.

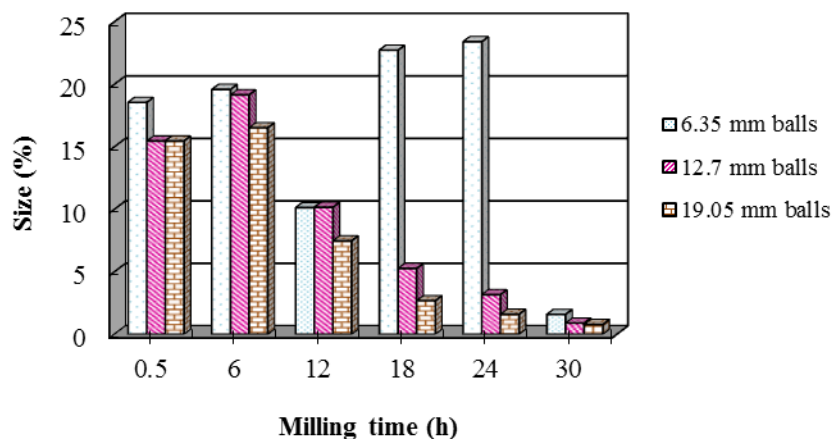


Figure 3B.4: Size (%) of ZnO (size $< 0.5 \mu\text{m}$) with milling time for different ball sizes

As the ball size decreases, more surfaces are generated and which results in more number of effective impacts. The particle breakage takes

place mostly at the contact sites of the balls. Hence, smaller balls possess a high milling efficiency because of the increased number of contact points between the balls [16]. The share of particles ball milled using 19.05 mm balls is low. Interestingly, after 6 h of wet milling of ZnO with balls having different diameters, the share of particles ball milled with 6.35 and 12.7 mm balls are almost same. This shows that, at lower milling time (up to 12 h), the effect of ball size on particle size reduction of ZnO is not much significant. Figure 3B.4 supports the result. However, increased milling time (18 h and 24 h) using balls with smaller diameters gave high share to lower sized particles showing effective impacts predominate over collision.

3B.3.5 Effect of ball size on stability of ZnO dispersions

The colloidal stability of wet ball milled ZnO with different ball sizes as a function of milling time is shown in Table 3B.1.

Table 3B.1: Magnitude of the zeta potential with ball sizes at various milling time

Milling time (h)	Zeta potential (mV)		
	6.35 mm balls	12.7 mm balls	19.05 mm balls
0.5	-40.4	-44	-42
6	-40.8	-39.8	-39.8
12	-39.1	-39.6	-39.3
18	-38.7	-37.2	-36.1
24	-36.8	-38	-35.6
30	-33.3	-35	-33.2

Zeta potential measurement brings detailed insight into the factors affecting the stability of dispersion, aggregation/flocculation *etc.* The zeta potential of ZnO wet ball-milled using different ball sizes did not change significantly. However, with increase in milling time, reduction in zeta value was observed in all cases. This indicates that the agglomeration tendency of the particles upon prolonged milling is high because the zeta potential values are low.

3B.4 Conclusions

ZnO was ball milled in aqueous medium using inert Al₂O₃-ceramic balls having different diameter (6.35, 12.7 and 19.05 mm) for different intervals (0.5, 6, 12, 18, 24 and 30 h) and the milling efficiency was analyzed. It was found that, small-sized balls increased the milling efficiency and it increases with increase in milling time. At lower milling time (up to 12 h), the average particle size (D50) of ZnO did not vary significantly with ball size. The highest share of lower sized particles (23.4 %) was achieved with 6.35 mm balls after 24 h of milling. The zeta potential of ZnO particles wet milled using different ball sizes was nearly the same.

References

- [1] M. A. Meitl, T. M. Dellinger, and P. V. Braun, *Adv. Functional Mater.*, **13**, 795 (2003).
- [2] L. C. Damonte, L. A. Mendoza Zelis, B. Marisoucase, and M. A. Fenollosa Hernandez, *Powder Technol.*, **148**, 15 (2004).
- [3] I. Ozdemir, S. Ahrens, S. Mucklich, and B. Wielage, *J. Mater. Process. Technol.*, **205**, 111 (2008).

- [4] B. S. Murty, and S. Ranganathan, *Intl. Mater. Rev.*, **43**, 101 (1998).
- [5] N. Salah, S. S. Habib, Z. H. Khan, A. Memic, A. Azam, E. Alarfaj, N. Zahed, and S. Al-Hamedi, *Intl. J. Nanomedicine*, **6**, 863 (2011).
- [6] N. Kotake, M. Kuboki, S. Kiya, and Y. Kanda, *Adv. Powder Technol.*, **22**, 86 (2011).
- [7] C. Wall, A. Pohl, M. Knapp, H. Hahn, and M. Fichtner, *Powder Technol.*, **264**, 409 (2014).
- [8] P. K. Giri, S. Bhattacharyya, Dilip K Singh, R. Kesavamoorthy, B. K. Panigrahi, and K. G. M. Nair, *J. Appl. Phys.* **102**, 093515 (2007).
- [9] S. Amirkhanlou, M. Ketabchi, and N. Parvin, *Mater. Lett.* **86**, 122 (2012).
- [10] A. Glushenkov, and Y. Chen, *Mater. Forum*, **30**, 1 (2006).
- [11] K. Anand, S. Varghese, and T. Kurian, *Powder Technol.*, **271**, 187 (2015).
- [12] N. Eom, M. H. Bhuiyan, T. S. Kim, and S. J. Hong, *Mater. Trans.*, **52**(8), 1674 (2011).
- [13] A. Johansson, "Correlation between process parameters and milling efficiency", Uppsala University Thesis, August 2012.
- [14] M. Ramezani, and T. Neitzert, *J. Achievements Mater. Manu. Engg.*, **55**(2), 790 (2012).
- [15] G. Du, Q. Xue, H. Ding, and Z. Li, *Ind. J. Engg. Mater. Sci.*, **20**, 7 (2013).
- [16] H. Shin, S. Lee, H. S. Jung, and J. B Kim, *Ceram. Intl.*, **39**, 8963 (2013).

**AQUEOUS DISPERSIONS OF LATEX COMPOUNDING INGREDIENTS
BY WET BALL-MILLING: EFFECT OF BALL SIZE AND MILLING TIME
ON DISPERSION QUALITY**

Contents	3C.1 Introduction
	3C.2 Experimental
	3C.3 Results and Discussion
	3C.4 Conclusions

Preparation of nanomaterials, their functionalization, evaluation and potential applications are active areas in materials science research. Preparation of ultra-fine/nano-sized particle dispersions and their stabilization is a great challenge among researchers where the high surface area and energy impedes the effective usage of nanomaterials. This study presents the effect of ball-milling on size and stability of aqueous dispersions of latex compounding ingredients (LCI) such as china clay, zinc diethyl dithiocarbamate (ZDEC), zinc 2-mercapto benzothiazole (ZMBT) and butylated reaction product of p-cresol and dicyclopentadiene (wingstay L). The particle size and stability were assessed through dynamic light scattering technique (DLS) and sedimentation test. By using lower sized balls for milling, the particle size of latex compounding ingredients can be reduced to a great extent.

*Part of work presented in this chapter has been published in **Transactions of the Indian Institute of Metals**, DOI: 10.1007/s12666-016-0957-x (2016).*

3C.1 Introduction

From the beginning of the era of nanoscience and nanotechnology, researchers are looking for the preparation of nano-sized materials through simple and easiest methods which are scalable commercially. Grinding is one of the most important operations used in chemical, pharmaceutical and food industries for the size reduction of materials [1]. Ball-milling is a technique used for particle size reduction. This technique could be applied for preparing dispersions and also for mixing of materials. The grinding or milling process is accompanied by the use of ceramic/steel balls along with the material to be comminuted in a cylindrical vessel or jar which rotates with a specific speed. Describing and understanding the milling process is very sophisticated because it is driven by several parameters like type of the mill, nature of milling (dry or wet), milling speed, ball size and type, ball to powder weight ratio, time of milling, temperature of milling *etc.* As the milling process advances, periodic fracture and coalescence of the particle continues [2]. The basic fragmentation mechanisms occurring in the comminution process includes: abrasion (occurs when low intensity stress is applied), cleavage (occurs when slow and relatively intense stresses are applied) and fracture (occurs by rapid application of intense stresses) [3]. In the long milling process, the lower sized particles generated undergoes agglomeration owing to its high specific surface area [4].

For the manufacture of latex based products, it is essential to add insoluble compounding ingredients to the latex as dispersions. Addition of ultra-fine/nano particle dispersions of compounding ingredients to the

latex results in products with superior quality and improved properties and can impart novel functionality to the product. Preparation of stable colloidal dispersions in the ultra-fine/nano size range is difficult because the particle will undergo agglomeration or flocculation. The degree of aggregation or agglomeration of the particles and the morphologies of agglomerated or aggregated structures dictate the final structure and subsequent properties (*e.g.*, solubility, mechanical strength, electrical and thermal conductivity, chemical affinity, *etc.*) [5].

Several researchers reported that the ball size used in a mill has a significant influence on the mill throughput, power consumption and the particle size of the material [6-8]. Effects of ball diameter on the crystalline size, induced strain, and atomic diffusion in Cu - 50 % Fe immiscible alloy system was investigated [9]. Recently, the effect of different ball size on particle size and stability of aqueous dispersions of zinc oxide by ball-milling has been attempted [10].

Use of smaller sized grinding media increases the milling efficiency and results in finer products having good quality. However, the main difficulty associated with the use of smaller ball size is the difficulty in discharging the mass from the milling vessel, especially for dry (powder type) materials. By reducing the grinding media size, the number of contact points between the charge and grinding media can be increased which results in improved shear and collision and are beneficial for particle size reduction.

The aim of the present work is to optimize the process parameters for the preparation of chemical dispersions of latex compounding ingredients *viz.* china clay, zinc diethyl dithiocarbamate (ZDEC), zinc 2-mercapto benzothiazole (ZMBT) and butylated reaction product of p-cresol and dicyclopentadiene (wingstay L). Effect of varying the ball size (6.35 mm, 12.7 mm, 19.05 mm and composite balls) and milling time on particle size and stability of aqueous dispersions of latex compounding ingredients were studied. Since most of the latex compounding ingredients are water insoluble, the study assumes greater importance for the latex based industry.

3C.2 Experimental

3C.2.1 Materials

Details of the chemicals (latex compounding ingredients) and balls used are given in experimental section [Table 2.10 & Table 2.9].

3C.2.2 Methods

Wet ball-milling was performed in a stainless steel vessel having a capacity of 2.5L (20.5cm diameter x 15.5cm height). The powder to ball-weight ratio was maintained as 1:5. Balls of different sizes (composite formulation) were configured in such a way that the free volume between the balls was minimum. The free volume was minimum for ball mixtures in the weight ratio 2:1:2 (large: medium: small). Free volume determination in a composite ball mixture has been explained later. Disodium methylene *bis*-naphthalene sulphonate (Dispersol F) was used as surfactant and has been added prior to start

the ball-milling. The concentration of dispersions was maintained at 30 per cent and the milling was carried out at 35 rpm. Samples were withdrawn at regular intervals of time (say 0.5, 3, 6, 9, 12, 15, 18, 24, 30 and 45 h). The first recording of particle size for each chemical was carried out after 30 min. of ball-milling. Particle size, specific surface area and cumulative size distributions of dispersions were measured using a particle size analyzer (Mastersizer 3000, Malvern, UK) by dynamic light scattering technique. Sedimentation test was used to examine the stability of wet ball-milled dispersions after different milling intervals.

3C.2.3 Free volume determination

For every ball sizes (say 6.35 mm) the free volume was measured after fully immersing a definite quantity of balls in a beaker with water. The weight of water is equivalent to the available free volume between the balls of a particular size. For composite ball system, different ball combinations were taken and the one having the minimum free volume was selected. It might be pointed out here that lower the free volume, higher was the grinding efficiency.

3C.2.4 Determination of stability of dispersion

Around 1-2g of each ingredients wet milled at various intervals (0.5, 3, 6, 9, 12, 15, 18, 24, 30 and 45 h) with different ball sizes (6.35 mm, 12.7 mm and 19.05 mm) were added to about 20 ml distilled water taken in a measuring vessel. The depth of sedimentation column was recorded after 24 h. Higher the length of the column; better the stability

of the dispersions. The sedimentation percentage of aqueous dispersions was determined by the following equation:

$$\text{Sedimentation (\%)} = \frac{H}{H_0} \times 100$$

where H (cm) is the length of the sedimentation column and H₀ (cm) is the total length of suspension [11]. Higher the magnitude better the dispersion stability.

3C.3 Results and Discussion

3C.3.1 Effect of ball size and milling time on D [4, 3]

The size of the particles which constitute the bulk of the dispersion volume is known as De Brouker Mean and is represented by D [4, 3]. It also gives an idea about the presence of larger particles in the size distribution. The D [4, 3] of wet-milled china clay with balls of different sizes (6.35 mm, 12.7 mm, 19.05 mm and their combination) at various milling intervals are shown in Figure 3C.1. D [4, 3] of china clay decreases with increase in milling time. Particle size (D [4, 3]) of unmilled (0 h milling) china clay was 5 μm and after 45 h of milling with 6.35 mm, 12.7 mm and 19.05 mm balls, it decreases to 1.68, 2.5 and 2.88 μm respectively. As the ball size increases, the free volume between the balls increases which resulted in particles with higher sizes. The combination of balls in definite proportions reported a particle size of 2.09 μm.

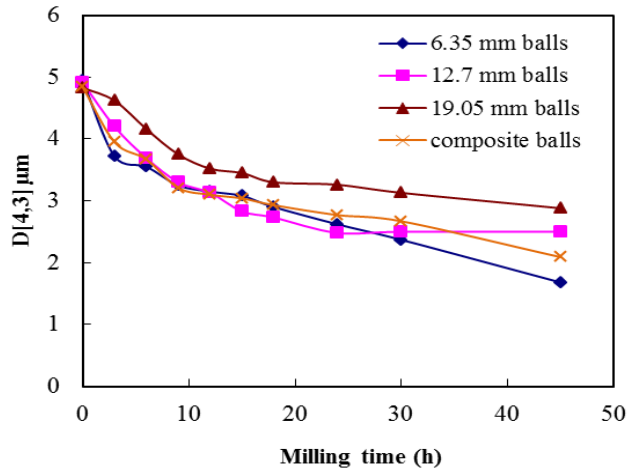


Figure 3C.1: Effect of ball size on D [4, 3] of china clay dispersions with milling time

Figure 3C.2 shows the effect of ball size and milling time on D [4, 3] of ZDEC. For unmilled ZDEC, the D [4, 3] was 17 μm and irrespective of the ball size, a sharp reduction was observed after 6 h of ball-milling and thereafter a gradual reduction in size was observed.

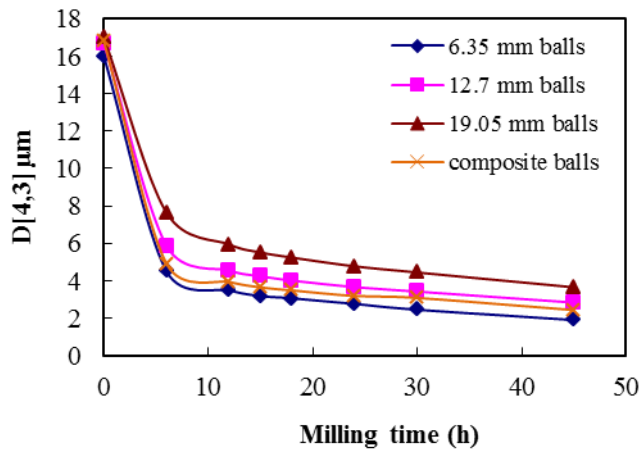


Figure 3C.2: Effect of ball size on D [4, 3] of ZDEC dispersions with milling time

The lowest size of 1.9 μm was observed after 45 h of milling with 6.35 mm sized balls whereas with 12.7 mm, 19.05 mm and composite balls, the sizes are 2.83, 3.65 and 2.43 μm respectively.

The D [4, 3] profile of ZMBT looks similar to that of ZDEC. The results are shown in Figure 3C.3.

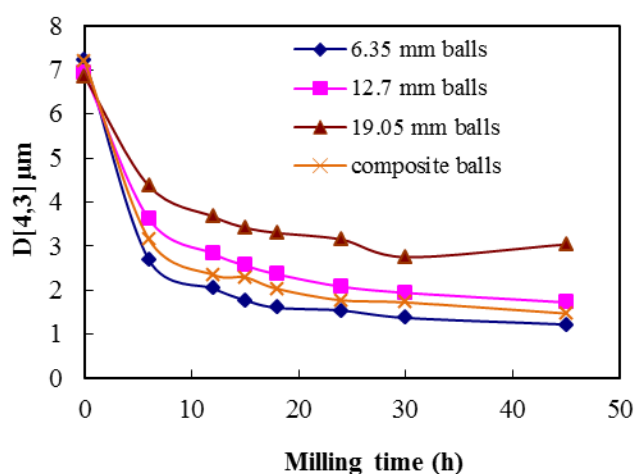


Figure 3C.3: Effect of ball size on D [4, 3] of ZMBT dispersions with milling time

For unmilled ZMBT, the D [4, 3] lies in the range of 7 microns. After 45 h of milling, it decreases to 1.22, 1.72, 3.04 and 1.47 μm by ball-milling with 6.35 mm, 12.7 mm, 19.05 mm and composite balls. Figure 3C.4 shows the effect of ball size and milling time on D [4, 3] of wingstay L dispersion. It is clear from Figure 3C.4 that the initial D [4, 3] of wingstay L was 50 μm and a sharp reduction in size occurs after 6 h of ball-milling. The D [4, 3] of wingstay L after 45h of ball-milling using various ball sizes (6.35 mm, 12.7 mm, 19.05 mm and composite balls) are 4.4, 5.9, 7.9 and 5.8 μm respectively.

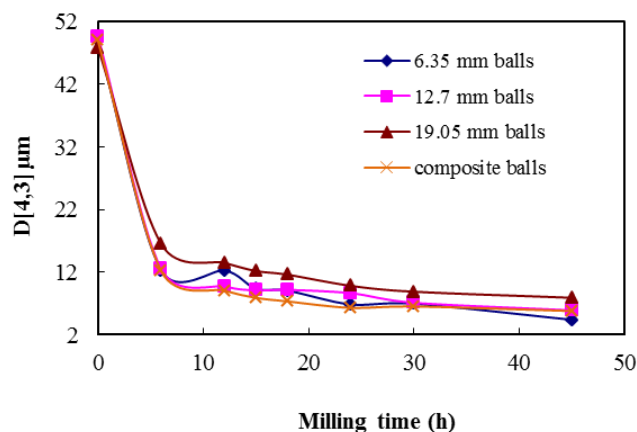


Figure 3C.4: Effect of ball size on D [4, 3] of Wingstay-L dispersions with milling time

Thus it can be concluded that irrespective of ball size, a significant size reduction was observed for ZDEC, ZMBT and Wingstay L after 6 h of ball-milling and thereafter size reduction is found to be slow. Interestingly, the size reduction achieved in ball-milling with composite balls is on par with that of smaller sized balls. From the results cited above, it is obvious that efficiency of balls in size reduction of aqueous dispersions of latex compounding ingredients follows the order 6.35 mm > composite balls > 12.7 mm > 19.05 mm.

3C.3.2 Effect of ball size on size (%)

The effect of ball size on the amount of lower sized particles (*i.e.* particles having size < 500 nm) of latex compounding ingredients (LCI) after 45 h of wet ball-milling is represented in Figure 3C.5. The size (%) of china clay (below 500 nm) after 45 h of wet-milling with 6.35 mm, 12.7 mm, 19.05 mm and composite balls are 23, 8, 5 and 7.3 per cent whereas for ZDEC the values are 9.7, 3.2, 2.4 and 4.5 per cent respectively. Among the LCI used, ZMBT retains highest share of lower sized particles

and wingstay L shows lowest share of lower sized particles in all the cases (with different ball sizes). The share (%) of ZMBT is 29.4, 23, 10.4 and 26 per cent after 45 h of wet-milling with 6.35 mm, 12.7 mm, 19.05 mm and composite balls respectively. In the case of wingstay L, the size (%) of lower sized particles obtained after 45 h of wet-milling with 6.35 mm and composite balls are nearly the same (1.2 per cent) and with 12.7 mm and 19.05 mm sized balls they are 0.91 and 0.74 per cent only. The size (%) of lower sized particles (size < 500 nm) obtained after 45 h of wet ball-milling was found to be high. However, wet-milling with lower sized balls (6.35 mm) retains highest share of lower sized particles in all the cases.

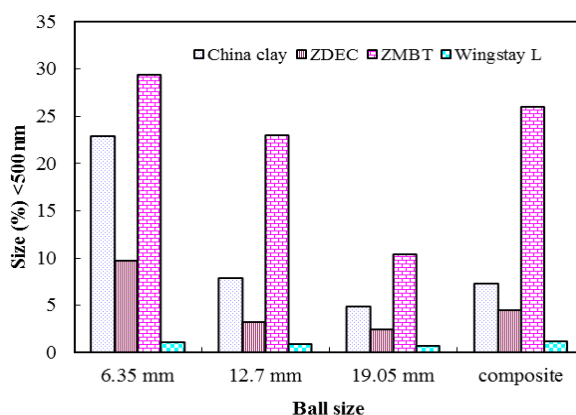


Figure 3C.5: Size (%) (below 500 nm) of latex compounding ingredients after 45h of wet ball- milling with 6.35 mm, 12.7 mm 19.05 mm and composite ball sizes

3C.3.3 Effect of milling time on specific surface area of latex compounding ingredients

The effect of milling time on specific surface area (SSA) of latex compounding ingredients milled with 6.35 mm balls is displayed in Figure 3C.6. It can be seen that irrespective of the materials used, the

specific surface area increases with milling time. However the extent of increase in SSA is different for different materials.

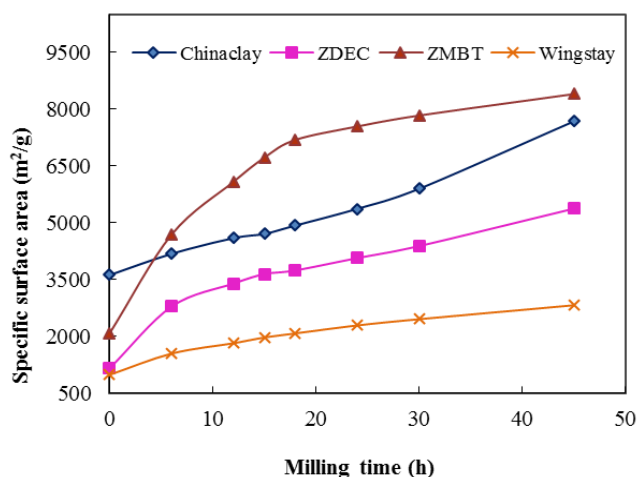


Figure 3C.6: Specific surface area of aqueous dispersions of latex compounding ingredients wet ball-milled with 6.35 mm balls at different milling intervals

The increase in SSA of ZMBT and ZDEC was quite high for the first 15 h of milling and it is more prominent in the case of ZMBT. The SSA of ZMBT is 2087 m²/g (unmilled) and increased to 6720 m²/g after 15 h of milling. Whereas the SSA of ZDEC is 1155 m²/g (unmilled) and after 15 h it is found to be 3653 m²/g only. The SSA of ZMBT and ZDEC after 45 h of ball-milling using 6.35 mm ball size are 8398 m²/g and 5370 m²/g respectively. The SSA of unmilled china clay is 3617 m²/g and it increased to 7675 m²/g after 45 h of ball-milling. The SSA of unmilled wingstay L is 982 m²/g only and registered the lowest SSA of 2819 m²/g among the dispersions evaluated after 45 h of ball-milling.

3C.3.4 Effect of milling time on cumulative size distribution of latex compounding ingredients

The cumulative size curves of latex compounding ingredients after 6, 12, 30 and 45 h of wet ball-milling with 6.35 mm ball size is shown in Figure 3C.7.

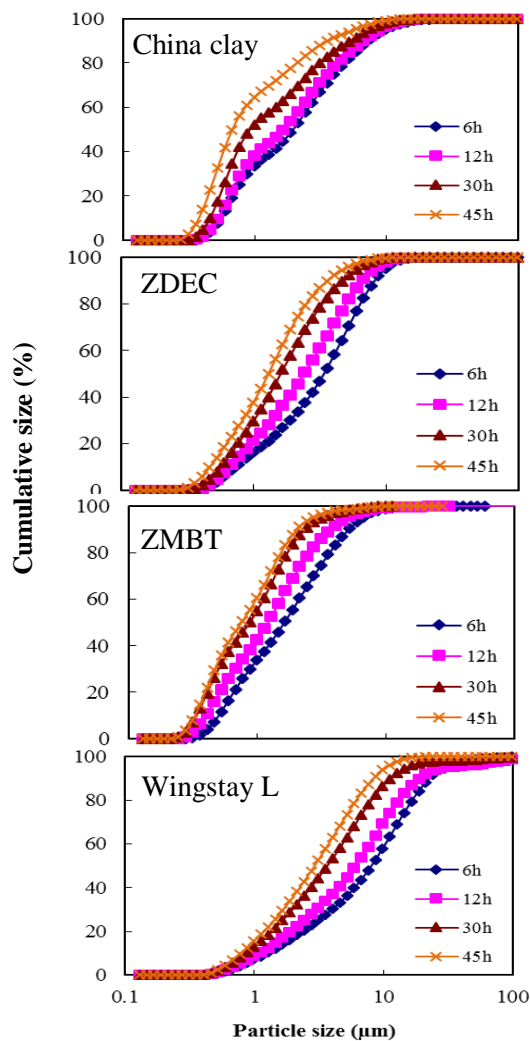


Figure 3C.7: Cumulative size curves of aqueous dispersions of latex compounding ingredients after 6, 12, 30 and 45 h of wet ball-milling with 6.35 mm sized balls

As anticipated, the particle size of ingredients decreases with increase in milling time. All the compounding ingredients showed higher size at 6 h of milling and it significantly reduced after 45 h of milling. A clear shift in peak towards left is evident after 45 h of wet-milling indicating size reduction. The millability of the chemical can be followed from the slope of the curve. The curve is more straightened (slope increases) as higher particles reduced to lower ones at extended milling time.

The reduction in particle size with prolonged milling using smaller sized balls indicates the formation of fresh surfaces during the course of grinding. As the milling time increases the cumulative size curves moves to the left indicating lower particle size as evident from the increase in specific surface area shown in Figure 3C.6. With 6.35 mm sized balls, there will be more number of balls in a unit volume and free volume will be minimum compared to other sizes. Consequently effective impacts on the dispersed materials will be high which results in particle size reduction.

A schematic illustration showing the effect of ball size on milling efficiency is shown in Figure 3C.8.

The size of grinding medium has an influence on milling efficiency [12]. Large grinding medium is useful since the weight of the balls will exert more kinetic energy to particles. The kinetic energy of the balls is related with ball size by the relation,

$$KE \propto d^4 \dots\dots\dots (3.2)$$

Thus, large balls transmit high energy and hence the amount of transferred energy per collision increases. However, with increase in ball size, the free space (void space) between the balls also increases (Figure 3C.8a). This results in reduced ball-to-ball contact and consequently fewer ball-to-material collisions. The free space (void space) can be reduced by using a mixture of balls (composite) having different sizes. A combination of balls having different sizes will form a close packed configuration due to the occupation of small balls in the void spaces (Figure 3C.8b).

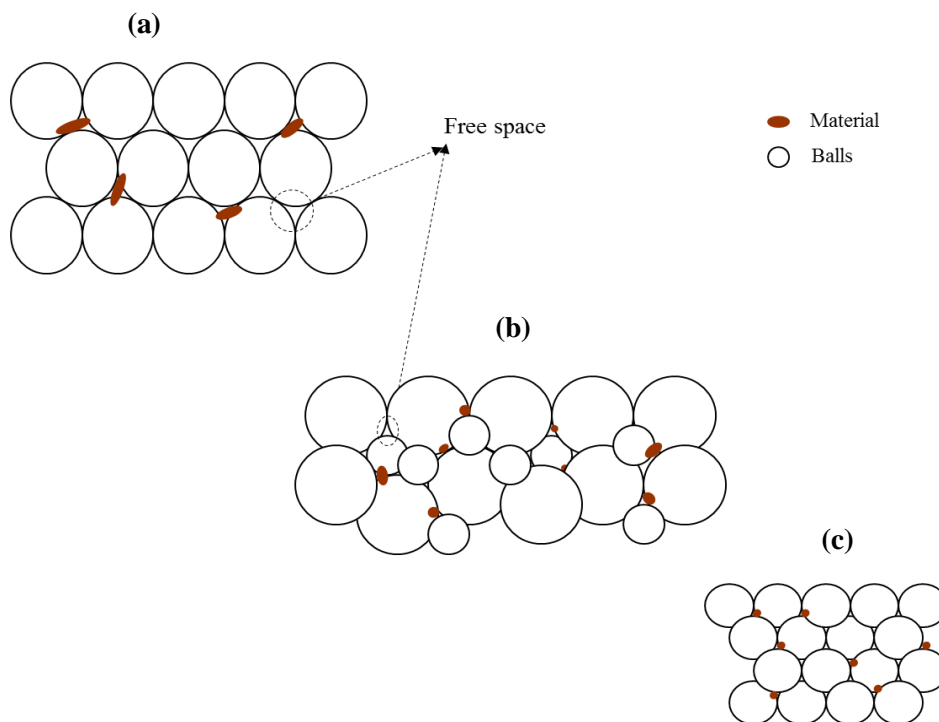


Figure 3C.8: Schematic representation showing the free volume in
(a) large sized balls (b) mixture of large and small sized balls
(c) small sized balls

Such configuration may presumably result in more ball-to-material impacts [13]. Using smaller sized balls, the total contact points (N) between the balls increases (Figure 3C.8c). As the ball size decreases, the number of balls (n) in the jar increases as $1/d^3$ (i.e. $N \propto n \propto d^{-3}$). Consequently, the rate of ball-to-ball contacts per unit time increases. As the particle breakage mostly occurs at the contact sites of the balls, smaller balls possess increased number of contact points between the balls [14]. Thus, the rate of breakage of particles by smaller sizes is higher [15]. Also, by reducing the ball size, the amount of entrapped powders increases and may result in fine particles of uniform size.

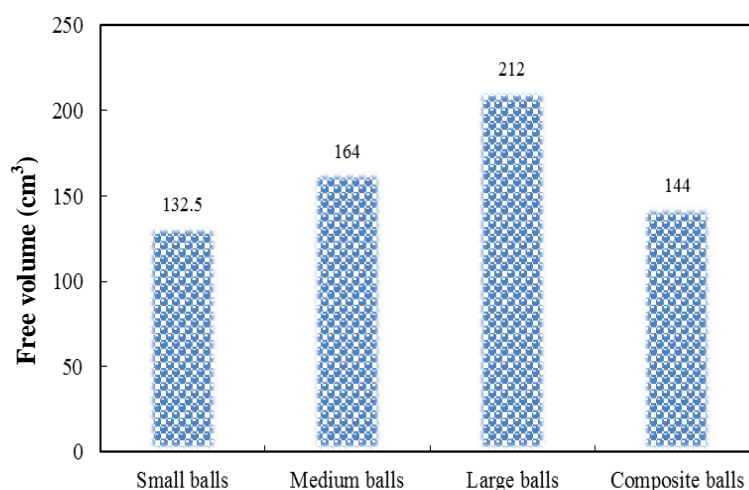


Figure 3C.9: Free volume available for small (6.35 mm), medium (12.7 mm), large (19.05 mm) and composite ball systems

Figure 3C.9 shows the free volume present in different systems each consisting of small (6.35 mm), medium (12.7 mm), large (19.05 mm) and combination of balls having these sizes.

The free space (free volume) present in the given system containing large balls are quite high (212 cm³) compared to medium (164 cm³) and smaller (132 cm³) sized ball systems. This results in reduced ball-to-ball contacts and fewer impacts. This can be ascribed to the reduced grinding efficiency observed for milling with large (19.05 mm) balls. Among the different ball combinations tried, small, medium and large balls in the ratio 2:1:2 by weight showed lowest free volume of 144 cm³, which is comparable to 132.5 cm³ offered by smaller (6.35 mm) sized balls.

3C.3.5 Stability of dispersions

The radar plots showing the stability of china clay, ZDEC, ZMBT and wingstay L dispersions wet-milled with different ball sizes (6.35 mm, 12.7 mm, 19.05 mm and composite balls) at different milling intervals (6, 12, 18, 24, 30 and 45h) are shown in Figure 3C.10. China clay shows better stability (95 %) after 12 h of milling with 6.35 mm sized balls. The better stability at lower milling time is expected to be due to the enhanced dispersion capability of china clay compared to other water insoluble latex compounding ingredients. ZDEC showed highest stability (96.24 %) after 30 h of wet-milling with 6.35 mm balls. In the case of ZMBT also, grinding with smaller sized balls (6.35 mm) shows better dispersion stability. Grinding with large, medium and combination of balls having different sizes are nearly the same in the case of ZMBT. Compared with other dispersions, the dispersion stability of wingstay L is found to be low *i.e.* a value of 90 % or above is highly desirable.

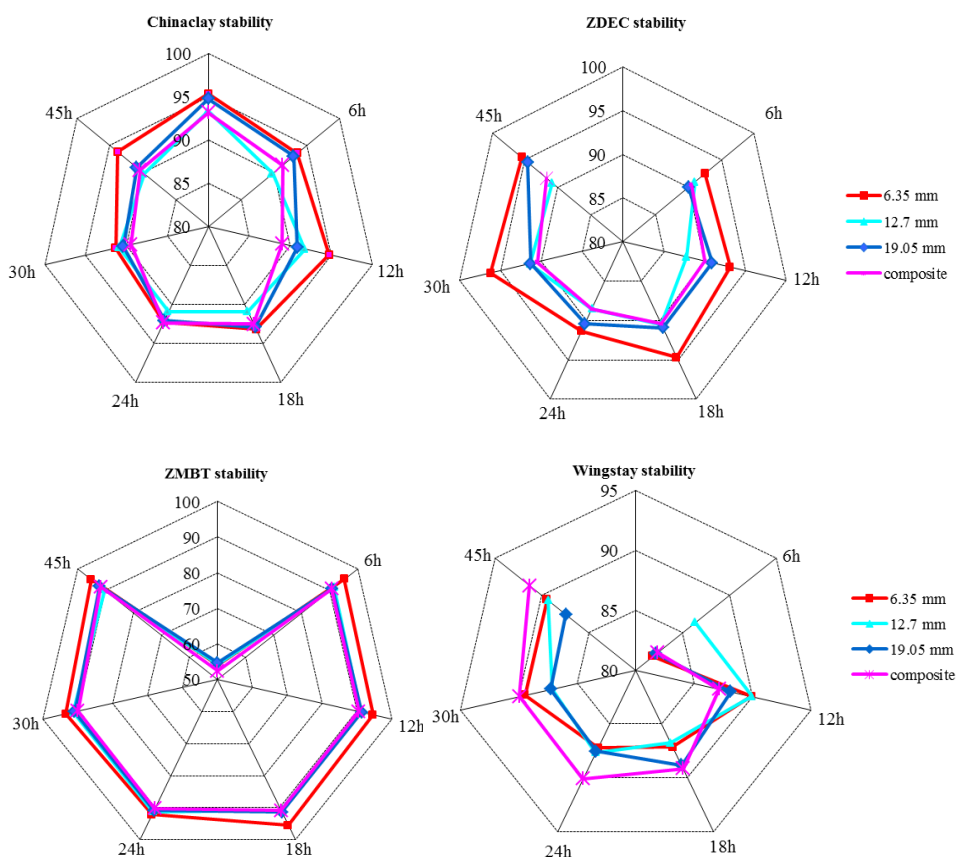


Figure 3C.10: Effect of ball size and milling time on stability of china clay, ZDEC, ZMBT and wingstay L dispersions

The presence of highly complicated non-polar nature of wingstay L prevents the easy dispersion in water even after prolonged period of milling (45 h). Interestingly, stability of wingstay L dispersion is found to be good (91.28 %) after 45 h of wet ball-milling with composite balls. To improve the stability further, addition of suitable colloid stabilizer should be exercised while preparing wingstay L dispersion.

3C.4 Conclusions

The effect of wet ball-milling on particle size and dispersion stability of aqueous dispersions of latex compounding ingredients (china clay, ZDEC, ZMBT and wingstay L) ball milled with different ball size was studied. Irrespective of the ball size, prolonged milling resulted in particle size reduction of the chemicals. However, maximum size reduction was achieved with smaller sized balls. By reducing the ball size, the number of effective impacts could be increased. The amount of free volume (space between the balls) was minimum in small sized balls. Both of these contributed to the effective grinding of the materials. Using composite balls *i.e.* large (19.05 mm), medium (12.7 mm) and small (6.35 mm) together for wet ball-milling resulted competent size reduction and was at par with that offered by smaller sized balls. The optimum ball combination was in the ratio 2:1:2 (by weight) respectively for large, medium and small sized balls. The D [4, 3] of china clay, ZDEC, ZMBT and wingstay L were 1.68, 1.9, 1.22 and 4.4 μm respectively after 45 h of milling with small (6.35 mm) sized balls. The dispersion stability was also found to be good. However, wingstay L dispersions with considerable stability could be achieved by wet ball-milling using composite balls.

References

- [1] C. F. Burmeister, and A. Kwade, *Chem. Soc. Rev.*, **42**(18), 7660 (2013).
- [2] M. Ullah, Md. E. Ali, and S. B. A. Hamid, *Rev. Adv. Mater. Sci.*, **37**(1/2), 1 (2014).
- [3] V. Monov, B. Sokolov, and S. Stoenchev, *Cybernetics and Information Technologies*, **12**(2), 51 (2012).

- [4] K. Anand, S. Varghese, and T. Kurian, *Powder Technol.*, **271**, 187 (2015).
- [5] C. Salties, Q. Chen, S. Manickavasagam, L. S. Schadler, R. W. Siegel, and M. P. Menguc, *J. Nanoparticle Res.*, **6**(1), 35 (2004).
- [6] L. G. Austin, K. Shoji, and P. T. Luckie, *Powder Technol.*, **14**(1), 71 (1976).
- [7] D. W. Fuerstenau, J. J. Lutch, and A. De, *Powder Technol.*, **105**, 199 (1999).
- [8] N. Kotake, K. Daibo, T. Yamamoto, and Y. Kanda, *Powder Technol.*, **143-144**, 196 (2004).
- [9] M. R. Vaezi, S. H. M. S. Ghassemi, and A. Shokuhfar, *J. Theo. Appl. Phys.*, **6**, 29 (2012).
- [10] K. Anand, S. Varghese, and T. Kurian, *Particulate Sci. Technol.* DOI: 10.1080/02726351.2016.1248258 (2016).
- [11] E. Tang, G. Cheng, and X. Ma, *Powder Technol.*, **161**, 209 (2006).
- [12] C. Suryanarayana, *Prog. Mater. Sci.*, **46**, 1 (2001).
- [13] T. M. Cook, and T. H. Courtney, *Metal. Mater. Trans.*, **26A**, 2389 (1995).
- [14] H. Shin, S. Lee, H. S. Jung, and J. B. Kim, *Ceram. Intl.*, **39**, 8963 (2013).
- [15] N. N. S. Lameck *M. Sc. Engg. Dissertation*, "Effects of grinding media shapes on ball mill performance" University of the Witwatersrand, Johannesburg October (2005).

.....✂.....

Chapter **4**

PREPARATION CHARACTERIZATION AND STABILIZATION OF ZINC OXIDE NANODISPERSIONS

Contents	Part A
	Synthesis of Zinc Oxide Nano Rods through Mechano-Chemical Route: A Solvent Free Approach
	Part B
	Role of Surfactants on the Stability of Nano Zinc Oxide Dispersions

SYNTHESIS OF ZINC OXIDE NANO RODS THROUGH MECHANOCHEMICAL ROUTE: A SOLVENT FREE APPROACH

Contents	4A.1 Introduction
	4A.2 Experimental
	4A.3 Results and Discussion
	4A.4 Conclusions

This section of the chapter reports an efficient and inexpensive route for the synthesis of zinc oxide (ZnO) nano rods through a two-step process. In this study, zinc acetate dihydrate and sodium hydroxide were used as precursors and cetyltrimethylammonium bromide (CTAB) was employed as a capping agent. Mechanochemically synthesized ZnO nanoparticles were characterized by X-ray diffraction (XRD), FT-IR spectroscopy, thermogravimetric analysis (TGA), dynamic light scattering measurements (DLS) and transmission electron microscopy (TEM). The highly crystalline nature of synthesized ZnO was confirmed from XRD analysis. The average particle size of ZnO nano rods obtained through the solid-state method was 35 nm in size.

4A.1 Introduction

In the domain of nanotechnology, oxide nano particles can exhibit unique chemical properties owing to their small size and high density of corner or edge surface sites [1]. Nano-ZnO as one of the multifunctional inorganic nano particle attracts researchers due to its physical and

*Part of work presented in this chapter has been published in **International Journal of Theoretical and Applied Sciences**, 6(1), 87-93, (2014).*

chemical properties such as chemical stability, high luminous transmittance, higher catalytic activity, effective antibacterial property, intensive UV and IR absorption *etc.* [2]. ZnO having a wide band gap of 3.37 eV, large bond strength, large excitation binding energy ($E_b=60$ meV) and higher melting temperature (2248 K) [3] has been widely used in many applications such as transparent conductive films, varistors [4, 5] and efficient photocatalysts [6]. The diverse applications exhibited by ZnO nano systems is because it can exist in different morphologies such as belts, wires, ribbons, tubes, rods, tetrapods, rings and needles [7-9]. Several methods for the synthesis of nano-ZnO were reported such as hydrothermal synthesis [10-12], micro emulsion hydrothermal process [13], chemical vapour deposition (CVD) [14] and sol-gel synthesis [15, 16].

Mechano-chemical reactions are suitable for large scale production of nano particles with good yield. Because such method doesn't involve the use of organic solvents for controlling the nano particle growth. Hence they are attractive and less expensive. Pillai *et al.* reported a mechano-chemical procedure for making nano-ZnO for varistor applications [4]. They have employed an annealing temperature of 500°C. In the current procedure a much lower temperature (*i.e.* 300 °C) was used to crystallize the zinc precursors to form ZnO.

In this study, a simple method for the preparation of hexagonal ZnO nano particles with the assistance of the surfactant cetyltrimethylammonium bromide (CTAB) is reported. The preparation procedure was described by Sun *et al.* [20] with the introduction of few modifications. This method is found to be cost effective, efficient and eco-friendly.

4A.2 Experimental

4A.2.1 Methods

4A.2.1.1 Preparation of nano-ZnO

In a typical synthesis 1M Zn(OAc)₂ 2H₂O and 0.3M CTAB were ground in an agate mortar for about 20 min. 6 g of NaOH was added to the above mixture and further ground for 45 min. at room temperature. The resulting pasty mass was washed with 100 ml de-ionized water (DW) for 2-3 times and sonicated. It is then centrifuged at 600 rpm. The resulting supernatant solution was decanted off. The precipitate is filtered, dried and calcined at 300 °C for 2 h. The yield of ZnO is 98%.

4A.2.1.2 Characterization

FT-IR spectra were recorded on a FT-IR spectrometer (Varian 660-IR model) (USA) in the wavelength range 400-4000 cm⁻¹. TG-DTA studies of nano-ZnO were carried out on a Perkin Elmer TGA 4000 model machine under N₂ atmosphere at a heating rate of 10°C/min. in the temperature range 30 - 900°C. For dynamic light scattering (DLS) studies, Malvern- Zetasizer (Nano S - UK) was used. TEM images were taken on HR-TEM machine (Model tecnai 30 G², Netherlands) operating at an accelerating voltage of 300 kV. The X-ray diffraction (XRD) of ZnO nano particles were recorded on PANalytical X'pert machine with Cu-K α radiation ($\lambda=1.54056$ Å). The mean grain size (D) of particle was determined from (XRD line broadening measurement) Scherrer equation [17].

4A.3 Results and Discussion

A solvent free, mechano-chemical reaction between zinc acetate and sodium hydroxide in presence of cetyltrimethylammonium bromide produced a pasty mass. This material was further washed and annealed and were subjected to various characterization methods.

4A.3.1 TG-DTA analysis

TG-DTA curve of synthesized nano-ZnO powder is shown in Figure 4A.1.

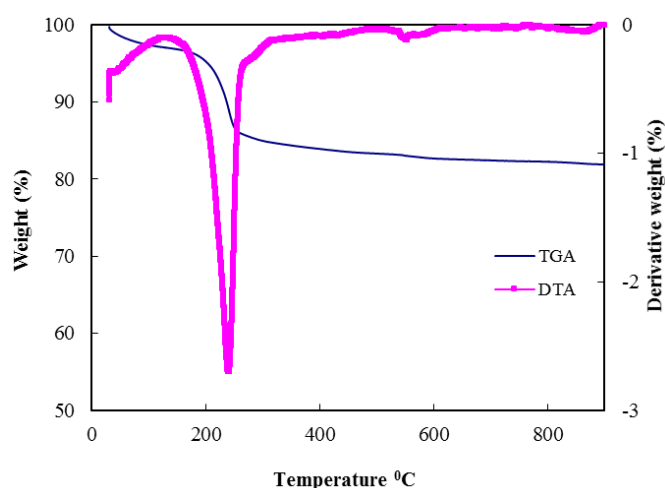


Figure 4A.1: TG-DTA curve of nanocrystalline ZnO powder precursor at a heating rate of 10 °C/min.

TGA curve showed 11.2 per cent weight loss at 241.1 °C and the corresponding DTA curve also showed an endothermic peak at this temperature. This might be due to the escape of remaining CH₃COOH and bonded water. Weight loss at 241.1 °C implies the complete removal of CH₃COOH unreacted if any present and loss of water molecules and other volatile impurities from the system and thereafter no significant

weight loss happened. Hence it is found that the purity of synthesized ZnO nano particles are high and temperature needed for the preparation is low compared with other methods. Using TG-DTA data, the zinc hydroxide obtained was decomposed at 300 °C and used for further study.

4A.3.2 XRD analysis

Figure 4A.2 shows the XRD pattern of synthesized nano-ZnO particles. The diffraction peaks from various planes and d- values are matching well with the reported JCPDS data of nano-ZnO [18].

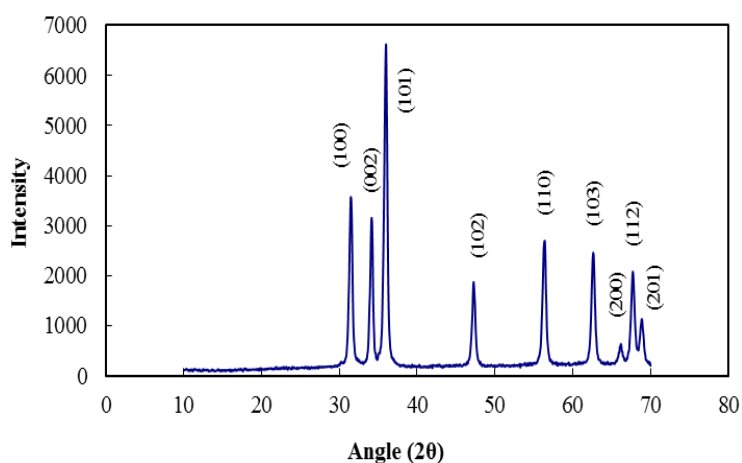


Figure 4A.2: XRD pattern of synthesized nano-ZnO powder after calcination at 300 °C

All the peak positions and relative peak intensities of ZnO product agrees well with standard JCPDS and no impurities such as Zn, Zn(OH)₂ or CTAB are observed. This indicates that the nano-ZnO prepared through the present low temperature, mechano-chemical method are of high purity. The phase structure of synthesized nano-ZnO belongs to

wurtzite structure (hexagonal phase). Moreover, the diffraction peaks of the product shows strong peak intensities indicating that the prepared ZnO nano particles have high crystallinity. They have an average grain size of 33.5 ± 0.5 nm calculated from Scherrer equation.

4A.3.3 FT-IR analysis

The formation of hexagonal phase ZnO in the prepared samples were supported by FT-IR spectra shown in Figure 4A.3. The broad band at 3380 cm^{-1} corresponds to vibrational mode of -OH group of water indicating the trace amount of water adsorbed on ZnO crystal surface. The band near 1650 cm^{-1} is due to the asymmetric stretching of zinc acetates or oxalates [19]. Band at 1533 cm^{-1} corresponds to C=O stretching vibration of small fractions of unreacted COO-Zn. The intense band around 500 cm^{-1} confirms the Zn-O vibration of ZnO.

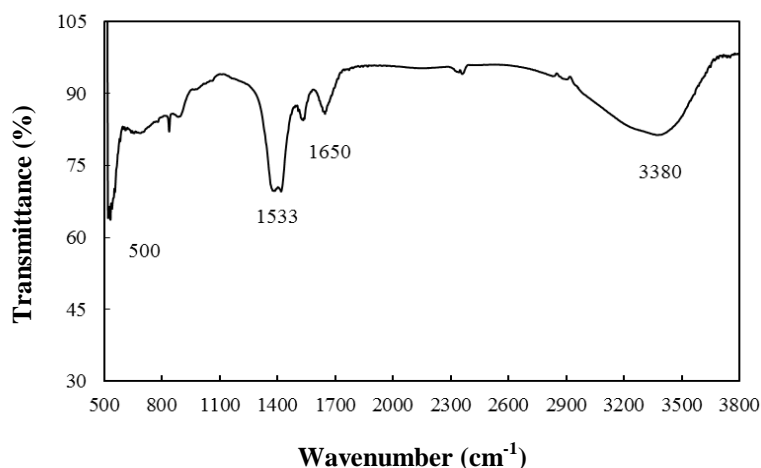


Figure 4A.3: FT-IR spectra of synthesized nano-ZnO

4A.3.4 DLS analysis

Figure 4A.4 shows the DLS measurements of ZnO nano particles dispersed in 0.1 % sodium lauryl sulphate (SLS). From the intensity statistics report it has been found that 16 % of particles having size below 100 nm. About 37 % particles showed size in between 100-200 nm. 48 % particles having size varies from 200-800 nm. Aggregation of particles was also observed and their size ranged from 4-5 μm . However, particles having size above 4 μm are less compared to the bulk. Particle aggregation occurs due to water absorption and also due to the lower surfactant concentration.

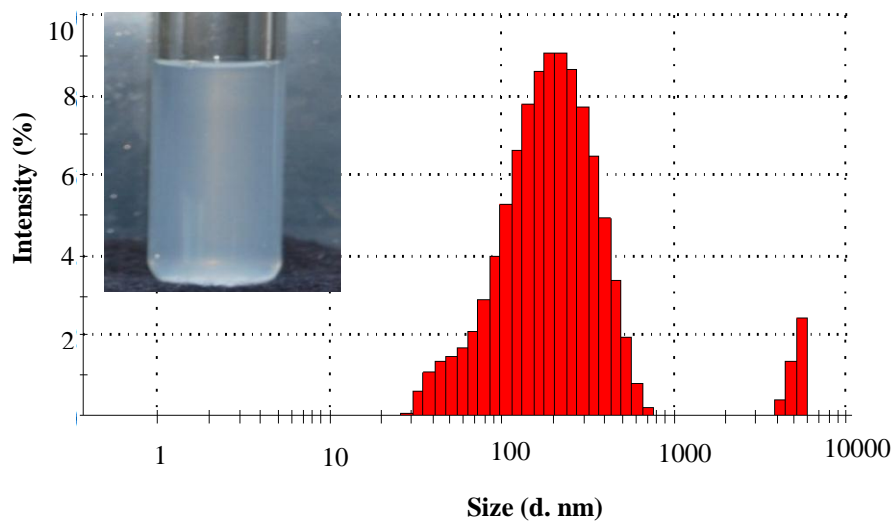


Figure 4A.4: Intensity distribution for synthesized ZnO nano particles dispersed in 0.1% sodium lauryl sulphate (SLS). The inset shows the stable ZnO nano dispersion

4A.3.5 HR-TEM analysis

The size and morphology of ZnO nano particles analyzed by HR-TEM technique is shown in Figure 4A.5.

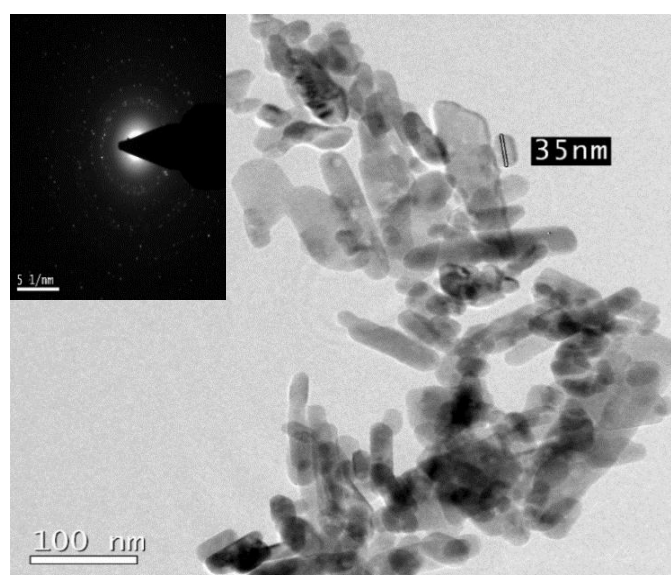


Figure 4A.5: HRTEM image of synthesized nano-ZnO. Inset shows electron diffraction (SAED) pattern of synthesized nano-ZnO

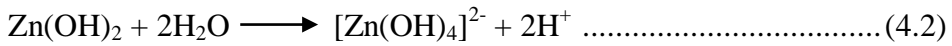
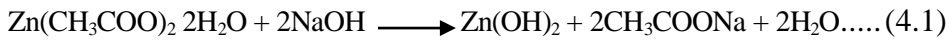
The image reveals that the product contained rod shaped particles with an average size range of 35-60 nm and is in good agreement with that estimated by Scherrer formula based on XRD pattern and DLS measurements.

4A.3.6 Mechanism of ZnO nanoparticle formation

In this typical process metal oxides are obtained by grounding metallic salts with sodium hydroxide, which is different from results obtained by hydroxides in solution [20]. It is expected that the

mechanism of formation of nano-ZnO under mechano-chemical method is as follows:

It was reported that $[\text{Zn}(\text{OH})_4]^{2-}$ nano particles are primarily produced by an exothermic reaction from Zn salt and NaOH as a result of the mechanical grinding (reaction 1 and 2) [21].



Freshly produced $[\text{Zn}(\text{OH})_4]^{2-}$ decomposes to produce ZnO nano particles at a low temperature within a short reaction time (reaction 3) [21].



The scheme of growth mechanism of ZnO nano rods is as shown in Figure 4A.6.

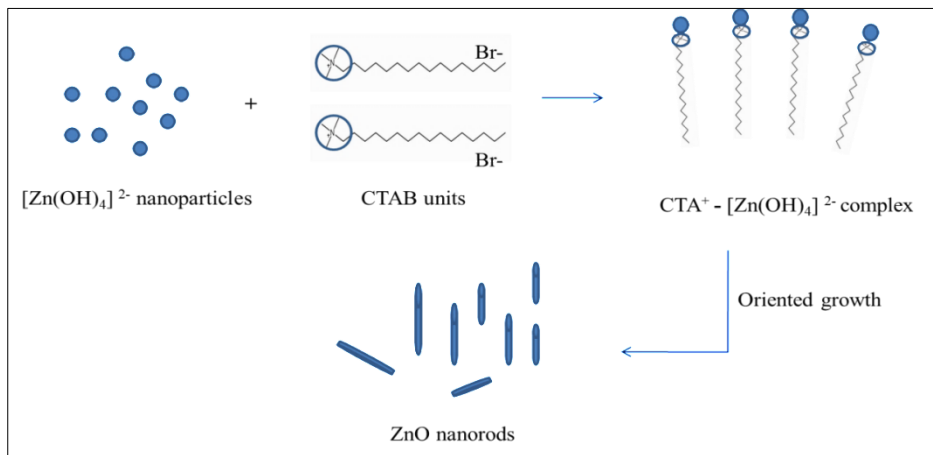


Figure 4A.6: Schematic diagram showing the mechanism of growth of ZnO

4A.3.7 Role of CTAB in morphology of ZnO nano particles

The choice of surfactant decides the morphology of products. It was reported that spherical ZnO nano particles can be prepared by using various alkyl amines [22, 23]. In the current study it is being expected that CTAB provides a long chain reaction interface and allows the particles to grow in one direction and as a result particles assumes a rod like morphology (Figure 4A.6). Bi-products if any formed during the process and formation of any other un-wanted impurities can be completely eliminated during washing. Thus the ZnO nanoparticle synthesized by this route is free from impurities, which is confirmed by XRD and TEM techniques.

4A.4 Conclusions

Present study envisages the formation of ZnO nano rods from zinc acetate dihydrate, sodium hydroxide and CTAB through a mechano-chemical process. The average size of particles obtained through this technique is in the range 35-60 nm. This method is convenient, effective and inexpensive method for synthesizing ZnO nano particles. It should also be noted that the reaction yield was about 98 %. Thermal studies revealed that the complete conversion of zinc hydroxide to zinc oxide happens at 241°C. TEM images showed that there is minimum aggregation of the synthesized nanoparticles and the purity of synthesized nano particles is good. FT-IR and XRD technique also support this finding. A suitable relationship between choices of substrates, concentration of substrates, type and dosage of surfactants on particle size as well as morphology of ZnO nanoparticles is still under debate.

References

- [1] C. R. Bhattacharjee, D. D. Purkayastha, S. Bhattacharjee, and A. Nath, *Assam Univ. J. Sci. Tech: Phys. Sci. Technol.*, **7**(II), 122 (2011).
- [2] J. Sawai, *J. Microbiol. Methods.*, **54**(2), 177 (2003).
- [3] A. Azam, F. Ahmed, N. Arshi, M. Chaman, and A. H. Naqvi, *Intl. J. Theo. Appl. Sci.*, **1**(2), 12 (2009).
- [4] S. C. Pillai, J. M. Kelly, D. E. McCormack, and R. Ramesh, *Mater. Sci. Technol.*, **20**, 964 (2004).
- [5] S. C. Pillai, J. M. Kelly, D. E. McCormack, and R. Ramesh, *Adv. Appl. Ceram.*, **105**(3), 158 (2006).
- [6] R. Georgekutty, M. K. Seery, and S. C. Pillai, *J Phys. Chem. C.*, **112**(35), 13563 (2008).
- [7] D. Ledwith, S. C. Pillai, G. W. Watson, and J. M. Kelly, *Chem. Commun.*, 2294 (2004).
- [8] S. C. Padmanabhan, D. Ledwith, S. C. Pillai, D. E. McCormack, and J. M. Kelly, *J. Mater. Chem.*, **19**(48), 9250 (2009).
- [9] S. C. Pillai, J. M. Kelly, D. E. McCormack, and R. Ramesh. *J. Mater. Chem.*, **14**(10), 1572 (2004).
- [10] W. J. Li, E. W. Shi, Y. Q. Zheng, and Z. W. Yin, *J. Mater. Sci. Lett.*, **20**, 1381 (2001).
- [11] B. Liu, and H. C. Zeng, *J. Am. Chem. Soc.*, **125**, 4430 (2003).
- [12] B. Cheng, and E. T. Samulski, *Chem. Commun.*, 986 (2004).
- [13] J. Jiang, Z. Huang, S. Tan, Y. Li, G. Wang, and X. Tan, *Mater. Chem. Phys.*, **132**(2-3), 735 (2012).
- [14] Y. J. Li, R. Duan, P. B. Shi, and G. G. Qin, *J. Cryst. Growth.*, **260**, 309 (2004).
- [15] M. J. Alam, and D.C. Cameron, *J. Vac. Sci. Technol. A.*, **19**(4), 1642 (2001).

- [16] M. Toyoda, J. Watanabe, and T. Matsumiya, *J. Sol-Gel Sci. Technol.*, **16**(1/2), 93 (1999).
- [17] L. Shen, N. Bao, K. Yanagisawa, K. Domen, A. Gupta, and C. A. Grimes, *Nanotechnology*, **17**, 5117 (2006).
- [18] JCPDS Card No. 36-1451.
- [19] N. T. Nolan, M. K. Seery, and S. C. Pillai, *Chem. Mater.*, **23**(6), 1496 (2011).
- [20] Z. P. Sun, L. Liu, L. Zhang, and D. Z. Jia, *Nanotechnology*, **17**, 2266 (2006).
- [21] N. C. Mamady, D. Khalid, Z. Hafid, A. Karima, L. Larbi, B. Mohammed, and J. Boujemaâ, *J. Mater. Sci. Engg. A.*, **1**, 985 (2011).
- [22] M. Shim, and P. Guyot-Sionnest, *J. Am. Chem. Soc.*, **123**, 11651 (2001).
- [23] P. D. Cozzoli, M. L. Curri, A. Agostiano, G. Leo, and M. Lomascolo, *J. Phys. Chem. B.*, **107**, 4756 (2003).

**ROLE OF SURFACTANTS ON THE STABILITY OF
NANO ZINC OXIDE DISPERSIONS**

Contents	4B.1 Introduction
	4B.2 Experimental
	4B.3 Results and Discussion
	4B.4 Conclusions

Now-a-days stable colloidal dispersions with ultra-fine or nano sized particles are getting importance due to their higher activity. This part of the chapter presents the methods for the preparation of stable aqueous dispersions of zinc oxide (ZnO) were discussed. The quality of the dispersion was improved by capping with different types of surfactants say non-ionic, cationic and anionic. Accordingly, Triton X 100, polyethylene glycol- 6000 (both non-ionic), cetyltrimethylammonium bromide (cationic) and sodium dodecyl sulphate (anionic) were selected for the study. Effect of these surfactants on particle size of ZnO was followed through dynamic light scattering (DLS) studies and zeta potential measurements. Particle size analysis and zeta potential measurement indicated that ZnO dispersions stabilized with anionic surfactants (sodium dodecyl sulphate) showed better stability. Further, the effect of ultrasonication on particle size distribution was examined and optimized.

Part of work presented in this chapter has been published in *Particulate Science and Technology*, DOI: 10.1080/02726351.2015.1131787 (2015).

4B.1 Introduction

A stable colloidal dispersion is expected to remain without sedimentation even after prolonged periods of storage. The settling behaviour of dispersions depends mainly on the size and density of the dispersed particles. Dispersion of nanopowders into liquids is a challenging task. The high surface area and surface energy which are responsible for the beneficial effects of nanomaterials prevents easy dispersion into liquids.

Stabilization of metal oxide nanoparticles are extensively studied over the past few years [1, 2]. As a promising semiconductor material, ZnO finds a lot of applications in optoelectronic devices, photocatalysts, cosmetics, pigments, paints, ceramics, solar cells, varistors, sensors *etc.* [3, 4]. The properties of ZnO can be varied by reducing the size. By reducing the size, the specific surface area gets increases which in turn increase the chemical activity.

Surfactants/capping agents are usually employed to control the size and dispersion of nanoparticles. The presence of capping molecule appears to affect the kinetics of nucleation and accretion in such a way that it slows down the growth of large particles. When no capping agents are introduced, particle-particle interaction will be much higher, accounting the instability of the sample [5]. Stabilization of colloidal dispersions of several commercial and synthesized metal oxide nanopowders by electrostatic and steric interactions were reported [6-8]. Synthesis of sulphur nanoparticles in aqueous media and the effect of different surfactants on particle size

were studied by Chaudhuri and Paria [9]. Naeini (2012) used UV-visible spectroscopy to investigate the dispersion and stability of titania nanoparticles in aqueous media with different types of dispersants [10]. Effect of dispersant types and concentration on dispersion of titania nanopowders were reported by Fazio [11]. They used zeta potential measurements and particle size distribution to characterize nano-titania suspensions.

The main difficulty associated with nanoparticles is in the area of dispersion. Though the benefits of nanoparticles are widely appreciated, there exist difficulties in the preparation and storage stability of such dispersions. The major problem is the particle agglomeration. *Van der Waals* and other attractive forces are responsible for the formation of aggregates or agglomerates. This impedes the effective usage of nanoparticles and makes the production cost much higher. With increasing energy costs and raw material prices, it is important to explore the efficiency of the manufacturing process associated with fine-particle dispersions.

Most of the nanomaterials are produced *via* dry process. As a result, they should be dispersed well in liquid formulations. Breakage of agglomerates is also a critical issue. Therefore, effective methods for de-agglomeration and dispersion of particles are required to exploit the full potential of nanoparticles in aqueous dispersions. Ultrasonication is a well-established method for particle size reduction. Further, storage stability of nano-dispersions is important for various applications.

In the present work, dispersion of synthesized ZnO nanopowder was treated with different types of surfactants. The stability of the resulting dispersion was assessed by particle size analysis, zeta potential measurements and sedimentation tests. Effect of ultrasonication on the size reduction was also attempted.

4B.2 Experimental

4B.2.1 Materials

The details of the surfactants used are shown in experimental section (Table 2.4).

4B.2.2 Methods

Synthesis of nano-ZnO is explained in chapter 4 [Part A].

4B.2.2.1 Preparation of ZnO dispersion

Surfactant solutions with a concentration of 0.22 wt. % was prepared by adding 0.11g of each surfactant in 50 ml pure water and stirred to get a homogeneous solution. It was then divided into four aliquots and nano-ZnO was added to each with continuous stirring. The concentration of resulting dispersion was maintained to 0.4-0.5 wt. %. The stirring process was continued to few more hours to get a uniform dispersion of ZnO. Around 13-15 ml of which is taken in 4 different test tubes (designated as **a**, **b**, **c** and **d**) and are used for the storage stability studies (sedimentation test). [*a and b represents ZnO dispersed in Triton X 100 and PEG 6000 respectively. c indicates ZnO dispersed in CTAB and d represents ZnO dispersed in SDS*].

4B.2.2.2 Characterization

Particle size analysis was performed in a particle size analyzer (Zetasizer Nano S, Malvern, UK) using dynamic light scattering (DLS) technique. A Vibra Cell ultrasonicator (model VCX-750) at a frequency of 20 kHz having 750W power rate was used to disperse the agglomerates in the dispersions. Zeta potential was measured by a Zetasizer (Nano Z, Malvern, UK) at 25 °C.

4B.3 Results and Discussion

4B.3.1 Impact of various surfactants on ZnO dispersion

4B.3.1.1 Particle size of ZnO in various surfactants

Figure 4B.1 displays the particle size distribution curves of aqueous dispersions of ZnO in the presence of different surfactants.

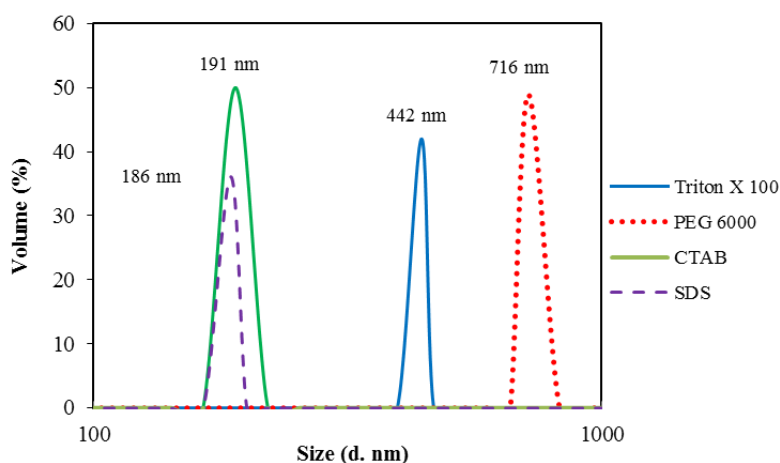


Figure 4B.1: Size distribution of ZnO in different surfactants

It can be seen that among the four kinds of surfactants used, nano-ZnO stabilized with SDS showed the lowest particle size (186 nm). The

share of particles (vol. %) were 36 per cent whereas in CTAB, almost 50 per cent particles recorded a size of 191 nm. Among the non-ionic surfactants tried, ZnO particles showed a size of 442 and 716 nm respectively in Triton X 100 and PEG 6000. The higher size exhibited by ZnO in PEG 6000 might be due to aggregation between ZnO nanoparticles.

4B.3.1.2 Size after storage

The storage stability of nano-ZnO dispersions stabilized using various surfactants were assessed after keeping the samples for 1 week followed by measurement of particle size. The size distribution curves are shown in Figure 4B.2.

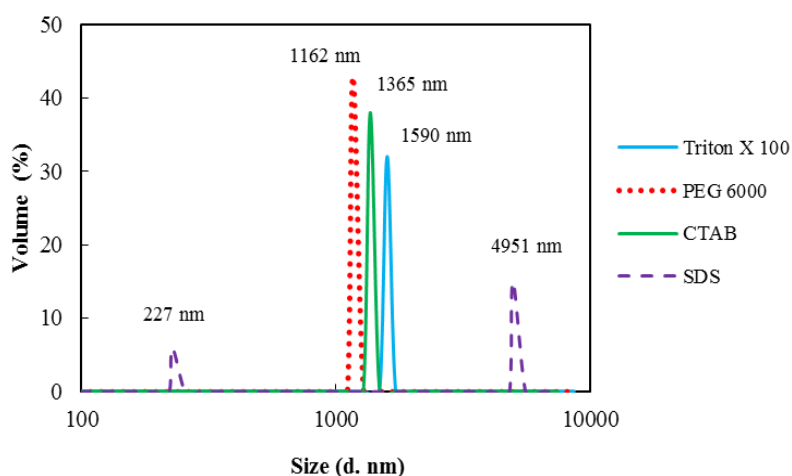


Figure 4B.2: Size distribution curves of ZnO in various surfactants after 1 week

In all the cases, the size of the particles is higher than the initial. The particle size of ZnO in Triton X 100, PEG 6000 and CTAB are 1590 nm (32 %), 1162 nm (43 %) and 1365 nm (38 %) respectively. A bimodal

distribution curve comprising of particles having sizes 227 nm and 4951 nm was observed for ZnO stabilized with SDS. The increased size is due to agglomeration which might be due to incomplete surface coverage of ZnO nanoparticles with SDS. Large surface area and high surface activity of nanoparticles cause agglomeration on prolonged storage. Also, smaller particles have a larger diffusion coefficient as compared with larger ones at the same mass and will aggregate rapidly in water by Brownian motion [13].

4B.3.1.3 Effect of sonication

Ultrasonication is an effective tool for preparing aqueous dispersions of ultra-fine/nanoparticles. Ultrasonic cavitation can break the primary particles and the *van der Waals* forces in agglomerates [14]. The effect of sonication on size distribution of ZnO dispersions stabilized in non-ionic (Triton X 100 and PEG 6000), cationic (CTAB) and anionic (SDS) surfactants are shown in Table 4B.1.

Table 4B.1: Effect of sonication on particle size of nano-ZnO dispersions

Surfactant Used	Sonication time (min.)		
	2	3	4
Triton X 100	201* (35%)**	223 (36%)	485 (25%)
PEG 6000	254 (48%)	3541 (16%)	370 (38%)
CTAB	114 (6%) 347 (17%)	805 (30%)	223 (18%)
SDS	195 (13%)	74 (21%) 868 (5%)	45 (32%) 317 (3%)

* Size of the particles (in nm) after sonication in different surfactants

** Volume (%) of particles with corresponding size.

The highest size of 3541 nm was observed for ZnO stabilized with PEG 6000 after 3 min. sonication (Table 4B.1). Earlier reports indicated that re-agglomeration process prevails even after sonication [6]. For CTAB stabilized system, in addition to a peak at 347 nm, particles having size closer to 100 nm (exactly 114 nm) are also observed after 2 min. sonication (Table 4B.1). The share of particles at this size range was only 6 per cent. By increasing the sonication time particle-particle interaction predominates which results in agglomeration. Sonication in presence of SDS reduces the agglomerates and hence the proportion of lower sized particles increases accordingly. In SDS, ZnO exhibited bimodal distributions after 3 and 4 min. sonication. Particle sizes of ZnO after 3 min. sonication were 74 nm (21 %) and 868 nm (5 %) which further decreased to 45 nm (32 %) and 317 nm (3 %) after 4 min. sonication. Increasing the sonication time (> 4 min.) leads to the growth of particles (Ostwald ripening).

4B.3.1.4 Stability of ZnO dispersion

The stability of colloidal suspensions can be assessed by measuring their zeta potential. The magnitude of zeta potential determines the stability of the dispersion. Surfactants added to aqueous solution will decrease the contact angle of solid particles and increase the energy barrier of particles which prevent re-agglomeration [15]. Figure 4B.3 illustrates the zeta potential stability of aqueous dispersions of nano-ZnO in various surfactants.

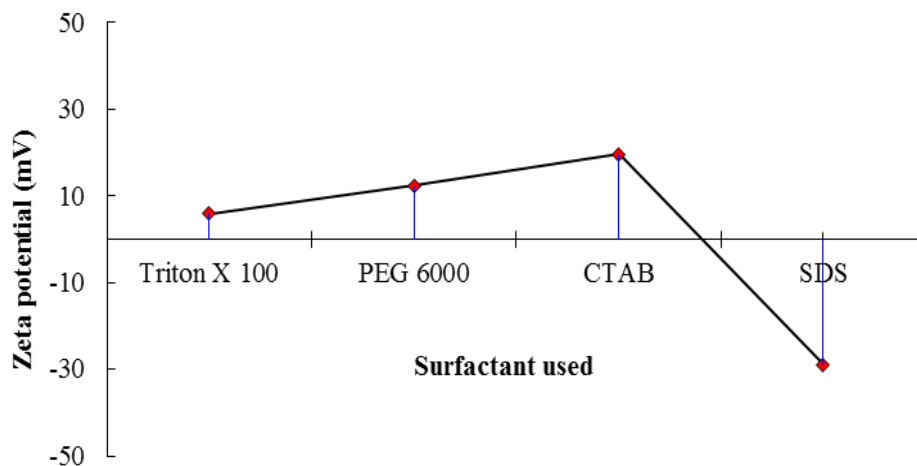


Figure 4B.3: Zeta potential of ZnO dispersion in various surfactants

Among different surfactants used, ZnO-SDS combination exhibited better stability. The zeta potential of resulting dispersion was -28.9 mV. This might be due to the higher level of adsorption of SDS molecules on ZnO surface. Zeta potential of ZnO in Triton X 100, PEG 6000 and CTAB are 5.92 mV, 12.3 mV and 19.6 mV respectively. Therefore, agglomeration tendency of ZnO nanoparticles in non-ionic surfactants are high because of low zeta potential values. To compare the storage stability of nano-ZnO, sedimentation tests were conducted. Photographs showing the dispersion state of ZnO nanoparticles in various surfactants are displayed (Figure 4B.4).

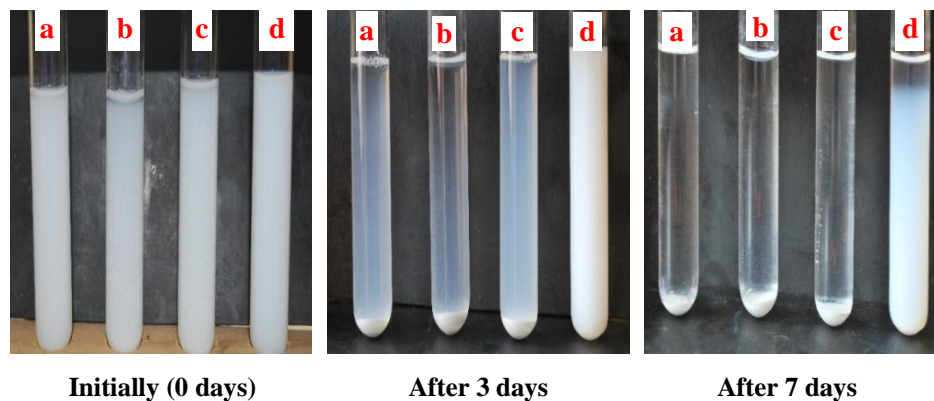


Figure 4B.4: Sedimentation of ZnO nanodispersions in a) Triton X 100 b) PEG 6000 c) CTAB and d) SDS

ZnO dispersed in non-ionic surfactants settles down after 3 days. ZnO dispersed in cationic surfactant (CTAB) too started sedimentation after 3 days but it was observed to be a slow process. After 3 days, complete sedimentation was observed for ZnO nanoparticles dispersed in both non-ionic and cationic surfactants (Figure 4B.4 [II]). The results are in accordance with zeta potential values. The lower the zeta value, lower will be the stability. Among the four kinds of surfactants used, nano-ZnO dispersed in SDS showed maximum stability even after 7 days. Particles settling velocity in dispersion medium is related to size and quality of the particle. The larger the particle, higher the settling velocity [16]. The results showed that ZnO dispersed in SDS has lesser agglomeration among the particles indicating better dispersion.

4B.4 Conclusions

The study mainly focused on the role of different surfactants on the stability and the particle size distributions of ZnO in aqueous media. Optimal dispersion conditions for the preparation of stable aqueous dispersion of nano-ZnO were presented. Surfactants play a major role in lowering the particle size. Among the non-ionic, cationic and anionic surfactants studied, the quality of dispersion was better with anionic surfactants (SDS). Dispersion of ZnO in SDS retained more number of particles in the nano-size range. Sonication in presence of SDS further enhanced the share of lower sized particles. As revealed from the zeta potential studies, the colloidal stability of ZnO dispersed in SDS was also found to be higher (-28.9 mV).

References

- [1] Y. Zhang, Y. Chen, P. Westerhoff, K. Hristovski, and J. C. Crittenden, *Water Res.*, **42**(8-9), 2204 (2008).
- [2] N. H. Tkachenko, Z. M. Yaremko, C. Bellmann, and M. M. Soltys, *J. Colloid Interface Sci.*, **299**, 686 (2006).
- [3] K. G. Kanade, B. B. Kale, R. C. Aiyer, and B. K. Das, *Mater. Res. Bull.*, **41**, 590 (2006).
- [4] M. Promsawat, A. Watcharapasorn, and S. Jiansirisomboon, *Nanoscale Res. Lett.*, **7**, 65 (2012).
- [5] L. Guo, S. Yang, C. Yang, P. Yu, J. Wang, W. Ge, and G. K. L. Wong, *Chem. Mater.*, **12**, 2268 (2000).
- [6] J. N. Mandzy, E. Grulke, and T. Druffel, *Powder Technol.*, **160**, 121 (2005).
- [7] J. Widegren, *J. Am. Ceram. Soc.*, **85**(3), 523 (2002).

- [8] S. G. J. Heijman, and H. N. Stein, *Langmuir*, **11**(2), 422 (1995).
- [9] R. G. Chaudhuri, and S. Paria *J. Colloid Interface Sci.*, **343**, 439 (2010).
- [10] Y. S. Naeini, M. Aminzare, F. G. Fard, F. Khorasanizadeh, and E. Salahi, *Iranian J. Mater. Sci. Engg.*, **9**(1), 62 (2012).
- [11] S. Fazio, J. Guzman, M. Colomer, A. Salomoni, and R. Moreno, *J. Euro. Ceram. Soc.*, **28**, 2171 (2008).
- [12] K. Anand, S. Varghese, and T. Kurian, *Intl. J. Theo. Appl. Sci.* **6**(1), 87 (2014).
- [13] C. P. Tso, C. M. Zhung, Y. H. Shih, Y. M. Tseng, S. C. Wu, and R. Doong, *Water Sci. Technol.- WST.*, **61**(1), 127 (2010).
- [14] K. Anand, S. Varghese, and T. Kurian, *Powder Technol.*, **271**, 187 (2015).
- [15] F. Zhang, and J. Yang, *Modern Appl. Sci.*, **3**(1), 89 (2009).
- [16] X. Y. Ni, J. Shen, and Z. H. Zhang, In: *Physicochemical properties and application of nanomaterials*. Beijing: Chemical Industry Press (2006).

.....❧.....

Chapter 5

EFFECT OF MICRO AND NANO ZINC OXIDE ON THE PROPERTIES OF PRE-VULCANIZED NATURAL RUBBER LATEX FILMS

Contents	5.1 Introduction
	5.2 Experimental
	5.3 Results and Discussion
	5.4 Conclusions

Zinc oxide (ZnO) nanoparticles were synthesized through a solution free mechano-chemical route and their effects on the properties of pre-vulcanized natural rubber latex films were investigated. Effect of nano-ZnO loading on swelling, antimicrobial, mechanical and ageing properties of pre-vulcanized latex vulcanizates were examined and compared with conventional micro ZnO filled vulcanizates. In comparison with micro ZnO filled system, nano ZnO filled system exhibits better performance in all respects. The ageing resistance of nano-ZnO incorporated latex films was found to be high.

*Part of work presented in this chapter has been published in **Progress in Rubber, Plastics and Recycling Technology**, 31(3), 145-156, (2015).*

5.1 Introduction

Pre-vulcanized natural rubber latex (PVL) is a convenient raw material for the manufacture of several latex products. Drying of PVL produces a crosslinked film that does not require further vulcanization. Crosslinking reaction in latex takes place over a range of conditions such as temperatures ranging from 20 °C to 90 °C for appropriate periods [1]. The crosslinking of rubber in latex can be effected by the reaction with sulphur [2], sulphur donors [3], peroxides [4] or by γ -radiation [5]. The attractive feature of PVL is that it requires shorter drying time and high product clarity. Pre-vulcanization of latex enables the removal of sedimentable impurities and unreacted ingredients which may cause blooming. The consistency of the properties of PVL products is excellent and they show minimum allergenic reactions.

Zinc oxide is an essential additive both in dry rubber and latex based formulations. Sulphur pre-vulcanized natural rubber latex is prepared by allowing rubber molecules to react with sulphur under the influence of one or more accelerator and zinc oxide. Being an activator of vulcanization, ZnO enhances the crosslinking efficiency in latex products. An important function of ZnO is to regenerate the accelerator as the vulcanization reaction proceeds.

It has been reported that the addition of ZnO reduces the latex stability and film clarity when used above 0.2 phr [6]. Moreover, ZnO is classified as a hazardous chemical and the excess release of which is highly toxic to aquatic species. For humans the recommended intake should not exceed 12-15 mg/day. Around 100000 tonnes of ZnO and other zinc

containing chemicals are consumed by rubber industry in European Union (EU) alone. Global consumption is much higher. To reduce the use of zinc in rubber products, “Eco Zinc” concept has been set up by EU. With increase in concern about the excess release of zinc to environment, rubber products manufacturers are looking for process/chemicals which can minimize the concentration of ZnO in their products.

The requirement of ZnO in latex based formulations could be considerably reduced by using nano-dispersions of ZnO [7]. By reducing the particle size of ZnO, the vulcanization time could be reduced and the mechanical properties could be improved. The smaller the particle, higher the surface to volume ratio and are expected to be more active.

Use of nano-ZnO as cure activator in natural rubber has been studied [8]. Addition of nano-ZnO decreases the cure time (t_{90}) and increases the cure rate index as compared with 5 phr micro ZnO. The optimum dosage of nano-ZnO as a cure activator in NR vulcanization was found to be 0.5 phr. Thomas *et al.* synthesized novel accelerators *N*-benzylimine aminothioformamide (BIAT)-capped-stearic acid-coated nano-ZnO (ZOBS), BIAT-capped ZnO (ZOB) and stearic acid-coated nano zinc phosphate (ZPS), to investigate their effects in NR vulcanization [9]. They found that BIAT-capped-stearic acid-coated nano-ZnO (ZOBS) exhibit superior curing and improved physico-mechanical properties compared with the reference mixture containing uncapped ZnO. NR/ZnO nanocomposites were prepared by blending NR latex with aqueous suspension of ZnO nanoparticles [10]. They exhibit excellent antibacterial characteristics and improved mechanical properties when the dosage of

ZnO is < 4 wt. %. Rathnayake *et al.* reported that the antibacterial activity of natural rubber latex foam can be improved by the addition of ZnO nanoparticles [11].

The objective of the present work is to study the performance of synthesized nano-ZnO on the properties of pre-vulcanized natural rubber latex and to compare them with control vulcanizate containing micro-ZnO. Effect of reducing the concentration of nano-ZnO on the mechanical properties of the vulcanizate has been evaluated. The antifungal activity of pre-vulcanized natural rubber latex films containing micro and nano-ZnO is also studied.

5.2 Experimental

5.2.1 Methods

Details of centrifuged natural rubber latex are given in the experimental section. Vulcanizing agents used were 50 % dispersions prepared by conventional ball-milling method.

Formulations of the compounding ingredients are given in Table 5.1.

Table 5.1: Formulation (dry weight) for the preparation of pre-vulcanized natural rubber latex

Ingredients	Formulations (Dry weight)			
	A	B	C	D
60% Centrifuged latex (<i>HA type</i> [#])	100	100	100	100
10% Potassium hydroxide solution	0.20	0.20	0.20	0.20
20% Potassium laurate solution	0.24	0.24	0.24	0.24
50% Sulphur dispersion	1.5	1.5	1.5	1.5
50% ZDC* dispersion	1.0	1.0	1.0	1.0
50% Micro-ZnO dispersion	0.5	-	-	-
5% Nano-ZnO dispersion	-	0.5	0.1	0.05

[#] High ammonia latex *Zinc-diethyldithiocarbamate

Pre-vulcanization was carried out at 70 °C for 3 h and films were casted. The mixtures were designated as A, B, C and D, based on the amount of ZnO. (A- 0.5 phr micro ZnO; B- 0.5 phr nano-ZnO; C- 0.1 phr nano-ZnO; D- 0.05 phr nano-ZnO). The stability and physical properties of latex vulcanizates containing micro and nano-ZnO dispersions are given in Table 5.2.

Table 5.2: Physical properties of pre-vulcanized latex films containing micro and nano ZnO

Formulations	Chloroform number	Viscosity (cPs)	pH	Elongation at break (%)	100% modulus (MPa)	500% modulus (MPa)
A	2	418	10.42	1005	0.81	3.45
B	3	500	10.48	940	0.95	3.51
C	2	130	10.49	1277	0.78	1.89
D	2	65	10.42	1460	0.72	1.64

For antifungal activity studies, 3 replicates from each vulcanizate (A, B, C and D) were cut into same dimension and inoculated with a common contaminant fungi of rubber sheets belonging to *Trichoderma sp.* and *Aspergillus sp.* under room temperature in moist atmosphere. After 2 months the samples were tested for any fungal and bacterial growth in PDA (Potato-Dextrose Agar) and NA (Nutrient Agar) respectively.

Ageing studies were performed in air oven at 100 °C for 22 h and physical properties of the aged samples were estimated.

5.3 Results and Discussion

5.3.1 Sorption behavior

Figure 5.1 shows the swelling characteristics of vulcanizates in toluene at 25 °C. From the graph it is clear that PVL vulcanizates with 0.5 phr nano-ZnO offers better resistance to swelling in toluene. This shows that there are restrictions for the solvent to penetrate through the matrix. Latex vulcanized with 0.05 phr nano-ZnO shows maximum swelling due to lower crosslink density as shown in Table 5.3. An interesting observation is that the crosslink density is almost same for PVL films containing 0.1 phr nano-ZnO (sample C) and 0.5 phr micro-ZnO (sample A), which indicates that nano-ZnO even at low loading can impart better solvent resistance.

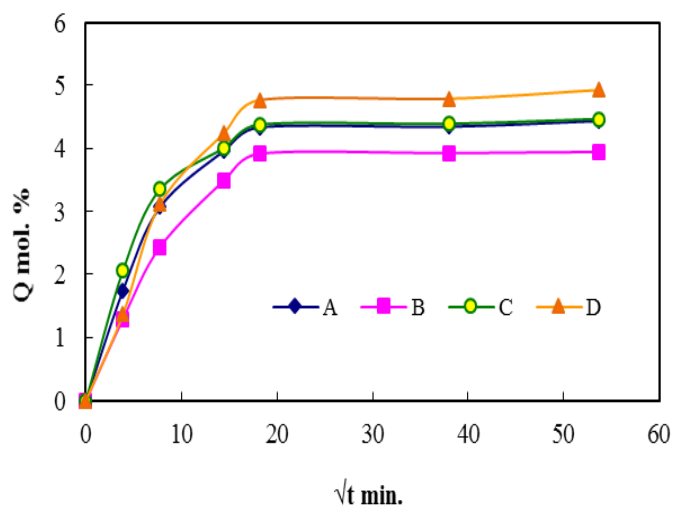


Figure 5.1: Swelling behaviour of pre-vulcanized latex films with micro and nano-ZnO

Table 5.3: Volume fraction of rubber and crosslink density of pre-vulcanized latex films containing micro and nano-ZnO

Sample type	Volume fraction of rubber (V_r)	Crosslink density $\times 10^5$ (mol/cm ³)
A	1.0477	12.3196
B	1.0685	14.1252
C	1.0524	12.1484
D	1.0512	10.7797

5.3.2 Antimicrobial activity

Antimicrobial activity of PVL films against the fungi *Trichoderma sp.* and *Aspergillus sp.* are shown in the Table 5.4.

Table 5.4: Antimicrobial properties of micro and nano ZnO incorporated pre-vulcanized NR latex films

Sample	Up to 6 weeks	After 6 weeks	After 2 months	
	Fungi	Fungi	Fungi	Bacteria
A	-	+	+	+
B	-	-	+	+
C	-	+	+	+
D	-	+	+	+

The bits of the film from all the four treatments (A, B, C and D) did not show any fungal growth up to 6 weeks. *Trichoderma sp.* and *Aspergillus sp.* isolated from the contaminated bits did not grow in any of the bits up to the period under observation. After 6 weeks visible growth was observed in A, C and D. In sample D, after 6 weeks, all the replicates showed visible growth with the inoculated fungi *Aspergillus sp.*

and *Trichoderma sp.* None of the replicates of sample B showed visible fungal infection. This shows that the nano-ZnO can impart better anti-fungal activity in pre-vulcanized latex films as compared to an equal dosage of the micro ZnO. However, when these samples were tested in PDA and NA after 2 months, fungal and bacterial growth was observed in all these samples. Photographs of the contaminated vulcanized films after 2 months are shown in Figure 5.2.

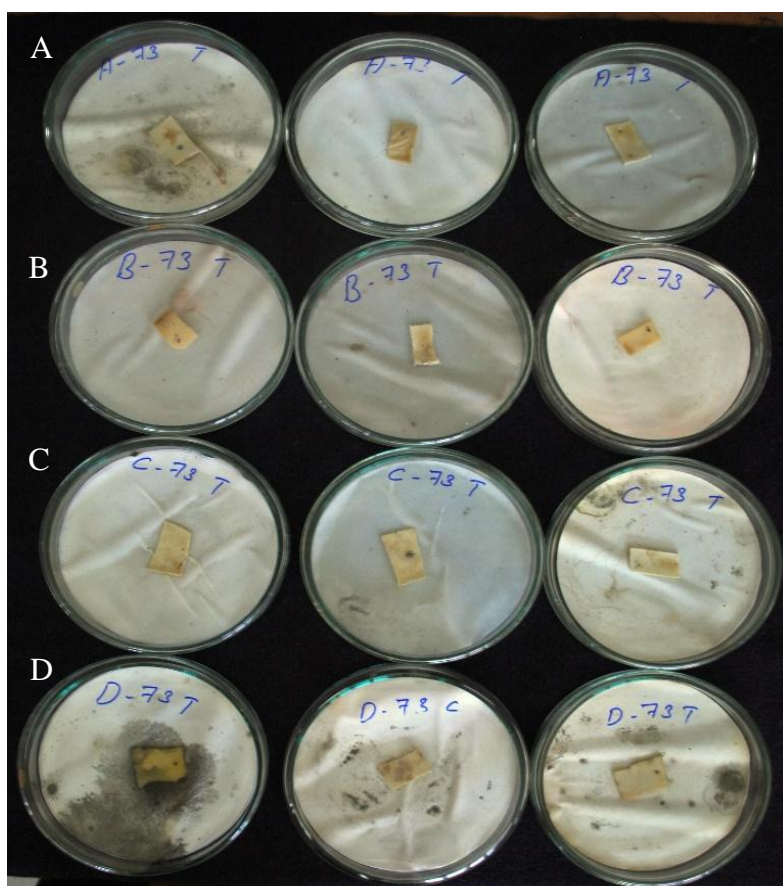


Figure 5.2: Photographs showing anti-fungal activity of ZnO in pre-vulcanized NR latex films with three replicates against fungi *Aspergillus sp.*

5.3.3 Mechanical properties

The stress-strain curves of vulcanizates are shown in Figure 5.3. Strain induced crystallization at large elongations ($> 300\%$ strain) plays a major role in the mechanical properties of natural rubber [15]. Presence of nano-ZnO at higher dosage (0.5 phr) in the latex based vulcanizate gives high initial modulus, indicating high reinforcement. As the concentration of nano-ZnO increases, the stress - strain curve is shifted towards high stress values indicating high level of crosslinks in nano-ZnO incorporated vulcanizates. As elongation increases to $> 400\%$, strain amplification (strain induced crystallization) come into play and increases proportionally with elongation. Strain induced crystallization of natural rubber is affected by filler content [16].

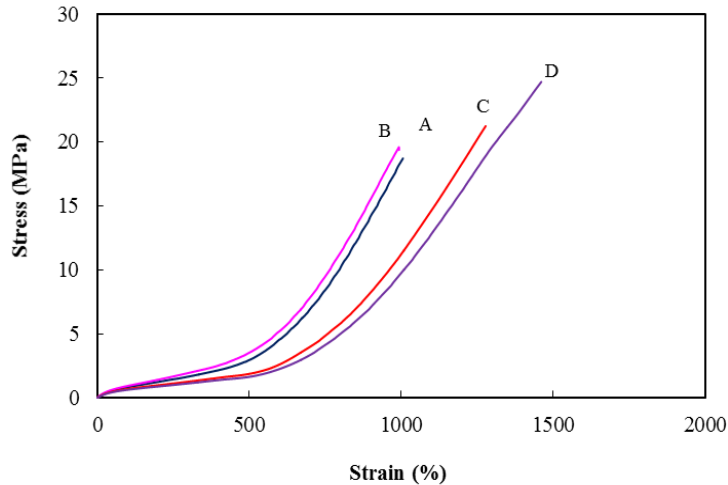


Figure 5.3: Stress strain behaviour of pre-vulcanized natural rubber latex films containing micro and nano ZnO

The tensile strength of micro and nano particulate filled composites depends on the effectiveness of stress transfer between matrix and fillers [17]. Figure 5.4 shows the effect of micro and nano-ZnO at various amounts (0.5 phr, 0.1 phr and 0.05 phr) on tensile strength of pre-vulcanized NR latex films.

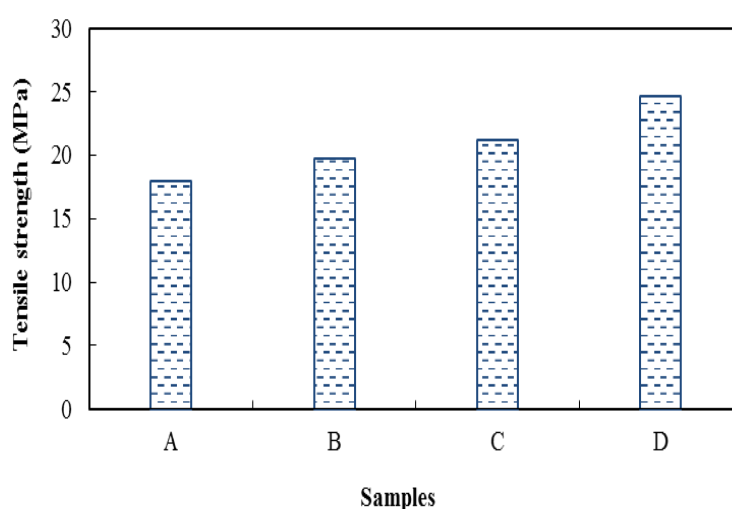


Figure 5.4: Tensile strength of pre-vulcanized natural rubber latex films containing micro and nano ZnO

From the graph it is obvious that nano-ZnO filled PVL films exhibited higher tensile strength than conventional ZnO incorporated films. By reducing the amount of nano-ZnO from 0.5 phr to 0.05 phr, tensile strength increases. Latex pre-vulcanized with 0.5 phr nano-ZnO, resulted in lower tensile strength. The decrease in tensile strength at higher nano-ZnO loading is due to particle-particle aggregation, resulting poor interaction with rubber matrix. However, this drop in tensile strength is still at par with the tensile strength offered by conventional ZnO. The crosslink density of 0.5 phr nano-ZnO

incorporated latex vulcanizate was found to be high. The formation of many crosslinks affects the degree of crystallinity of rubber during stretching [18]. The tensile strength of pre-vulcanized films is governed not only by introducing crosslinks but also the ability of particles to coalesce among themselves. When the film is prepared from highly crosslinked latex, coalescence of rubber particles become more and more difficult, resulting in lower tensile strength [19]. The agglomeration of ZnO nanoparticles at higher levels also leads to lower tensile properties [20].

Modulus is the ratio of stress to strain in the linear region of stress-strain curve. It is a bulk property and depends primarily on the geometry, particle size distribution and concentration of filler [21]. Other parameters attributed to an increase in modulus are the aspect ratio of the filler and the orientation of fillers. Figure 5.5 displays the modulus of PVL films containing conventional micro-ZnO and nano-ZnO at 700 % elongation. The modulus value decreased on decreasing the concentration of nano-ZnO. The modulus of elongation of the sample containing 0.5 phr nano-ZnO was 8.04 MPa whereas modulus of the vulcanizate containing the same loading of micro-ZnO was 7.63 MPa. From this it is clear that nano-ZnO has better activity compared to micro ZnO. Further the particle size of nano-ZnO is ~ 55 nm so that the surface area is high and the activity provided by them will be higher.

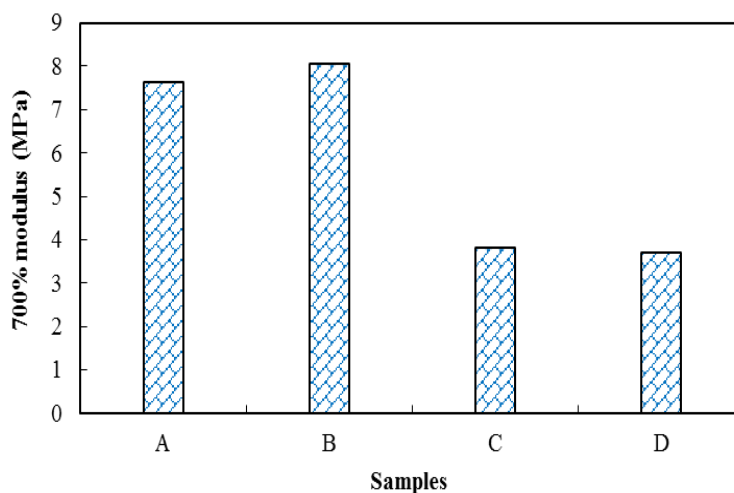


Figure 5.5: Modulus at 700 % elongation of pre-vulcanized natural rubber latex films containing micro and nano ZnO

5.3.4 Effect of ageing

The effect of ageing at 100 °C for 22 h on tensile strength and modulus of pre-vulcanized films containing micro and nano-ZnO are shown in Table 5.5.

Table 5.5: Effect of micro and nano ZnO on mechanical properties of pre-vulcanized natural rubber latex films after ageing at 100 °C for 22 h.

Sample	Tensile strength (Before ageing) MPa	Tensile strength (After ageing) MPa	Retention in tensile strength %	100% modulus MPa	500% modulus MPa	700% modulus MPa
A	18	3.50	19.44	0.29	1.00	2.11
B	19.7	8.67	44	0.36	1.06	2.25
C	21.24	4.58	21.57	0.3	1.03	2.15
D	24.68	3.60	14.59	0.25	0.87	1.98

It was observed that ageing resistance was improved by adding nano-ZnO. After ageing, the tensile strength of the vulcanizate incorporated with 0.5 phr nano-ZnO was 8.67 MPa whereas the corresponding value for micro-ZnO filled films were 3.50 MPa only. This shows that addition of nano-ZnO offers better retention in tensile strength after ageing compared to the conventional micro ZnO. But, by reducing the concentration of nano-ZnO, tensile strength decreases.

Elongation at break (EB) indicates the maximum extension of samples under tension. Elongation at break for PVL films containing micro and nano-ZnO before and after ageing is shown in Figure 5.6.

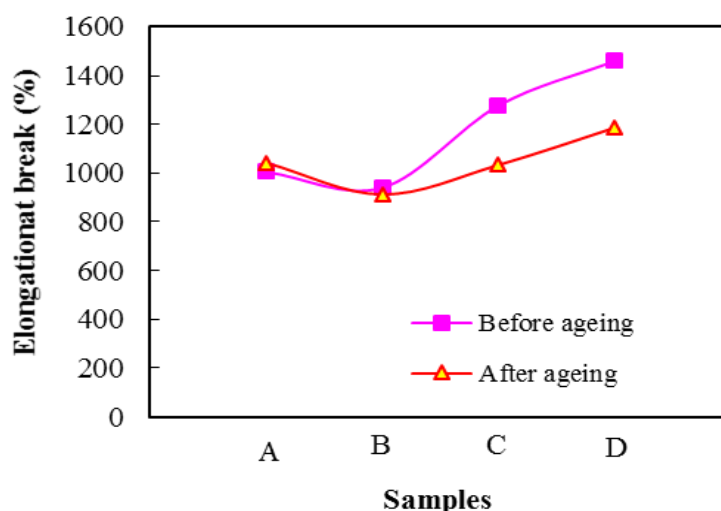


Figure 5.6: Elongation at break of micro and nano ZnO filled pre-vulcanized NR latex films before and after ageing

The EB depends on the level of vulcanization in the rubber. By reducing the amount of nano-ZnO from 0.5 phr to 0.05 phr, the

elongation at break increased. This increase in elongation at break is due to the variation in crosslink density in the rubber matrix. The reduction in elongation at break in the case of vulcanizates containing higher loading of nano-ZnO is apparently due to the higher crosslink density in the matrix. However, the vulcanizates containing higher amounts of ZnO (micro and nano - 0.5 phr each) showed lower reduction in elongation at break after ageing compared to the vulcanizates containing lower dosages of ZnO.

5.4 Conclusions

Lower solvent up-take (in toluene) was noticed in pre-vulcanized natural rubber latex films containing 0.5 phr nano-ZnO. Also, the swelling behaviour of pre-vulcanized films containing 0.1 phr nano-ZnO and 0.5 phr conventional micro ZnO are the same. Nano-ZnO imparts better antifungal activity in pre-vulcanized latex films as compared to an equal dosage of the micro ZnO. The tensile strength and elongation at break of the pre-vulcanized latex films increases with decreasing the concentration of nano-ZnO indicating better crosslinking induced by nanoparticles in the rubber matrix. At higher dosage (0.5 phr nano-ZnO loading), agglomeration among the high surface area ZnO nano particles also leads to reduction in tensile strength and elongation at break. Modulus of latex films increases by increasing nano-ZnO addition. Compared with micro ZnO, incorporation of nano-ZnO results in better retention of mechanical properties after ageing.

References

- [1] K. F. Gazeley, A. D. T. Gorton, and T. D. Pendle, *Natural Rubber Science and Technology* (Ed. A.D Roberts); Oxford University Press: Oxford, United Kingdom, Chap 3. 85 (1988).
- [2] K. K. Sasidharan, R. Joseph, S. Palaty, K. S. Gopalakrishnan, G. Rajammal, and V. Pillai, *J. Appl. Polym. Sci.*, **97**, 1804 (2005).
- [3] M. W. Philpott, *J. Rubber Res. Inst. Malayasia.*, **22**, 441 (1969).
- [4] G. B. Feild, W. S Ropp, *US Patent 2802891 A*, Hercules Powder Co. Ltd. (1957).
- [5] K. M. Zakir Hossain, A. M. Sarwaruddin Chowdhury, M. E. Haque, N. C. Dafader, and F. Akhtar, *Polym. Plast. Technol. Engg.*, **49**, 136 (2010).
- [6] T. D. Pendle, Latex Technology educational symposium (18) (1987) 131st meeting Rubber division ACS Canada **1987**.
- [7] A. Chapman, and T. Johnson, *KGK Kautschuk Gummi Kunststoffe*, **58**, 358 (2005).
- [8] P. Bindu, and S. Thomas, *Polym. Engg. Sci.*, **53**, 1337 (2013).
- [9] S. P. Thomas, E. J. Mathew, and C. V. Marykutty, *J. Appl. Polym. Sci.*, **124**, 3099 (2012).
- [10] M. Z. Lv, L. Fang, P. W. Li, and C. L. Yang, *Adv. Mater. Res.*, **936**, 394 (2014).
- [11] W. G. I. U. Rathnayake, H. Ismail, A. Baharin, I. M. C. C. D. Bandara, and S. Rajapakse, *J. Appl. Polym. Sci.*, **131**, 1 (2014).
- [12] K. Anand, S. Varghese, and T. Kurian, *Intl. J. Theo. Appl. Sci.*, **6**, 87 (2014).
- [13] B. Ellis, and G. N. Welding, *Rubber Chem. Technol.*, **37**, 571 (1964).
- [14] A. P. Mathew, S. Packiriswamy, M. Kumaran, and S. Thomas, *Polymer*, **36**, 4935 (1995).

- [15] B. Ozbas, S. Toki, B. S. Hsiao, B. Chu, R. A. Register, I. A. Aksai, R. K. Prud'homme, and D. H. Adamson, *J. Polym. Sci. PART B: Polym. Phys.*, **50**, 718 (2012).
- [16] A. N. Gent, S. Kawahara, and J. Zhao, *Rubber Chem. Technol.*, **71**, 668 (1998).
- [17] S. Y. Fu, X. Q. Feng, B. Lauke, and Y. W. Mai, *Composites: PART B.*, **39**, 933 (2008).
- [18] R. Roslim and M. Y. Amir Hashim, *J. Rubber Res.*, **13**, 125 (2010).
- [19] N. M. Claramma, and N. M. Mathew, *J. Appl. Polym. Sci.*, **65**, 1913 (1997).
- [20] M. Altan, H. Yildirim, and A. Uysal, *The Online J. Sci. Technol.*, **1**, 25 (2011).
- [21] S. S. Ochigbo, and A. S. Luyt, *Intl. J. Composite Mater.*, **1**, 7 (2011).

.....✪✪.....

Chapter 6

DEGRADATION BEHAVIOUR OF NANO SILICA AND NANO TITANIA FILLED NATURAL RUBBER LATEX NANOCOMPOSITES

Contents	6.1 Introduction
	6.2 Experimental
	6.3 Results and Discussion
	6.4 Conclusions

The shelf-life of natural rubber latex products are highly dependent on various environmental factors. To improve the quality as well as performance, fine particle dispersions are employed in their formulations. The degradation behaviour of silica (SiO₂) nanoparticles and titania (TiO₂) nanoparticles incorporated natural rubber latex (NR) nanocomposites against various degrading agents viz. thermal, γ - radiation, UV radiation and chlorination were studied. The properties such as tensile strength, elongation at break and modulus were recorded after exposing the latex films to various degrading environments. Compared to the gum vulcanizates, addition of nano SiO₂ and nano TiO₂ improved the tensile strength even after ageing. Enhanced UV resistance was noticed for nano titania latex composites from mechanical property measurements. Nano SiO₂ (0.3 phr) imparted maximum tensile strength after chlorination.

Part of work presented in this chapter has been published in *Rubber Science*, 28(3), 294-304, (2015).

6.1 Introduction

Natural rubber (NR) exhibits unique mechanical properties due to highly stereo regular microstructure resulting from its high molecular weight [1]. However, its resistance to heat, oxygen and ozone is poor due to the presence of large number of double bonds in the chemical structure [2]. Degradation of NR can be affected by a variety of factors such as elevated temperatures, light, humidity, impurities, radiation, chemicals *etc.* The shelf-life of rubber products are dependent on such environmental factors.

Natural rubber on prolonged exposure to heat undergoes thermo-oxidative degradation, which in turn adversely affect the properties. When NR products are exposed to UV radiation, free radicals are produced. These free radicals abstract H atom from poly-isoprene chains thereby producing more free radical sites in the chain. These alkyl free radicals react with oxygen in atmospheric air to produce hydroperoxides. The free radical chain reaction process continues until the entire rubber gets degraded [3]. Light ageing in rubber can be retarded by adding UV resistant materials and by the use of antioxidants which will inhibit any subsequent oxidation. Chlorination, a process commonly used in the manufacture of powder-free gloves, may have detrimental effects on the mechanical and barrier properties after exposure to elevated temperatures [4]. Crack generation, discolouration and poor heat resistance were observed for un-vulcanized NR latex films after chlorination [5]. Degradation of NR by γ - radiation is also a serious issue, where it is exposed for sterilization purpose.

It would be quite interesting to study the effect of nano-fillers on degradation resistance of NR latex films. Development of nanocomposites consisting of TiO₂ and SiO₂ nanoparticles in organic polymeric matrix is positively perceived now-a-days [6]. TiO₂ is a well-known inorganic material with good optical and photo catalytic properties. Due to high refractive index and excellent light scattering capacity, it is effectively used as white pigments. Besides, it provides better protection against UV light. Incorporation of TiO₂ nanoparticles in to polymer matrix results in improved thermal stability and mechanical strength [7, 8]. Natural rubber/silica (NR/SiO₂) nanocomposite with a SiO₂ loading of 4 wt. % was developed by latex compounding with self-assembly technique [9]. The resulting nanocomposites showed enhanced thermal resistance. Several publications are available regarding the reinforcement of natural rubber with nano-fillers [10 -13]. The ageing properties of NR and filled rubber vulcanizates are studied by various authors [14-19].

The oxidation process requires contact between rubber and oxygen which normally can occur at the surface of the product. The diffusion of oxygen in to the bulk of the rubber is a slow process; consequently, oxidation is confined to the surfaces of thick articles whereas latex based thin articles suffer more from the effects of oxidation [20]. The major reactions operating under accelerated ageing conditions are polymer chain scission, crosslinking and crosslink breakage.

The main objective of the present study is to analyze the effect of ageing conditions including thermal, chlorination, UV and γ - radiation on the mechanical properties of NR latex vulcanizates filled with nano

TiO₂ and nano SiO₂. The mechanical properties of latex vulcanizates containing different filler content were compared with the gum (un-filled) vulcanizate. The swelling index and crosslink density of all the vulcanizates prior to exposure to the ageing atmosphere was also measured.

6.2 Experimental

6.2.1 Methods

The specifications of centrifuged natural rubber latex and filler dispersions used are given in experimental section. Dispersions of the other compounding ingredients were prepared by conventional ball milling method. Latex compounding formulations used are given in Table 6.1.

Table 6.1: Formulation of the latex compound

Ingredients	Dry weight (phr)
60% Centrifuged latex (High ammonia type)	100
10% Potassium hydroxide solution	0.20
20% Potassium laurate solution	0.10
50% Sulphur dispersion	1.5
50% ZDEC* dispersion	1.0
50% Zinc oxide dispersion	0.5
20% Nano SiO ₂ dispersion	Variable
37% Nano TiO ₂ dispersion	Variable

*Zinc diethyldithiocarbamate

Before adding the compounding ingredients, the total solid content of the latex was maintained at 55 per cent. The compounded NR latex was matured for 24 h at room temperature.

6.2.1.1 Preparation of latex films

The compounded NR latex was mixed with varying amount of nano SiO₂ and nano TiO₂ dispersions and gently stirred for getting uniform distribution. The compounded latex was then poured on side raised glass plates (inside dimensions 13 cm x 10 cm x 2 mm) and films were casted. Drying of the latex films were carried out at 45 °C in air oven. Post-vulcanization was carried out at 100 °C for 1 h to ensure maximum strength to the composite films. The vulcanized latex films are designated as G, T1, T3, T5, S1, S3 and S5. G represents gum vulcanizate whereas T and S denote nano TiO₂ and nano SiO₂ filled vulcanizates respectively. The numbers (1, 3, 5) indicate vulcanizates containing 0.1, 0.3 and 0.5 phr filler respectively.

The details regarding swelling index measurements, crosslink density determination and degradation studies are explained in experimental part and mechanical properties are measured thereafter.

6.3 Results and Discussion

The particle size distribution curves of silica and titania nanoparticles are displayed in Figure 6.1. The average particle size (Z-average) of nano TiO₂ and nano SiO₂ dispersions are 84 nm and 297 nm respectively. For nano TiO₂, 49.8 per cent of the particles showed size < 100 nm and 50.2 per cent showed size in the range of 100-500 nm. In the case of nano SiO₂, majority of the particles (94.5 per cent) showed size in the range 100 - 500 nm. Particles having size below 100 nm was absent in the case of nano SiO₂.

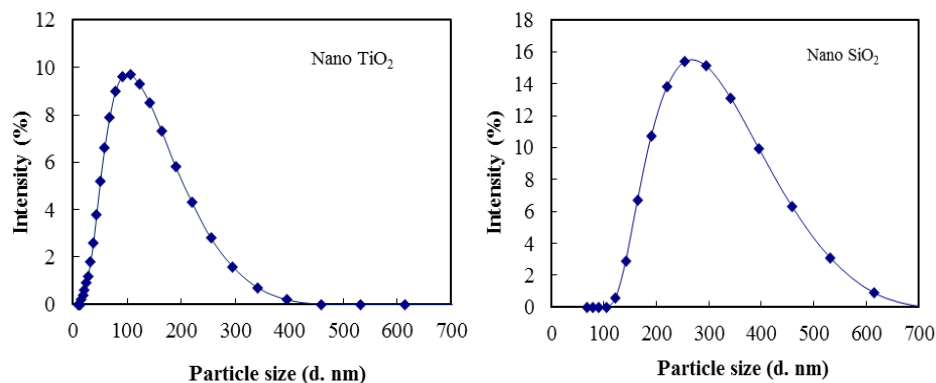


Figure 6.1: Particle size distribution of nano titania (TiO_2) and nano silica (SiO_2) dispersions

6.3.1 Swelling studies

The swelling indices of the gum and the composite latex films are shown in Table 6.2.

Table 6.2: Swelling index and crosslink density of vulcanized latex films

Samples	Swelling index	Cross link density ($\times 10^5$) (moles/ cm^3)
G	4.119	5.618
T1	4.142	5.562
T3	4.084	5.987
T5	3.944	6.246
S1	4.141	5.454
S3	3.973	5.975
S5	3.485	6.561

The crosslink density of the sample is related to swelling index. In comparison with the gum vulcanizates, swelling indices of the filled vulcanizates are lower and the reduction is more pronounced at higher filler loadings. This indicates that the extent of vulcanization is higher in

the filled specimen than the virgin specimen. Among all, vulcanized latex films incorporated with 0.5 phr nano silica dispersion exhibited the lowest swelling index values. The crosslink densities of filled systems (Table 6.2) are higher compared to gum sample and are more pronounced at higher filler loading (0.5 phr). The presence of high surface area nanoparticles and their homogeneous distribution in the rubber matrix provides more hindrance to the solvent molecules thereby improving the solvent resistance capacity.

6.3.2 TGA studies

The percentage weight of NR/TiO₂ and NR/SiO₂ nanocomposites retained at various temperatures is determined from TGA studies and is given in Table 6.3.

Table 6.3: Weight % retention of gum and nanocomposite samples at various temperatures

Temperature (°C)	wt. % retained						
	<i>Gum</i>	<i>T1</i>	<i>T3</i>	<i>T5</i>	<i>S1</i>	<i>S3</i>	<i>S5</i>
250	96.7	97.2	97.1	96.9	97.2	96.2	96.3
300	94.4	95.1	95.2	95.0	95.1	93.7	94.0
350	89.8	89.7	90.1	87.2	90.1	84.6	87.3
400	32.8	33.1	35.5	27.8	36.2	28.9	31.6
450	3.6	4.3	5.1	4.0	5.3	4.2	6.7
500	1.3	2.1	3.0	2.9	3.1	2.4	4.8

The thermal stability of the composite is proportional to the weight retained at a particular temperature. Latex composites containing nano TiO₂ and nano SiO₂ imparts better thermal stability to the vulcanizates. At 500 °C, the weight % retained for 0.1, 0.3 and 0.5 phr nano TiO₂ filled

composites were 2.1, 2.3 and 2.9 respectively, whereas it was 3.1, 2.4 and 4.8 for nano SiO₂ filled composites. For gum vulcanizate it was only 1.33.

6.3.3 Effect of thermal ageing

In rubber compounds, high temperature causes two competing reactions- crosslink formation and chain scission. This will affect the mechanical properties of the composites. The variation in tensile strength, elongation at break (EB) and modulus of the NR latex nanocomposites can be explained based on these processes.

The percentage retention of tensile strength of NR/TiO₂ and NR/SiO₂ nanocomposites after thermal ageing is shown in Figure 6.2.

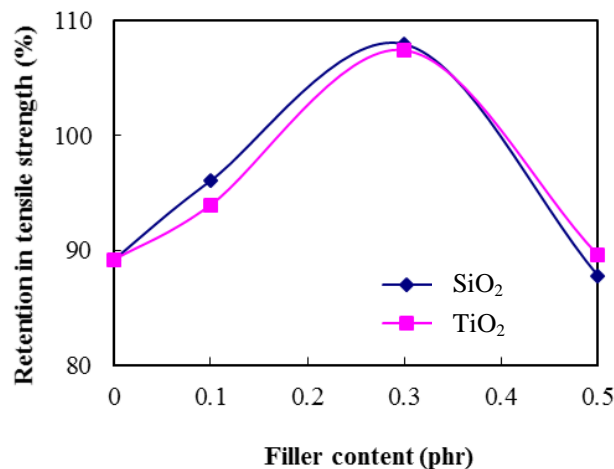


Figure 6.2: Percentage retention in tensile strength of nanocomposites after thermal ageing

After ageing at 70 °C for 7 days, the retention values of both the composite increases (107 %). This is much higher than (89 %) the retention of the gum vulcanizate. High retention in tensile strength value has been attained for the composites with the addition of 0.3 phr filler.

Further increase in filler concentration (*i.e.* 0.5 phr) causes reduction in tensile strength. A slight reduction in tensile strength is observed for SiO₂ filled systems at higher loadings. This might be due to the adsorption of sulphur on the surfaces of the silica particles. Due to this adsorption, sulphur available for crosslinking will be minimum which leads to mono-sulphidic linkages. Further, the strain induced crystallization of rubber will be hindered by high filler content and may affect the strength [21].

The flexibility of rubber composites can be expressed using the parameter elongation at break (EB). Variation of EB of thermally aged latex nanocomposites with filler content is given in Figure 6.3.

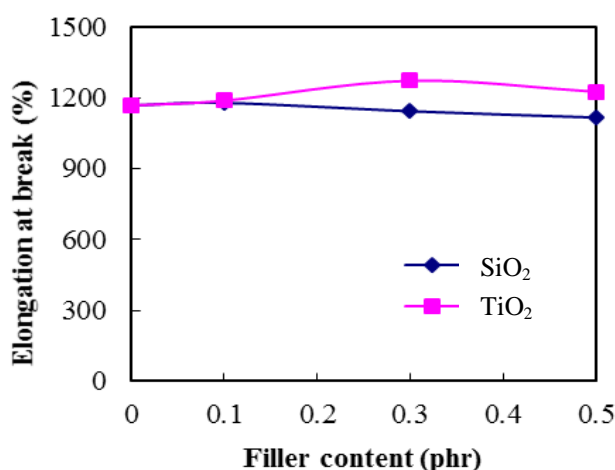


Figure 6.3: Effect of filler content on elongation at break of nanocomposites after thermal ageing

At higher filler loadings, NR/TiO₂ nanocomposites showed higher EB compared to NR/SiO₂. Highest EB of (1272) was registered for latex vulcanizates containing 0.3 phr nano TiO₂. For NR/SiO₂ nanocomposites, EB value has decreased with increase of SiO₂ content. This reduction is

due to stiffening of the matrix. Modulus increases due to additional crosslink formation and this reduces the elongation. Also, the improved adhesion of nano SiO_2 restricts the mobility of NR chain thereby causing reduced elongation. As more crosslinks are formed, the segmental mobility of the rubber chain decreases. This also leads to a gradual reduction in EB for NR/ SiO_2 nanocomposites.

Figure 6.4 illustrates the variation of M100 (modulus at 100 per cent elongation) of aged nanocomposites with filler loadings.

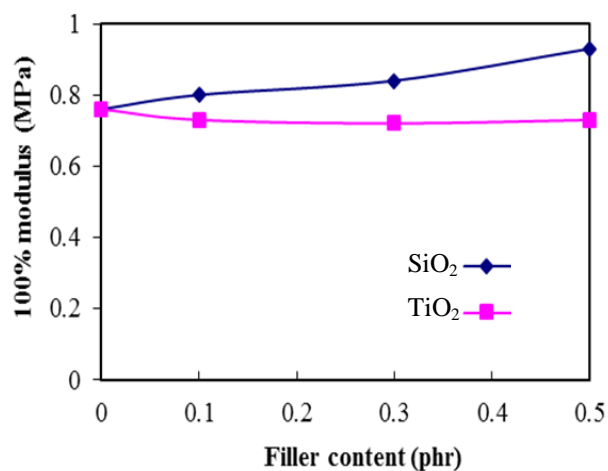


Figure 6.4: Effect of filler content on modulus (M100) of nanocomposites after thermal ageing

Modulus changes are directly associated with changes in the original crosslink structure, such as main chain scission and crosslink modifications [16]. NR/ SiO_2 nanocomposite exhibited higher modulus than NR/ TiO_2 and it increases with increase in filler content whereas the M100 of NR/ TiO_2 nanocomposites were not affected by TiO_2 content. Incorporation of 0.5 phr nano SiO_2 resulted in highest M100 (0.93 MPa) after ageing. The increase

in modulus with SiO₂ content is due to the reinforcing action of the filler. These data clearly indicates that nano TiO₂ and nano SiO₂ can impart better thermal stability to NR. It has been reported that on loading with TiO₂ pigment and china clay, good retention of tensile strength, modulus and EB is obtained for RVNRL films after thermo oxidative ageing [22].

6.3.4 Effect of chlorination

Chlorination is a method used for de-proteinization and sterilization of medical latex goods including gloves, catheters, surgical tubings *etc.* Chlorination removes the allergenic proteins and improves the donnability of the product.

Figure 6.5 displays the effect of nanoTiO₂ and nano SiO₂ on tensile properties of NR latex composite films after chlorination.

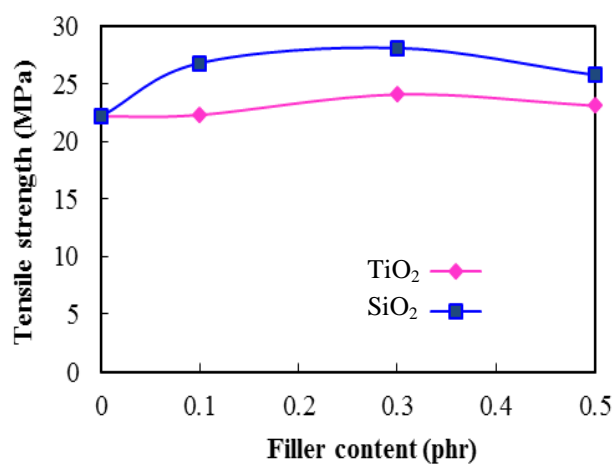


Figure 6.5: Effect of filler content on tensile strength of nanocomposites after chlorination

The high strength of gum vulcanizate is due to strain induced crystallization. It has been found that tensile strength increases with

increase of nano-filler content and reaches the maximum when the filler content is 0.3 phr. Significant increase in tensile strength for NR/SiO₂ nanocomposites is due to the addition of high surface area SiO₂ nanoparticles which will be in contact with rubber causing high stress transfer between rubber matrix and SiO₂ particles. Further increase in filler concentration causes reduction in tensile strength. Among the two, SiO₂ filled vulcanizates exhibited higher tensile strength as compared to the TiO₂ filled vulcanizates.

It can be seen in Figure 6.6 that latex vulcanizates containing nano SiO₂ showed a steady increase in M100 with filler content. Maximum modulus of 0.91 MPa was obtained for the composite with 0.5 phr nano SiO₂. On the other hand, nano TiO₂ incorporated latex composites gave the highest modulus of 0.78 MPa, which is slightly higher than the M100 of gum vulcanizate. The increase in modulus with increasing filler levels was more marked for SiO₂ than TiO₂.

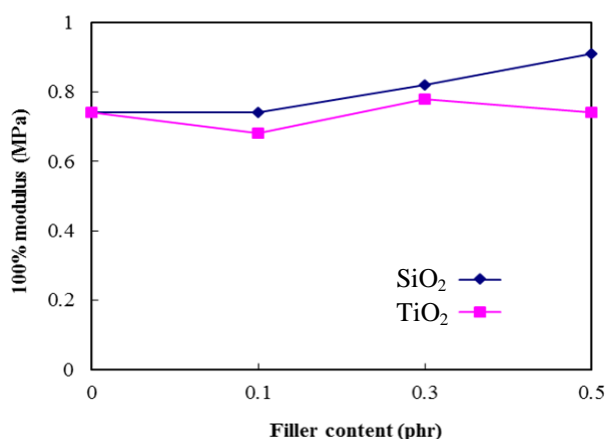


Figure 6.6: Effect of filler content on modulus (M100) of nanocomposites after chlorination

6.3.5 Effect of UV light

NR hydrocarbon produces free radicals by absorbing energy from UV radiation in the region 290-350 nm [23]. During UV irradiation chain scission may occur as a result of the following reactions [24].

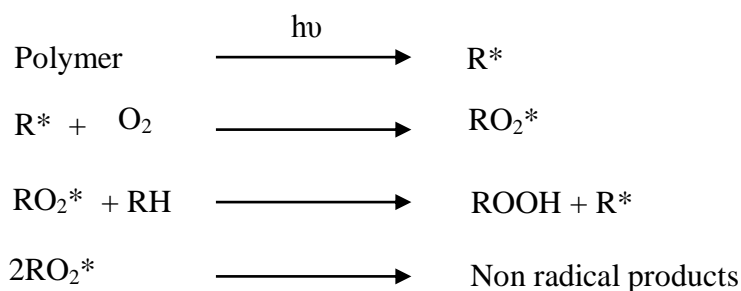


Figure 6.7 depicts the variation in tensile strength of NR/SiO₂ and NR/TiO₂ nanocomposites after exposure to UV light for 72 h. An increase in tensile strength was observed with nano TiO₂ filled samples than nano SiO₂ filled systems, with filler loadings. This indicates the better UV resistance capacity of TiO₂ based nanocomposites.

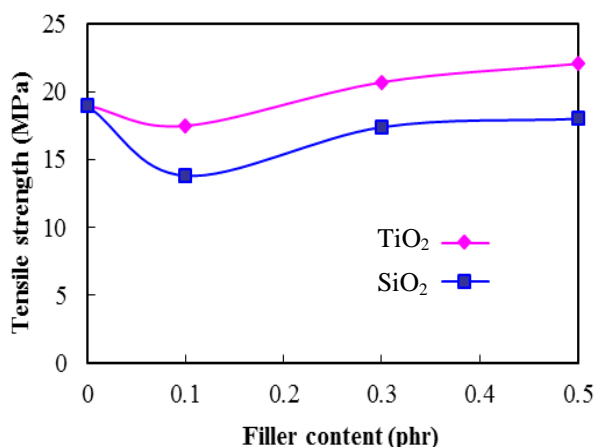


Figure 6.7: Effect of filler content on tensile strength of nanocomposites after UV ageing

Optical photographs of the UV aged latex composites containing 0.5 phr filler (nano SiO₂ and nano TiO₂) incorporated films are shown in Figure 6.8.

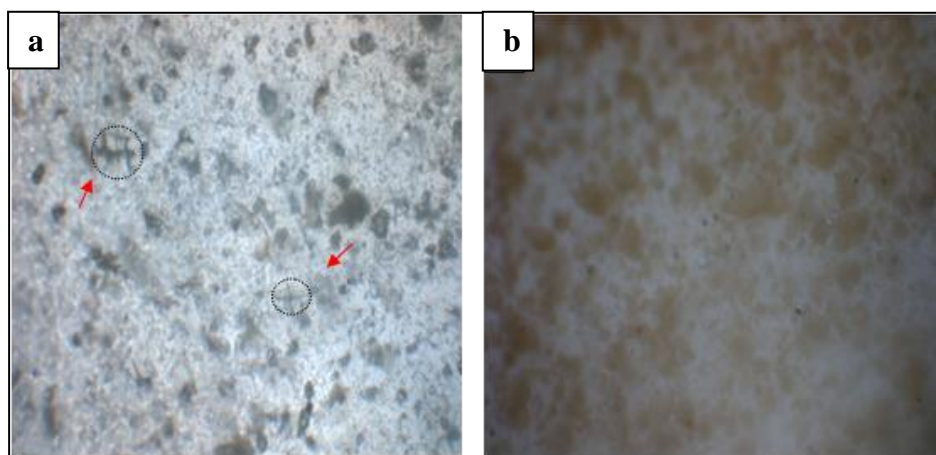


Figure 6.8: Optical photographs of UV aged latex vulcanizates containing a) 0.5 phr nano SiO₂ b) 0.5 phr nano TiO₂

After 72 h of UV irradiation, micro-cracks can be observed in NR/SiO₂ nanocomposites. The drop in tensile strength could be attributed due to the formation of surface cracks resulting in earlier sample rupture. However, for both the composites containing 0.1 phr nano fillers, a drop in tensile strength is observed. It has been presumed that reduction in tensile strength for NR/SiO₂ nanocomposites is expected to be due to the presence of OH⁻ groups, co-ordinatively unsaturated metal atoms and free radicals present on the surface of the filler *etc.* [25].

6.3.6 Effect of gamma radiation

Effect of radiation dose on tensile strength of nano filler incorporated (0.3 phr) latex vulcanizates is shown in Figure 6.9.

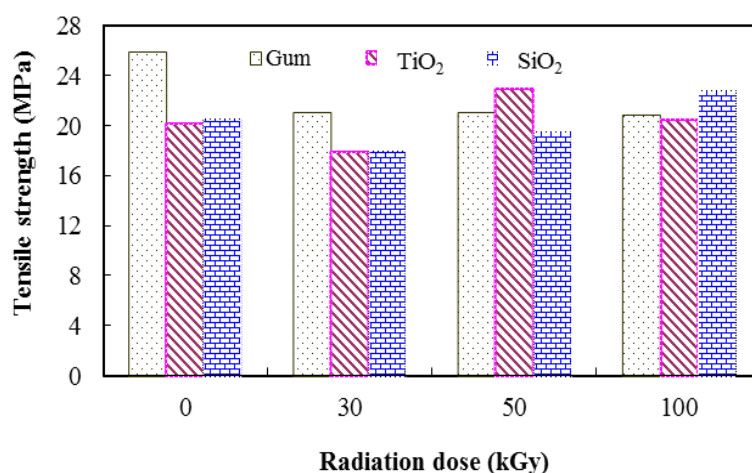


Figure 6.9: Effect of radiation dose on tensile strength of nanocomposites

The tensile strength of gum vulcanizates is initially high (25 MPa) and it decreased to 21 MPa after γ - irradiation (30 kGy). Further increase in radiation dose did not affect the tensile strength. NR/TiO₂ nanocomposite showed a higher tensile value of 23 MPa after exposure to 50 kGy radiation dose. Upon irradiation, different type of functionalities present in the surface of TiO₂ may take part in physical and chemical bond formation at the interface between TiO₂ and rubber. In the case of SiO₂ filled nanocomposites, tensile strength increases with increase in radiation dose. Moreover, the trend observed here are in accordance with the earlier reports for other rubber composites [26]. This shows that, the mechanical properties of NR/SiO₂ and NR/TiO₂ latex nanocomposites

on exposure to γ - radiation are highly dependent on filler type and its surface characteristics.

6.4 Conclusions

Incorporation of nano particles of silica and titania improved the degradation resistance of NR latex films. Retention in tensile strength was observed for the composites with 0.3 phr filler addition after thermal ageing. Silica nanocomposites exhibited better strength after chlorination. There is no colour change for the composites upon chlorination. The UV resistance capacity was found to be better for NR/TiO₂ nanocomposites. The reduction in tensile strength for NR/SiO₂ nanocomposites upon UV irradiation is due to the formation of micro-cracks on the surface of the films. In the case of SiO₂ filled nanocomposites, tensile strength increases with increase in radiation dose. A progressive increase in modulus of NR/SiO₂ composites with filler dosage can be attributed to more crosslink formation as evident from low swelling index values. Thus, the addition of suitable quantities of nano silica and nano titania in natural rubber latex can result in products having improved shelf-life.

References

- [1] M. J. Wang, *Rubber Chem. Technol.*, **71**(3), 520 (1998).
- [2] K. O. Nwanorkh, and M. E. Enyiegbulam, *Chi. J. Polym. Sci.*, **16**(2), 170 (1998).
- [3] N. R. Peethambaran, and A. P. Kuriakose, *KGK Kautchuk Gummi Kungstoffe*, **42**(12), (1989).
- [4] D. L. Walsh, D. J. Chwirut, and R. M. Kotz, *ASTM* **27**(6), pages 6, November (1999).

- [5] C. C. Ho, and M. C. Khew, *Intl. J. Adhesion Adhesives*, **19**(5), 387 (1999).
- [6] L. Rejinders, *Polym. Degrad. Stab.*, **94**, 873 (2009).
- [7] G. Wu, S. Gan, L. Cui, and Y. Xu, *Appl. Surface Sci.*, **254**, 7080 (2008).
- [8] A. Chatterjee, and M. S. Islam, *Mater. Sci. Engg. A*, **487**, 574 (2008).
- [9] S. D. Li, Z. Peng, L. X. Kong, and J. P. Zhong, *J. Nanosci. Nanotech.*, **6**, 541 (2006).
- [10] S. Varghese, and J. Karger-Kocsis, *Polymer*, **44**, 4921 (2003).
- [11] A. P. Meera, S. Said, Y. Grohens, and S. Thomas, *J. Phys. Chem. C*, **113**(42), 17997 (2009).
- [12] K. Kueseng, and K. I. Jacob, *Euro. Polym. J.*, **42**(1), 220 (2006).
- [13] A. K. Anand, S. T. Jose, R. Alex, and R. Joseph, *Intl. J. Polym. Mater.*, **59**, 33 (2010).
- [14] L. R. Baker, *NR Technol.*, **19**(2), 28 (1988).
- [15] A. D. T. Gorton, *NR Technol.* **20**(4), 65 (1989).
- [16] Y. S. Rohana Yahya, A. R. Azura, and Z. Ahmad, *J. Phys. Sci.*, **22**(2), 1 (2011).
- [17] K. M. Zakir Hossain, A. M. S. Chowdhury, M. E. Haque, N. C. Dafader, and F. Akhthar, *Polym. Plast. Technol. Engg.*, **49**, 136 (2010).
- [18] B. Kosikova, A. Gregorova, A. Osvald, and J. Krajcovicova, *J. Appl. Polym. Sci.*, **103**, (2007).
- [19] S. Mathew, S. Varghese, and R. Joseph, *Prog. Rubber Plast. Recyc. Technol.*, **29**(1), 1 (2013).
- [20] P. M. Lewis, *MRPRA Tech. Bulletin*, **46**, 49 (1987).
- [21] Y. Wang, H. Zhang, Y. Wu, J. Yang, and L. Zhang, *J. Appl. Polym. Sci.*, **96**, 318 (2005).

- [22] J. K. Kurian, *Ph.D. thesis*, “Studies for improving the degradation resistance of natural rubber latex vulcanizates with special reference to heat and UV-radiation” *Mahatma Gandhi University*, Kottayam, Kerala, p 102 October (2002).
- [23] D. J. Carlsson, A. Garton, and D. M. Wiles, *Developments in polymer stabilization*, I. G. Scott Ed. *Applied Science Publishers*, London p 219 (1979).
- [24] V. R. Gowariker, N. V. Viswanathan, and J. Sreedhar, *Polymer Science*, Chapter 10, 278 (1996).
- [25] M. T. Bryk, *Degradation of filled polymers*, *Ellis Horwood Ltd.*, Chichester, England, 74- 75, 78-79, 84-88 (1991).
- [26] M. Khalid, A. F. Ismail, C. T. Ratnam, Y. Faridah, W. Rashmi, and M. F. Al Khatib, *Rad. Phys. and Chem.*, **79**, 1279 (2010).



Chapter 7

EFFECT OF STARCH NANOCRYSTALS ON NATURAL RUBBER LATEX VULCANIZATE PROPERTIES

Contents	7.1 Introduction
	7.2 Experimental
	7.3 Results and Discussion
	7.4 Conclusions

The incorporation of bio-nano fillers such as starch nanocrystals (SNC) in polymer matrices received much attention owing to their biodegradable nature. In this work, starch nanocrystals have been isolated from modified corn starch by acid hydrolysis and their efficacy as a potential bio-filler for natural rubber latex (NR) has been explored. The quality of the SNC suspension was confirmed from dynamic light scattering (DLS) studies and X-ray diffraction (XRD) measurements. For the fabrication of nanocomposites of NR with corn starch crystals, a simple latex stage mixing procedure was employed. The platelet-like morphology of corn starch nanocrystals improved the barrier properties of NR based vulcanizates with the addition of the SNC suspension.

7.1 Introduction

Starch is a naturally occurring biodegradable polysaccharide produced by almost all green plants and is a major source of energy in the world of flora. It is the second most abundant biomass material in nature and found abundantly in plant roots, stalks, crop seeds and staple crops such as rice, corn, wheat, tapioca and potato [1, 2]. Starch is composed of two polysaccharides, amylose and amylopectin, whereas, glucose units are joined by glycosidic bonds. The amorphous (amylose) and crystalline (amylopectin) components of native starch granules are arranged alternatively encircling the point of initiation known as hilum [3].

The total worldwide starch utilization in 2008 was 66 million tons, with US being the largest starch manufacturer with bioethanol and fructose syrups together totalling 72 per cent of starch output [4]. The modified starch output is expected to experience a growth of 4.1 per cent in 2013-2018. In India, NPCS estimates that the production of starch and its derivatives was 970000 tonnes in 2010 and is anticipated to reach 2749000 tonnes by the year 2017 [5]. Low density, cost-effectiveness, environmental safety and abundant supply of these materials demand applications in various industries.

Starch nanocrystals (SNC) are formed as distinct crystalline platelets due to the disruption of the semi-crystalline structure of starch granules by the acid hydrolysis of amorphous parts [6]. Acid hydrolysis for the isolation of SNCs is cumbersome process due to several factors, such as time of hydrolysis, concentration and type of acid used, temperature *etc.* Therefore, proper control over these parameters is crucial for the

fabrication of starch nanoplatelets. The distinct platelet-like morphology, strong interfacial interaction and rigidity of the starch nanocrystal ensure improved mechanical performance, reduced solvent penetration and improved barrier properties when incorporated to polymer matrix.

With increasing environmental awareness, replacement of conventional non-renewable inorganic fillers like clay, silica *etc.* with eco-friendly bio-fillers like starch, cellulose *etc.* is getting wide acceptance for various industrial applications, particularly in rubber and allied industries where fillers are essential for improved product performance. It is also possible to develop novel functional materials with the incorporation of suitable nanofillers. Goodyear Tire and Rubber (USA) has recently developed tyres with a 30 per cent reduction in rolling resistance. They used nanoparticles derived from corn starch for partial replacement of carbon black and silica. Goodyear has been working on the corn starch-based filler since the mid-1990s and launched a tire, the GT3 BioTread, in 1999 [7].

The structural and mechanical properties of natural rubber latex filled with starch nanocrystals extracted from different sources were investigated before [8]. Waxy maize starch nanocrystals (2-50 wt. %) were incorporated into a natural rubber latex matrix and the properties of the nanocomposites such as morphology, crystallinity, swelling behaviour, barrier properties for water vapour and oxygen, thermal properties and mechanical properties were investigated [9]. Tang *et al.* used different modifying agents to improve the interaction of starch

with SBR and studied the curing behaviour, thermal properties and mechanical properties of the rubber compounds [10].

In the present study, starch nanocrystals have been isolated from modified corn starch and investigated their effect on natural rubber latex vulcanizate properties. The morphology and microstructure of the isolated corn starch nanocrystals were also studied. Finally, the mechanical properties of the composites obtained from the experimental results are compared with theoretical predictions.

7.2 Experimental

7.2.1 Materials

Details of the modified corn starch and the reagents used are mentioned in the experimental section.

7.2.2 Methods

7.2.2.1 Preparation of starch nanocrystals

Corn starch nanocrystals were isolated from modified corn starch by acid hydrolysis. Briefly, 120 g modified corn starch was mixed with 816 ml 3.16 M conc. H_2SO_4 using a magnetic stirrer in a water bath maintained at 45 °C for 5 days. The resultant aqueous suspension was centrifuged at 10000 rpm for 15 min. and washed several times with distilled water until neutral (pH = 7). The supernatant solution was discarded and the gel like precipitate thus obtained was scooped off and collected. The solid fraction of the suspension had a concentration of about 11.8 per cent. The resulting suspension was sonicated for about 10 min. and a portion of it was used for DLS and XRD analyses.

7.2.2.2 Characterization

Wide angle and small angle 2D-X-ray scattering were measured using Xeuss simultaneous WAXS/SAXS instruments. Cu-K α was the X-ray source with a collimated area of 0.64 mm². Silver behenate was used for distance calibration. 2D-X-ray scattering data were azimuthally integrated using Fit-2D software. The hydrolyzed starch samples were placed in a sample holder for X-ray measurements. The crystallinity of the corn starch nanocrystals was calculated using the reported method [11]. Scanning electron microscopy (SEM) analysis of hydrolyzed sample was performed using Zeiss EVO 18 Cryo SEM special edition with variable pressure working at 15 - 30 kV. The sample was prepared by the drop casting method on a carbon tape.

7.2.2.3 Composite preparation

Corn starch crystal suspensions were mixed well with compounded natural rubber latex at various proportions (0.69, 1.38 and 2.75 phr) and films were casted at room temperature and kept overnight. The formulation of the mixes is given in Table 7.1. The cast films were dried at 70 °C for 2.5 h and then vulcanized at 105 °C for 35 min.

Table 7.1: Formulation of the mixes

Ingredients	Dry weight (phr)
60% Centrifuged latex (High ammonia type)	100
10% Potassium hydroxide solution	0.3
50% Sulphur dispersion	1.5
50% ZDC* dispersion	1
50% ZnO [#] dispersion	0.4
30% Wingstay (A/O) dispersion	0.75
Corn starch suspension	0 (gum), 0.69, 1.38, 2.75

*Zinc diethyl dithiocarbamate

[#]Zinc oxide

7.2.2.4 Mechanical property measurements

Tensile pieces were punched from the cast films and were used to measure the mechanical properties. Six replicates were used and the average value was considered. Tension set was measured as per IS 4148 and the procedure is explained in experimental section.

Leaching of the latex films were carried out in distilled water for about 4 h and then the films were dried and kept in a desiccator overnight. The mechanical properties were tested on the next day.

The modulus of the composite films were predicted using the theoretical models (Einstein equation, Guth equation, Brinkman equation and Ponte Castaneda equation) and compared with the experimental results. The theoretical models studied are explained in experimental section.

7.3 Results and Discussion

7.3.1 DLS analysis

The particle size (DLS) curves of native corn starch (modified) and acid hydrolysed (5 days) corn starch is displayed in Figures 7.1(a) and 7.1(b), respectively.

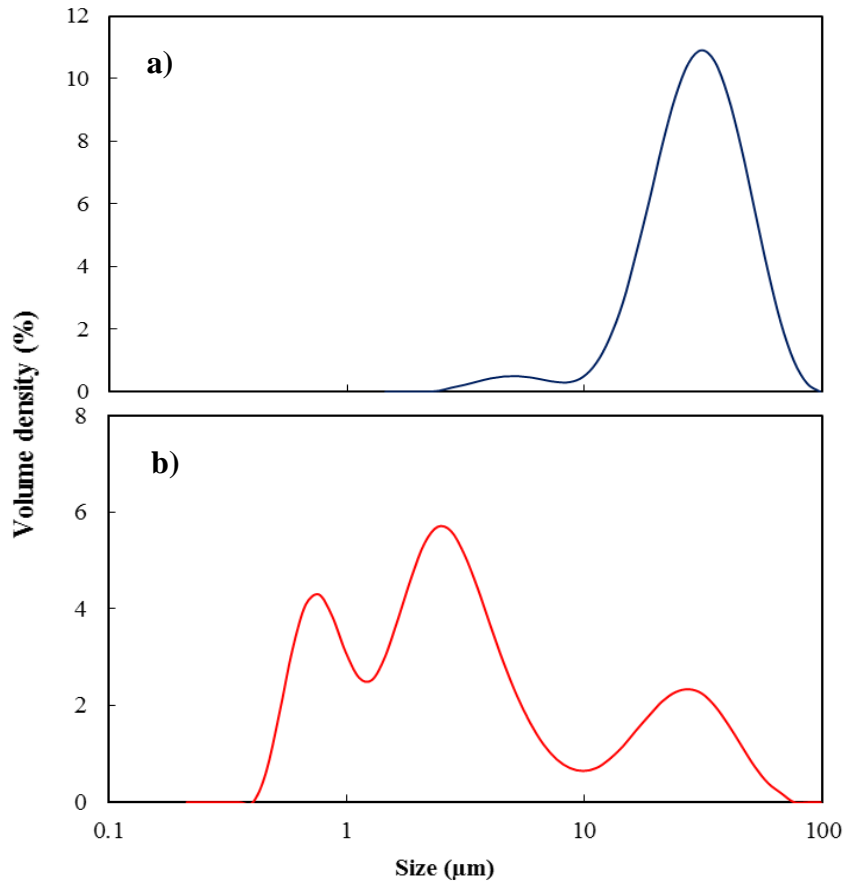


Figure 7.1: Size distribution curves of (a) native corn starch (modified) and (b) acid hydrolyzed corn starch

The mean particle size (D50) of native corn starch was 31.9 μm and it reduced to 2.84 μm after acid hydrolysis. D50 represents the particle diameter below which 50 per cent of the sample volume exists. It is also known as Mass Median Diameter (MMD). Also, the specific surface area (SSA) of native corn starch (modified) was 238 m^2/kg only and it increased to 3035 m^2/kg after acid hydrolysis confirming the presence of corn starch nanocrystals. It is well known that smaller

particles possess higher surface area. However, moderate agglomeration/flocculation of starch nanocrystals can also be seen from Figure 7.1 (b). This can be attributed to bonding of smaller particles obtained after hydrolysis of partially hydrolyzed particles [12].

7.3.2 XRD analysis

The XRD pattern of corn starch nanocrystals is shown in Figure 7.2.

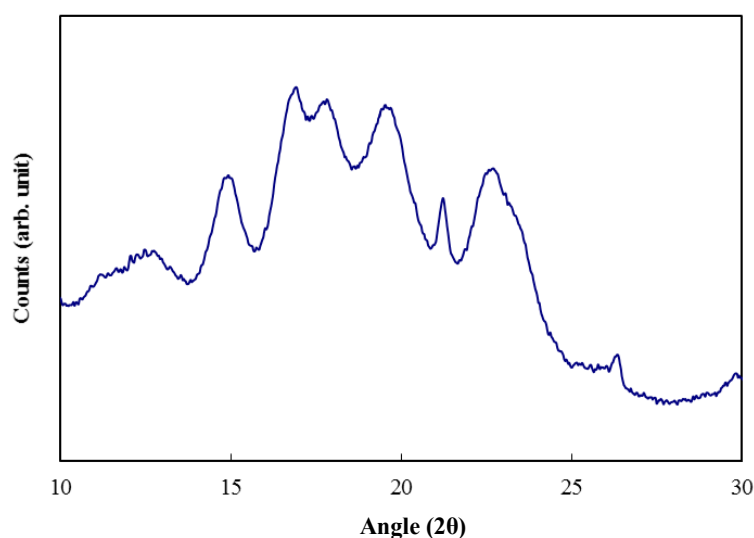


Figure 7.2: X-ray diffraction pattern of corn starch nanocrystals

Hibi *et al.* studied the effect of high pressure on the crystalline structure of corn, rice and potato starch granules. They found that high pressure changed the A-type crystalline structure to B- type [13]. The strong peaks obtained at $2\theta = 15^\circ$, 17° , 17.9° and 22.9° confirms that the crystal structure is A-type. The results are in accordance with the earlier findings [14, 15]. The peak at $2\theta = 17^\circ$ is much more prominent than other peaks. The sharper peak obtained after hydrolysis indicates that the crystallinity of

the starch increased and might be attributed to the hydrolysis of amorphous regions of starch granules. After 5 days of hydrolysis, the crystallinity index of the starch nanocrystal was 33.11 per cent.

7.3.3 SEM analysis

The morphology of acid hydrolyzed (5 days) modified corn starch was observed by SEM and is shown in Figure 7.3. As revealed from the figure, an irregular platelet like crystalline morphology was observed for SNC. The surface was not smooth. The surface roughness and heterogeneity in shapes can be understood due to the adhesion between starch granules and the surface erosion and fracture induced by continuous stirring [14]. Also, during acid treatment the starch granules undergo morphologic alterations [16].

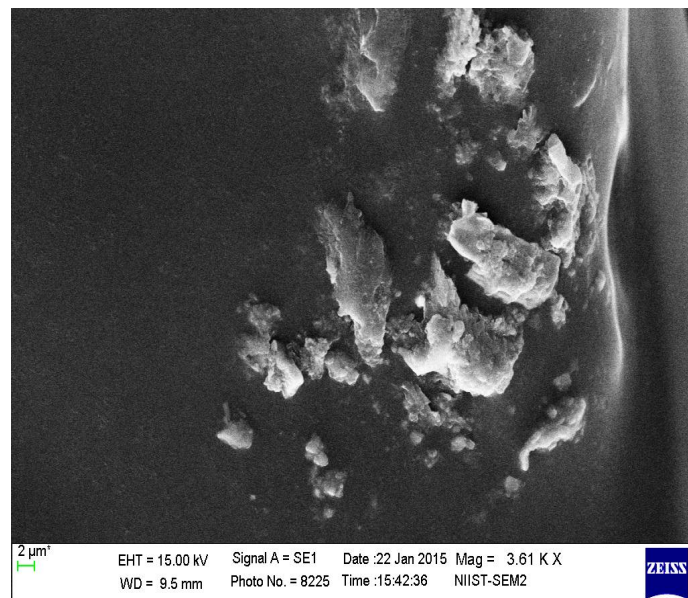


Figure 7.3: SEM image of modified corn starch granules after 5 days of acid hydrolysis

7.3.4 Swelling studies

The swelling behaviour of the gum and starch nanocrystals filled vulcanizates (0.69, 1.38 and 2.75 phr) in toluene was evaluated and the swelling index (%) of vulcanizates as a function of square root of time is displayed in Figure 7.4.

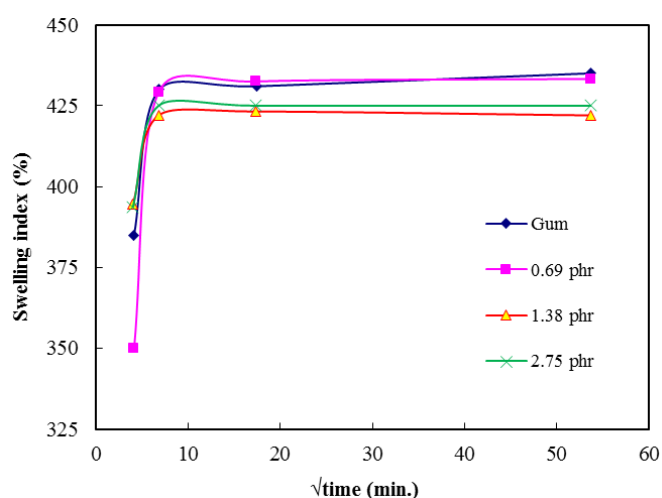


Figure 7.4: Swelling characteristics of SNC filled NR vulcanizates

The swelling measurements were carried out up to 48 h ($\sqrt{t}=53.3$ min.) and equilibrium was considered to be reached at this immersion time. Initially, except for the 0.69 phr SNC incorporated system, the vulcanizates (gum, 1.38 and 2.75 phr SNC filled) exhibited a higher swelling index. However, after 48 h, the swelling index of gum and 0.69 phr SNC filled systems were almost the same and are 435 and 433.3 respectively. The lowest swelling index of 422 was achieved by 1.38 phr SNC loading whereas it is slightly higher (425) for NR containing 2.75 phr SNC. The toluene uptake and sorption coefficient of gum and

filled vulcanizates are given in Table 7.2. Here also, the lowest values were obtained for the 1.38 phr SNC loaded systems. The platelet like morphology and more uniform distribution of SNC in polymer matrix also offer reduced sorption and organic solvent uptake. The slight increase in toluene uptake and sorption coefficient for highly filled systems (2.75 phr SNC loading) might be due to agglomeration among starch nanocrystals.

Table 7.2: Toluene uptake and sorption coefficient of gum and filled vulcanizates

	Gum	CS 0.69	CS 1.38	CS 2.75
Toluene uptake (mol. %)	4.72	4.7	4.58	4.61
Sorption coefficient (%)	535	533	522	525

7.3.5 Mechanical properties

The mechanical properties of gum and SNC filled vulcanizates (0.69, 1.38 and 2.75 phr) are given in Table 7.3.

Table 7.3: Mechanical properties of gum and filled vulcanizates

Properties	Gum	CS 0.69	CS 1.38	CS 2.75
Tensile strength (MPa)	24.4	23	17.5	19.8
Elongation at break (%)	1388	1399	1379	1246
100 % modulus (MPa)	0.69	0.71	0.74	0.84
500 % modulus (MPa)	1.74	1.7	1.87	2.33
Tension set	2.5	5	5	7.5

The reinforcing capability of SNC is evident from the modulus values. Modulus is a bulk property and it depends mainly on the geometry, particle size and distribution of the filler as well as the

concentration of the filler. The monotonic increase in 500 % modulus of NR vulcanizates with filler content can be ascribed to increased specific surface area (SSA) and aspect ratio resulting in high interaction between SNC and rubber matrix.

7.3.6 Effect of leaching

The effect of leaching on the variation in tensile strength of the resulting vulcanizates (gum and filled) is shown in Figure 7.5. The leaching process was performed on most of the dipped products, threads and moulded foams to obtain improved properties. It is also crucial for medical goods and electrician gloves where the presence of hydrophilic materials would cause absorption of atmospheric moisture and consequently accounts for reduction in electrical resistance [17]. The leaching process imparts increased tensile strength and modulus values.

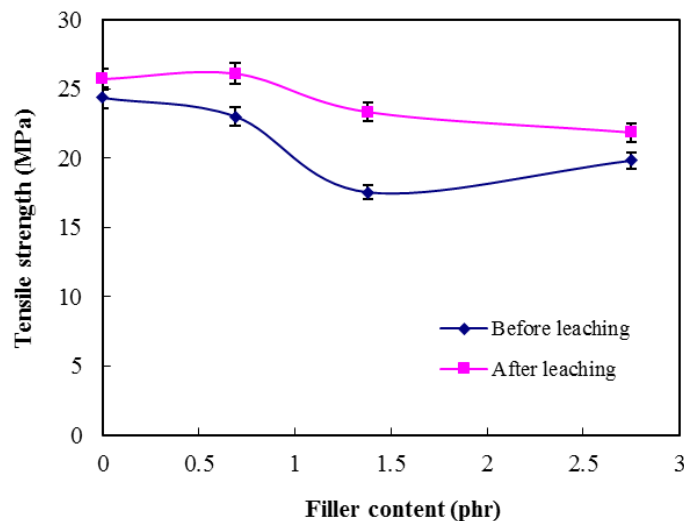


Figure 7.5: Tensile strength of SNC incorporated NR composites before and after leaching

As anticipated, after leaching, all the vulcanizates showed improved tensile strength, which is more pronounced in the filled systems. The tensile strength of gum and SNC filled vulcanizates (0.69, 1.38 and 2.75 phr loading) are 24.4, 23, 17.5 and 19.8 MPa respectively (Table 7.3), and after leaching the values increased to 25.7, 26, 23.3 and 21.8 MPa respectively. The improved tensile strength for filled latex films after leaching could be attributed to the removal of acidic and amorphous components (unhydrolyzed if any present) and favoured enhanced coalescence among rubber particles and increased polymer-filler interaction.

The percentage retention in elongation at break (EB) of gum and SNC filled vulcanizates after leaching is displayed in Figure 7.6.

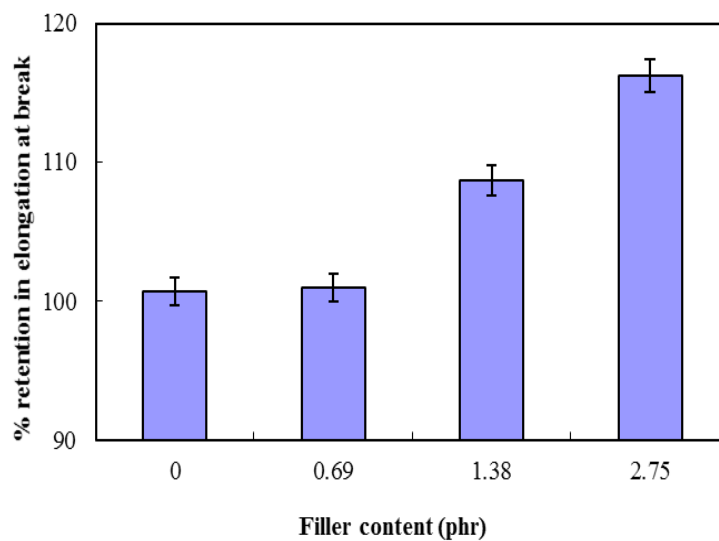


Figure 7.6: Percentage retention in elongation at break (EB) of SNC incorporated NR composites after leaching

It is obvious that, the percentage retention in elongation at break of filled vulcanizates increases with filler loading. This can be attributed to

increased water absorption by the filler during leaching. Since the filler is highly hydrophilic in nature, higher filler content causes increased water absorption. The increase in tension set (%) values of filled vulcanizates (particularly at higher filler loadings) also supports this. The improved elongation at break is also due to increased interaction between latex and SNC. The increase in modulus with filler content (Table 7.3) and increase in EB indicate that corn starch nanocrystals reinforce the latex vulcanizates without losing elasticity.

7.3.7 Theoretical predictions

The relative moduli (E'/E_0) of the composite films obtained from the experimental results were compared with theoretical predictions. The theoretical predictions are plotted with the experimental results in Figure 7.7.

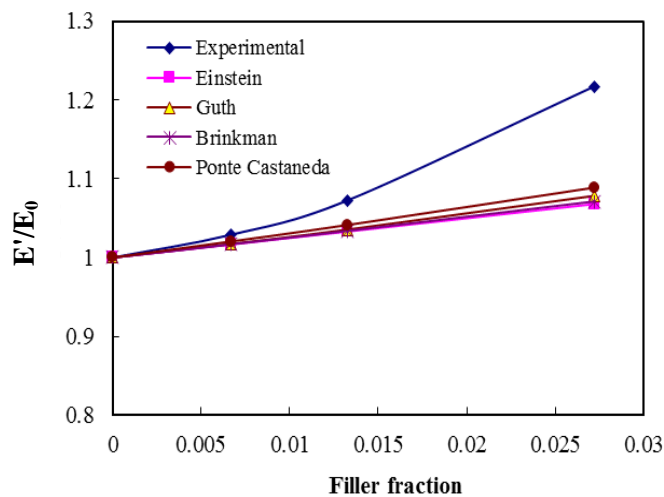


Figure 7.7: Theoretical modelling of the relative moduli of SNC incorporated NR composites

It can be seen that at higher filler loading, the modulus value calculated from the experimental results are higher than predicted. The difference in experimental result with the theoretical assumptions at higher loadings indicates considerable interaction between polymer and filler [18].

7.4 Conclusions

Starch nanocrystals (SNC) were separated from modified corn starch by an acid hydrolysis method. The resulting corn starch crystal suspensions were characterized by DLS and XRD analysis and confirmed the presence of corn starch nanocrystals. Natural rubber latex-corn starch crystal nanocomposites were prepared by compounding method, and the vulcanizate properties and swelling index were measured. An optimum SNC loading of 1.38 phr imparted improved solvent resistance to the NR latex film. The mechanical properties of SNC incorporated vulcanizates were found to be good.

References

- [1] D. LeCorre, J. Bras, and A. Dufresne, *Biomacromolecules*, **11**, 1139 (2010).
- [2] R. L. Whistler, and E. F. Paschall, *Starch: Chemistry and Technology*, Academic Press: New York, (1965).
- [3] N. Lin, J. Huang, P. R. Chang, D. P. Anderson, and J. Yu, *J. Nanomater.* **2011**, 13 pages (2011).
- [4] www.starch.dk/ISI/market/index.asp.
- [5] NPCS team, NIIR Project Consultancy Services (2014).
- [6] D. LeCorre, J. Bras, and A. Dufresne, *J. Nanopart. Res.*, **13**, 7193 (2011).

- [7] <http://www.rubbernews.com/>.
- [8] D. LeCorre, J. Bras, and A. Dufresne, *Macromol. Mater. Engg.*, **297**, 969 (2012).
- [9] H. Angellier, S. M. Boisseau, L. Lebrun, and A. Dufresne, *Macromolecules*, **38(9)**, 3783 (2005).
- [10] H. Tang, Q. Qi, Y. Wu, G. Liang, L. Zhang, and J. Ma, *Macromol. Mater. Engg.*, **291**, 629 (2006).
- [11] J. Xin, Y. Wang and T. Liu, *Adv. J. Food Sci. Technol.*, **4(5)**, 270 (2012).
- [12] D. LeCorre, J. Bras, and A. Dufresne, *Biomacromolecules*, **12**, 3039 (2011).
- [13] Y. Hibi, T. Matsumoto, and S. Hagiwara, *Cereal. Chem.*, **70(6)**, 671 (1993).
- [14] R. G. Utrilla-Coello, C. H. Jaimes, H. C. Navas, F. Gonzalez, E. Rodriguez, L. A. B. Perez, E. J. V. Carterand, and J. A. Ramirez, *Carbohydrate Polym.*, **103**, 596 (2014).
- [15] S. Song, C. Wang, Z. Pan, and X. Wang, *J. Appl. Polym. Sci.*, **107**, 418 (2008).
- [16] C. Beninca, I. M. Demiate, L. G. Lacerda, M. A. S. C. Filho, M. Ionashiro, and E. Schnitzler, *Ecl. Quim., Sao Paulo*, **33(3)**, 13 (2008).
- [17] N. M. Claramma, *Ph. D. thesis*, "Studies on pre-vulcanization of rubber latex with special reference to influence of storage and after treatments on properties of films" Cochin University of Science and Technology, Kochi (1997).
- [18] T. P. Selvin, J. Kuruvilla, and S. Thomas, *Mater. Lett.*, **58**, 281 (2004).

.....✂.....

**PROPERTIES OF RADIATION VULCANIZED
NATURAL RUBBER LATEX (RVNRL) - GRAPHENE
NANOCOMPOSITES**

Contents	8.1 Introduction
	8.2 Experimental
	8.3 Results and Discussion
	8.4 Conclusions

Graphene related materials such as graphene oxide (GO)/exfoliated graphene oxide (XGO) and reduced graphene oxide (RGO) recently achieved much interest in nanocomposite research. In this chapter, synthesis of RGO by a green route and the exploration of its efficacy as potential filler for radiation vulcanized natural rubber latex (RVNRL) was reported. The synthesized XGO and RGO suspensions were characterized by different analytical and spectroscopic tools. The mechanical, morphological and electrical properties of the RVNRL-XGO/RGO nanocomposites were evaluated as a function of filler content. The percolation threshold of RVNRL-RGO composite was 0.1 wt. %. Compared to gum RVNRL, significant improvement in tensile strength and elongation at break was obtained for RVNRL-XGO nanocomposites at 1wt. % XGO loading indicating increased polymer-filler interaction. The morphological results showed aggregation of filler particles at a concentration of 1.25 wt. %.

8.1 Introduction

Radiation vulcanized natural rubber latex (RVNRL) is commercially important as it can be directly used for the fabrication of various latex products. In RVNRL, crosslinking of rubber is brought about by γ -radiation and is different from conventional sulphur pre-vulcanized natural rubber latex. Biodegradability, absence of nitrosamines, very low cytotoxicity, low protein allergy response, no contamination of effluent with zinc oxide, less formation of ashes when burned, better transparency and softness *etc.* makes RVNRL an attractive candidate for the manufacture of gloves, medical tubes, condoms, catheters, teats, endoscopic balloons dental dams and several other medical products [1].

Now-a-days polymer-graphene nanocomposites (PGN's) are emerging field in materials science. A huge volume of literature is available in the area of graphene-elastomer nanocomposites. Xing *et al.* prepared graphene/natural rubber (GE/NR) nanocomposites by a modified latex mixing method combined with *in situ* chemical reduction [2]. Mensah and co-workers prepared graphene oxide reinforced acrylonitrile-butadiene rubber nanocomposites *via* solution mixing [3]. Derivatives of graphite such as graphene oxide (GO) and reduced graphene oxide (RGO) is incorporated into natural and synthetic rubber as a filler to improve the properties as well as to impart novel functionalities [4-8].

Graphene is a flat monolayer of carbon atoms tightly packed in to a two-dimensional honeycomb lattice, having completely conjugated sp^2 hybridized planar structure and is the basic building block for zero-

dimensional fullerenes, one- dimensional nanotubes and three- dimensional graphite [9]. It is considered as the “thinnest material in the universe” and has remarkable properties such as high thermal conductivity, superior mechanical properties and excellent electronic transport properties [10]. The excellent conductive properties of graphene is attributed to the enhanced electron-hole mobility in its planar structure due to perfect overlap of neighbouring π -orbitals [11].

Like other nanomaterials, graphene can be synthesized *via* top-down and bottom-up approach. Top-down methods include mechanical milling, mechanical exfoliation of graphite by sonication and chemical oxidation followed by exfoliation and reduction of graphene oxide (GO). The bottom-up synthesis route includes epitaxial growth on SiC and other substrates, CVD and arc discharging method [9]. Zhong *et al.* reviewed the scalable methods of graphene production with recent progresses and challenges [12].

Chemical oxidation and exfoliation followed by reduction method is widely practiced for the large scale production of graphene. This route is simple and inexpensive. Further, oxidative-exfoliation technique increases the distance between carbon layers thereby weakening the *van der Waals* forces of interaction and facilitates the exfoliation process [13]. The exfoliated graphene oxide (XGO) obtained after the oxidation followed by exfoliation and reduction using hydrazine derivatives yielded reduced graphene oxide (RGO)/graphene. Considering the high toxicity associated with hydrazine, a green and eco-friendly approach for the reduction of graphene stimulated much interest now-a-days.

Production of multi-layer graphene dispersion by ultrasound exfoliation of graphite in a weakly basic solution is reported by Ricardo *et al.* [14]. Loryuenyong *et al.* synthesized reduced graphene oxide sheets *via* water based exfoliation and reduction method and characterized using FT-IR, XRD, TGA, Raman spectroscopy, SEM and TEM methods [15]. Liao *et al.* synthesized graphene sheets from graphite oxide by reduction with simple de-ionized water at 95⁰C under atmospheric pressure [16]. Haghighi *et al.* used rose water as a green reducing agent for the synthesis of reduced graphene oxide nanosheets. Through XRD analysis, the oxygen containing functional groups of exfoliated GO can be removed easily after its reduction by rose water [17]. A detailed review on the techniques and mechanisms associated with the reduction of graphene oxide is available [18].

Solution mixing is a simple and effective method for the preparation of graphene based nanocomposites. The process involves mixing of colloidal suspensions of graphene-based materials with the desired elastomer either with latex form or by dissolving in a solvent [19]. In this chapter, a hydrazine- free route for the synthesis of reduced graphene oxide (RGO) and the preparation of RVNRL-RGO/XGO nanocomposites *via* simple solution mixing was demonstrated.

8.2 Experimental

8.2.1 Materials

The formulation and preparation of RVNRL is given in the experimental section. The specifications of graphite used are also given.

8.2.2 Methods

8.2.2.1 Preparation of exfoliated graphene oxide (XGO) dispersion

Graphene oxide was synthesized from flake graphite using modified Hummers method reported by Loryuenyong *et al.* with some modifications [15]. Briefly, 6 g graphite was added to 300 ml conc. H₂SO₄ taken in a RB flask with continuous stirring. The mixture has been cooled in an ice bath. After completely adding graphite, 24 g KMnO₄ added slowly into the above mixture with continuous stirring and cooling. After 30 min. stirring, the mixture was removed from the ice bath and again stirred for 45 min. at room temperature. Then 150 ml distilled water was added slowly into the above mixture and stirred for 15 min. Finally, 40 ml 30 % H₂O₂ solution was added to the above mixture and stirred well. The solid fraction was filtered washed and centrifuged three times with distilled water at 10000 rpm for 5 min. The obtained graphene oxide (GO) was dried at 45 °C for about 48 h in an air oven. For the preparation of graphene oxide dispersion, around 0.255 g GO powder was added to 150 ml distilled water and stirred at 700 rpm for about 5 h. The concentration of the resulting suspension was 0.043 wt. %.

The GO dispersion was ultrasonicated for about 30 min. to obtain exfoliated graphene oxide dispersion (XGO). To avoid overheating, the mixture was cooled occasionally in an ice bath.

8.2.2.2 Preparation of reduced graphene oxide (RGO) dispersion

0.266 g GO powder was dispersed in 100 ml distilled water stirred at 600 rpm for 5 h and then sonicated for 30 min. with occasional

cooling in an ice bath. The resulting XGO suspension was transferred to a RB flask kept in an oil bath followed by continuous stirring and heating at 95 °C for 4 days. The concentration of the RGO suspension was 0.00389 %.

8.2.2.3 Preparation of nanocomposites

Before adding XGO and RGO dispersions to RVNRL, the pH of the latex was adjusted to ~ 11 using 10 % potassium hydroxide solution. For the preparation of XGO-RVNRL nanocomposites, appropriate amount of XGO dispersion was added to RVNRL. Details showing the amount of XGO/RGO added for the preparation of nanocomposites are shown in the Table 8.1.

Table 8.1: Amount of filler (XGO and RGO) used for the preparation of nanocomposites

Filler wt. %	0	0.1	0.25	0.5	1	1.25
<i>RVNRL-XGO nanocomposites</i>						
Weight of RVNRL latex (g)	20.05	20.04	20.03	20.05	20.03	20.03
Weight of XGO (g)	0	1.101	2.682	5.364	10.668	13.352
<i>RVNRL-RGO nanocomposites</i>						
Weight of RVNRL latex (g)	20.00	20.00	20.00	20.00	20.02	20.01
Weight of RGO (g)	0	1.072	2.696	5.345	10.693	13.386

RVNRL-XGO and RVNRL-RGO represents radiation vulcanized natural rubber latex-exfoliated graphene oxide and reduced graphene oxide nanocomposites respectively. The filler concentrations were kept at 0, 0.1, 0.25, 0.5, 1 and 1.25 wt. %.

The latex mixture has been stirred well and matured for 45 min. and films were casted as per the formulation made above (Table 8.1) and kept in hot air oven for drying at 60 °C for 40 min. The films are then leached in distilled water and dried again until they are free from moisture.

For the preparation of RVNRL - RGO nanocomposites, RGO was initially dispersed in Triton X 100 (1 % solution) by vigorous stirring for 30 min. and was prepared as given in Table 8.1. The filler content (XGO and RGO) in the composite has been varied from 0 to 1.25 wt. % (*i.e.* 0, 0.1, 0.25, 0.5, 1 and 1.25 wt. %). The amount of filler (XGO and RGO) required for this has been calculated based on dry weight of the polymer. For example, 20 g latex having a total solid content of 53.49 % may contain 10.698 g dry rubber. Therefore the amount of filler required for the preparation of composite having 1.25 wt. % of XGO/RGO is 13.372 (10.698 x 1.25). Similarly, the amount of filler required to prepare latex composites having various concentrations of filler (XGO/RGO) can be calculated.

8.2.2.4 Characterization

Particle size analysis of GO and XGO was monitored in a particle size analyzer (Zetasizer Nano S, Malvern, UK) using dynamic light scattering technique. Vibra Cell ultrasonicator (model VCX-750) at a frequency of 20 kHz having a power rate of 750 W was used for the exfoliation of GO to XGO. The FT-IR spectra were recorded on Varian FT-IR spectrometer (Varian 660-IR model) in the wavelength 600 - 3600 cm⁻¹. The UV-visible spectra of XGO and RGO were recorded on

a spectro UV-VIS double beam spectrometer (model UVD-3500) of Labomed Inc., CA.

High resolution Raman spectrometer (Horiba JY) band analysis with a resolution in the order of $0.3 - 1 \text{ cm}^{-1}$ was used to record the Raman spectra of XGO and RGO. Ar ion laser operating at 514 nm was used for this purpose. AFM analysis of RGO was measured on a WITec Alpha 300RA, GmbH using tapping mode on a thin film casted on a glass substrate. HRTEM carried out in Jeol/JEM 2100 operated with a voltage of 200 kV having a magnification of 2000x - 1500000x.

The morphological images of the nanocomposites were taken with a Wild Heerbrugg (M8) zoom stereomicroscope (Switzerland) connected with Leica digital camera (model DFC 320), Germany. The mechanical properties of the composite films are measured using a Zwick universal testing machine (Model 1474) according to ASTM D 412.

8.3 Results and Discussion

8.3.1 Particle size analysis

Particle size analysis of GO and XGO is shown in Figure 8.1. It is clear from the figure that, the size and size distribution of XGO decreased considerably after ultrasonication. The size range of sub-micron sized GO particles is 712 - 825 nm whereas it is in the range of 295 - 531 nm for XGO. A slight increase in the size of XGO particles in the nano size range ($< 100 \text{ nm}$) might be due to agglomeration of lower sized particles generated after prolonged sonication. A significant size

reduction of XGO indicates the high extend of exfoliation of GO after ultrasonication.

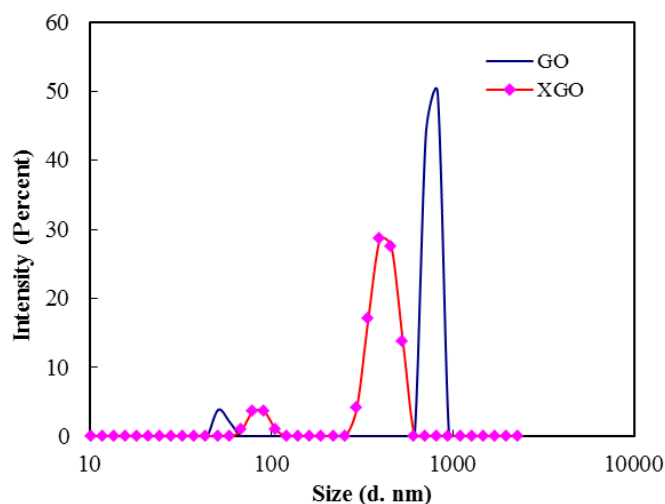


Figure 8.1: Particle size distributions of graphene oxide (GO) and exfoliated graphene oxide (XGO).

8.3.2 FT-IR analysis

Figure 8.2 represents FT-IR spectra of exfoliated graphene oxide (XGO) and reduced graphene oxide (RGO). The stretching vibrations of O-H (3450 cm^{-1}), C=O (1728 cm^{-1}) and C-O (epoxy) (1229 cm^{-1} and 1071 cm^{-1}) are specific for XGO [15]. The evidence for the reduction of XGO to RGO is confirmed by the disappearance of C=O peak (1728 cm^{-1}) and C-O alkoxy stretching (1071 cm^{-1}). Significant weakening of O-H peak (3450 cm^{-1}) also indicates the efficient reduction of XGO to RGO [20].

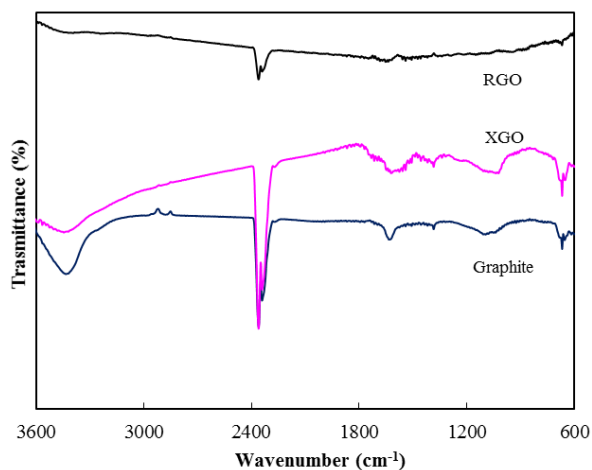


Figure 8.2: FT-IR spectra of graphite, exfoliated graphene oxide (XGO) and reduced graphene oxide (RGO)

8.3.3 UV-Visible analysis

The UV-Visible spectrum of XGO and RGO is displayed in Figure 8.3. The absorption peak at 224 nm is attributed to π - π^* transition of aromatic C=C bonds [21] whereas the RGO peak is shifted to 246 nm due to decrease in oxygen functional groups and an increase in aromatic rings causing electrons to be excited easily at lower energy [15]. The red shift of the peak to 246 nm (>238 nm) indicates the restoration of π -conjugation network in reduced graphene oxide (RGO) [22]. The inset shows stable high concentration aqueous dispersions of XGO and RGO.

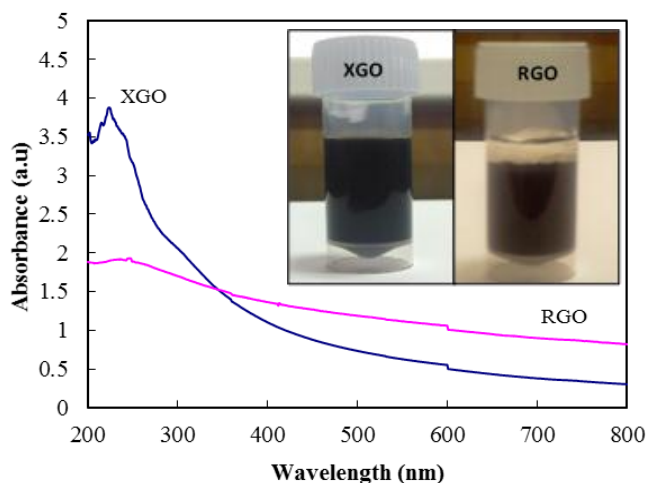


Figure 8.3: UV-Visible absorbance spectra of XGO and RGO. Inset showing photographic images of XGO and RGO suspensions in water

8.3.4 Raman analysis

Raman spectroscopy can be used to illustrate the structural changes happening during the oxidation and reduction process. Figure 8.4 exhibits the Raman spectra of XGO and RGO. Raman spectrum of RGO contains both D and G bands at 1345 cm^{-1} and 1579 cm^{-1} with an increased I_D/I_G ratio corresponds to a decrease in the average size of sp^2 domains [23, 24]. Raman spectrum of XGO showed broad and highly intense D band compared to RGO indicating higher disorder or defects in the former [25]. The structural defects induced by oxygen-containing functional groups during oxidation of graphite intensified the D band [13]. In hydrothermal reduction route, besides dehydrating/reducing the XGO, also recovers the aromatic structures [22]. The I_D/I_G ratio of RGO reported here is much lower (1.03) than hydrazine reduced GO (1.44) reported by Zhou *et al.*

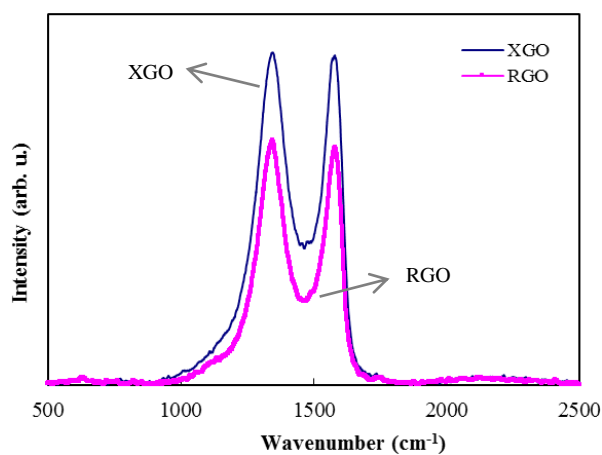


Figure 8.4: Raman spectra of XGO and RGO

8.3.5 AFM analysis of RGO

Tapping mode AFM image and the corresponding height profile of RGO sheets deposited on a glass substrate by drop casting is shown in Figure 8.5. The scan area was 5 μm x 5 μm .

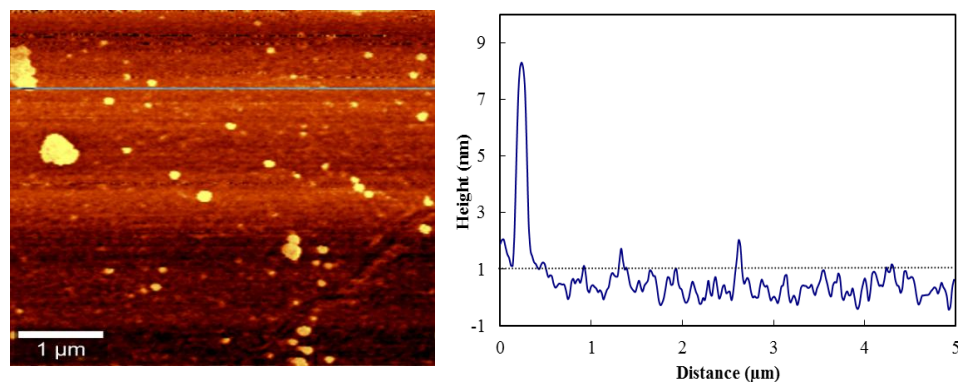


Figure 8.5: Tapping mode AFM image of RGO with corresponding height profile

Height profile shows mono, bi and multi-layered sheets of graphene. The thickness of mono layer graphene was found to be 1.32 nm. The

thickness values are in accordance with monolayered (1.25 ± 0.08 nm) and bi-layered (2.23 ± 0.11 nm) graphene reported earlier [26].

8.3.6 TEM analysis of RGO

The characterization of exfoliated graphene can be carried out by transmission electron microscopy (TEM) and is shown in Figure 8.6(a-b).

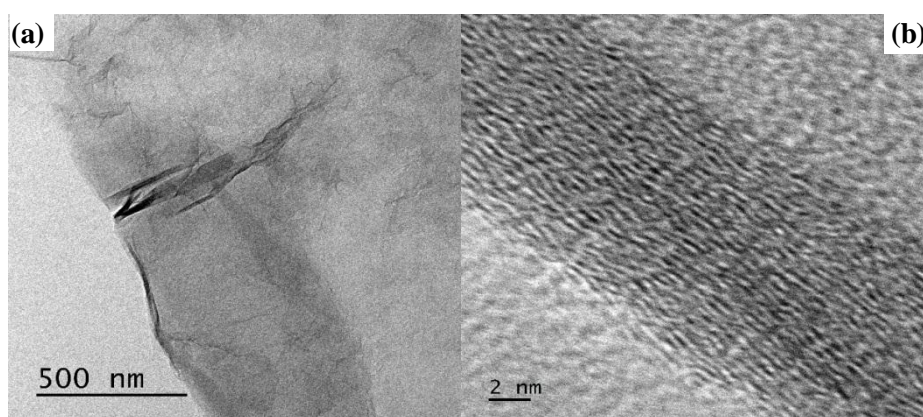


Figure 8.6: TEM image of RGO with partial foldings (a) and (b) HRTEM image of (a)

TEM analysis reveals the presence of single and multi-layered sheets of RGO. After analyzing a large number of TEM images, it has been found that major portion of the dispersion contains mono layer graphene however; partially folded crumpled sheets are also present (Figure 8.6a). High resolution TEM image of partially folded/aggregated sheets of graphene is shown in Figure 8.6b.

8.3.7 Visual features of the composite

Optical photographs of dried latex composite films containing XGO and RGO is shown in Figure 8.7(a-j).

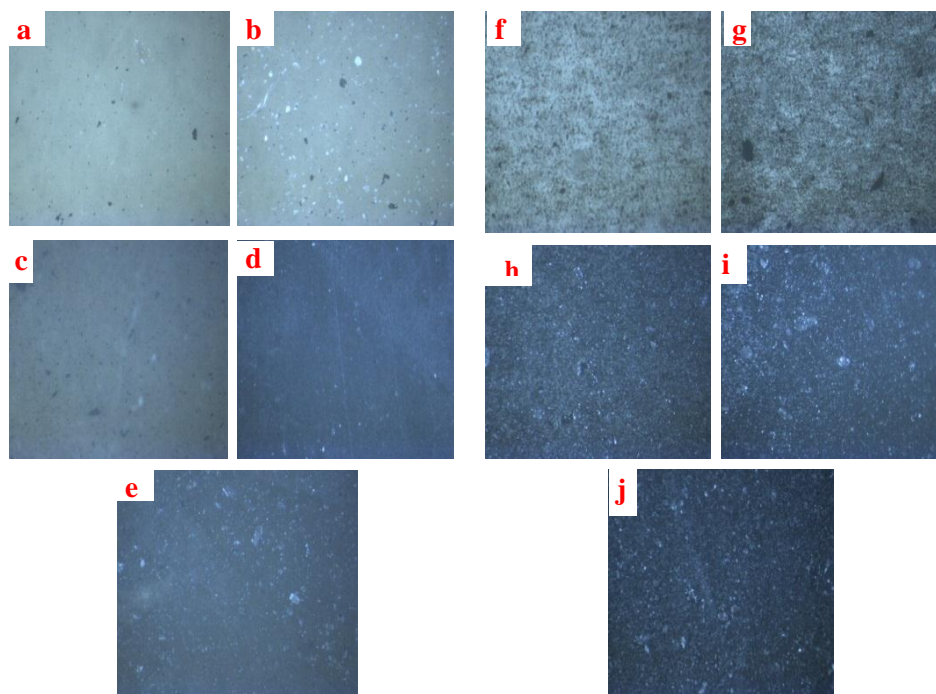


Figure 8.7: (a-j) Photographic images of RVNRL-XGO/RGO nanocomposites. (a-e) with various amounts of XGO (0.1, 0.25, 0.5, 1 and 1.25 wt. %) and (f-j) RGO (0.1, 0.25, 0.5, 1 and 1.25 wt. %).

The stable aqueous dispersion of XGO is uniformly dispersed throughout the polymer matrix up to a loading of 1 wt. % XGO. Above this concentration (1.25 wt. %), slight agglomeration was observed whereas for RGO incorporated composite films, homogeneous distribution of RGO in the polymer matrix can be achieved up to 0.5 wt. % and further loading resulted in higher rate of agglomeration.

8.3.8 Electrical conductivity studies

The effect of filler concentration on the conductivity of RVNRL nanocomposite films is displayed in Figure 8.8.

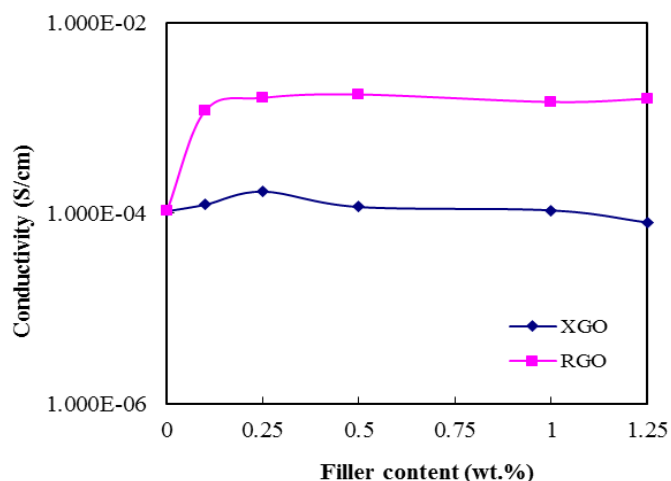


Figure 8.8: Electrical conductivity as a function of filler content for RVNRL nanocomposites containing XGO and RGO

The pure RVNRL showed a conductivity of 10^{-4} S/cm. Even at a low percolation threshold of 0.1 wt. %, the conductivity of RVNRL-RGO nanocomposite was of the order of 10^{-3} S/cm. *i.e.* almost 10 fold increase in conductivity. The addition of RGO yielded significant improvement in conductivity. The uniform distribution of RGO in the polymer matrix (Figure 8.7 f) resulted in the formation of continuous network of RGO and imparts high electrical conductivity. Potts *et al.* reported higher electrical conductivity of solution treated RGO-natural rubber (NR) nanocomposites compared to mill mixed composites. The high electrical conductivity in the former is attributed to the provision of more conducting pathways whereas in the latter case, RGO platelets will get coated with a sheath of polymer which inhibits the electrical conductivity [27]. The addition of XGO did not improve the conductivity. Graphene oxide itself is an insulating material because it lacks labile π - conjugated orbital system [28].

8.3.9 Mechanical properties

The mechanical properties (tensile strength, elongation at break and modulus at 100% elongation (M_{100}) of XGO and RGO incorporated latex composite films are represented in Figures 8.9(a-c). It is clear that the tensile strength and elongation at break increases with increase in XGO loading and reaches a maximum at 1 wt. % XGO content and above this concentration the properties decreases (Figures 8.9a & 8.9b). The increase in tensile strength and elongation at break is due to more uniform distribution of XGO in the polymer matrix (Figure 8.7d). XGO-RVNRL composite film showed a tensile strength of 24 MPa at 1 wt. % filler loading, which is 60 per cent higher than the initial value.

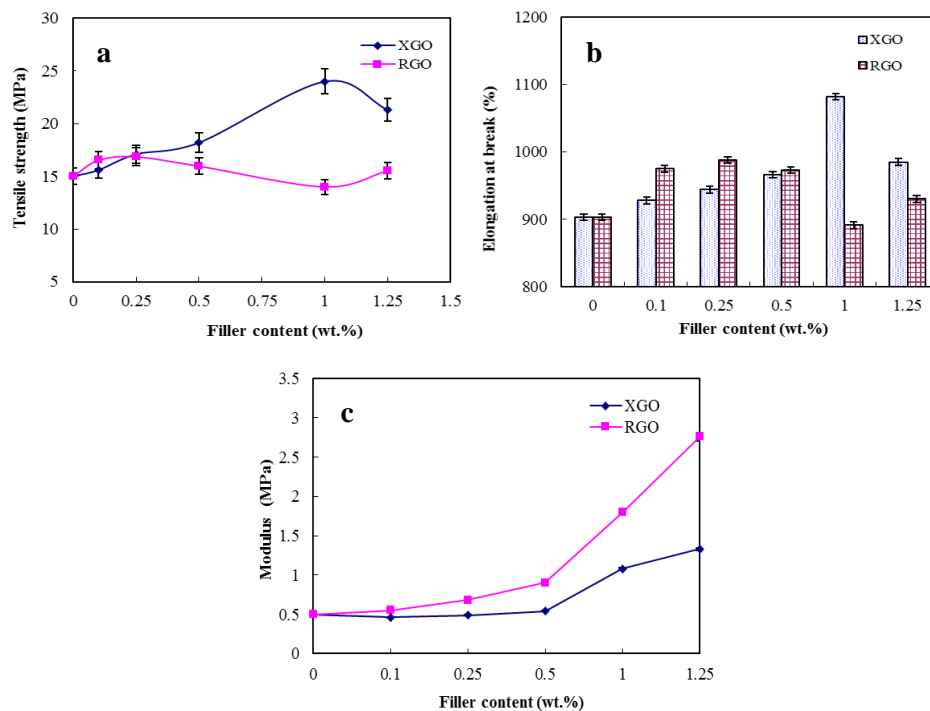


Figure 8.9: (a-c) Mechanical properties of RVNRL nanocomposites with various amounts of filler (XGO and RGO). Variation of tensile strength (a), elongation at break (b) and modulus (c) with filler content

The increased rubber-filler interaction results in effective stress transfer from rubber to filler particles and in turn increases the tensile strength. On the other hand, the tensile strength of RGO incorporated latex composites registered the highest tensile value of 17.1MPa at 0.25 wt. % RGO loading and then gradually decreases with RGO content. The variation in elongation at break of RGO-RVNRL composite follows the same trend. The maximum elongation at break of 1488 was noticed for latex films with 0.25 wt. % RGO loading. The reduction in tensile strength and elongation at break of latex composites at higher RGO loading (1 wt. %) can be attributed to agglomeration of RGO nano-sheets in the polymer matrix as evident from Figure 8.7i. The unexfoliated agglomerates resulted in more stress concentration, and will end up with reduced tensile strength [29]. The strong interaction between polymer matrix and the filler is reflected in modulus results (Figure 8.9c). The modulus (M_{100}) value increases with the filler content. At 1.25 wt. % filler loading, the modulus of RGO and XGO incorporated composite films are 3.18 and 1.33 MPa respectively.

8.3.10 Theoretical modelling

Halpin Tsai model is an effective tool to predict the mechanical properties of filled composites. It is obvious from Figure 8.10 that the M_{100} values obtained from experimental calculation agrees with the theoretical predictions and the values fits well with values (M_{100}) of RVNRL-RGO nanocomposite films with random arrangement of RGO in the RVNRL matrix.

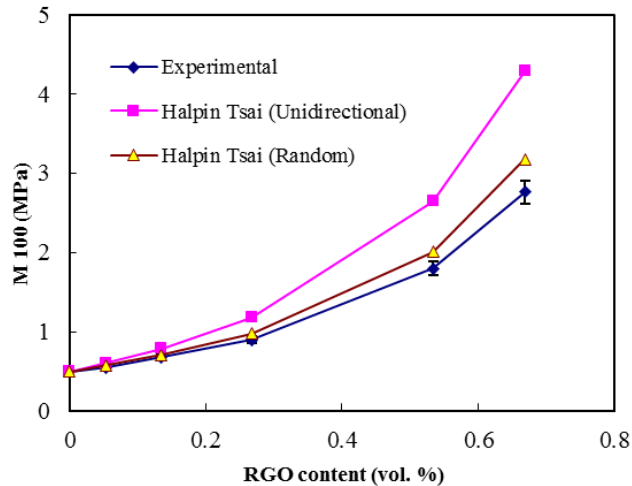


Figure 8.10: Experimental data of tensile modulus (M100) and Halpin Tsai theoretical model fitting for RVNRL-RGO nanocomposites.

8.4 Conclusions

For the synthesis of graphene sheets, a hydrazine free “green route” was attempted and radiation vulcanized natural rubber latex (RVNRL)-graphene based nanocomposites has been prepared *via* simple solution mixing. Uniform dispersion of filler (XGO and RGO) in the polymer matrix and improved polymer-filler interaction is reflected in mechanical properties. Theoretical predictions showed random distribution of graphene sheets in RVNRL matrix. The effect of filler content on the electrical properties of nanocomposites showed a lower percolation threshold (0.1 wt. % for RGO). The study opens up new possibilities for the preparation of RVNRL based nanocomposites for novel applications.

References

- [1] K. Makuuchi, *An Introduction to Radiation Vulcanization of Natural Rubber Latex*, T.R.I Global Co., Ltd. Thailand, Chapter 11, p 144 (2003).
- [2] W. Xing, J. Wu, G. Huang, H. Li, M. Tang, and X. Fu, *Polym. Intl.*, **63**(9), 1674 (2014).
- [3] B. Mensah, S. Kim, S. Arepalli, and C. Nah, *J. Appl. Polym. Sci.*, **131**(16), 40640 (2014).
- [4] C. F. Matos, F. Galembeck, and A. J. G. Zarbin, *Carbon*, **78**, 469 (2014).
- [5] X. Bai, C. Wan, Y. Zhang, and Y. Zhai, *Carbon*, **49**, 1608 (2011).
- [6] H. Lian, S. Li, K. Liu, L. Xu, K. Wang, and W. Guo, *Polym. Engg. Sci.*, **51**, 2254 (2011).
- [7] J. S. Kim, J. H. Yun, I. Kim, and S. E. Shim, *J. Ind. Engg. Chem.*, **17**, 325 (2011).
- [8] S. Araby, Q. Meng, L. Zhang, H. Kang, P. Majewski, Y. Tang, and J. Ma, *Polymer*, **55**(1), 201(2014).
- [9] K. Singh, A. Ohlan, and S. K. Dhawan, *Polymer graphene nanocomposites: Preparation, Characterization, Properties and Applications in Nanocomposites-New trends and Developments*, InTech Open Chapter 3, 37 (2012).
- [10] T. Kuilla, S. Bhadra, D. Yao, N. H. Kim, S. Bose, and J. H. Lee, *Prog. Polym. Sci.*, **35**, 1350 (2010).
- [11] Y. J. Park, S. Y. Park, and I. In, *J. Ind. Engg. Chem.*, **17**, 298 (2011).
- [12] Y. L. Zhong, Z. Tian, G. P. Simon, and D. Li, *Mater. Today*, 1 (2014).
- [13] S. Abdolhosseinzadeh, H. Asgharzadeh, and H. S. Kim, *Sci. Rep.*, **5**, 10160 (2015).
- [14] K. B. Ricardo, A. Sendeci, and H. Liu, *Chem. Commun.*, **50**, 2751 (2014).
- [15] V. Loryuenyong, K. Totepvimarn, P. Eimburanaprat, W. Boonchompoo, and A. Buasri, *Adv. Mater. Sci. Engg.*, **2013**, 5pages (2013).

- [16] K. H. Liao, A. Mittal, S. Bose, C. Leighton, K. A. Mkhoyan, and C. W. Macosko, *ACS nano*, **5**(2), 1253 (2011).
- [17] B. Haghighi, and M. A. Tabrizi, *RSC Adv.*, **3**, 13365 (2013).
- [18] S. Pei, and H. M. Cheng, *Carbon*, **50**(9), 3210 (2012).
- [19] K. K. Sadasivuni, D. Ponnammam, S. Thomas, and Y. Grohens, *Prog. Polym. Sci.*, **39**(4), 749 (2014).
- [20] Y. Zhan, J. Wu, H. Xia, N. Yan, G. Fei, and G. Yuan, *Macromol. Mater. Engg.*, **296**, 590 (2011).
- [21] N. M. Huang, H. N. Lim, C. H. Chia, M. A. Yarmo, and M. R. Muhamad, *Intl. J. Nanomed.*, **6**, 3443 (2011).
- [22] Y. Zhou, Q. Bao, L. A. L. Tang, Y. Zhong, and K. P. Loh, *Chem. Mater.*, **21**, 2950 (2009).
- [23] S. Stankovich, D. A. Dikin, R. D. Piner, K. A. Kohlhaas, A. Kleinhammes, Y. Jia, Y. Wu, S. B. T. Nguen, and R. S. Ruoff, *Carbon*, **45**, 1558 (2007).
- [24] E. Y. Choi, T. H. Han, J. Hong, J. E. Kim, S. H. Lee, H. W. Kim, and S. O. Kim, *J. Mater. Chem.*, **20**, 1907 (2010).
- [25] T. V. Cuong, V. H. Pham, J. S. Chung, E. W. Shin, D. H. Yoo, S. H. Hahn, J. S. Huh, G. H. Rue, E. J. Kim, S. H. Hur, and P. A. Kohl, *Mater. Lett.*, **64**, 2479 (2010).
- [26] Inhwa Jung, M. Pelton, R. Piner, D. A. Dikin, S. Stankovich, S. Wacharotone, M. Hausner and R. S. Ruoff, *Nano Lett.*, **7**(12), 3569 (2007).
- [27] J. R. Potts, O. Shankar, L. Du, and R. S. Ruoff, *Macromolecules*, **45**, 6045 (2012).
- [28] Y. Si, and T. Samulski, *Nano Lett.*, **8**(6), 1679 (2008).
- [29] J. Yang, L. Q. Zhang, J. H. Shi, Y. N. Quan, L. L. Wang, and M. Tian, *J. Appl. Polym. Sci.*, **116**, 2706 (2010).
- [30] X. She, C. He, Z. Peng, and L. Kong, *Polymer*, **55**, 6803 (2014).



Chapter 9

SUMMARY AND CONCLUSIONS

A brief explanation of the major findings and the results obtained is summarized in this chapter. Future possibilities from the work done are also presented.

Natural rubber latex comprises rubber particles dispersed in aqueous medium. For the preparation of various latex products, the chemical dispersions of latex compounding ingredients are added to natural rubber latex and the process is known as latex compounding. Wet ball milling is one of the commonly practiced technique for the preparation of dispersions of the chemicals. Since ball milling is a highly complicated process, several parameters such as time of milling, milling speed, milling atmosphere, ball to powder weight ratio, ball size, concentration of the surfactant, *etc.* influence the milling efficiency. The particle size and stability of the dispersions plays a crucial role in latex processing and technological properties of resulting vulcanizates. Addition of ultra-fine/nanoparticles in latex compound formulations, avoids the sedimentation problem, which is common with conventional

micro dispersions and enhances the technological properties. Moreover, they are highly active and hence the amount required can be reduced significantly. Zinc oxide (ZnO) is an ubiquitous ingredient in the vulcanization process and replacement of conventional ZnO with nano ZnO can reduce the overall amount of chemical required and it improves the thermal stability and mechanical properties of the vulcanizates. In addition, the problems associated with the release of zinc through the effluent can be minimized.

As most of nanomaterials are very expensive, the concept of stable ultrafine dispersions with uniform size distribution is getting commercial importance. Dispersion of ZnO has been a consistent issue because of their strong tendency to form aggregates. The combined effect of ball milling followed by ultrasonication to produce stable aqueous dispersions of ZnO with low particle size was studied. The decrease in specific surface area was monitored after prolonged ball-milling. A higher reduction in the size of the ZnO has been achieved by wet ball-milling followed by ultra-sonication. It was found that six hours of ball milling of the zinc oxide dispersion with 3 wt. per cent PCA followed by ultrasonication resulted the formation of particles having size below 500 nm. The stability of the ZnO dispersion decreases with the concentration of the process control agent, as evident from decrease in zeta potential values.

The effect of ball size on milling efficiency of ZnO was assessed. ZnO dispersion was ball-milled using inert Al₂O₃-ceramic balls having different diameter (6.35, 12.7 and 19.05 mm) for different intervals

(0.5, 6, 12, 18, 24 and 30 h). It was found that smaller sized balls improved the milling efficiency and the highest share of lower sized particles was achieved with 6.35 mm balls after 24 h of milling. At lower milling time (up to 12 h), the variation in average particle size with ball size was not much significant.

Optimization of the process parameters for the preparation of chemical dispersions of latex compounding ingredients (LCI) *viz.* china clay, zinc diethyl dithiocarbamate (ZDEC), zinc 2- mercapto benzothiazole (ZMBT) and butylated reaction product of p-cresol and dicyclopentadiene (wingstay L) was carried out. The effect of varying the ball size (6.35 mm, 12.7 mm and 19.05 mm and composite balls) and milling time on particle size and stability of aqueous of dispersions of latex compounding ingredients were assessed. Prolonged milling resulted size reduction of the chemicals irrespective of ball size, however, maximum size reduction was achieved with smaller sized balls. Using composite balls *i.e.* large (19.05 mm), medium (12.7 mm) and small (6.35 mm) in the weight ratio 2:1:2 (by weight) respectively for large, medium and small sized balls resulted in competent size reduction and is on par with that offered by smaller sized balls. Also, the wingstay L dispersions with considerable stability was achieved by milling with composite balls.

ZnO nanoparticles were synthesized through solvent-free mechano-chemical process. Zinc acetate dihydrate, sodium hydroxide and CTAB were used as precursors. The average particle size of the prepared ZnO particles was found to be in the range of 35-60 nm with rod shaped morphology. The reaction yield was high compared to other

methods. TEM images showed that aggregation of the synthesized ZnO nanoparticles was minimum and the purity was good. The complete conversion of zinc hydroxide to zinc oxide occurs at 241 °C as revealed from thermal analysis.

Dispersions of synthesized ZnO nanoparticles were made and the evaluation of the stability of the prepared nano ZnO dispersions was carried out. Various types of surfactants/stabilizers namely; Triton X - 100, polyethylene glycol - 6000 (both non-ionic), cetyltrimethylammonium bromide (cationic) and sodium dodecyl sulphate (anionic) were selected for this purpose. It was found that, among the non-ionic, cationic and anionic surfactants studied, the quality of dispersion was better with anionic surfactants (SDS). ZnO with SDS retained more number of particles in the nano-size range. Sonication in presence of SDS further enhanced the share of lower sized particles. Further, the colloidal stability of ZnO dispersed in SDS was also found to be high (-28.9 mV).

Effect of nano-ZnO (synthesized) on swelling, antimicrobial, mechanical and ageing properties of pre-vulcanized latex vulcanizates were examined and compared with micro-ZnO filled vulcanizates. The better solvent resistance was shown by pre-vulcanized natural rubber latex films containing 0.5 phr nano-ZnO. Nano-ZnO imparts better antifungal activity in pre-vulcanised latex films as compared to an equal dosage of the micro-ZnO. The mechanical properties (tensile strength and elongation at break) of the pre-vulcanized latex films increases with decreasing the concentration of nano ZnO indicating better activation of nanoparticles on rubber crosslinking. Also, pre-vulcanized latex films

with nano-ZnO showed better retention of mechanical properties after ageing. Modulus of latex films also increased with nano-ZnO addition.

With increasing environmental awareness, replacement of conventional non-renewable inorganic fillers with eco-friendly bio-fillers like starch, cellulose *etc.* is getting wide acceptance for various industrial applications, particularly in rubber and allied industries where fillers are essential for improved product performance. Starch is composed of crystalline and amorphous components arranged alternatively. Starch nanocrystals (SNC) have been isolated from modified corn starch by acid hydrolysis and their efficacy as a potential bio-filler for natural rubber latex (NR) has been explored. Natural rubber latex–corn starch crystal nanocomposites were fabricated and estimated the important vulcanizate properties such as swelling index and mechanical properties. It was found that, an optimum SNC loading of 1.38 phr imparted improved solvent resistance capacity to the natural rubber latex film. The mechanical properties of SNC incorporated vulcanizates were also found to be good.

Graphene related materials such as graphene oxide (GO)/ exfoliated graphene oxide (XGO) and reduced graphene oxide (RGO) received much interest in materials science research. A hydrazine free “green route” was employed for the synthesis of graphene sheets and fabricated radiation vulcanized natural rubber latex (RVNRL)-graphene based nanocomposites by simple solution mixing route. RVNRL is having commercial importance and is widely used for the manufacture of various industrial products such as gloves, medical tubes, condoms, catheters, etc. Uniform dispersion of filler (XGO and RGO) in the

polymer matrix and improved polymer-filler interaction were reflected in mechanical properties. Theoretical predictions showed random distribution of graphene sheets in RVNRL matrix. The electrical properties of nanocomposites showed a lower percolation threshold (0.1 wt. per cent for RGO).

Future scope

It is expected that the results of the present investigations will encourage research in the area of nano-sized dispersions, particularly in the area of their use in latex technology. Possibilities for the preparation and use of novel chemicals/fillers in the nano regime for latex compounding can be explored. As already known, in-addition to size, the stability of dispersions also matters. There is ample scope for improving the stability of dispersions used in latex compounding. Preparation of stable chemical dispersions of latex compounding ingredients using different types of surfactants or capping agents which may not have any detrimental effect on latex stability, processing and end properties would be quite interesting. Addition of rubber chemicals as fine particle dispersion in latex technology will improve the product clarity and also will reduce the rejection rates in thin-walled products like gloves, condoms *etc.* Large abundance, low cost and eco-friendliness of bio-materials such as starch, cellulose, chitin, *etc.*, opens up the scope for research to explore their suitability as alternative candidates for conventional inorganic fillers in rubber industry. The biodegradable nature of these materials offers several other advantages also. They can be used either in natural or synthetic latex formulations or in blend

systems as cheap filler. Graphene based polymer nanocomposites is another emerging area for further research. Graphene is a widely discussed material due to its unique properties. The synthesis of graphene by different methods with good quality and large yield is still a challenge and its use in polymer solutions (natural/ synthetic/ blends) for tailor-made applications would be highly interesting. Graphene based polymer nanocomposites are still in the embryonic stage and cutting-edge research in this field will open up new avenues for materials like natural rubber. Also, synthesis, characterization and evaluation of several multi-functional nanomaterials and their adoption in latex technology will open new possibilities and processing techniques.

.....❧.....

List of Abbreviations and Symbols

A	Area of cross-section
a.u	Arbitrary unit
AAM	Anodic alumina membranes
AFM	Atomic force microscopy
APS	Aminopropyl triethoxy silane
ASTM	American Society for Testing and Materials
BA	Boric acid
BdR	Bound rubber
BIAT	N-Benzylimine aminothio formamide
BIS	Bureau of Indian Standards
BPR	Ball to powder ratio
C	Specific heat capacity
CB	carbon black
CEC	Cation exchange capacity
CIIR	Chlorobutyl rubber
c-MWCNT	Carboxylated multi-walled carbon nanotube
CNF	Carbon nanofibres
CNT	Carbon nanotube
CPS	Chloropropyl trimethoxy silane
cPs	Centipoise
CR	Polychloroprene rubber
CSDPf	Carbon-silica dual phase filler
CSM	Chlorosulphonated polyethylene
CTAB	Cetyltrimethyl ammonium bromide
CTE	Coefficient of thermal expansion
CVD	Chemical vapour deposition
D	Diameter of ball/ball size
D [4, 3]	Volume weighed mean
D50	Average/mean particle size
Dispersol- F	Disodium methylene <i>bis</i> - naphthalene sulphonate
DLS	Dynamic light scattering
DPG	Diphenyl guanidine

List of Abbreviations and Symbols

DRC	Dry rubber content
DTA	Differential thermal analysis
DTT	Dithiothreitol
DW	De-ionized water
DWCNT	Double walled carbon nanotube
E	Voltage
E'	Tensile modulus of filled samples
E ₀	Tensile modulus of gum samples
EB	Elongation at break
EDTA	Ethylene diamine tetra acetic acid
E _g	Young's modulus of RGO
E _m	100% modulus of unfilled RVNRL
ENR	Epoxidized natural rubber
EPDM	Ethylene propylene diene monomer
EPT	Ethylene – propylene terpolymer
E-SBR	Styrene – butadiene copolymer
EU	European Union
eV	Electron volt
FGS	Functionalized graphene sheets
FHT	Fluorohectorite
FT-IR	Fourier transform infrared spectroscopy
G'	Storage modulus
G''	Loss modulus
GCB	Grafted carbon black
GE	Graphene
GO	Graphene oxide
GPa	Giga pascal
HA	High ammonia
HAF	High abrasion furnace
HNBR	Hydrogenated nitrile rubber
HNT	Halloysite nanotube
I	Current
IR	Synthetic <i>cis</i> 1, 4 polyisoprene
IS	Indian Standards
JCPDS	Joint Committee on Powder Diffraction Standards

KE	Kinetic energy
kGy	Kilo gray
KOH	Potassium hydroxide number
kV	Kilo volt
LA	Low ammonia
LATZ	Low ammonia TMTD-ZnO
LCI	Latex compounding ingredients
l_g	Average length of reduced graphene oxide
LR	Laboratory reagent
M	Magnetization
MAA	Methacrylic acid
MBE	Molecular beam epitaxy
MBT	Mercapto benzothiazole
meV	Milli electron volt
M_H	Maximum torque
min.	Minute
M_L	Minimum torque
mm	Millimeter
MMA	Methyl methacrylate
MMD	Mass median diameter
MMT	Montmorillonite
MOCVD	Metal – organic chemical vapour deposition
MPa	Mega pascal
MPS	Methacryloxy propyl trimethoxy silane
M_R	Remanent magnetization
M_S	Saturation magnetization
MST	Mechanical stability time
mV	Milli volt
MWCNT	Multi-walled carbon nanotube
N	Total contact points
n	Number of balls
NA	Nutrient agar
Na-MMT	Sodium montmorillonite
n-BA	n- butyl acrylate
NBR	Nitrile rubber

List of Abbreviations and Symbols

nm	nanometre
NR	Natural rubber
NRS	Non-rubber solids
NXT	3-octanoylthio-1-propyl triethoxy silane
ODA	Octadecylamine
PCA	Process control agent
PDA	Potato – dextrose agar
PEG	Polyethylene glycol
PGN	Polymer – graphene nanocomposite
phr	Parts per hundred rubber
PINC	Polymer/inorganic particle based nanocomposite
PVL	Pre-vulcanized latex
PVP	Polyvinyl pyrrolidone
Q	Swelling index
R	Resistance
RGO/rGO	Reduced graphene oxide
RP	Rubber powder
RPA	Rubber process analyzer
rpm	Rotations per minute
RSO	Rubber seed oil
RVNRL	Radiation vulcanized natural rubber latex
SA	Surfactant
SBR	Styrene butadiene rubber
S/cm	Siemens per centimeter
SEM	Scanning electron microscopy
SIR	Silicone rubber
SLS/SDS	Sodium lauryl/dodecyl sulphate
SNC	Starch nanocrystals
SPP	Sodium pentachlorophenate
SRSO	Sodium salt of rubber seed oil
SSA	Specific surface area
SWNT	Single walled carbon nanotube
TEM	Transmission electron microscopy
TESPT	<i>bis</i> (3-triethoxysilyl propyl) tetra sulphide
T _g	Glass transition temperature

t_g	Average thickness of reduced graphene oxide
TGA	Thermogravimetric analysis
TMTD	Tetramethyl thiuram disulphide
TPa	Tera pascal
Triton X 100	Polyoxyethylene octyl phenyl ether
TU	Toluene uptake
UV	Ultra violet
VFA	Volatile fatty acid
V_g	Volume fraction of RGO
V_r	Volume fraction of rubber
V_s	Molecular weight of solvent
Wingstay- L	Butylated reaction product of p-cresol and dicyclopentadiene
XGO	Exfoliated graphene oxide
XNBR	Carboxylated nitrile rubber
XRD	X-ray diffraction
XSBR	Carboxylated styrene butadiene rubber
ZDC/ZDEC	Zinc diethyl dithiocarbamate
ZMBT	Zinc-2-mercaptobenzo thiazole
α	Thermal conductivity
θ	Theta
λ	Specific heat capacity
μm	Micrometre
ξ	Shape fitting parameter
χ	Rubber-solvent interaction parameter
ζ	Zeta potential
χ_i	Initial susceptibility
μ_i	Initial permeability
γ	Gamma
ρ_r	Density of the polymer
σ	Conductivity
ϕ	Volume fraction of rubber
Ω	Ohm

.....❧.....

||| List of Publications |||

Publications in International/National Journals

- [1] **Anand K.**, Siby Varghese and Thomas Kurian. "Synthesis of ZnO Nanorods Through Mechano-chemical Route: A Solvent Free Approach" *International Journal of Theoretical and Applied Sciences* 6(1) (2014) 87-93.
- [2] **Anand K.**, Siby Varghese and Thomas Kurian. "Preparation of Ultra-fine Dispersions of Zinc oxide by Simple Ball-milling: Optimization of Process Parameters" *Powder Technology* 271 (2015) 187-192.
- [3] **Anand K.**, Siby Varghese and Thomas Kurian. "Effect of Micro and Nano-ZnO on the Properties of Pre-vulcanized Natural Rubber Latex Films" *Progress in Rubber Plastics and Recycling Technology* 31(3) (2015) 145-156.
- [4] **Anand K.**, Siby Varghese and Thomas Kurian. "Degradation Behavior of Nano Silica and Nano Titania Filled Natural Rubber Latex Nanocomposites" *Rubber Science* 28(3) (2015) 294-304.
- [5] **Anand K.** and Siby Varghese. "Role of Surfactants on the Stability of Nano-Zinc Oxide Dispersions" *Particulate Science and Technology* DOI: 10.1080/02726351.2015.1131787 (2015).
- [6] **Anand K.**, Siby Varghese and Thomas Kurian. "Aqueous Dispersions of Latex Compounding Ingredients By Wet Ball-Milling: Effect of Ball Size and Milling Time on Dispersion Quality" *Transactions of the Indian Institute of Metals* DOI: 10.1007/s12666-016-0957-x (2016).
- [7] **Anand K.**, Siby Varghese and Thomas Kurian. "Effect of Ball Size on Milling Efficiency of Zinc Oxide Dispersions" *Particulate Science and Technology* DOI: 10.1080/02726351.2016.1248258 (2016).
- [8] **Anand K.**, Siby Varghese and Thomas Kurian. "Morphology and Microstructure of Starch Nanocrystals Isolated from Modified Corn Starch and Their Effect on Natural Rubber Latex Vulcanizate Properties" (Accepted for publication in *Progress in Rubber Plastics and Recycling Technology*).
- [9] **Anand K.**, Siby Varghese and Thomas Kurian. "Mechanical Morphological and Electrical Properties of Radiation Vulcanized Natural Rubber Latex (RVNRL) - Graphene Based Nanocomposites" (Communicated to *Polymers and Polymer Composites*).

International/National Conferences

- [1] **Anand K.**, Siby Varghese and Thomas Kurian. ‘Nano Zinc Oxide in Pre-vulcanized Natural Rubber Latex: Antimicrobial, Mechanical and Swelling Characteristics’ *International Conference on Advances in Polymer Technology (APT’16)*, Cochin University of Science and Technology (CUSAT), 25 & 26 February 2016.
- [2] **Anand K.**, Siby Varghese and Thomas Kurian. ‘Preparation and Properties of Natural Rubber (NR) Latex-Corn Starch Crystal Based Bio-nanocomposites’ *National Seminar on Nano and Bio-Materials (NBM’15)* Department of Polymer Science and Rubber Technology, CUSAT, 28th February 2015.
- [3] **Anand K.**, Siby Varghese and Thomas Kurian. ‘Nanodispersions of ZnO: Preparation Characterization and Stabilization’ *National Conference on Materials Science and Technology (NCMST 2014)* Indian Institute of Space Science and Technology (IIST), Valiyamala, Trivandrum, 28 - 30 July 2014.
- [4] **Anand K.**, Siby Varghese and Thomas Kurian. ‘Wet Milling of ZnO Dispersion: Optimization of Process Parameters’ **26th Kerala Science Congress** Kerala Veterinary and Animal Sciences University (KVASU), Pookod, Wayanad, 28 - 31 January 2014.
- [5] **Anand K.**, Siby Varghese and Thomas Kurian. ‘Synthesis and Characterization of Nano ZnO and its Effect on Latex Preservation’ *International Rubber Conference (IRC-2012)* Kovalam, Kerala, India, 28 – 31 October 2012.

.....❧.....

Curriculum Vitae

Anand K.

NMC 8/325 (OLD 13/277)
Near Ganapathy Temple
Pazhavadi Street
Nedumangad 695 541
Thiruvananthapuram District
Kerala, India
Ph:+91-9895914592
E mail: anand.rrii@gmail.com



Personal Profile

Date of birth : 20-05-1987
Sex : Male
Marital Status : Single
Nationality : Indian
Religion & Caste : Hindu - Brahmin

Permanent Address : Anand K.
NMC 8/325 (Old 13/277)
Near Ganapathy Temple
Pazhavadi Street
Nedumangad 695 541
Thiruvananthapuram District
Kerala, India.

Academic Qualifications

M.Sc. Chemistry : S D College, Alappuzha.
B.Sc. Chemistry : University College, Trivandrum
Hindi Sahityaacharya : Kerala Hindi Prachar Sabha, Trivandrum

Achievements

- Top Performing Faculty Award from Amal Jyothi College of Engineering, Kanjirappally, India.
- Honour Code Certificate from IITBombayX, an online learning initiative of Indian Institute of Technology, Bombay.
- Second prize in quiz competition held in connection with National Science Day celebrations sponsored by KSCSTE –Trivandrum & DST – New Delhi.
- Travancore Brahmana Janasabha prize for securing highest mark in final B.Sc. examination among the Brahmin student of the University College - Trivandrum.

Professional Experience

Research: Five years research experience in Polymer Science and Rubber Technology at Rubber Research Institute of India, Kottayam, India.

Ten months research experience in Physico-chemical Characterization and Evaluation of Metal Based Siddha Medicines at PG & Research Department of Chemistry, Sree Narayana College, Chempazhanthy, Trivandrum.

Teaching: Assistant Professor (Chemistry) at Amal Jyothi College of Engineering, Kanjirappally, Kerala, India (Present).

Faculty of Chemistry in Co-operative Arts and Science College, Trivandrum, controlled by Dept. of Co-operation, Govt. of Kerala (1 year)

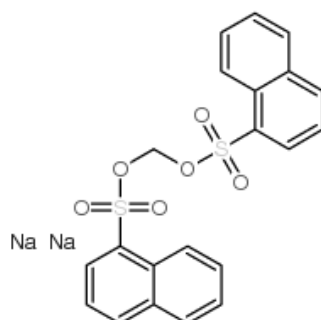
.....✍.....

Reply to thesis examiners comments

(Reviewer I)

C1. In chapter 3, optimization of process parameters to obtain ultra-fine dispersions of zinc oxide by ball-milling is presented. Here, the structure of surfactant used in the study should be shown. Also, some rationale for the choice of surfactant, Dispersol F, should be given. In fact, in addition to reporting the influence of surfactant concentration, a comparison of common surfactants could have been a valuable addition. It is not clear how D [4,3] is calculated and should be included.

The structure of the surfactant used was given below:



In this study the surfactant used was disodium methylene *bis* naphthalene sulphonate (Dispersol F). The selection of a surfactant for the use in latex depends upon several factors such as its activity, cost, residual action in the products etc. Generally anionic surfactants are more preferred in latex industry. Accordingly, the most preferred surfactant for making dispersions of latex ingredients is disodium methylene *bis* naphthalene sulphonate. There are several other surfactants which are widely used in latex industry e.g. Ammonium laurate (anionic), ammonium oleate (anionic), sodium dodecylsulphate (SDS-anionic), hexadecyl trimethyl ammonium bromide (CTAB-cationic), polyethylene oxide condensate (Vulcastab VL-non-ionic) etc. Exploring the effect of all the surfactants is beyond the scope of this study.

D [4,3] is the volume weighed mean, also known as De Brouckere Mean. It is the weighted average volume diameter, assuming spherical particles of the same volume as the actual particles. It is most sensitive to the presence of large particulates in the size distribution.

$D[4,3] = \Sigma d^4 / \Sigma d^3$ where 'd' is the diameter of the particle.

C2. Many abbreviations are written multiple times in text starting with Chapter 3 and these should be removed.

Abbreviations written multiple times in chapter 3 were removed and the modified thesis is prepared accordingly. (*Page 99, line 1; page 100, line 23; page 101, line 3; page 109, line 22; page 119, line 2; page 128, line 3 and line 24; page 129, line 8; page 134, line 15*).

C3. The decrease in specific surface area at longer times has been attributed to aggregation of zinc oxide particles, however, it is unclear why SSA does not increase at all in the beginning also for any of the concentrations investigated? Also, it is important to include how SSA is calculated? Although it is suggested that the use of higher surfactant concentration could potentially eliminate aggregation, no report is included to confirm this assertion.

The particle size reduction and hence the increase in SSA for a particular system depends on factors like the size of the balls, materials of the ball, activity of the surfactant, speed of rotation, milling time etc. Once the milling process started, the size decreases slowly and reaches the lowest possible size and thereafter it increases. The reason for this slow reduction and no change thereafter in all systems has been described in Figure 3A.7. (Page 108). The SSA is obtained directly from machine (Mastersizer 3000 Malvern, UK) and is calculated as stated below.

Specific surface area = $6 / D[3,2]$, where D[3,2] is the surface area moment mean or Sauter mean diameter

Dispersol - F is the commonly recommended surfactant for preparing aqueous dispersions of latex compounding ingredients. However, excess usage of the chemical can cause discoloration to the finished product. Hence higher surfactant concentration is not generally recommended.

C4. In Chapter 4, is the IR spectrum shown (Fig 4A.3) that of annealed sample? The band at 1650 cm^{-1} has been assigned to acetate or oxalate, please check? Also, the TGA graph shows two step weight-loss, an initial weight loss which extends up to 200°C and a second one around 241°C ? What do these correspond to?

The IR spectrum of the annealed sample is displayed in Fig. 4A.3. The band near 1650 cm^{-1} is attributed to asymmetric stretching of residual zinc acetate [**Ref:** N.T. Nolan, M. K. Seery and S.C. Pillai. (2011). *Chem. Mater.*, 23(6) 1496]. This has been corrected in the thesis (page 151). Initial small weight loss (below 200°C) corresponds to the volatile impurities. Weight loss at 241°C might be due to the decomposition of unreacted CH_3COOH .

C5. In Chapter 5, the effect of micro and nano sized dispersions on various physical properties are presented. Here, and in subsequent chapters, it is imperative to add the error in the data in the tables as well as show the error bars on the graphs. In Chapter 6, comparative studies are presented between the use of SiO_2 and TiO_2 , however, direct comparison would have been better justified if the particle sizes of the two were comparable as well.

The graphs were re-plotted and error-bars were included. The modified graphs are shown below:

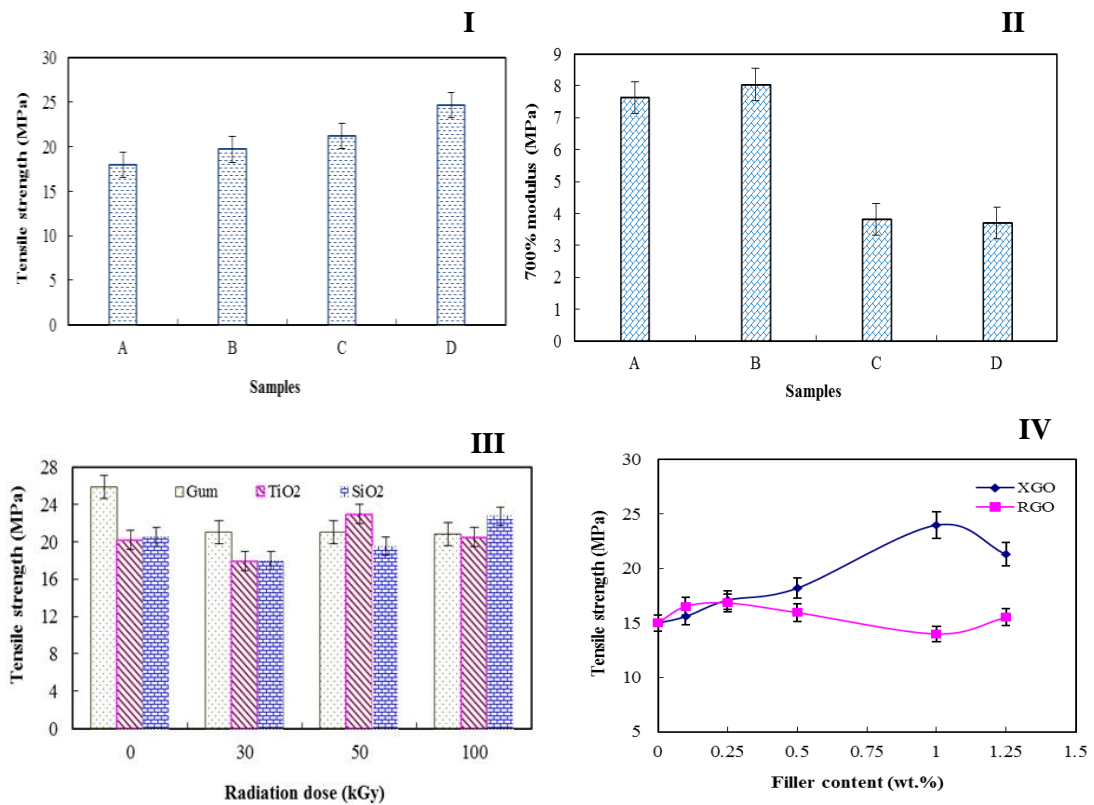


Fig. I: Tensile strength of pre-vulcanized latex films containing micro and nano ZnO

Fig. II: Modulus at 700% elongation of pre-vulcanized latex films containing micro and nano ZnO

Fig. III: Effect of radiation dose on tensile strength of nanocomposites

Fig. IV: Variation in tensile strength of XGO and RGO filled RVNRL nanocomposites

Both SiO₂ and TiO₂ nano dispersions having comparable size (< 200 nm) were purchased from the manufacturer. However, an increase in the particle size was noted for SiO₂ dispersions after the size analysis. This might be due to agglomeration of nanoparticles during sample preparation for DLS measurements.

(Reviewer II)

C1. The author has carried out the sorption behavior of zinc oxide NR, degradation behavior of nano silica/titania NR, swelling studies for starch nano crystal NR and electrical studies for graphene nanocomposites. It is also better to take same properties and study across different dispersions. This will give real comparison of same properties across different dispersion in common media (latex).

The dispersions which included in the study were ZnO, silica, titania, starch nanocrystals and graphene derivatives. In latex technology, ZnO is activator, silica and titania are inorganic fillers, starch is a bio-filler and graphene is a conductive filler. For example property wise silica is non-conductive filler whereas graphene is a conductive one. As the effect of all these materials in latex is different, the evaluation of the dispersions was conducted separately.

C2. It is better if you can add the actual photographs of ultrasonication in the chapter for a better understanding whether horn type or normal method used (suggestion only).

In this study horn type sonicator was used. The photograph is shown below:



C3. The author has carried out the effect of milling time, surfactant, ultrasonication etc. on the size of the particle formation based at a fixed rpm of 35. What is the basis of fixing rpm as 35?

There optimum speed of rotation which ensures the cascading action of balls was calculated using the equation $29.92/\sqrt{R} \text{ min}^{-1}$, where R is the radius of the container in meters. Accordingly an optimum speed of 35 rpm has been selected.

C4. The mechanical properties results normally represented with standard deviation of five specimens. In this work only the results of starch nano crystal filled latex shows with standard deviations. What about the other matrices?

For other materials also, standard deviation of five specimens were taken.

C5. Effect of ultrasonication on the specific surface area of the zinc oxide particles studied for dispersions of zinc oxide. The effect of ultrasonication for making stable dispersion also could have been attempted. Ultrasonication could have been helped for stable dispersion of micro and nano zinc oxide on pre-vulcanized natural rubber latex films in chapter 5.

On ultrasonication, the size distribution of the dispersions changes continuously. Preparation of stable dispersions was followed accordingly.

C6. Percolation threshold is mentioned as 0.1 wt. % for RGO in chapter 8. It is better to do one more formulation for 0.05 wt. % before declaring 0.1 wt. % as the threshold value.

The declared threshold value was correct as the abrupt increase in conductivity was occurred at this loading.

C7. It is better to study the stability of RVNRL-graphene nanocomposite dispersions also in chapter 8.

In almost all industrial process, the compounded latex is immediately converted to useful products and hence the stability-

evaluation of RVNRL-graphene nanocomposites for prolonged periods is beyond the scope of this study.

(Reviewer III)

C1. The volume-weighted mean size increases after 30 h with 2 wt. % SA (Fig. 3A.1). The specific surface area decreases marginally (Fig. 3A.2) for the same case. A significant decrease in surface area would be expected if there is agglomeration. Similarly, the average particle size after 30 h of wet ball milling does not appear to be reflected in Fig. 3A.3. Please clarify.

The results of the Figure 3A.1 have been rechecked and it was found that the size increase after 30h was an experimental error. After 30 h of wet-ball milling (Figure 3A.3), the size is expressed in percentage and is as expected.

C2. PVA is biodegradable (page 23)? Relevant reference may be incorporated. Does literature give some basis to conclude that PVA is biodegradable?

Polyvinyl alcohol (PVA) is recognized as one of the very few vinyl polymers soluble in water and is biodegradable. (Ref: E. Chiellini, A. Corti, S. D'Antone and R. Solaro (2003) Biodegradation of poly (vinyl alcohol) based materials, *Progress in polymer science* 28(6) 963-1014).

Chapter IV

C1. The yield of zinc oxide may be given in the Experimental section at the end of section 4A.2.1.1 in addition to what is given in the conclusion section.

The yield of the ZnO is included in the Experimental section of the modified thesis (*Page 148, line 10*).

C2. The interpretation of the result presented in Fig. 4A.1 is different in pages 149 and pages 150. (decomposition of zinc hydroxide at 300°C is implied here instead of the loss of volatiles as presented in page 149) and 155 (conclusion in which the decomposition of zinc hydroxide is

suggested). In the light of the factual data presented in the interpretation given in page 149 requires clarification.

From the TGA results, it has been observed that the complete conversion of Zn(OH)_2 to ZnO occurs at 241°C . There is no weight loss after 241°C . The complete removal of volatile impurities if any, bound water, unreacted zinc acetate and acetic acid formed occurs at this temperature. Therefore the synthesized ZnO nano powder was annealed at 300°C in order to ensure complete removal of residual chemicals if any.

C3. In page 151 (Fig. 4A.3), the C=O stretching vibration in zinc acetate is assigned as the peak appearing at 1533 cm^{-1} . Is there any reference for this assignment? If so, the same may be mentioned.

It has been reported that the symmetric C=O stretching of zinc acetate is observed at 1515 cm^{-1} [Ref: F. Z. Haque, M. R. Parra, H. Siddiqui, N. Singh, P. Pandey and K.M. Mishra (2016). PVP assisted shape-controlled synthesis of self-assembled 1D ZnO and 3D CuO nanostructures, *Optika i Spektroskopiya* 120(3):427-433].

C4. The FT-IR data suggests the presence of zinc acetate impurity in the zinc oxide synthesized while the PXRD suggests otherwise. Hence this may be qualified (page 150: From this limits of detection of PXRD no impurities could be found in the nanoparticles of zinc oxide).

PXRD is not sensitive enough to detect the small amount of zinc acetate in the sample as observed in FTIR.

In addition to the above, the following suggestions put forwarded by the examiner were also included in the respective places of thesis:

Page 1, line 5: “.....preparation of nanomaterials **are** explained.....”

Page 5, last line: “.....propionic may **be** generated.....”

Page 27, line 8: “**of** mechanical strength....”

Page 37, 7th line: zinc acetate **dihydrate**

Page 60, line 5: “**amount the amount**” should be “amount”

Page 151: **The** band near 1650 cm^{-1}

Page 167, first line: ZnO dispersed in non-ionic surfactants settles down after 3 days.

Page 208, Section 7.2.2.1: “....distilled water until **neutral** (pH = 7).

Anand K (Research Scholar)

Dr. Siby Varghese (Guide)